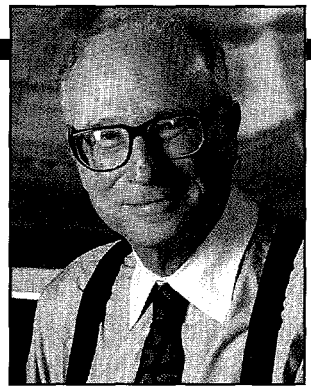

There's a popular song that says, "Nobody does it better." The song refers to James Bond, the fictional British spy, but the same sentiment also holds true for Argonne's Intense Pulsed Neutron Source, now marking the 15th anniversary of its operation. IPNS is one of Argonne's premier success stories.

Although based on equipment cannibalized from earlier projects and given only bare-bones funding, IPNS continues to provide the nation's most reliable source of neutrons for the study of atomic arrangements and motions in liquids and solids, known as condensed-matter physics.

And that persistence in quality has been rewarded. Under the Scientific Facilities Initiative approved by Congress last year, the operating budget of IPNS has been increased by 50%, allowing a substantial increase in operating time. In addition, the proposed IPNS Upgrade – a one-megawatt pulsed source with 2 target stations and 36 beamlines – has the support of scientists nationwide. It is the Laboratory's first construction priority.

The reasons for the success of IPNS are simple. First, the facility established new, higher standards of "user friendliness" early on. It attracts biologists and chemists, as well as physicists, because of its organization and staff, who provide outstanding assistance to visiting researchers. And finally, the facility's reliability – more than 95% availability of beam – allows users to plan research with confidence and gain maximum results from their time at the facility.

On this 15th anniversary, all of us at Argonne National Laboratory share with the IPNS staff their pride in a job well done, and we look forward to many more years of successful operations on behalf of scientific research and societal progress.

Alan Schriesheim
Director and Chief Executive Officer

Foreword

The 15th Anniversary Edition of the IPNS Progress Report is being published in recognition of the Intense Pulsed Neutron Source's first 15 years of successful operation as a user facility. To emphasize the importance of this milestone, we have made the design and organization of the report significantly different from previous IPNS Progress Reports.

This report consists of two volumes. For Volume I, authors were asked to prepare articles that highlighted recent scientific accomplishments at IPNS, from 1991 to present; to focus on and illustrate the scientific advances achieved through the unique capabilities of neutron studies performed by IPNS users; to report on specific activities or results from an instrument; or to focus on a body of work encompassing different neutron-scattering techniques. Articles were also included on the accelerator system, instrumentation, computing, target, and moderators.

A list of published and "in press" articles in journals, books, and conference proceedings, resulting from work done at IPNS since 1991, was compiled. This list is arranged alphabetically according to first author. Publication references in the articles are listed by last name of first author and year of publication. The IPNS experimental reports received since 1991 are compiled in Volume II. Experimental reports referenced in the articles are listed by last name of first author, instrument designation, and experiment number.

From the startup of IPNS in 1981, our goal has been the optimization of research opportunities for the neutron user community. The accomplishments described in the pages of this report are a tribute to the people who work at IPNS. There have been rough and, occasionally, uncertain times, but the scientific productivity has remained extremely high. With the dedication we're seeing to our scientific program and the exciting prospect of the IPNS Upgrade, the future looks bright for IPNS.

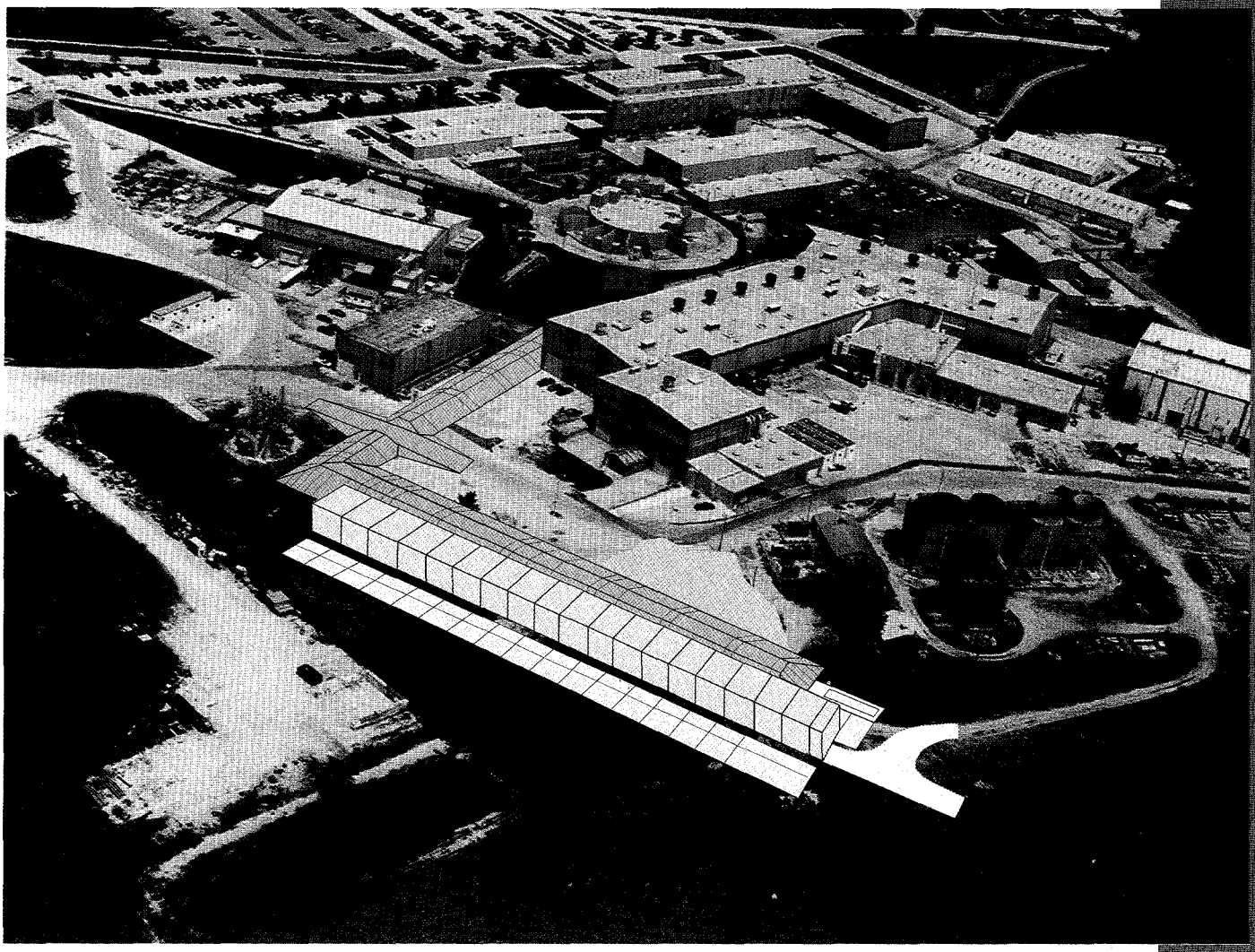

Layout of the IPNS Upgrade, which is based on a proton accelerator producing 500 μA at 2 GeV. Such an upgrade could provide a total beam power of 1 MW.

IPNS Division personnel.

Chapter I

INTRODUCTION

15TH ANNIVERSARY 1981 - 1996

IPNS

I Introduction

In May 1981, the proton beam was first delivered to the Intense Pulsed Neutron Source (IPNS) target at Argonne National Laboratory and now, in May 1996, the 15th anniversary of this historic event is being celebrated. In addition, this special IPNS Progress Report, which contains a summary of developments and scientific accomplishments, is being disseminated.

In the five years since the 10th anniversary, a great deal of activity took place at IPNS, and many improvements were made. More than 1,300 experiments were performed, and more than 900 scientists conducted at least one experiment during any given year. Many of the scientific results achieved at IPNS were significant, and they involved a broad range of disciplines.

During this time, several new instruments were added:

- The glass, liquid, and amorphous materials diffractometer (GLAD) was added to the user program in 1992.
- The small-angle diffractometer (SAND) was commissioned in 1993.
- The chemical excitations spectrometer (CHEX) was constructed in record time during the summer of 1995. CHEX was put on the beamline formerly occupied by PHOENIX, which had been very successful in performing deep inelastic scattering for 10 years and, more recently, in performing diffraction experiments in quantum systems.

Fiscal year (FY) 1996 has been especially exciting because the IPNS operating budget has increased by 50% as part of the Scientific Facilities Initiative. This funding will enable IPNS to double its operating time and provide the scientific and technical support necessary to allow all instruments involved in the user program to be operated at their full capacity.

Argonne also made a major contribution to the development of pulsed sources in the last five years, conceiving, developing, and documenting a feasibility study for a new, world-class pulsed spallation source. This "IPNS Upgrade" was originally designed to be a 1-MW source with two target stations and 36 beamlines, having six times the beam power of ISIS (the most powerful source operating in the world) and saving $175 million by using existing buildings and infrastructure. The feasibility study was reviewed in April 1995. In response to guidance from the U.S. Department of Energy (DOE), the design was scaled down to a 400-kW source with 18 beamlines and 2.5 times the power of ISIS. This plan is now under review by DOE's Basic Energy Sciences Advisory Committee. In addition, an effort has begun to design and prepare a detailed cost estimate of an ISIS-level source (150 KW), which would again realize large savings by using existing buildings.

Already, the scientific capabilities of the four short pulsed spallation sources that operate worldwide have been shown to be significant. It is therefore vital that the United States have

a plan to enhance its own capabilities. The 1-MW IPNS Upgrade is the best documented and most thoroughly reviewed option for a future spallation source.

Argonne's accomplishments and innovations with regard to spallation sources over the past 20 years and its dedicated operation of IPNS as a user facility demonstrate the Laboratory's commitment and credibility. The IPNS Upgrade would represent an important step forward in the technological expertise that the United States could offer the neutron scattering community. Details of the IPNS Upgrade are discussed in Chapter 8 on future plans.

Members of the IPNS Division Management Team include: (from left to right) Chun Loong, Ira Bresof, Bill Ruzicka, Kent Crawford, Tom Worlton, Gerry McMichael, Frank Brumwell (standing), and Bruce Brown and Jack Carpenter (seated).

Intense Pulsed Neutron Source control room. William Sullivan is updating the accelerator log book, and James Spindler is at the accelerator controls.

Chapter II

THE IPNS ACCELERATOR SYSTEM

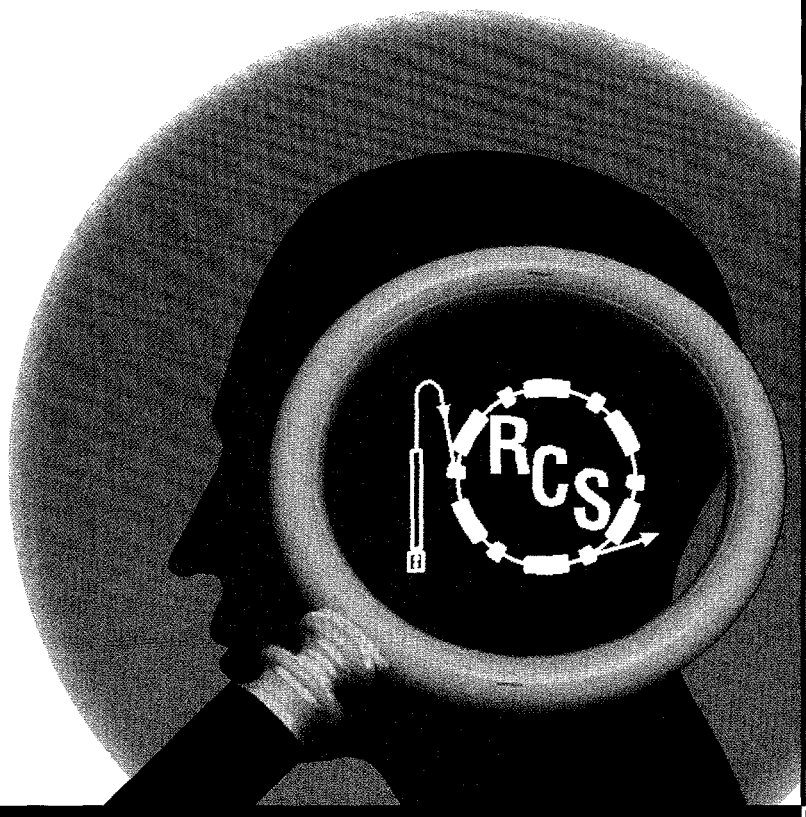

15TH ANNIVERSARY 1981 – 1996

IPNS

II

The IPNS Accelerator System

F. R. Brumwell and G. E. McMichael, IPNS Division, Argonne National Laboratory

Introduction

The IPNS accelerator, which delivered its first beam to the IPNS target on May 5, 1981, is poised to mark the 15th anniversary. However, parts of this machine can claim a much earlier start; the first beam was injected and coasted in the synchrotron on April 4, 1977; the injector and linac are in their 34th year, having accelerated the first beam to the Zero Gradient Synchrotron (ZGS) in 1962. What these anniversaries represent in "people years" is left to the reader. Suffice it to say that, like a fine wine, the IPNS accelerator has continued to improve with age (higher average beam current, better availability). Sometime late next year, it should record its five-billionth pulse on target, and we confidently expect the eight-billionth pulse well before its 25th anniversary on May 5, 2006.

Accelerator Description

The IPNS Accelerator System

The accelerator system consists of an H^- ion source, a Cockcroft-Walton preaccelerator, a 50-MeV Alvarez linac, a 500-MeV Rapid Cycling Synchrotron (RCS), and transport lines and ancillary subsystems (controls, diagnostics, services). Figure 1 shows the layout of the IPNS accelerator, including linac, RCS, and spallation target. The accelerator normally operates at an average beam current of 14 to 15 μA, delivering pulses of approximately 3×10^{12} protons at 450 MeV to the target, at a rate of 30 times per second (30 Hz).

The Ion Source and Preaccelerator

The H^- ion source and associated equipment are housed in the terminal of a 750-kV Cockcroft-Walton preaccelerator. The H^- ion source is a magnetron type in which negative ions are extracted directly from the hydrogen plasma on the surface of the source cathode. The extractor electrode and magnet poles are at terminal ground potential; the source itself, including the pulsed arc supply, pulsed hydrogen gas supply, and cesium supply (cesium greatly increases the H^- generation), is pulsed to a negative 20-kV potential. The H^- beam is extracted, bent 90° (to remove electrons from the H^- beam) by a magnetic dipole, focused by a set of three quadrupole magnets, and injected into the high-voltage column of the preaccelerator. The preaccelerator produces approximately 30-mA, 750-keV, 70-μs pulses at a repetition rate of up to 30 Hz.

The Low-Energy Beam Transport System (LEBT)

The LEBT is a 4-m line between the preaccelerator and the linac. It contains quadrupole magnets to confine the beam and focus it into the linac, two steering magnets, a 200-MHz single-gap buncher cavity to improve the capture in the linac, a beam chopper to establish the beam rate, beam diagnostics, and a beam stop (Faraday cup).

The Linac

The linac is a copper-clad-steel structure 0.94 m in diameter and 33.5 m long. Along with the preaccelerator and LEBT, it was originally commissioned in 1962 and provided beam for the ZGS accelerator until that facility's shutdown in October 1979. (Its lineage can actually be traced back even further, because the copper-clad steel was some of that produced in the early 1950s for the then-top-secret MTA accelerator at Livermore.) The linac was constructed in seven sections, which are bolted together. It contains 124 drift tubes, each with a dc quadrupole magnet. The magnets are divided into 12 series groups and powered by 12 dc power supplies, located on the service floor. Transistorized shunts are attached to each of the first 58 magnets, allowing remote control of individual magnets. Nominal vacuum level in the linac is 2-3 x 10^{-7} torr, maintained by seven ion and two cryo pumps. The linac is water-cooled with a closed-loop system, which is temperature-regulated to within 0.2°F to keep the cavity tuned during normal operation to 200.07 MHz ± 1 kHz. The 200-MHz pulsed rf power is obtained from a four-stage amplifier; the output stage is a 7835 triode with a normal operating level of 3 MW and a peak-power rating of 5 MW. The 50-MeV beam exiting from the linac is about 1 cm in diameter; the pulsed current is about 10 mA; the 70-μs pulses can be delivered at a repetition rate of up to 30 Hz.

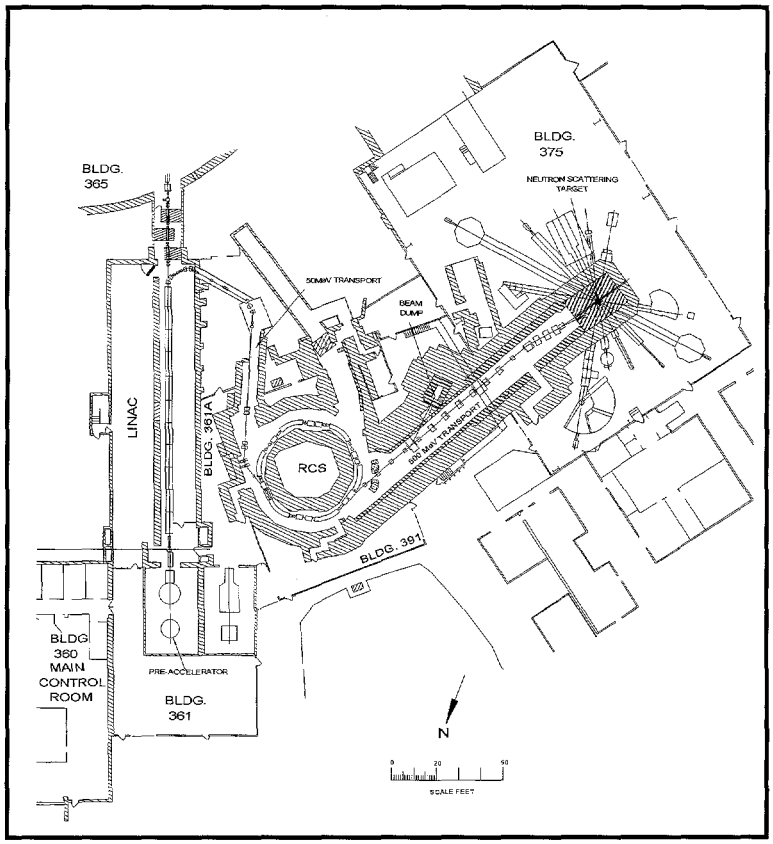

FIGURE 1.
Layout of the IPNS accelerator, including linac, RCS, and spallation target.

The 50-MeV Transport Line

The 50-MeV beamline transports the H^- beam from the high-energy end of the linac approximately 38 m to the RCS accelerator. Beam steering and focusing is provided by a total of eight horizontal and two vertical dipole magnets and 16 quadrupole magnets. To avoid excessive gas stripping of the H^- beam, the vacuum level in the 50-MeV line is kept below 2×10^{-6} torr.

The Rapid Cycling Synchrotron (RCS)

The RCS was originally designed as a booster for the 12.5-GeV ZGS high-energy physics accelerator, the intent being to provide increased ZGS beam intensity by injecting higher-energy (boosted) particles and taking advantage of the higher space-charge limit that would result. However, since the ZGS could only accept 8 pulses every 4 seconds, 90% of the beam from the RCS would have been available for other uses – specifically, for a pulsed neutron source. Although a 300-MeV beam was extracted toward the ZGS from the RCS in 1977 (two years before the termination of the ZGS program), it was stopped at the ZING experimental target and never injected into the ZGS because, with shutdown imminent, priority was given to exploiting the ZGS's uniqueness as the world's only producer of high-energy polarized proton beams.

Over the next four years, the IPNS accelerator took on much of its present form. The extraction point from the RCS was moved to permit beam delivery to the present IPNS target location, and improvements were made to injection and extraction regions. The kicker magnet system, ac and dc septum magnet systems, and the extraction beamline were completed. By May 1981, the RCS was delivering 10-μA pulses at 300 MeV or 4.5-μA pulses at 400 MeV to the new neutron Radiation Effects Facility (REF) target.

The RCS is a strong-focusing, combined-function synchrotron. It is a six-period machine with a magnet structure of DOOFDFO and a circumference of 42.95 m. The ring magnets, part of a biased 30-Hz resonant circuit driven from twin solid-state power supplies, generates a magnetic field from 0.28 to 1.0 Tesla so that the beam orbital radius remains constant during the acceleration from 50 to the design maximum of 500 MeV. Two pairs of sextupole magnets, powered by 30-Hz programmable power supplies, provide betatron tune correction and manipulation.

H^- stripping injection, pioneered on the Booster I experiment for the ZGS, is accomplished on the RCS with a carbon stripper foil located on the inside radius of a long straight section (L-1) outside the limit of the circulating proton beam. The equilibrium orbit is deformed in the injection region into the foil by a series of three small, pulsed "bumper" magnets. The H^- beam is injected through a singlet ring magnet so that, at the stripper foil, its path matches the deformed orbit. During injection, the bumper magnet current decays at a controlled exponential rate, moving the closed orbit away from the stripper foil and uniformly filling the horizontal aperture.

The accelerated proton beam is accelerated from the injection energy (50 MeV) to the final energy (currently 450 MeV) by two ferrite-loaded coaxial cavities. The frequency swing for the first-harmonic acceleration cycle is from 2.20 to 5.29 MHz, with a 22-kV peak accelerating voltage for 500 MeV (2.0 to 5.14 MHz for 450 MeV). Lost beam, which causes radiation and activates beamline components, ultimately determines operational limits. Because beam loss

is a complicated function of both current and extraction energy, beam is extracted before the maximum energy (500 MeV) is reached; by so doing, neutron production in the target is maximized for a given beam loss in the RCS. The accelerated beam is extracted in a single turn by two ferrite-loaded kicker magnets and two septum magnets, one pulsed and one dc. The rise time of the kicker magnet is ≈100 ns, with a 100-ns flat-field region. The first septum magnet is pulsed by a half sine wave current at a 30-Hz rate. The extracted beam (450-MeV, 70-80 ns pulses, peak current ≈12 A) is then transported through the "500 MeV" beamline to the neutron-generating target.

The 500-MeV Transport Line

The 500-MeV transport line, a 37-m-long beamline that includes three horizontal (bending), two vertical (steering), and 15 quadrupole (focusing) magnets, transports the beam from the RCS in Building 391 to the neutron-generating target in Building 375.

Controls and Diagnostics

All of the accelerator operations can be handled by one operator, thanks in part to the control and diagnostics system. Recently, the two Data General control computers (left over from the late 1970s) were replaced. The new control system is based on EPICS (Experimental Physics and Industrial Control System), a constantly evolving, distributed, real-time, control and instrumentation system developed jointly by Argonne (Advanced Photon Source) and other national laboratories/research facilities. The system is customized for the individual needs of the IPNS accelerator.

An EPICS system consists of one or more Input/Output Controllers (IOCs) and one or more Operator Interfaces (OPIs), all connected together via an ethernet. The data collection and control functions are handled by the IOCs and are built up of simple building blocks called records. A set of these records is put into a database to perform a required function. Readout and operator input functions are handled by the OPIs. Any type of display (meter, bar, number, etc.) may be made for any record in any IOC and may be displayed on any OPI.

Currently, the IPNS control and diagnostics system comprises three IOCs and two OPIs. Since either OPI can get information from any of the IOCs, this new system greatly improves the ease with which the operator can retrieve necessary information. Either OPI can do the whole job of displaying information if necessary, and spare parts for them and the IOCs are readily available. This substantially improves system reliability and minimizes downtime in the event of a failure.

Work is under way to upgrade the remaining parts of the old computer control system, including the replacement of pushbuttons and digital readouts by LCD touch screens.

The upgrading of the Linac Source Control System with an EPICS-based system is also beginning. The current system suffers many of the problems that the main control system suffered in terms of reliability and availability of spare parts.

There are also two PC-type computers in the control room. One monitors the 50-MeV beam position and losses at six points in the line; the other monitors beam losses at 14 points in

the accelerator. These computers are not part of the EPICS system and are not essential to operations, but they offer useful feedback to the operators. Indeed, the loss monitor computer has been set up specifically to indicate "better" or "worse" than a starting point the operator chooses. This provides the operator with an opportunity to see whether a tuning change is better or worse, both overall and over time.

Accelerator Operations

Three performance measures for the IPNS accelerator are beam current delivered to the target, system availability, and total operating hours:

- Beam current is primarily a machine parameter; however, it is the engineers' and technicians' fixing of faults and improvements to the hardware, and the skill of the operators in "tuning," that has allowed what was initially a machine with a current of 10-12 μA to consistently achieve average currents of 14-15 μA.
- System availability is undoubtedly the most important measure, from the user's perspective. Although it has a strong machine component, major credit for IPNS's enviable record (availability consistently hovering around 95%) must go to the skill, dedication, and attention to detail of all the people who maintain and operate the machine.
- Operating hours on IPNS have, almost from turn-on in 1981, been funding-limited rather than machine-limited. This situation is now changing. The Scientific Facilities Initiative (SFI) funding included in the FY 1996 budget provides for an increase in operating time for IPNS from 16 weeks/year to possibly as much as 32 weeks/year.

Proton Beam Current

Figure 2 shows the weekly-average proton current on target, from turn-on in 1981 down to the present. Prior to 1983, current was limited by the ion source. Since then, it has been limited ultimately by "beam loss" – as more beam is injected, the fraction of the beam that is "spilled" in the accelerator reaches some limit (usually determined by radiation levels) that it is not prudent to exceed because of the requirement of hands-on maintenance. Because beam spill is a complicated function of vacuum level in beam lines, "noise" in power supplies or controls, achievable fields in cavities, etc., the challenge for the operator is to find the optimum "tune" for the conditions at the moment, to maximize beam-on-target while keeping beam spill to

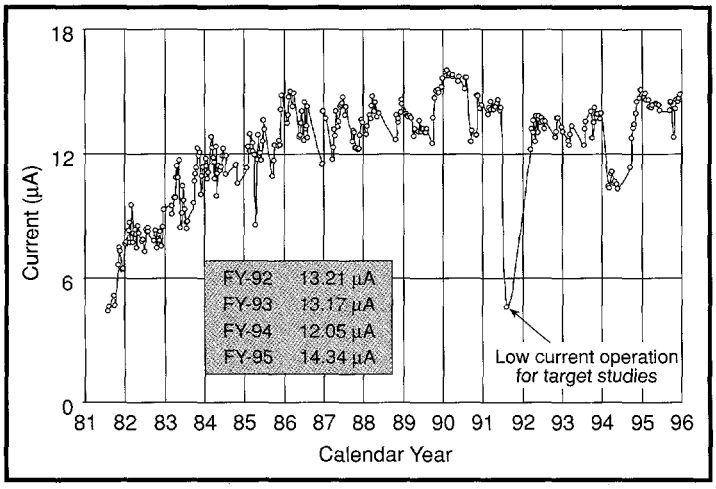

FIGURE 2.
Weekly-average proton current on target, from turn-on in 1981 down to the present.

manageable levels. Over the course of a year, operators must cope with a host of changes brought about by vacuum leaks, weak or noisy supplies, and other glitches that arise during a run and can only be repaired following that or a subsequent run. In many cases, a cool-down time is required for access to the area or component requiring repair. With the exception of one run in 1991 (where low current was required for target studies) and during much of 1994 (when a damaged septum magnet limited operation to about 10 μA), average current has exceeded 13 μA, with occasional operation exceeding 15 μA.

Accelerator System Availability

At the conclusion of each run (typically a period of 2-3 weeks, during which beam is scheduled to be available to the users 24 hours a day), availability is calculated as the ratio of beam hours available to beam hours scheduled. Achieved availability since 1981 is plotted in Figure 3, one point for each scheduled run. For the last ten years, availability for a single run has very rarely dropped below 80%, and yearly averages are close to or exceeding 95%. The challenge for the coming years will be to maintain this level while at the same time doubling the total number of hours per year that neutrons are produced for users.

Yearly Operating Schedule

Scheduled and actual operating time (weeks/year) are shown in Figure 4. For several years, budget constraints have limited operation to about 16 weeks per year. The SFI funding has allowed us to increase scheduled operation for 1996 to 25 weeks and should eventually result in an operating schedule of 32 weeks per year.

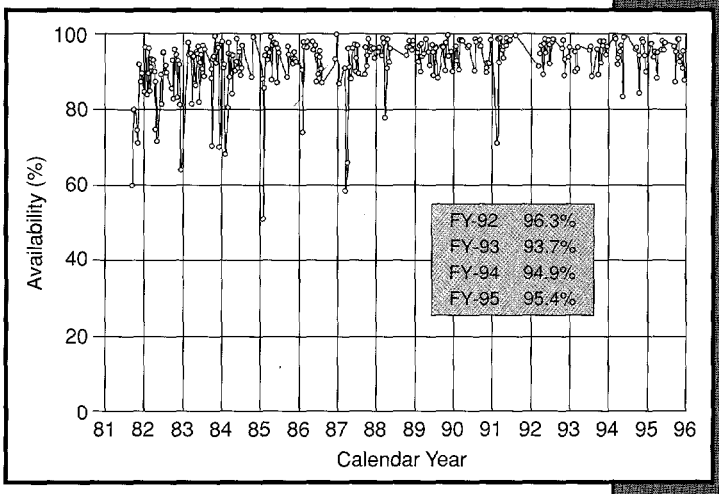

FIGURE 3.
Availability is calculated as the ratio of beam hours available to beam hours scheduled. Achieved availability since 1981 is plotted, one point for each scheduled run.

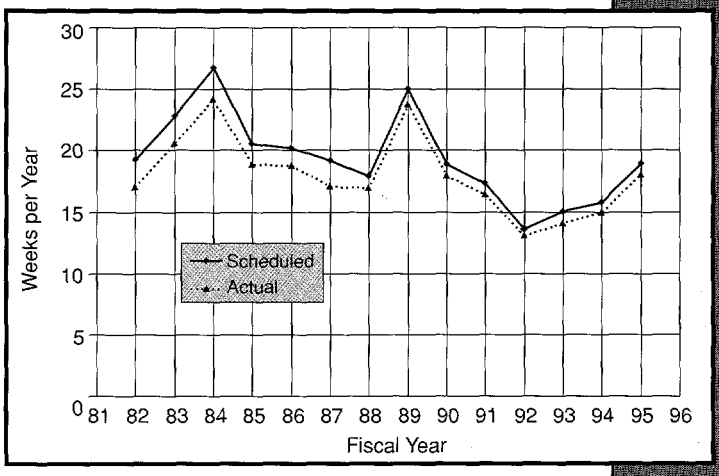

FIGURE 4.
Scheduled and actual operating times (weeks/year).

Pappannan Thiyagarajan loads a colloidal sample into the automatic sample changer at the Small Angle Diffractometer to measure structures in a size range of 1 to 100 nm.

Chapter III

SCIENCE AT IPNS

- GENERAL PURPOSE POWDER DIFFRACTOMETER
- SCIENCE ON THE SPECIAL ENVIRONMENT POWDER DIFFRACTOMETER
- SINGLE CRYSTAL DIFFRACTOMETER
- SMALL ANGLE NEUTRON SCATTERING
- REFLECTIVITY AT IPNS
- QUASIELASTIC NEUTRON SPECTROMETER AND CHEMICAL EXCITATIONS SPECTROMETER
- DIFFRACTION STUDIES OF HYDROGENOUS MATERIALS AT GLAD
- ADVANCED TECHNICAL CERAMICS
- THE STRUCTURE AND DYNAMICS OF ZEOLITE FRAMEWORKS AND ADSORBATES
- MUCH ADO ABOUT SOMETHING
- NEUTRON IRRADIATION EFFECT STUDIES AT IPNS

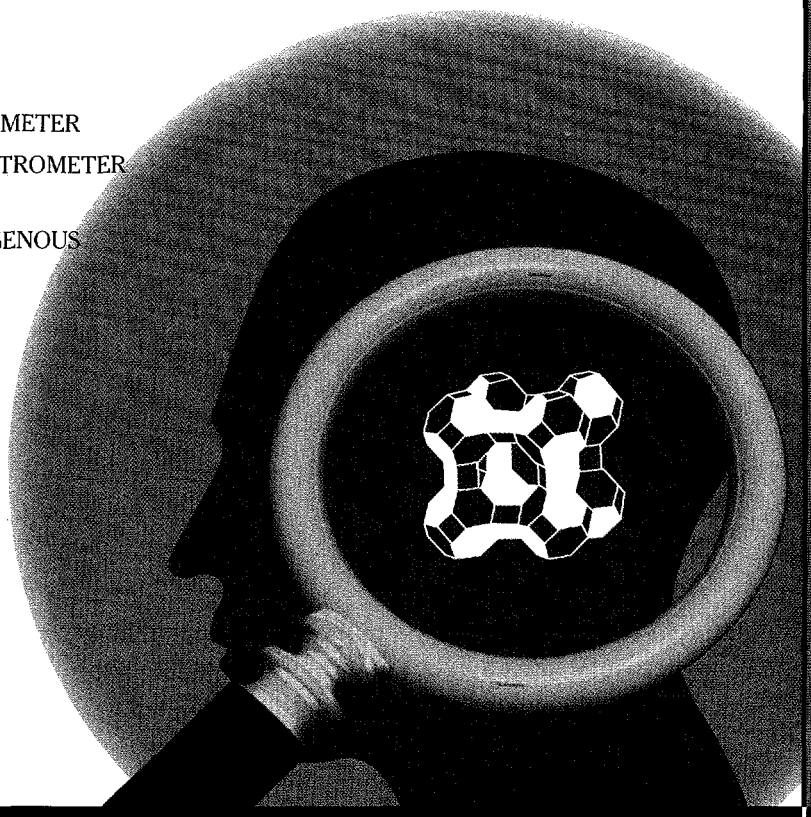

III

General Purpose Powder Diffractometer

J. W. Richardson, Jr., IPNS Division, Argonne National Laboratory

The General Purpose Powder Diffractometer (GPPD) at IPNS continues to be a very versatile instrument. Although the majority of GPPD users (about 30 outside users per year) come to do experiments involving structure refinements of powder samples, there is an increasing emphasis on the study of advanced materials in operational configurations. The instrument was designed and constructed for basic research, but the unique characteristics of time-of-flight (TOF) neutron powder diffraction (NPD) provide incentives for scientists to participate in cooperative research with industry, where real-world (messy) scientific problems exist.

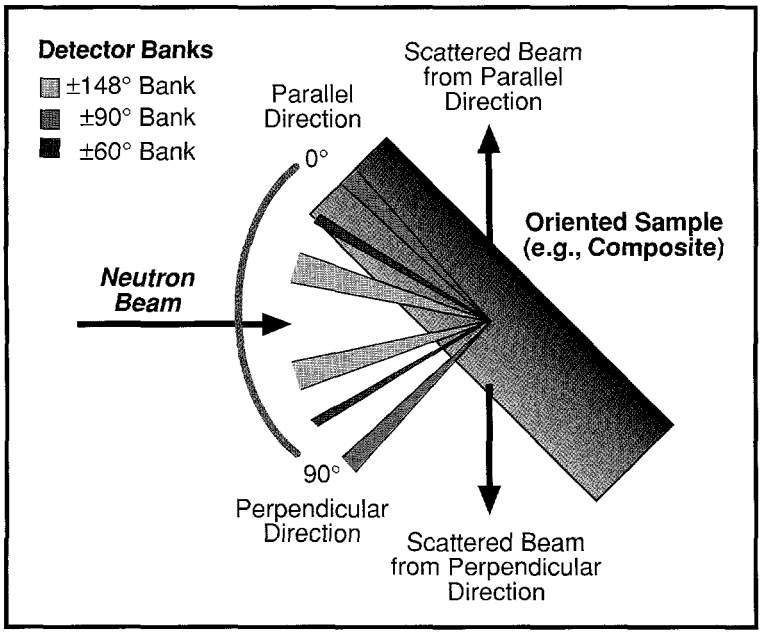

FIGURE 1.
With detector banks centered at 2θ values of ±148°, ±90°, and ±60°, a single GPPD dataset contains microstructural data, such as texture, residual strain, or dislocation strain, corresponding to six different orientations within the sample. For instance, when strongly oriented samples, such as fiber-reinforced composites, are oriented with their major axes 45° to the incident beam (above), the respective banks measure properties covering orientations between those parallel and perpendicular to the major axis.

The GPPD provides a flexible experimental platform for exploring a diverse range of microstructural parameters. Its multiple detector banks centered at 2θ values of ±148°, ±90°, and ±60° allow us to measure anisotropy in any of a variety of structural parameters (see Figure 1). Well-characterized peak profiles and good resolution ($\Delta d/d = 2.5 \times 10^{-3}$ at $2\theta = 148°$) provide sensitivity to the presence of minority phases. The GPPD can be used in high-temperature experiments to probe chemical synthesis, phase transformations, and strain relief. Inherent gamma radiation discrimination, together with extensive shielding around the instrument and remote access, allow users to study highly radioactive samples.

Coincident with developments in neutron scattering instrumentation has been the coming of age of the Rietveld profile refinement technique. Rietveld refinement provides a powerful analytical platform for quantifying such materials properties as crystal structure, phase composition in multicomponent systems, short-range interatomic correlations in crystalline/amorphous mixtures, residual macrostrain, microstrain, grain size distribution, and crystallographic texture.

Determining the structures of complex inorganic oxides, such as zeolites, has long been a strength of neutron powder diffraction. The GPPD's inherently high resolution throughout reciprocal space, coupled with strong scattering from oxygen, has facilitated the solution of many previously unknown topologies. As the capabilities have been refined, ever more complex mixtures of zeolites have been studied. Recent applications on GPPD have included (1) topological transformations among $AlPO_4$ molecular sieves (Richardson, GPPD: #D1991; Richardson et al., 1992a), and (2) zeolite-A and sodalite as immobilization media for low-level radioactive waste (see Trouw and Richardson, pg. 80; Lewis, GPPD: #1490; Richardson et al., 1994a).

Scientific activities that make use of the GPPD remain diverse, as demonstrated by the discussion of highlights that follows.

Residual Stress

Fabrication-induced residual stress can be the factor that limits the performance of manufactured components incorporating composites, and it can be the root cause of failure in welded or bonded structures. The measurement of residual stress in the constituents of composites, therefore, is critical in designing and processing these materials for optimal mechanical properties, reliability, and life expectancy.

Strain is typically measured as a fractional change in bulk lattice spacing corresponding to the average response of polycrystalline aggregates to external stresses. Stress is calculated as the product of measured strain and elastic constants characteristic of the material. Recent experiments have studied (1) in-situ measurement of residual strains in a Ti/SiC composite rotor assembly (Kupperman, GPPD: #D1992), (2) strain relaxation and high-temperature chemical transformation of a WC/Co metal matrix composite (Krawitz, GPPD: #1644; Mari et al., 1996), (3) residual stress and texture in superconductor-silver composites (Kupperman, GPPD: #P1994), and (4) strain anisotropy in Ag-Cu composites (Lawson, GPPD: #2013). The first two of these are described in more detail below to illustrate the current capabilities at IPNS.

On the GPPD, strains in each component of a composite are simultaneously measured in a multitude of directions with respect to the composite geometry, thus providing a measure of anisotropy. A recent experiment measured strains in a compressor rotor assembly from the first man-rated jet engine to incorporate metal-matrix composite rotors (Kupperman, GPPD: #D1992). The rotor assembly was manufactured from silicon-carbide-reinforced titanium metal matrix composites. Strains were calculated from data obtained with the rotor centered in the GPPD, oriented at 45° to the incident beam, and rotating at 1 rpm. Strain anisotropy (Figure 2) relative to the fiber axis was observed.

Typical residual stress experiments on GPPD involve measuring the temperature-dependence of strains to determine the strain-free temperature, an important parameter in models used to predict mechanical behavior at operational temperatures. WC-Co composites, for example, are widely used for cutting tools. WC-11wt% Co exhibits three distinct mechanical property domains, depending on temperature: elastic and brittle from room temperature to 900 K; tough, with limited plasticity, between 900 and 1100 K; and easily deformable above 1100 K. Measurements were made to relate these properties to residual strain (Krawitz, GPPD: #1644; Mari et al., 1996). WC and Co are under compressive and tensile thermal strain, respectively, at room temperature, because of a difference in coefficients of thermal expansion (CTE). Upon heating, WC reaches a minimum in compressive strain at 1000 K, after which compression again increases (see Figure 3). Measurements made during cooling follow a similar curve, but the strain maximum in WC is tensile, with corresponding compression in Co, and is shifted to lower temperatures (i.e., hysteresis is observed). A second heating and cooling cycle showed reproducibility. The unusual increase in compressive strain magnitude in WC upon heating above 1000 K is attributed to W dissolution into Co to form WCo_3. The hysteresis is thought to result from a difference between the heating and cooling kinetics of solution-precipitation of W from WC and WCo_3.

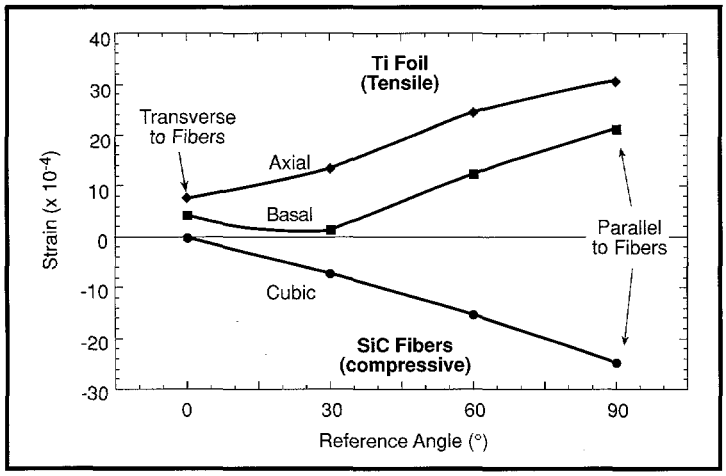

FIGURE 2.
Residual strains in a Ti-SiC metal-matrix composite (MMC) turbine rotor illustrate the GPPD's ability to measure strain anisotropy in a single diffraction experiment. From data obtained with the composite oriented with the continuous SiC fibers 45° to the incident neutron beam, the 2θ = ±148° and ±90° detector banks characterize the residual strain anisotropy between the axial (parallel to the fibers) and transverse (perpendicular) directions. An additional degree of anisotropy is observed between the basal and axial crystallographic directions within the (hexagonal) Ti matrix.

Engineered Materials

In work involving engineered materials, the diffraction experiment must conform to the material's specifications. Catalytic support structures must be studied in their sintered form, metallurgical samples in their quenched state, oxygen sensors and electro-optic materials at operating temperature and oxygen partial pressure, electrochemical cell electrodes in their electrolyte solution and formed into an operational geometry, thermal barrier coatings at optimal thickness, and formed metallic sheets in whatever configuration their applications dictate.

TOF NPD offers simultaneous access to many microstructural parameters, including structure (relative positions and intensities of Bragg peaks), strain state (absolute positions of Bragg peaks), texture/preferred orientation (absolute intensities of peaks), microstrain and grain size (peak breadths), and presence of minority phases. Engineered materials often exhibit strong anisotropy in these parameters, so each scattering direction defines the parameters for its corresponding sample orientation. Because so many important parameters are accessible from a single measurement, this will surely be a growth area for TOF NPD in the future.

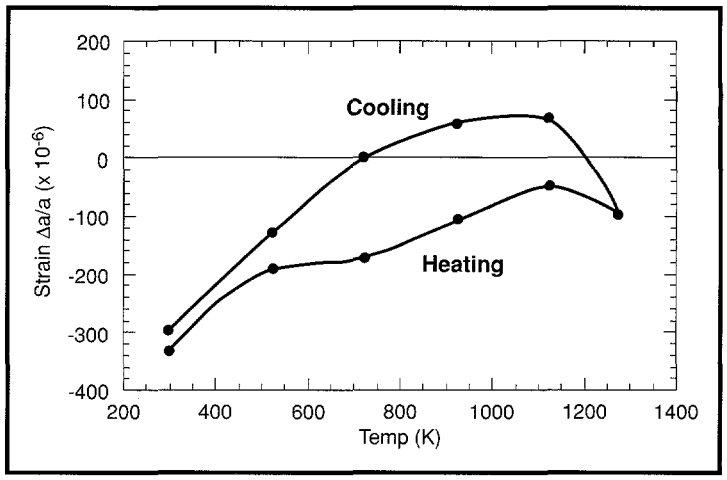

FIGURE 3.
Residual strains in the basal plane of WC in a WC-Co composite are plotted as a function of temperature. Heating the composite relieves the compressive strain in WC, up to 1100 K, where compressive strain is regenerated, presumably due to W dissolving in Co to form WCo_3. Hysteresis upon cooling (WC actually becomes tensile) is thought to be due to differences in the heating and cooling kinetics of solution-precipitation of W from WC and WCo_3.

Recent experiments have included (1) identification of static, oxygen-vacancy-induced atomic displacements in high-surface-area lanthanide-doped zirconia catalytic supports (Ozawa, GPPD: #2068; Loong et al., 1994g, 1995c); (2) phase characterization of Si_3N_4-Al_2O_3 ceramic alloys (Ozawa, GPPD: #1971; Loong et al., 1996a); (3) study of cation mobility in doped $KTiOPO_4$ (KTP) electro-optic harmonic generators at temperatures up to 1100°C (Kaduk, GPPD: #1599); (4) operation of a metal-hydride battery in the GPPD to discover the role of Al substitution in performance enhancement of $LaNi_{5-y}Al_yD_x$ electrodes (Redey, GPPD: #2158); and (5) microstructural characterization of aluminum (MacEwen, GPPD: #P1994).

Neutron Irradiation/Amorphization/Structures of Nuclear Materials

There is a growing emphasis on studies of transuranic materials. This is in some ways an outgrowth of the neutron irradiation effect studies described elsewhere in this volume (see Birtcher, pg. 92); structure characterization on GPPD has been an important part of those studies. Because GPPD detectors have inherent gamma radiation discrimination and are positioned 1.5 meters from the sample position, samples with activity as high as 100 R/h can be dealt with. Remote handling (Figure 4) precludes personnel exposure. Once appropriate precautions have been taken in preparing and encapsulating the hazardous samples (double encapsulation is required) and in documenting isotope compositions and potential hazards, the diffraction experiments provide the same structural detail available for more traditional materials.

Examples include (1) amorphization of U_3Si and U_3Si_2, including simultaneous modeling of crystalline and amorphous components (Birtcher, GPPD: #1494; Birtcher et al., 1995, 1996a) and subsequent recrystallization (Birtcher, GPPD: #2156); (2) identification of an intermetallic reaction product between 80% burned-up U_3Si_2 and Al fuel plates (Hofman, GPPD: #D1994; Hofman et al., 1996); (3) a study of $Pu_{0.6}U_{0.4}$ at high temperature, including determination of the complex (10 atoms in the asymmetric unit) structure of ζ-U/PU (Lawson, GPPD: #1837; Lawson et al., 1996); and (4) identification of corrosion products created upon failure of the first IPNS neutron scattering target, from a 200-mg sample containing small amounts of UO_2, β-UH_3, UO_3, and α-U (Richardson, GPPD: #D1993).

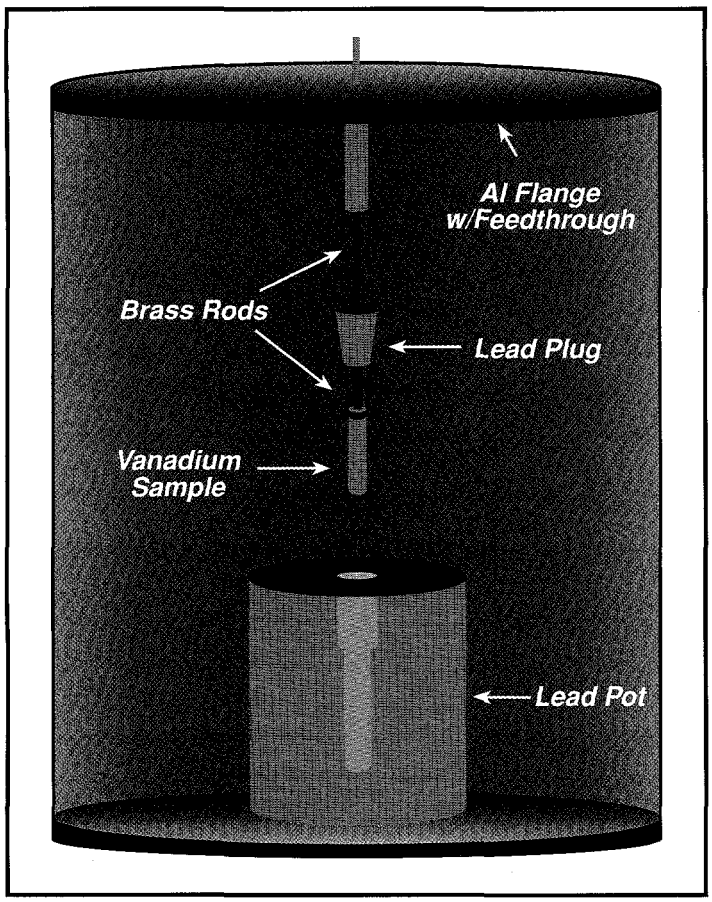

FIGURE 4.
Highly radioactive samples (up to ~100 R/hr at the surface) can be studied on the GPPD using the remote handling apparatus illustrated above. Doubly encapsulated samples are attached to a support assembly, which in turn is sealed in a lead cask for transportation to the GPPD. Once the lead cask is placed in the GPPD and brass rods are attached to the sample assembly, the sample can be raised into scattering position (in the center of the chamber) by pulling the rods up through an aluminum support flange remotely, without exposing personnel to high radiation fields. Using this arrangement, no detector banks are shielded from the sample, and the entire range of available d-spacings can be used.

Neutron diffraction is ideally suited for reactor fuel studies because of the penetrating power of the neutron beam and its enhanced sensitivity to light elements. Fuels are studied without compromising their structural integrity, and fundamental modifications due to irradiation, involving such light elements as hydrogen, oxygen, and sodium, can be recognized. One recent experiment probed the structure of a mixed-oxide $(U_{0.75}Pu_{0.25})O_{2-x}$ reactor fuel and the fuel-sodium-reaction-product (FSRP) that forms on the surface of the fuel, between the fuel and its cladding, as a result of cladding breach in a sodium-cooled liquid metal reactor (Strain, GPPD: #P1992). For this experiment, a pre-irradiation defect was introduced and sodium coolant reacted with the fuel. Metallographic examination indicated

reaction to a depth of about 0.25 mm. A segment was cut from the fuel pin for the neutron diffraction experiment. Contributing to the diffraction pattern were four cubic phases corresponding to the stainless-steel cladding, mixed-oxide fuel, FSRP, and vanadium sample container. Analysis of the data (see Figure 5 for Rietveld profile fit) resulted in (1) successful modeling of the dual (110)/(112) texture in the stainless-steel cladding, (2) assessment of the stoichiometry of the fuel, (3) confirmation of the basic structure of the reaction product, and (4) calculation of volume fractions for each constituent, which were found to be quantitatively in line with previous calculations. These results are being used by fuel designers to better understand fuel behavior during various operating and accident scenarios.

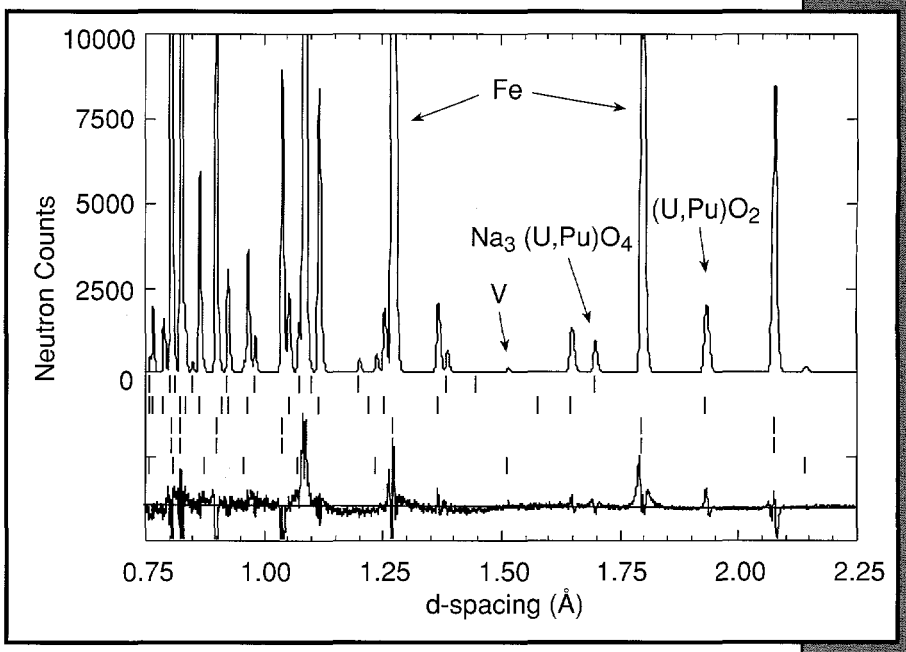

FIGURE 5.
Neutron beams are highly penetrating. One recent experiment on the GPPD identified the reaction product $Na_3(U,Pu)O_4$ in situ, where it was formed between a buried surface of $(U,Pu)O_2$ reactor fuel and Na coolant that had passed through a breach in stainless-steel cladding. Shown in the Rietveld profile plot above are the observed diffraction data after background subtraction; calculated data from a crystalline model including five phases, steel in two different texture representations, $(U,Pu)O_2$ fuel, $Na_3(U,Pu)O_4$, and vanadium (from the capsules); and the difference plot. Also shown are vertical bars representing the positions of Bragg peaks for the respective phases.

III

Science on the Special Environment Powder Diffractometer

J. D. Jorgensen and S. Short, Materials Science Division, Argonne National Laboratory

Introduction and Background

The Special Environment Powder Diffractometer (SEPD) has continued to operate, with no down times due to instrument problems exceeding one or two hours, for the last five years. In the late 1980s and early 1990s, the study of high-T_c oxide superconductors dominated SEPD use, but as interest in high-T_c materials has begun to subside, the scientific program on the SEPD has become more diverse. Major topics being studied by in-house and user scientists include new battery electrode and solid electrolyte materials, "bucky balls" intercalated with various gases, giant magnetoresistive materials, and ferroelectric materials. The SEPD has been unexpectedly popular for pair-distribution-function (PDF) studies of a variety of materials, even though it was not originally designed for that purpose. The somewhat higher resolution of the SEPD, compared with GLAD, has made it the instrument of choice for a number of studies involving noncrystalline materials, as well as crystalline materials for which PDF techniques have been used to probe local structural features that are not manifest in the average crystal structure.

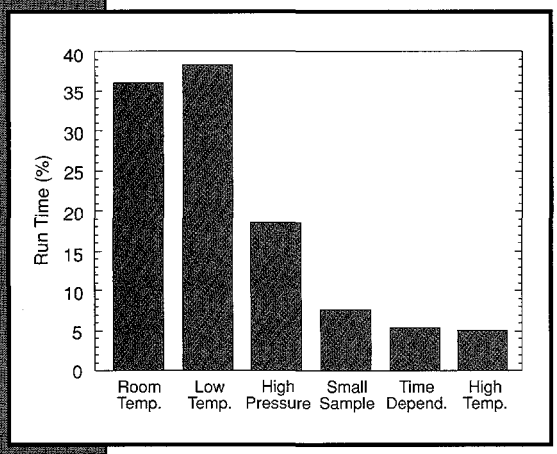

FIGURE 1.
Distribution of various kinds of experiments run on SEPD during the five-year period 1991-1995. The percentages add to more than 100% because some experiments involved more than one special technique (for example, high pressure and low temperature). Small samples are those under 200 mg.

The major emphasis on the SEPD continues to be the use of special sample environments. Figure 1 shows the distribution of experimental time over the last five years. Of the total running time, 36% is spent on data collection at room temperature under ambient conditions. The average data collection time for such experiments is about two hours. The use of a computer-controlled sample changer, which will cycle up to ten samples into the beam, has been critical to the overall efficiency in running these samples. Typically, the sample changer is loaded once daily. Because of the fast turnaround for room-temperature data collection, we have recently initiated a new mode of user access for such experiments (room temperature; no special sample handling problems; data collection less than one day). After calling the instrument scientist to learn the current backlog, users can mail their samples for data collection. Data are

collected as time becomes available, and the user is informed of where to access the data on the IPNS computers.

The remaining time on the SEPD (64%) has been devoted to data collection in some form of special environment, such as low temperature, high temperature, or high pressure. The percentages for each of these techniques (Figure 1) add to more than 100% because two or more of these techniques often are combined – as, for example, in a high-temperature experiment where a time-dependent chemical reaction process is studied. Time spent doing low-temperature experiments has actually exceeded that spent at room temperature. Essentially all of the low-temperature experiments are done using a computer-controlled, closed-cycle helium refrigerator (Displex). Because of manpower limitations, cryostats are not yet in routine use on the SEPD. We hope to remedy this situation in the near future as support levels are increased with new funding from the Scientific Facilities Initiative. Because low-temperature experiments are so routine, they are not discussed further here, but the other special environment capabilities available on the SEPD are discussed in detail below.

High-Pressure Experiments

Experiments at high pressure account for a growing amount of time on the SEPD – almost 20% of the running time averaged over the last five years. Two pressure cells are available: a helium-gas pressure cell capable of pressures to about 0.6 GPa and a piston-in-cylinder, supported-aluminum-oxide cell that can reach about 3 GPa. The latter pressure cell is an upgraded version of a cell first used by Bob Brugger and Tom Worlton at the MTR reactor in Idaho in the late 1960s and later at the CP-5 reactor at Argonne-East. In the last five years, this cell has seen very little use. It is labor-intensive to use, and data collection is rather slow – typically 24 hours or more for one run. During the same five-year period, requests for experiments in the helium-gas pressure cell have grown steadily.

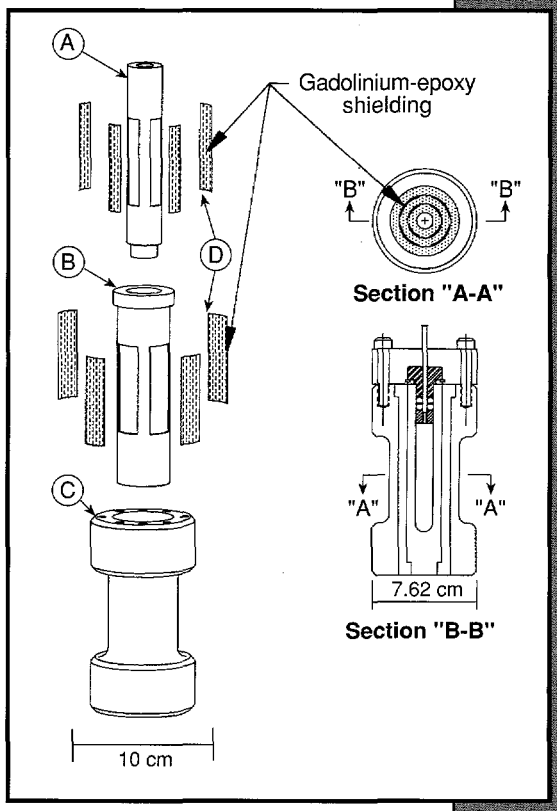

FIGURE 2.
Exploded view of the helium-gas pressure cell used on SEPD. The cell is constructed from three concentric cylinders of 7075-T6 alloy aluminum. Windows for the incident, transmitted, and scattered neutron beams are formed by collimating with internal gadolinium-epoxy shielding.

The helium-gas pressure cell, built ca. 1986, is patterned after earlier designs by Bill Daniels, except that it is optimized for time-of-flight diffraction, where only a single scattering angle is needed (Jorgensen et al., 1990a). The cell design is shown in Figure 2. The use of three concentric aluminum alloy cylinders allows gadolinium-epoxy shielding to be placed "inside" the cell – close to the sample, where it is most effective.

This accomplishes two things: (1) nearly the full sample can be viewed at a 90° (±5°) scattering angle, with no Bragg peaks from the aluminum; and (2) the internal shielding minimizes multiple-scattering background that would otherwise result from the rather large volume of aluminum surrounding the sample. Another advantage is that the pressure is perfectly hydrostatic and can be changed and measured from an external pumping station without removing the cell from the SEPD. This maintains the full precision of the instrument throughout a series of pressures and temperatures that may constitute a high-pressure experiment (Takahashi et al., 1992a). Cooled by the Displex, the cell can reach about 20 K, although the low-temperature limit for most experiments is determined by the freezing point of helium.

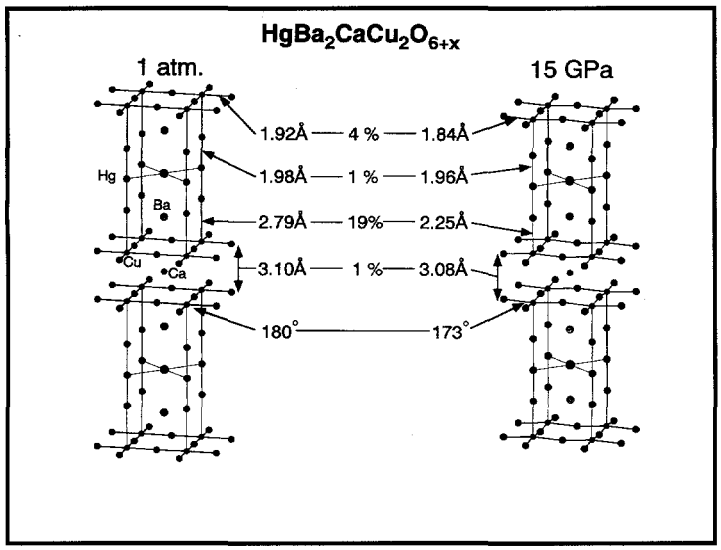

FIGURE 3.
Structure of the $HgBa_2CaCu_2O_{6+x}$ high-T_c superconductor at 1 atm and 15 GPa (based on extra-polation from data at 0.6 GPa). Individual atom-atom distances respond very differently to the applied pressure, leading to changes in the structure that cause a 25-K increase in T_c.

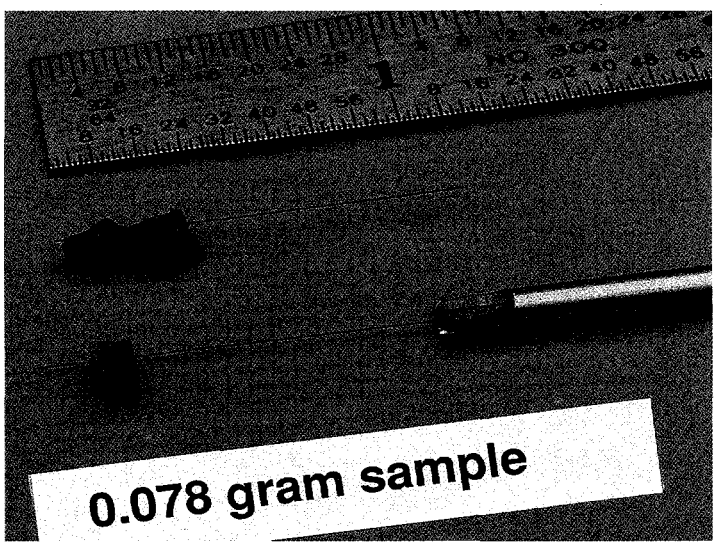

FIGURE 4.
Example of a small sample glued to an amorphous-boron-coated tungsten fiber for study in the SEPD.

Early experiments with the helium-gas cell included studies of KNO_3-IV (Worlton et al., 1986), NDF_4-II (Lawson et al., 1989), Li (Smith et al., 1990), and Na (Smith et al., 1991). After the high-T_c oxide superconductors were discovered and it was realized that pressure had rather dramatic effects on the superconducting properties, which could provide important insights into the underlying physics, a number of high-pressure neutron diffraction experiments were performed on these materials.* Much of this work was done in collaboration with

* *At least nine different high-T_c materials have been studied with respect to pressure. Most of the work can be found by referring to Kamiyama et al. (1994) and Shaked et al. (1994a) and the references cited therein.*

Dr. Fujio Izumi (National Institute for Research in Inorganic Materials, Tsukuba, Japan) and other collaborators. Perhaps the most informative experiment was one done on Hg-Ba-Ca-Cu-O compounds. Discovered in 1993, these materials still hold the record-high T_c, 135 K for Hg-1223, and exhibit the remarkable property that T_c can be increased by another 25 K with the application of high pressure. There was great interest in learning the structure of the material under high pressure, where T_c was ~160 K. Measurements done on the SEPD showed how the structure was modified by the application of pressure (Hunter et al., 1994) and enabled band-structure calculations that explained how this modification changed the electronic structure to produce the high-T_c behavior (Novikov et al., 1994). The structures of $HgBa_2CaCu_2O_8$ at 1 atm and 15 GPa (extrapolated on the basis of data taken at 0.6 GPa) are shown in Figure 3.

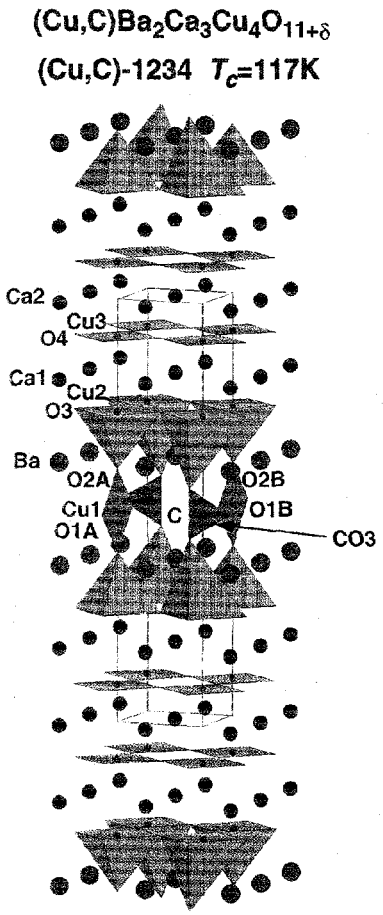

FIGURE 5.
Crystal structure of $(Cu,C)Ba_2Ca_3Cu_4O_{11+x}$ refined by using data from a 190-mg sample mounted as shown in Figure 4.

Small Samples

During the last three years, we have developed techniques for obtaining high-quality data from small samples on the SEPD. Interest in doing this was motivated by the discovery of many new high-T_c superconductors by means of high-pressure synthesis techniques (up to 10 GPa, using multiple-anvil presses).** The samples made in this way are small, typically 50-200 mg, because of the limited volume in the high-pressure synthesis apparatus. The very low intrinsic background on the SEPD makes it possible to study such small samples if ways can be found to minimize the background that would normally be contributed by a sample can.

We have developed two methods for the study of small samples. If the sample is in the form of a small pellet or chunk, we glue it with a minimum amount of five-minute epoxy to a tiny amorphous-boron-coated tungsten fiber and hang the sample in the beam. Figure 4 shows a typical sample glued onto one of these fibers. The boron-coated fiber contributes no background whatever, and the size of sample that can be studied in this way depends mostly on how long one is willing to collect data. Using this technique, we have taken data of quality sufficient for meaningful Rietveld refinement from samples as small as 17 mg (which required a 45-hour data collection) (Shaked et al., 1995). Other small samples studied by this technique have ranged in size from 40 to 190 mg (Jorgensen et al., 1993b; Shimakawa et al., 1994c; Shaked et al., 1994a; Shimakawa et al., 1994a; Argyriou et al., 1995). In one case, we studied an 82-mg sample in the helium-gas pressure cell by suspending it in the center of the cell on

** *See, for example, Radaelli and Jorgensen (1993a) and references cited therein.*

a boron-coated fiber (Shaked et al., 1994a). The most complex structure refined from a small sample (in this case, 190 mg) was that of $(Cu,C)Ba_2Ca_3Cu_4O_{11+x}$, which was the first four-layer copper-oxide superconductor to be synthesized in single-phase form (Shimakawa et al., 1994a). The structure of this compound is shown in Figure 5.

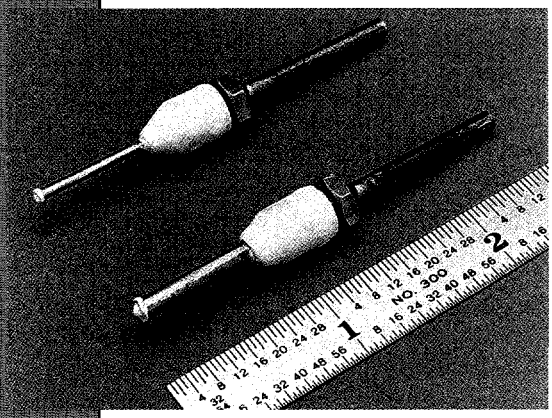

FIGURE 6.
Vanadium microcans designed for data collection from small samples.

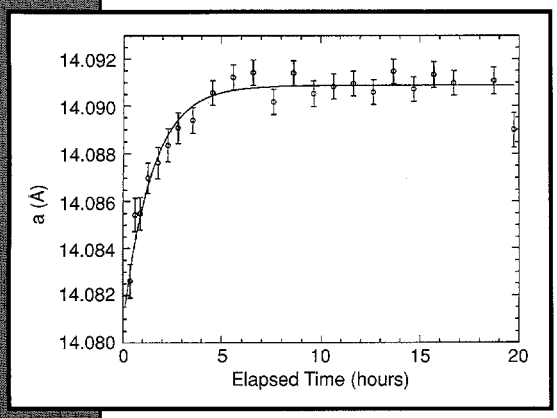

FIGURE 7.
Variation of the lattice parameter, a, of C_{60} as Ne enters the lattice, following a sudden change in Ne pressure from 0 to 30,000 psi at room temperature.

When the sample is in the form of a powder, rather than a pellet or chunk, the technique shown in Figure 4 cannot be used. For such cases, we have developed two sizes of microcans, shown in Figure 6. These cans are made by thinning a sheet of vanadium foil to about 0.004 mm, using acid etching techniques, and rolling the foil to form a tube. The bottom end of the tube is sealed with gadolinium epoxy. The top end, where there is a fixture that allows filling the can and mounting the sample, is also shielded with gadolinium epoxy. These cans provide background levels almost as low as the boron-coated-fiber method. To date, only a few experiments have been done using the microcans. These are available for user experiments, but because they are very delicate, IPNS staff prefer to do the sample loading themselves.

Time-Dependent Experiments

The initial interest in time-dependent experiments on the SEPD was for the study of *in-situ* reaction chemistry, such as the reaction processes involved in the formation of $Ba_{1-x}K_xBiO_3$ (Pei et al., 1991) or the Bi-Ca-Sr-Cu-O superconductor that is the material of choice for wire applications (Garbauskas et al., 1990 and 1991). In the latter work, done in collaboration with Mary Garbauskas and Ronald Arendt from General Electric Corporate Research and Development, important information leading to improved melt-processing synthesis techniques was obtained. About the same time, Jorgensen et al. (1990b) studied time-dependent room-temperature ordering processes in $YBa_2Cu_3O_{6+x}$. These experiments showed for the first time that short-range oxygen diffusion and ordering processes that occur on the time scale of minutes to hours at room temperature in $YBa_2Cu_3O_{6+x}$ manifest themselves as changes in the average crystal structure and can have a surprising effect on the superconducting properties (Jorgensen, 1991). The shortest time window used in these experiments was 15 min. With the use of a large sample (~15 g), these data-collection times allowed Rietveld refinements with enough precision to see the time-dependent changes of individual bond lengths. Later, the area of the back-scattering detector banks on the SEPD was doubled to increase the

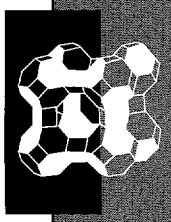

counting rate. In more recent time-dependent experiments, five-minute data-collection times have been used for experiments in which full Rietveld refinements are desired; if only lattice parameters are required, the data-collection time can be considerably shorter.

Also more recently, time-dependent experiments have been done to investigate the intercalation kinetics of various gases into C_{60} ("bucky balls"). Gas atoms that are small enough, such as He and Ne, penetrate the C_{60} structure and occupy sites between the C_{60} balls (Schirber et al., 1995). These experiments are done in the gas pressure cell, using various gases (e.g., He, Ne, or Ar) as the pressure medium. The rate of intercalation of He into C_{60} is too fast to measure, but Ne atoms, being larger, intercalate more slowly. The intercalation kinetics is studied by making a sudden change in pressure (for example, suddenly increasing the Ne pressure from 0 to 30,000 psi) and monitoring the lattice parameter of the C_{60} as the gas intercalates. A typical Ne loading curve is shown in Figure 7. At 30,000 psi, the Ne content in the C_{60} saturates after about five hours. The intercalated Ne exerts an "internal pressure" that counteracts part of the external Ne pressure, resulting in a lower measured compressibility than for C_{60} pressurized in a gas that does not intercalate, such as Ar. The pressure dependence of the intercalation rate is rather unusual: higher external gas pressure results in slower intercalation, not faster. This surprising behavior is being investigated further.

Summary

In this progress report, we reviewed some of the experimental capabilities recently developed for use on the SEPD. In each case, these new capabilities were initially developed to satisfy particular scientific interests, but they clearly have much broader utility. Our hope is that SEPD users will become more aware of these capabilities and make more use of them in their proposed experiments.

References

D.N. Argyriou, J.D. Jorgensen, R.L. Hitterman, Z. Hiroi, N. Kobayashi, and M. Takano, Phys. Rev. B **51** (1995), 8434 .

M.G. Garbauskas, R.H. Arendt, J.D. Jorgensen, and R.L. Hitterman, Mat. Res. Soc. Symp. Proc., Vol. 169 (1990), 129; Appl. Phys. Lett. **58** (1991), 2987.

J.D. Jorgensen, S. Pei, P. Lightfoot, D.G. Hinks, B.W. Veal, B. Dabrowski, A.P. Paulikas, and R. Kleb, Physica C **171** (1990a), 93.

J.D. Jorgensen, S. Pei, P. Lightfoot, H. Shi, A.P. Paulikas, and B.W. Veal, Physica C **167** (1990b), 571.

J.D. Jorgensen, Nature **349** (1991), 565.

A.C. Lawson, R.B. Roof, J.D. Jorgensen, B. Morosin, and J.E. Schirber, Acta Cryst. B **45** (1989), 212.

D.L. Novikov, O.N. Myrasov, and A.J. Freeman, Physica C **222** (1994), 38.

H.G. Smith, B. Berliner, J.D. Jorgensen, M. Nielsen, and J. Trivisonno, Phys. Rev. B **41** (1990), 1231.

H.G. Smith, B. Berliner, J.D. Jorgensen, and J. Trivisonno, Phys. Rev. B **43** (1991), 4524.

T.G. Worlton, D.L. Decker, J.D. Jorgensen, and R. Kleb, Physica B **136** (1986), 503.

III Single-Crystal Diffractometer

A. J. Schultz, IPNS Division, Argonne National Laboratory

The single-crystal diffractometer (SCD) at IPNS has been highly reliable over the past five years, allowing a variety of experiments to be performed successfully. This time-of-flight (TOF) Laue SCD employs a 30 cm x 30 cm position-sensitive area detector that enables a solid volume of reciprocal space to be sampled for each sample setting. This feature allows researchers to easily characterize satellite and superlattice peaks while also measuring the fundamental Bragg reflections. The SCD is also used to conduct texture analyses of polycrystalline samples. In addition to various software upgrades, a major improvement for the SCD was the design and fabrication of a new vacuum container. The walls of the new container are 7.6 cm from the sample, rather than 1.3 cm as in the past. Furthermore, a turbomolecular vacuum pump has been mounted in the χ circle, eliminating a rubber vacuum hose that had been positioned between the sample container and a diffusion pump. These improvements, which provide better heat shielding and better vacuum, enable lower temperatures to be achieved over extended periods of time. Another improvement was to the detector electronics, which were upgraded with the addition of a computer-controllable, multichannel high-voltage power supply for the 49 photomultiplier tubes. Some highlights of recent experiments are described below.

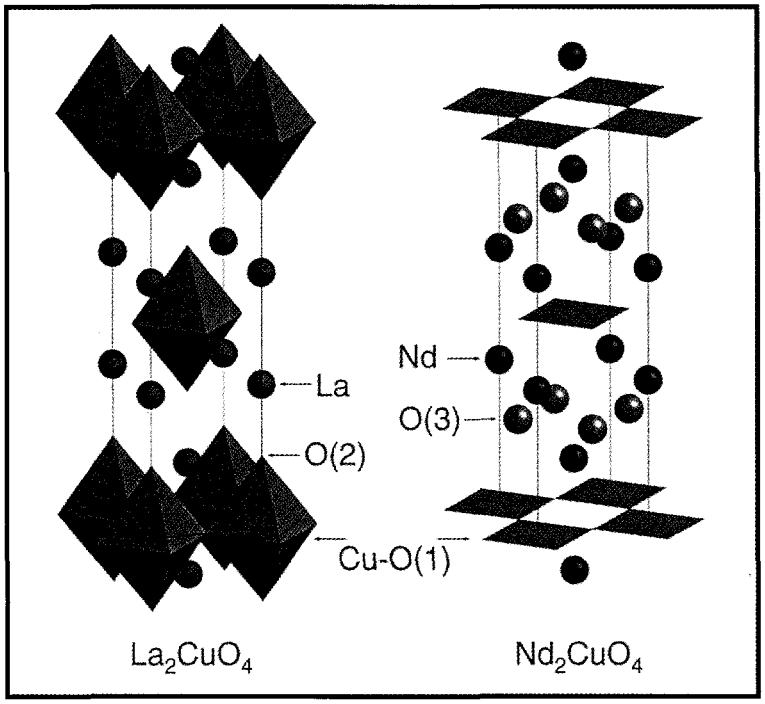

FIGURE 1.
Idealized structures of La_2CuO_4 and Nd_2CuO_4 (For consistency, O(1) refers to oxygen atoms in the CuO_2 plane; O(2), to the apical oxygen atoms. O(3) sites are sandwiched between the La or Nd planes.)

High-T_c Superconductors

Oxygen-rich $La_2CuO_{4+\delta}$ is a superconductor with T_c = 40 K for $\delta \approx 0.1$. The SCD was used to study a crystal prepared by room-temperature electrochemical oxidation

of La_2CuO_4 (Radaelli et al., 1993b). It was shown to be single-phase with *Fmmm* symmetry. The absence of any evidence of a (*Bmab*) phase, which is the stoichiometric nonsuperconducting compound La_2CuO_4, indicated that the sample has a composition beyond the phase-separated region of the phase diagram for this material. An analysis of the fundamental Bragg peaks revealed that the excess oxygen is located between adjacent La-O(2) layers at the interstitial O(3) sites (Figure 1). The introduction of interstitial oxygen atoms also led to a splitting of the apical oxygen site, O(2), into four positions to avoid unfavorable O(2)-O(3) contacts. In addition, satellites arising from a modulation of the defect structure were clearly identified in the single-crystal data, as shown in Figure 2, for the l = 5.67 reciprocal lattice plane. The reciprocal lattice defined by the satellites appeared to be commensurate with the original one; all observed reflections could be indexed by using an *F*-centered 10*a* x 10*b* x 6*c* supercell. However, because of twinning, the observed satellite pattern could have resulted from the superposition of more than one set of superlattice reflections, each with a smaller supercell.

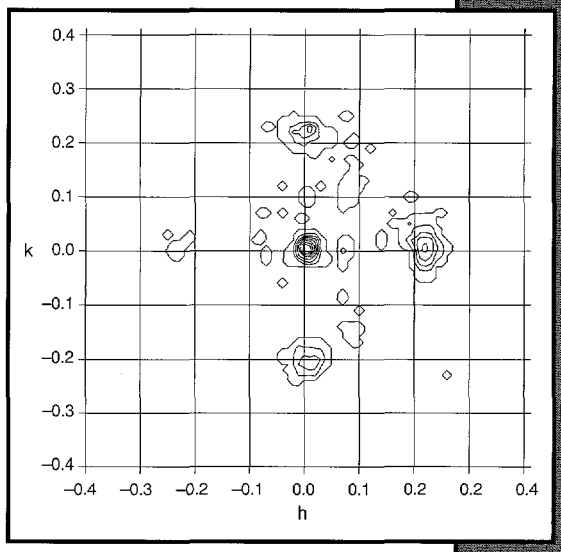

FIGURE 2.
Intensity contour plot of reciprocal space derived from SCD data for the l = 5.67 plane of $La_2CuO_{4.1}$ at 18 K (Satellites with propagation vectors of (±0.1, ±0.1, -0.167) (not shown), (0, ±0.2, -0.333), and (±0.2, 0, -0.333) appear around the tail of the [0,0,6] Bragg reflection.)

$Nd_{2-x}Ce_xCuO_y$ ($y \approx 4$) is one of the few known examples of electron-doped cuprate superconductors. It is superconducting only within a narrow range of Ce doping ($x \approx 0.15$-0.20) and only after it has been annealed in a reducing atmosphere. The *T'* structure of $Nd_{2-x}Ce_xCuO_y$ consists of infinite square planar CuO_2 layers with oxygen atoms sandwiched between the Nd/Ce layers (the "interstitial" sites in the $La_2CuO_{4+\delta}$ structure described above) rather than between the apical Cu sites as in the *T* structure of La_2CuO_4 (Figure 1). The IPNS single-crystal time-of-flight diffractometer was used to measure data on oxygenated and reduced samples of Nd_2CuO_y (Radaelli et al., 1994) and $Nd_{2-x}Ce_xCuO_y$ (Schultz et al., 1996). For Nd_2CuO_y, structural refinements indicated that the occupancy of the apical oxygen, O(2), is ~0.10 for the oxygenated sample and ~0.04 for the reduced one. The occupancies of the in-plane oxygens, O(1), do not vary. The results from the data analysis of reduced (T_c = 24 K) and oxygenated $Nd_{1.85}Ce_{0.15}CuO_y$ were less conclusive, as expected from the small changes obtained with TGA measurements. However, evidence for changes similar to those observed in the undoped crystals was obtained from difference Fourier maps in the region of the O(2) site.

A Pressure-Switchable Jahn-Teller Distortion

The Jahn-Teller theorem has proven extremely useful in interpreting many aspects of the behavior of a range of transition-metal compounds. Particular interest has been shown in the isomorphous series of Tutton salts of the general formula $A_2[M(H_2O)_6](SO_4)_2$, where A is an alkali metal ion or ammonium and M is a divalent transition metal ion. For the case where M

is copper and the cation A is ammonium, $(NH_4)_2[Cu(H_2O)_6](SO_4)_2$, a rhombic distortion occurs around the copper atoms, oriented 90° from the distortion occurring in the salts in which A is an alkali metal. In the perdeuterated salt, $(ND_4)_2[Cu(D_2O)_6](SO_4)_2$, there is an isotope-induced Jahn-Teller distortion switch such that the distortion becomes identical to that in the alkali metal salts. The first example of a pressure-induced Jahn-Teller distortion switch was unexpectedly observed (Simmons et al., 1993) using the SCD equipped with a helium pressure apparatus which mounts on the closed-cycle helium refrigerator. As shown in Figure 3, application of 1.5 kbar of pressure switched the long axis of the Jahn-Teller distortion by 90° in the deuterated ammonium copper Tutton's salt, $(ND_4)_2[Cu(D_2O)_6](SO_4)_2$. The Cu-O(7) bond length changed from 2.022(2) to 2.290(2) Å, and the Cu-O(8) bond length changed from 2.310(2) to 2.014(2) Å. Thus, the high-pressure phase of the deuterated salt is isostructural with the hydrogenous salt, but not with the alkali metal salts. The switching of the long axis of the Jahn-Teller distortion is also associated with a rotation of the ND_4^+ cation, with concomitant changes in the hydrogen bonding of the coordinated water molecules with the SO_4^{2-} anions. The resulting adiabatic potential energy surfaces were calculated by using tetragonal and orthorhombic strain parameters estimated from the temperature variation of the Cu-O bond lengths. Results showed that the two forms differed by only ≈250 cm^{-1} (30 meV). The key parameter deciding the relative stability of the two forms is apparently the nonequivalence of the lattice strain acting along the Cu-O(7) and Cu-O(8) bond directions. A quite small lattice strain, sufficient to cause bond length differences of ~0.02 Å in the absence of Jahn-Teller coupling, is greatly amplified by this effect, resulting in the large distortions. The change in structure of $(ND_4)_2[Cu(D_2O)_6](SO_4)_2$ at 1.5 kbar may be explained if the nonequivalence of the lattice strain changes sign at high pressure, becoming similar to that of the hydrogenous complex.

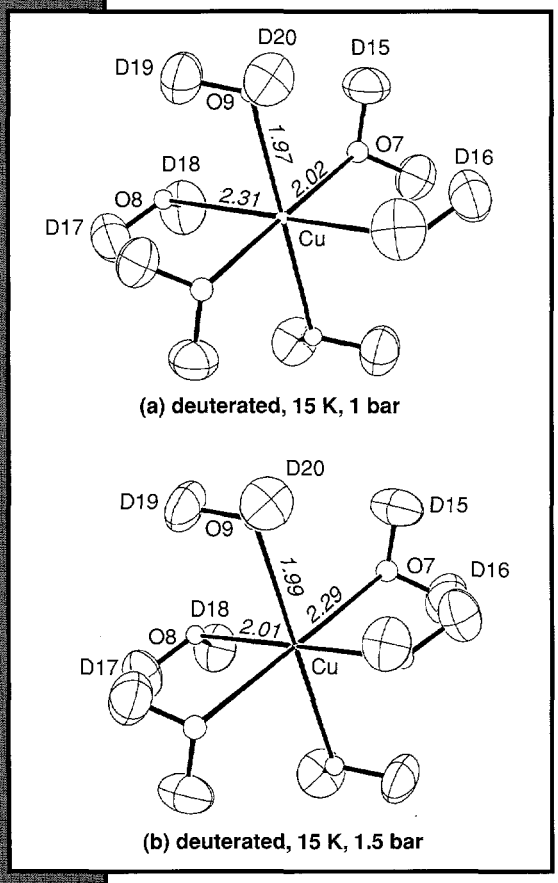

FIGURE 3.
Coordination sphere around the copper atoms in $(ND_4)_2[Cu(D_2O)_6](SO_4)_2$ at (a) T = 15 K, P = 1 bar and (b) T = 15 K, P = 1.5 kbar. (Note the switch in the Cu-O(7) and Cu-O(8) bond lengths between a and b.)

Metal-Metal Exchange in a Heterometallic Hydride Complex

Heterometallic hydride complexes have been studied extensively, partly because of their potential utility in catalytic reactions. A neutron study unexpectedly provided evidence that $HMn_2Re(CO)_{14}$ (compound **1**, below left) co-crystallizes with $HMnRe_2(CO)_{14}$ (compound **2**, below right) (Bullock et al., 1992). In the initial analysis of the structure of compound **1**, shown in Figure 4, the displacement parameters for both the Re and Mn(2) sites were physically unreasonable unless their scattering lengths were also refined. For the Re site, the value of b_{Re} = 9.54(6) fm was consistent with a value of 9.55(6) fm

derived from data obtained at Brookhaven National Laboratory's HFBR reactor on an unrelated compound. These results imply that the literature value for b_{Re} of 9.2(2) fm is underestimated. For the Mn(2) site, the refined value of ^{b}Mn(2) suggests partial occupancy of this site by rhenium (9.2%). This result led to a further investigation of the Mn/Re exchange equilibrium in this system. A mechanism has been proposed to account for the metal-metal exchange reaction that transforms compound **1** and $HRe(CO)_5$ into compound **2** and $HMn(CO)_5$, as shown below:

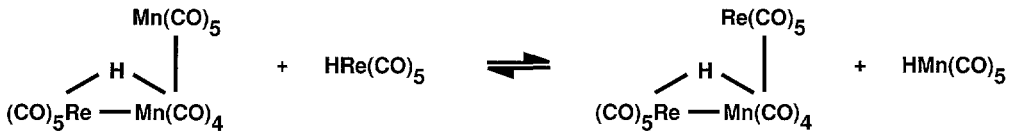

1 **2**

The equilibrium constant derived from ^{1}H NMR experiments indicates that the Re-Mn bond is stronger than the Mn-Mn bond by about the same amount as the difference in the bond dissociation enthalpy of $H\text{-}Re(CO)_5$ vs. $H\text{-}Mn(CO)_5$.

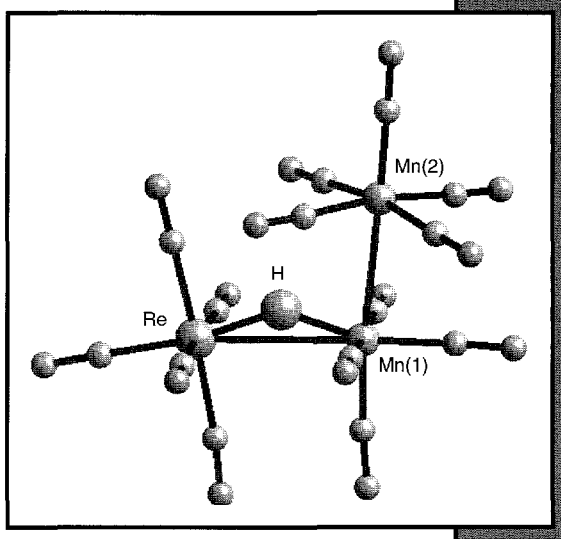

FIGURE 4.
Structure of $(CO)_5Re(\mu\text{-}H)\text{-}Mn(CO)_4Mn(CO)_5$ at 15 K.

III

Small-Angle Neutron Scattering

P. Thiyagarajan, IPNS Division, Argonne National Laboratory

Introduction

Small-angle neutron scattering (SANS) is a general-purpose technique for probing the structure and interaction of systems ranging from 10 to 1,000 Å in size, a region that is not easily accessible by other methods. SANS is especially useful for studying systems under realistic conditions (e.g., behavior of proteins and their complexes in solution, detergent solutions in bulk and in porous media, phase separation in metallic alloys, polymer blends, colloidal dispersion under temperature, pressure, and shear, etc.). The technique is applicable to a wide range of fields, including structural biology, metallurgy, ceramics, polymer physics, colloidal science, disordered composites, and porous materials.

The small-angle diffractometer (SAD) at IPNS, a time-of-flight-SANS (TOF-SANS) instrument, has been successfully serving the scientific community in the United States and abroad over the past 10 years. In general, TOF-SANS instruments at pulsed neutron sources provide data over a wide dynamic range in the scattering vector q [$q = 4\pi\sin(\theta/\lambda)$, where θ is half the scattering angle and λ is the wavelength of the probing neutrons], yielding structural information in a wide range of length scales. To obtain data over such a wide q region, reactor-based SANS instruments require repetition of measurements at several instrument configurations. Such reconfigurations have different instrumental smearing effects on the data; hence, the data measured at different settings may not overlap. The data from the TOF-SANS instruments, on the other hand, do not suffer from such overlap problems, because the data over the whole q region are produced in a single measurement.

SAD uses pulsed neutrons with wavelengths in the range of 0.5 to 14 Å and a fixed sample-to-detector distance of 1.54 meters. The scattered neutrons are measured by using a 64 x 64 array of position-sensitive, gas-filled 20 cm x 20 cm proportional counters, while the wavelengths are measured (time-of-flight) by binning each pulse to 67 constant $\Delta\lambda/\lambda = 0.05$ time channels. This instrument can provide useful SANS data in the q range of 0.005 to 0.35 $Å^{-1}$ in a single measurement. SAD is considered successful for several reasons: (1) it provides data for which the quality and absolute calibration are comparable with those at established reactor-based SANS instruments; (2) a number of ancillary equipment items (see Table 1) – such as a sample changer, furnaces, a temperature-controlling bath, a temperature-controlling electric heater, magnet, displex, pressure cells that can vary the temperature and pressure, a stretching device for elastic polymers, and a sample rotator (for samples that may slowly settle over time) – are available to create a wide range of sample conditions; (3) the automation of sample changer, furnaces, displex, temperature-controlling electric heater, and transmission monitor through computerized data acquisition makes the experiments easier and more efficient; (4) easy access to several data analysis software packages for the users, even

ANCILLARY EQUIPMENT AT SAD		
EQUIPMENT	ENVIRONMENT	EXPERIMENTAL CONDITIONS
SAMPLE CHANGER seven positions, with circulating bath	*Air*	*0-75°C*
BIOLOGICAL WELL with circulating bath with resistance heater with pressure cell with rotator with sample stretcher for polymer with displex	*Air* *Air* *High-pressure liquid* *Air* *Air* *High vacuum*	*-10 to 100°C* *20-200°C* *1-2,500 bar, 0-80° C* *20°C* *20°C* *20-300 K*
METALLURGICAL CONFIGURATION with electromagnet with electromagnet and furnace with electromagnet and displex with furnace in ceramic tube	*Vacuum* *Air* *He purge gas* *High vacuum* *He purge gas*	*20°C* *10 kilogauss @ 1in.,* *5 kilogauss @ 2 in.* *20-750°C* *20-300 K* *100-1,700°C*

TABLE 1. Ancillary Equipment at SAD

after they return to their home institutions, enables them to conveniently analyze their data; and (5) the technical help provided by the IPNS support staff helps users efficiently adapt the samples and equipment on the instrument. SAD has made a significant contribution to the scientific community from academic institutions and industry, from the United States and from abroad, providing quality SANS data on both static and dynamic systems (*in-situ* measurements). This instrument has been consistently oversubscribed for several years, with proposals exceeding operating time by a factor of two to three. The number and the quality of the proposals have steadily increased over the years, requiring increased run times at our facility. In order to meet the beam time requirements of the community, a second, more sophisticated instrument is being developed. The new instrument (see Instrumentation and Computing Developments at IPNS, pg. 98) will be capable of accessing a larger dynamic range in q, as well as providing higher-resolution data than the present SAD. The near completion of the new instrument and the recent increase in funding for the IPNS as part of the Scientific Facilities Initiative (see Future Plans, Enhanced Operation, pg.140) are timely. We hope to provide adequate beam time for the best proposals and also accommodate more proposals in the coming years.

During the past five years, SAD has been used to study a number of systems in a wide range of fields. Details of all the experiments can be found in the experimental reports. The following examples illustrate the nature of the science that can be done by using SAD: detergent behavior relevant to membrane protein crystallization, solution structure of membrane

proteins in different detergents, *in-plane* SANS to determine the interaction mechanism of amphiphathic peptides with membranes, *in-situ* SANS on the phase separation of paraffins in bulk and on a surface, and decomposition in a new family of metallic glasses.

Solution Structures of Supramolecular Assemblies

SANS enables the resolution of the solution structure of molecular assemblies that (1) cannot be readily accessed by crystallography, such as inherently disordered assemblies like micelles or vesicles; or (2) contain multiple-protein-component complexes that cannot be easily crystallized. Scattering measurements on solution samples yield direct correlations between structural features of supramolecular assemblies and their spectroscopically determined functions. Parameters that can be resolved by SANS include the size, shape, polydispersity, molecular weight, volume, and internal packing for multiple-component protein complexes. This information can be used to discriminate among possible molecular models for supramolecular structures.

Detergent Phenomena Related to Membrane Protein Crystallization

An understanding of membrane protein crystallization is of central importance to structural biology. To be solubilized in aqueous media, integral membrane proteins require detergent solutions. However, the presence of detergent greatly complicates the phase map for protein crystallization, because both detergent and protein solubilities are altered by chemical additives, such as polyethylene glycol (PEG), salts, and small amphiphiles, used for crystallization. So far, success in membrane protein crystallization has been achieved with two detergents, lauryl-dimethylamine-N-oxide (LDAO) and n-octyl b-D-glucoside (OG), which were used to crystallize the photosynthetic reaction center (RC). However, the physical processes underlying the micelle-micelle and micelle-protein interactions in the presence of other chemical additives have not been well documented.

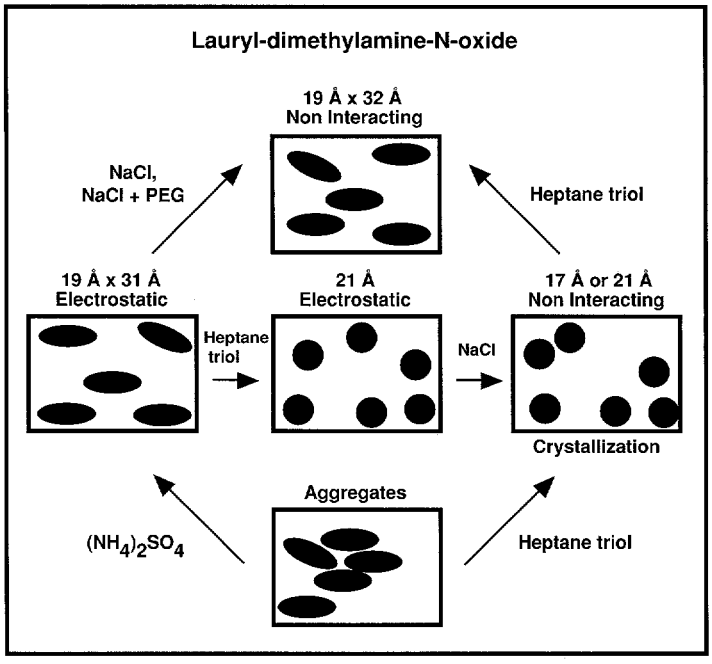

FIGURE 1.
Schematic of LDAO micelle structure and intermicelle interaction under solution conditions relevant to membrane protein crystallization.

As a first step toward gaining a better knowledge of the physical principles involved in membrane protein crystallization, Thiyagarajan and Tiede (Argonne National Laboratory)

have used SANS to compare LDAO and OG micelle size and micelle-micelle interactions under the different sets of chemical conditions used for RC crystallization (Thiyagarajan and Tiede, 1994). They systematically examined the effects of sodium chloride, ammonium sulfate, PEG, and heptane triol, when added alone and in combination for RC crystallization, on the behavior of LDAO and OG solutions. The main results from this study are schematically shown in Figures 1 and 2, respectively, for LDAO and OG behavior. A key difference between LDAO and OG was that the change in micelle size induced by the addition of heptane triol was larger for OG than for LDAO under the conditions used for crystallization. This effect may have implications for the differences in chemical conditions that are observed when these two detergents are used for RC crystallization.

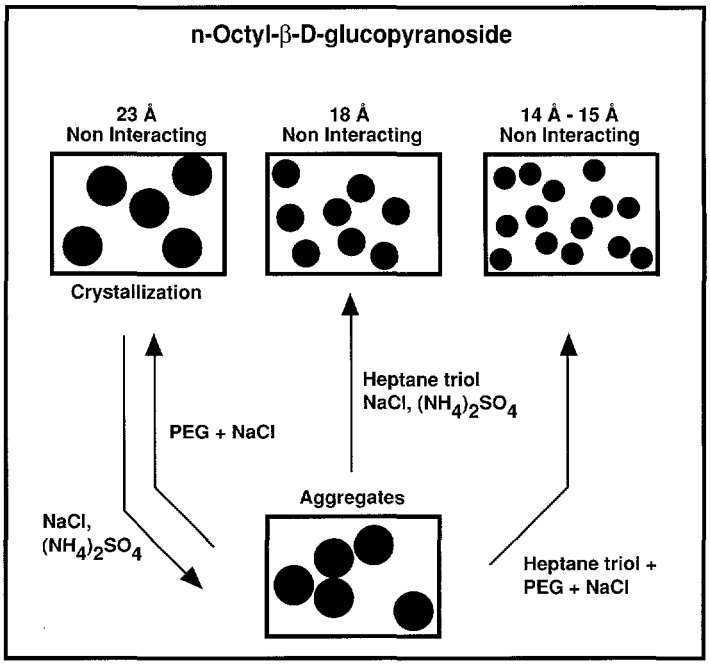

FIGURE 2.
Schematic of OG micelle structure and intermicelle interaction under solution conditions relevant to membrane protein crystallization.

Structure of Reaction Center in Detergent Solutions

SANS has been used to characterize the effect of ionic strength and detergents on RC aggregation and the solution structure of supramolecular assemblies in photosynthesis. Studies on the behavior of RC under conditions relevant for its crystallization were done. To enhance the differential scattering cross section for proteins in detergent solutions, deuterated RCs (D-RCs) from *Rb. sphaeroides* R-26 cells were grown on a medium enriched to >98% with ^2H (Wraight, 1979). RCs were solubilized in either 0.06% LDAO or 0.8% OG solutions. The D_2O/H_2O ratios were adjusted by dialysis at 5% and 17%, respectively, for LDAO and OG samples. Under these deuterated conditions, the scattering length densities of the solvent and the respective micelles became equal (contrast matched); hence, the scattering from the micelles became insignificant. The measured SANS signals from the proteins in the detergent solutions were solely from the proteins. The measured SANS data for the D-RC in a 0.06% LDAO solution containing 5% D_2O were compared with the calculated profile from the crystal coordinates (Figure 3). The agreement between the experimental and calculated profiles indicates that the structure of the RC is similar in both the crystalline and solution states. This agreement indicates that the aggregation states of RC in solutions under different temperatures, as well as upon addition of PEG, ethylene glycol, heptane triol, and salts could be modeled effectively by using the crystal coordinates of RC. Systematic studies have been conducted

on RC solutions under a number of relevant conditions; the data were modeled by using the crystal coordinates of RC (Tiede and Thiyagarajan, 1996a; Tiede et al., 1996b). The main conclusion from these studies is that the behavior of RC in solution is strongly dependent on the detergent type and ionic strength. RC does not seem to aggregate in the case of LDAO solution, even when the ionic strength is up to 2M NaCl. On the other hand, it aggregates in OG solution at higher ionic strengths, possibly as a result of the aggregation of OG micelles at high ionic strength, leading to a depletion of micelles required for the solubilization of RC. In solutions containing OG and PEG4000, RC aggregation was observed at PEG concentrations far lower than those required for RC precipitation and crystallization. It is expected that the observed equilibrium between the monomeric and aggregated RC states would be shifted toward the aggregate as crystallization mixtures progressively decreased the solubility of RC, either by increasing the ionic strength with a fixed PEG concentration or by simultaneously increasing both PEG and salt concentrations. The existence of this equilibrium may have direct implications for the mechanism of RC crystallization, because protein monomers may serve as intermediates in crystallization.

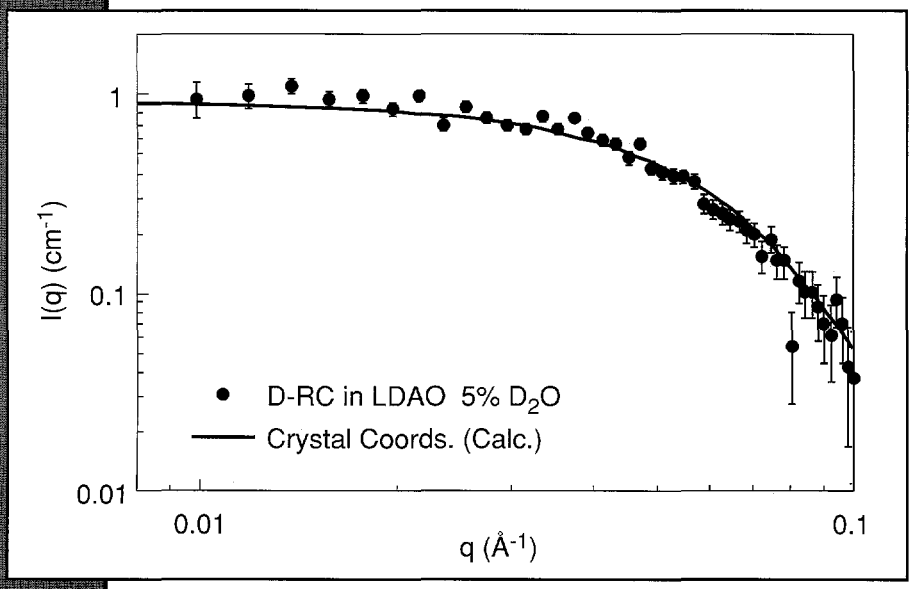

FIGURE 3.
Comparison of measured SANS data and that calculated from crystal coordinates for per-deuterated-RC in LDAO in 5% D_2O buffer.

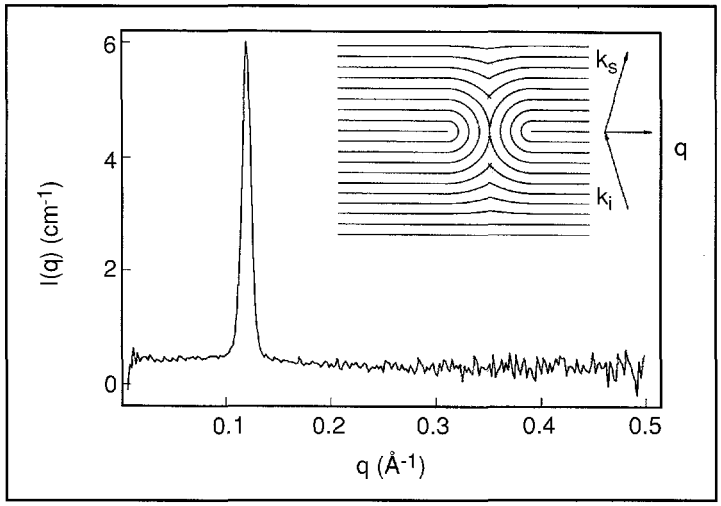

FIGURE 4.
Neutron in-plane scattering of pure DLPC bilayers hydrated with D_2O. The peak at q ~ 0.12 Å^{-1} corresponds to a defect shown in the inset. Perfectly aligned bilayers will not exhibit such lamellar peaks.

Antimicrobial Peptide Pores in Membranes by In-Plane SANS

A new class of antimicrobial agents has been discovered in the host defense systems

of animals in the past 15 years (Hultmark et al., 1980; Zasloff, 1987; Boman et al. (eds.), 1994). Unlike conventional antibiotics, these antimicrobials, which are in the form of small peptides, have been shown to act directly on the lipid bilayer of the cellular membrane. The mechanism by which the antimicrobial action is elicited is not well understood, because there is no technique sufficiently sensitive to visualize the structures formed by these peptides in membranes. Spectroscopic methods, such as solid-state NMR and oriented circular dichroism, detect only the orientation of the individual peptides in a membrane, leaving the high-order structures of the peptides unresolved. Recently, Huang and co-workers from Rice University (He et al., 1996) have shown that an *in-plane* neutron scattering technique used on oriented membranes is effective in delineating the structural details of the antimicrobial peptides in membranes.

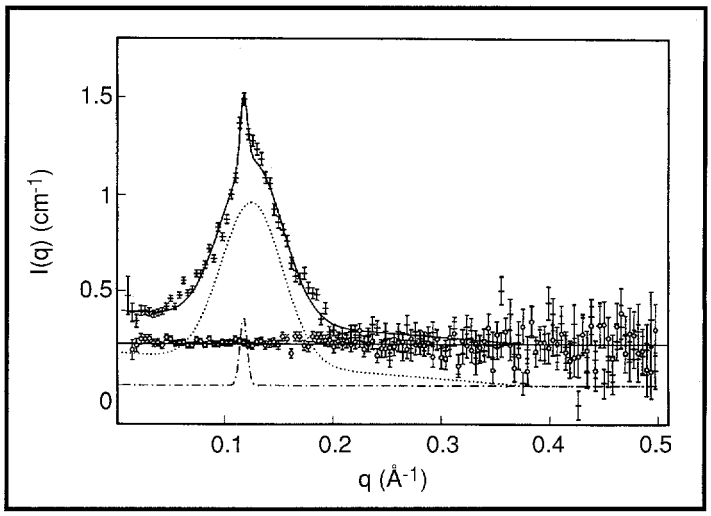

FIGURE 5.
Neutron in-plane scattering of alamethicin inserted in DLPC layers hydrated with D_2O (+). Exposure to H_2O vapor for 20 hours made the peak disappear (o), implying that the peak is indeed associated with the channels filled by D_2O. The data (+) have been modeled to indicate a lamellar peak ($q \sim 0.12$ Å^{-1}) due to smectic defects (dash-dot line), scattering from alamethicin pores (dotted line), and the incoherent background (solid line).

He et al. used the lipids 1,2-dilauroyl-sn-glycero-3-phosphatidylcholine (DLPC) and 1,2-diphytanoyl-sn-glycero-3-phosphatidylcholine and the peptide alamethicin in their study. The lipid and peptide at a desired molar ratio were co-dissolved in chloroform/methanol. The solvent was removed by a slow nitrogen purge and dried under vacuum. D_2O was added to the peptide-lipid film. The mixture was homogenized with a sonicator to break up the large aggregates and then lyophilized, and the powder was hydrated with D_2O vapor. The lipid without peptide was prepared in a similar way, as a control sample. The fully hydrated liquid crystalline peptide/lipid mixtures were aligned between clean quartz plates (thickness = 0.25 mm). The peptide orientation was monitored by oriented circular dichroism. Six thin layers of a D_2O-hydrated sample were held between seven parallel plates for SANS measurements. A polarized microscope was used to examine the condition of each layer for smectic defects. These defects in multilayer samples produce strong lamellar peaks in the *in-plane* scattering data (Figure 4); such defects should be absent, or at least minimal, for good *in-plane* scattering measurements.

The *in-plane* neutron scattering data for alamethicin inserted in DLPC bilayers and hydrated with D_2O are shown in Figure 5 (+). To establish that the peak in the scattering pattern was caused by the presence of D_2O, the experimenters exposed the same sample to H_2O vapor for

20 hours and measured the SANS data. As expected, the peak disappeared after the sample was exposed to H_2O (o), because of the lack of contrast between the DLPC bilayers and H_2O. Quantitative modeling was carried out on the SANS data (Figure 5) for alamethicin inserted into DLPC bilayers and hydrated with D_2O (+). The scattering data were decomposed into (a) an incoherent background due to the DLPC and alamethicin (solid line); (b) a lamellar peak (dashed-dotted line) due to smectic defects, obtained by a gaussian fit to the peak at 0.12 $Å^{-1}$ (thickness = 52.3 Å); and (c) the scattering from alamethicin pores (dotted line).

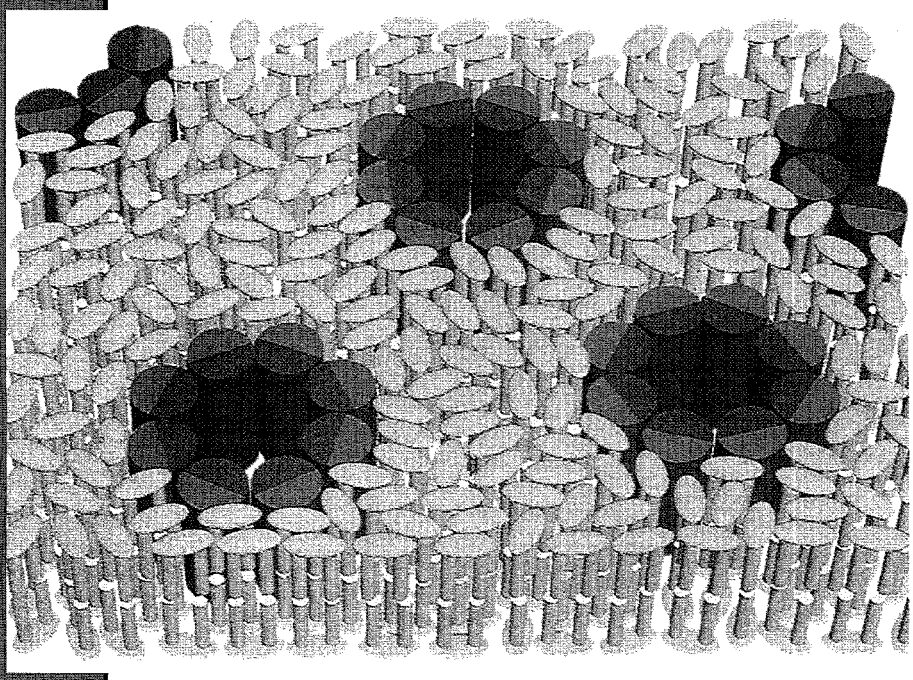

FIGURE 6.
Schematic of pores created by alamethicin in DLPC layers. Each pore consists of 8 alamethicin monomers. Each peptide has a cylindrical shape, with a diameter of 11 Å. The inner diameter of the pore is 18 Å, and the outer diameter is about 40 Å. The surface density of the pores is such that the alamethicin:lipid ratio is about 1:10.

These experiments took advantage of SAD's wide dynamic range in dealing with samples that are delicate, expensive, and hard to prepare; use of SAD also eliminated the possibility of exposure of these samples to atmospheric water vapor (which could affect the stability of the samples, especially if repetitive experiments were required to measure the data in a wide q region, as might be the case with reactor-based SANS instruments). These studies demonstrate that the antimicrobial peptides enter the membrane when its concentration exceeds a critical value dependent on the chemical nature of the lipids (Figure 6). The peptides then form aqueous pores that are more than 18 Å in diameter. The density of the pores was consistent with all these peptides being involved in pore formation; moreover, no pores were seen below the critical concentration of these peptides. These studies prove that the molecular mechanism of the antimicrobial action is through concentration-dependent pore formation in the cell membranes of the microbes.

Microphase Separation of Binary Paraffin Mixtures

Certain binary mixtures of n-alkanes, when quenched from the melt to room temperature, undergo spontaneous demixing from the solid solution. Mazee (1958) was the first to report

the phenomenon of demixing in alkanes for a mixture of $C_{30}H_{62}$:$C_{35}H_{72}$. Using X-ray diffraction, he observed that after about one year the mixture produced a pattern that indicated an ordering of the molecules in the direction of the paraffin chains. When the chain length difference was increased, Dorset (1986) and Snyder et al. (1993), using DSC, electron diffraction, and infrared and Raman spectroscopy, found that demixing took place in $C_{30}H_{62}$:$C_{36}H_{74}$ over a period of hours. They suggested that the mechanism by which the microphase was formed might be an intermediate between a vacancy and reptation model, with the paraffin chains moving primarily in the longitudinal direction and slipping along their long axes to "separate" into lamellar components (Snyder et al., 1992).

This phenomenon is superficially similar to such processes in metals, but it includes an additional, interesting effect associated with the anisotropy of the intermolecular potential due to the rod-like molecular shape of the paraffin. The use of SANS, with isotopic labeling of one of the components in the mixture, readily allows the study of the structure, kinetics of formation (Gilbert et al., unpublished), and isotopic dependence (White et al., 1990) of the resultant microphases. The microphase separation of binary mixtures of $C_{30}H_{62}$:$C_{36}D_{74}$ and $C_{30}D_{62}$:$C_{36}H_{74}$ in the bulk, as well as that adsorbed

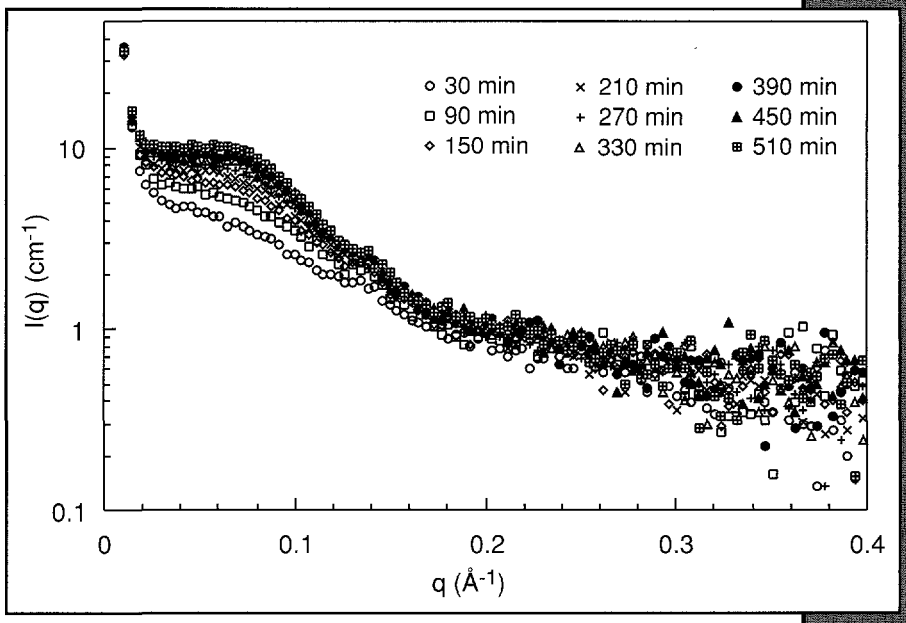

FIGURE 7.
In-situ SANS studies of phase separation of bulk 1:1 $C_{30}H_{62}$: $C_{36}D_{74}$ after quench at 20°C.

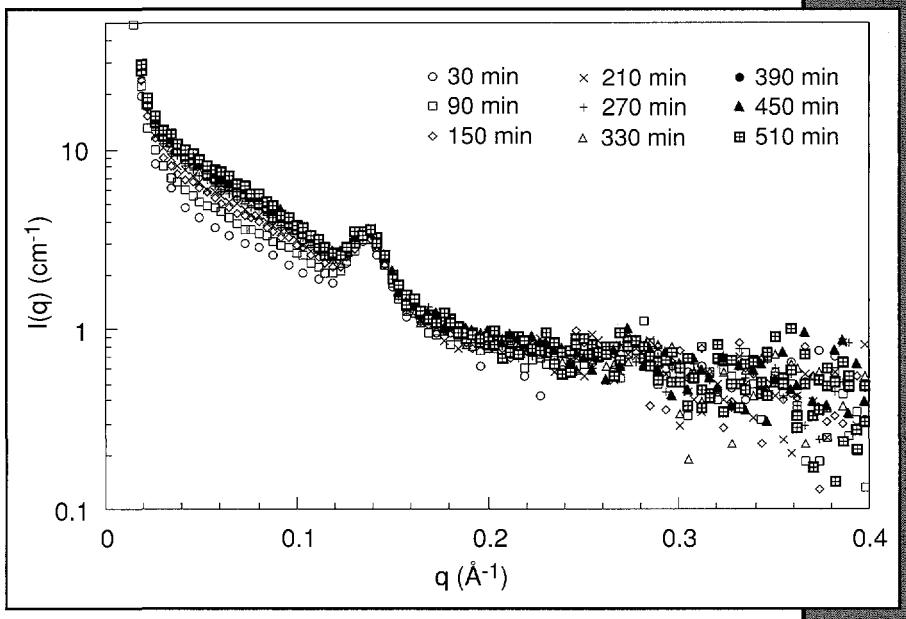

FIGURE 8.
In-situ SANS studies of phase separation of bulk 1:1 $C_{30}D_{62}$: $C_{36}H_{74}$ after quench at 20°C.

into the pores of exfoliated graphite, were studied by White et al. (Australian National University, Canberra) and Snyder et al. (University of California, Berkeley).

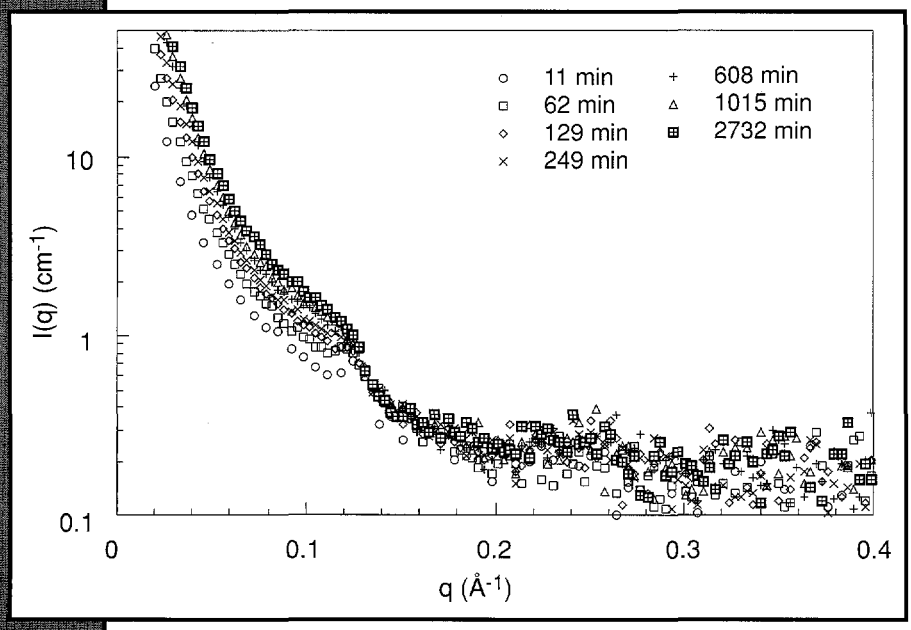

FIGURE 9.
In-situ SANS studies of phase separation of 1:4 $C_{30}H_{62}$:$C_{36}D_{74}$ on graphite after quench at 27°C.

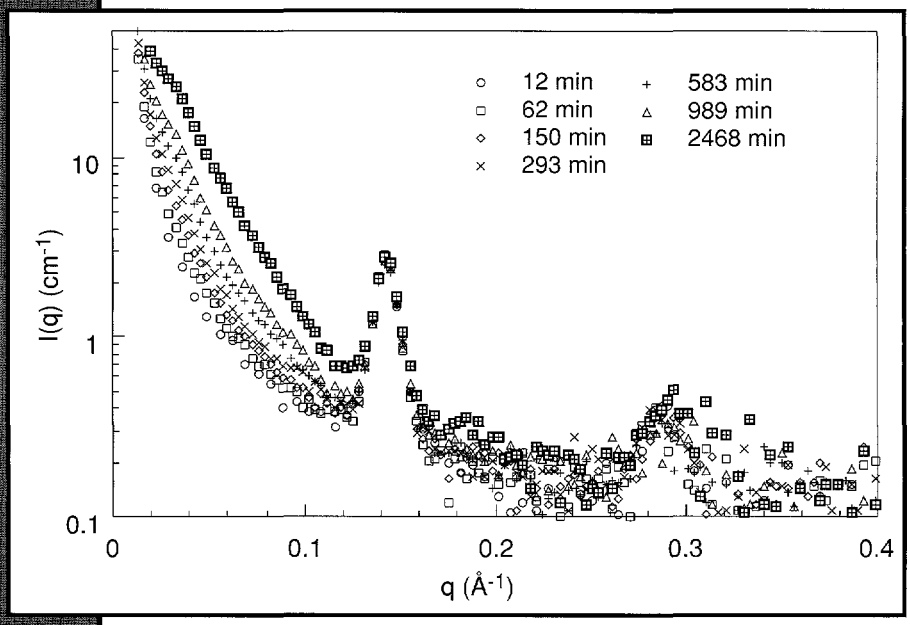

FIGURE 10.
In-situ SANS studies of phase separation of 4:1 $C_{30}D_{62}$:$C_{36}H_{74}$ on graphite after quench at 27°C.

Microphase Separation in the Bulk

The time-resolved SANS for an equimolar mixture of pure $C_{30}H_{62}$:$C_{36}D_{74}$ quenched from the liquid state (80°C) to 20°C showed the evolution of a diffuse peak in the mid-q region, at q = 0.078 Å^{-1} (Figure 7). This peak corresponds to a d-spacing of 81 Å and is associated with microphase formation (White et al., 1990). As the intensity increases with time, there is a progressive reduction in peak width, indicating a longer coherence length. The isotopic dependence of this phenomenon has been demonstrated for the equivalent 1:1 $C_{30}D_{62}$:$C_{36}H_{74}$ system (Figure 8). After 510 min of annealing, the system had only a rather poorly defined peak corresponding to a d-spacing of 81 Å, with significantly less intensity (White et al., unpublished). However, the peak corresponding to a repeat distance of *ca.* 45 Å was more pronounced in the case of the 1:1 $C_{30}D_{62}$:$C_{36}H_{74}$ system (Figure 8) than that for the 1:1 $C_{30}D_{62}$:$C_{36}H_{74}$ system (Figure 7), indicating that there is an isotopic effect in the microphase separation in these systems. In fact, extensive *in-situ* experiments carried out on these

paraffins at several annealing temperatures and molar compositions indicated the occurrence of the peak corresponding to the 45 Å repeat distance.

Microphase Separation at the Graphite Interface

In the past, there has been considerable interest in the influence of graphite on hydrocarbons. Early thermodynamic work showed that *n*-alkanes had a high affinity for the surface of graphite and that this affinity increased with carbon number (Groszek, 1970). Later work showed that when an alkane was introduced to the surface of graphite above its fusion temperature, prefreezing took place at the surface with the occurrence of molecular ordering (Ash and Findenegg, 1970). This order extended over several molecular layers, propagating away from the surface, with the degree of orientational correlation decreasing steadily (Kern et al., 1977). Scanning tunneling microscopy showed that the *n*-alkane molecules formed lamellar structures, which tended to order themselves in an all-*trans* conformation, with the long-axis of the alkane chain aligned parallel to the graphite basal plane (Gilbert et al., 1994). In the present system, two competing processes may be at work: longitudinal phase separation parallel to the graphite surface and demixing lateral to the surface because of the effect of the graphite surface forces. These processes significantly affect the kinetics of the microphase separation of these systems.

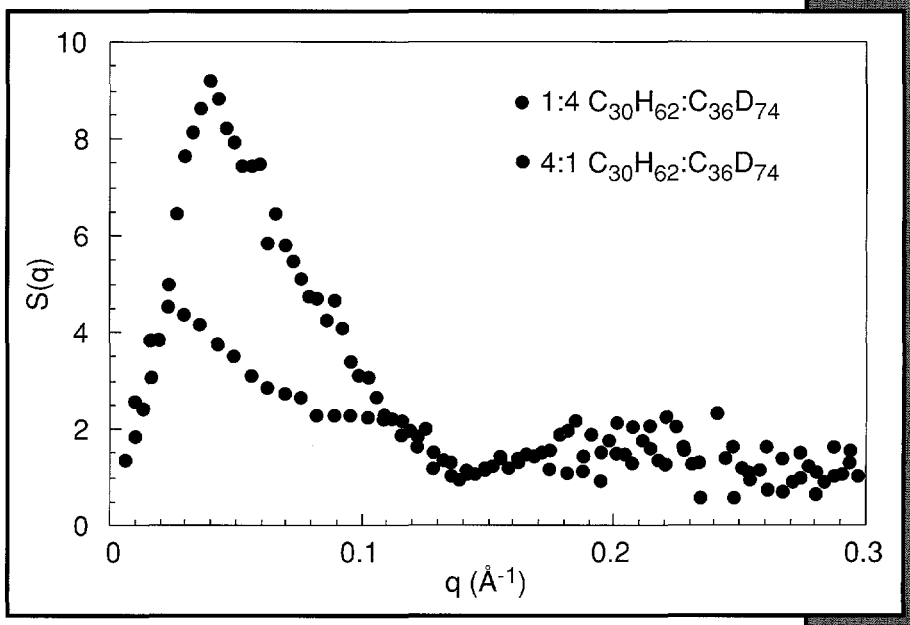

FIGURE 11.
Isotopic effect of phase separation and order in n-alkanes adsorbed on graphite.

Figure 9 displays the time-resolved SANS data for a 1:4 mixture of $C_{30}H_{62}$:$C_{36}D_{74}$ doped into the porous graphite substrate and quenched at 27°C. *In-situ* measurements were taken at intervals, and the initial stages of phase separation were studied for several hours. The major features observed were a diffuse peak at 0.12 Å^{-1} (d = 52.3 Å) and a progressive increase in scattering in the region q < 0.1 Å^{-1} with annealing time. The sample annealed for 15 min showed high intensity in the low-q region because of the graphite/alkane interface, due to the large contrast between the alkane mixture in the larger cavities of the graphite and the graphite substrate.

When isotopic substitution was employed in the binary alkane system, resulting in a 4:1 mixture of $C_{30}D_{62}$:$C_{36}H_{74}$ doped into graphite, significantly different features were observed in the scattering (Figure 10). Three peaks evolved at q = 0.04 Å^{-1}, 0.14 Å^{-1}, and 0.28 Å^{-1}. The first diffuse peak (clearly seen in Figure 11) resulted from the microphase separation, while the latter two were the first- and second-order peaks corresponding to a repeat distance of about 45 Å. This feature occurred for $C_{30}D_{62}$:$C_{36}H_{74}$ at all quenching temperatures and in all molar compositions studied, with no observable change in position with time. The peaks of these mixed solid solutions resulted from a (002) repeat in the orthorhombic form, as shown by Craig et al. (1994) by means of synchrotron x-ray powder diffraction.

To demonstrate that the scattering in the low-q region in Figures 9 and 10 did indeed result from microphase separation, the SANS data for a 1:4 mixture of $C_{30}H_{62}$:$C_{36}D_{74}$ at different annealing times were divided by the data for the 15-min annealing, and the ratios [(S(q)] were determined over the whole q region. A number of such arrays of S(q) vs. q data were also generated for the 4:1 mixture of $C_{30}H_{62}$:$C_{36}D_{74}$ for different annealing times. The signature for the occurrence of phase separation in these systems is a peak in the S(q) data, where the peak's position in q should be constant, but its height should continuously increase with annealing time. Indeed, such peaks were observed in the S(q) data for both systems. Figure 11 depicts the S(q) vs. q curves for both systems, annealed for about 2,500 min at 27°C. The repeat distance for the 1:4 mixture of $C_{30}D_{62}$:$C_{36}H_{74}$ was 230 Å, and that for the 4:1 mixture of $C_{30}D_{62}$:$C_{36}H_{74}$ was 157 Å. The differences in the repeat distance and molecular order between these systems resulted from the isotopic effect.

Shortly after quenching, in all the samples studied, the systems showed a relatively disordered structure with a broad distribution of repeat spacing, which developed over time into a more ordered lamellar structure. A comparison of the scattering patterns produced for both isotopic pairs in the presence and absence of papyex showed that the graphite substrate suppressed the substantial isotopic difference that had been evident in the bulk system. A comparison of the increase in the rate of intensity in the bulk and graphite-adsorbed alkane systems indicated that the kinetics of the demixing was faster in the presence of graphite. This result may be related to the significant surface-stabilization imposed by the graphite, which was effective not only at the surface but also some distance into the pore.

Phase Separation in Bulk Metallic Glasses

More than 30 years ago, Klement, Willens, and Duwez (1960) showed that metallic glasses can be formed by the rapid solidification of liquid metals at cooling rates of about 10^6 K/s. For many years, the application of rapid quenching techniques was the only way to obtain metallic glasses. The thickness of such quenched samples was restricted to less than 50 mm, and their low thermal stability did not allow extended heat treatment procedures.

More recently, a new family of multicomponent metallic alloys with excellent glass-forming ability and a wide supercooled-liquid region has been found (Inoue et al., 1989; Zhang et al., 1991; Peker and Johnson, 1993a). Some of these amorphous alloys can be prepared at cooling rates of less than 100 K/s, and even as low as 1 K/s (Peker and Johnson, 1993b). For the first time, this excellent glass-forming ability permits three-dimensional specimens of amorphous metals to be prepared. Their high thermal stability offers a unique opportunity to investigate

thermodynamic and atomic transport properties in both the solid and the supercooled liquid states. The thermal stability of the amorphous phase, however, is limited by crystallization. To study thermal stability, a detailed knowledge of the crystallization process is required. Analytical field ion microscopy of the slowly cooled, bulk, amorphous $Zr_{41.2}Ti_{13.8}Cu_{12.5}Ni_{10.0}Be_{22.5}$ samples shows inhomogeneities of the Zr and Be concentrations on a scale of about 500 Å. Scanning Auger electron spectroscopy measurements of the surfaces of as-prepared, freshly broken glassy samples also reveal fluctuations of the Be composition on a comparable scale. These results indicate that chemical decomposition processes take place in the $Zr_{41.2}Ti_{13.8}Cu_{12.5}Ni_{10.0}Be_{22.5}$ alloy. Such decomposition behavior was proposed for conventional metallic glasses, but it could not be proved systematically because of limitations in thermal stability, sample size, and a large surface-to-bulk ratio (Lamparter and Steeb, 1986). Differential scanning calorimetry and TEM investigations also showed that the primary crystallization of $Zr_{41.2}Ti_{13.8}Cu_{12.5}Ni_{10.0}Be_{22.5}$ is caused by a Ti-rich nanocrystalline phase (Schneider, unpublished). The formation of nanocrystals inside the amorphous matrix causes an embrittlement of the alloy. For the sake of technical applications of this alloy, as well as fundamental research on it, it is important to determine if the primary crystallization is triggered by the decomposition of the amorphous phase.

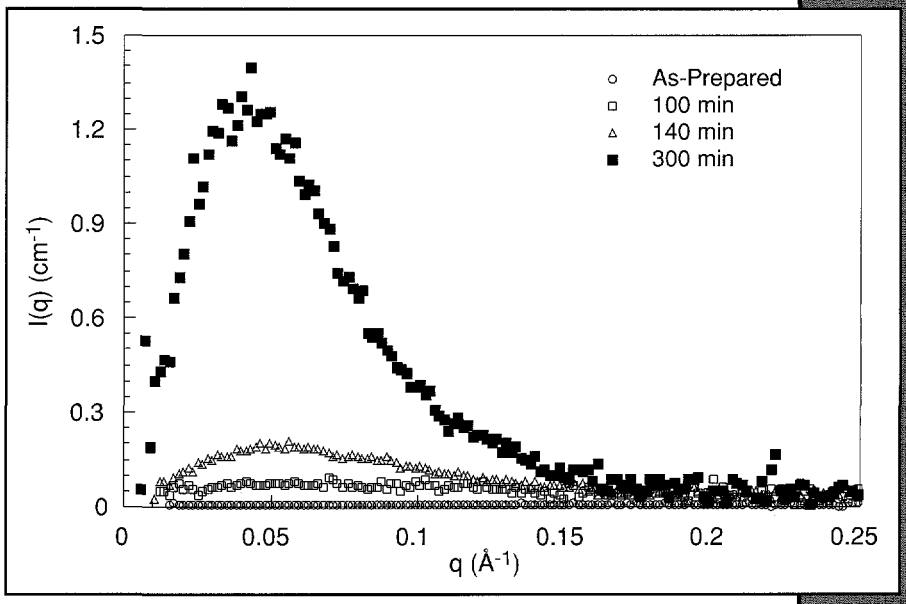

FIGURE 12.
Phase separation in amorphous $Zr_{41.2}Ti_{13.8}Cu_{12.5}Ni_{10}Be_{22.5}$ alloys annealed at 623 K.

To investigate the chemical decomposition in $Zr_{41.2}Ti_{13.8}Cu_{12.5}Ni_{10.0}Be_{22.5}$ alloy at a finer length scale, researchers at the California Institute of Technology have conducted systematic SANS experiments on a series of samples annealed at different temperatures and for different times by using SAD (Schneider et al., 1996a; Schneider et al., 1996b). Homogeneous samples were made from a mixture of the pure elements by means of induction-melting on a water-cooled silver "boat" under a Ti-gettered atmosphere. Ingots of $Zr_{41.2}Ti_{13.8}Cu_{12.5}Ni_{10.0}Be_{22.5}$ were remelted in a silica tube with an inner diameter of 14 mm and then water-quenched at a cooling rate of 10 K/s. For the SANS measurements, disks with a thickness of about 2.7 mm were cut from the rod. These disks were annealed near the glass transition temperature at 623 K for different lengths of time.

The scattering data of an as-prepared $Zr_{41.2}Ti_{13.8}Cu_{12.5}Ni_{10.0}Be_{22.5}$ sample and of samples heat-treated for three different times at 623 K are shown in Figure 12. The as-prepared sample, as

expected, exhibited no scattering in the low-q region. Samples annealed for up to 80 min also showed no significant signal in the low-q region. The samples annealed for 100, 140, and 300 min showed interference peaks at q = 0.046 $Å^{-1}$ (d = 137 Å). The position of the peak did not change with the annealing time, but the intensity of the peaks increased with annealing time, indicating an increase in the volume fraction of the inhomogeneities in the system. These peaks appear to have resulted from spatially periodic fluctuations in the scattering length density in the $Zr_{41.2}Ti_{13.8}Cu_{12.5}Ni_{10.0}Be_{22.5}$ alloy. Guinier analysis of the data showed that the radius of gyration increased with annealing time, from 10 Å for the sample aged for 100 min to 21.6 Å after an annealing time of 300 min. The SANS features of these representative samples have been explained as follows: the as-prepared sample lacked a SANS signal because of its amorphousness and the almost homogeneous atomic density; the onset of the peaks for the sample annealed at 623 K after 100 min resulted from a periodic variation in the composition of at least one component of the alloy and/or a periodic local change in atomic density.

The most striking results reported by Schneider et al. (1996a, 1996b) are the existence of an incubation time for crystallization and the periodic arrangement of the nanocrystals. The primary crystallization in the $Zr_{41.2}Ti_{13.8}Cu_{12.5}Ni_{10.0}Be_{22.5}$ alloy during isothermal annealing at the glass transition temperature resulted in the formation of spatially periodically arranged Cu-Ti-rich nanocrystals. The authors propose that the arrangement is preceded by a modulated chemical decomposition process. The time scale for phase separation and subsequent crystallization seems to be determined by the mobility of the slower-moving Cu species.

Conclusion

The above examples clearly demonstrate the power of the SAD instrument in studying systems that require data over a wide q range. The large dynamic range in q available at SAD provides unique capabilities for studying systems undergoing transformation, those that are delicate, expensive, and/or not easily reproducible, and those at extreme temperature, pressure, and shear conditions, which require characterization at wider length scales. The future looks bright for the availability of beam time in the IPNS facility, and we encourage the scientific community to take advantage of this opportunity.

References

S.G. Ash and G.H. Findenegg, *Special Disc. Faraday Soc.* **1** (1970), 105-111.

H.G. Boman, J. Marsh, and J.A. Goody, Eds., "Antimicrobial Peptides," *Ciba Foundation Symposium* 186, John Wiley & Sons, Chichester, England (1994).

S.R. Craig, G.P. Hastie, K.J. Roberts, and J.N. Sherwood, *J. Mater. Chem.* 4 (1994), 977-981.

D.L. Dorset, *Macromolecules* **19** (1986), 2965-2973.

E.P. Gilbert, J.W. White, and T.J. Senden, *Chem. Phys. Lett.* **227** (1994), 443-446.

E.P. Gilbert, P.A. Reynolds, and J.W. White, unpublished research.

A.J. Groszek, *Proc. Roy. Soc. Lond.* A. **314** (1970), 473-498.

D. Hultmark, H. Steiner, T. Rasmuson, and H.G. Boman, *Eur. J. Biochem.* **106** (1980), 7-16.

A. Inoue, M. Kohinata, K. Otera, A.P. Tsai, and T. Masumoto, *Mater. Trans. JIM* **30** (1989), 378.

H. Kern, W. Rybinski, and G.H. Findenegg, *Journal of Colloid and Interface Science* **59** (1977), 301-307.

W. Klement, R. Willens, and P. Duwez, *Nature* **187** (1960), 869.

P. Lamparter and S. Steeb, *J. Non-Cryst. Sol.* **88** (1986), 388.

W.M. Mazee, *American Chemical Society Division of Petroleum, Chemistry Preprints* 3 (1958), B35-47.

A. Peker and W.L. Johnson, *Appl. Phys. Lett.* **63** (1993a), 2342.

A. Peker and W.L. Johnson, "Be Bearing Amorphous Metallic Alloys Formed at Low Cooling Rates," U.S. Patent No. 5, 288, 344 (1993b).

S. Schneider, unpublished research.

R.G. Snyder, M.C. Goh, V.J.P. Srivatsavoy, H.L. Strauss, and D.L. Dorset, *J. Phys. Chem.* **96** (1992), 10008-10019.

R.G. Snyder, G. Conti, H.L. Strauss, and D.L. Dorset, *J. Phys. Chem.* **97** (1993), 7342-7350.

J.W. White, D.L. Dorset, J.E. Epperson, and R.G. Snyder, *Chemical Physics Letters* **166** (1990), 560-564.

J.W. White, P.W. Zhu, J.E. Epperson, D. Wozniak, and R.G. Snyder, unpublished research.

C.A. Wraight, *Biochem. Biophys. Acta* **548** (1979), 500-515 .

M. Zasloff, *Proc Nat. Acad Sci. USA* **84** (1987), 5449-5453.

T. Zhang, A. Inoue, and T. Masumoto, *Mater. Trans. JIM* **32** (1991), 1005.

III

Reflectivity at IPNS

G. P. Felcher, Materials Science Division, and A. P. Y. Wong, S. Adenwalla, and R. J. Goyette, IPNS Division, Argonne National Laboratory

Neutron reflectivity can measure density profiles with spatial resolutions in the tens of Angstroms, a resolution that is unmatched by other techniques. Such information is vital to the basic understanding of magnetic, metallic, oxide, biological, and polymeric thin films and interfaces. One might say that neutron reflectometers have been springing up like bamboo shoots after the rain. Acronyms like POSY at IPNS, SURF at ISIS, and SPEAR at LANSCE decorate the directories of every major current and future neutron source. Despite the plentiful supply of reflectometers, the demand remains high. A combination of novel instrumentation and clever experimentation brings new dimension and insight to the technique as it continues to breathe new excitement into the field.

The reflectometers at IPNS, built around two horizontally split beams from the same beam port, employ a vertical reflection geometry so that the normal to the surface of the sample is horizontal. The first reflectometer (POSY I) is designed to measure the reflectivity of polarized neutrons. By strategic use of a polarizer, a flipper, and an analyzer, POSY I is optimized to measure the two different reflectivities with the neutron polarization parallel and antiparallel to the applied magnetic field. It is particularly suitable for studies of magnetism on thin film samples. The second reflectometer (POSY II), designed to handle high-intensity, unpolarized neutron reflection, is capable of measuring up to six decades of reflectivity with a maximum q-range up to 0.25 $Å^{-1}$. It has been optimized for studies of polymeric, oxide, and biological thin film samples. Both reflectometers can measure specular and off-specular reflectivity signals simultaneously by taking advantage of position-sensitive detectors and the pulsed nature of IPNS.

The POSY instruments are parts of the user facility of IPNS. In light of the Scientific Facility Initiative, the available beam time on these machines will be increased significantly in FY 1996. Much effort is devoted to enhancement of the user programs. The reflectometers are highly adaptable to accommodate the various requirements for different experiments, including vacuum, humidity control, high- and low-temperature control, and a multiple sample changer. The fully automated data acquisition and analysis system is designed to be as user-friendly as possible. Moreover, the whole infrastructure of the user program is streamlined to provide maximum support to users, enabling them to use the beam time efficiently and productively. Instrument scientists are always available for scientific exchange and discussion about the experiments.

To illustrate the power of polarized neutron reflectometry (PNR), we describe an experiment performed in 1995 that clearly demonstrated the presence of biquadratic coupling in a

multilayer (Adenwalla et al., 1996). It is known that ferromagnetic films separated by nonferromagnetic spacers can exhibit an oscillatory exchange coupling between the ferromagnetic layers as a function of spacer thickness. The amplitude of this oscillation decreases with increasing thickness of the spacer layer. We studied a [Fe (14 Å)/Cr (74 Å)]$_{20}$ superlattice, which is in the region of large spacer thickness where the ferromagnetic (FM) and antiferromagnetic (AFM) exchange couplings are very small. Using polarized neutron reflectometry (with spin analysis), we were able both to demonstrate the 90° alignment of the Fe layers and to show that the sample was in a single-domain state over an area on the order of a square centimeter.

We measured four reflectivity curves – R^+, R^-, R^{++} and R^{-+} – over a region extending from the critical edge to the chemical Bragg peak. There were two Bragg peaks present: the FM peak (corresponding to the superlattice periodicity and resulting from both the nuclear scattering from the layers and components of the Fe-layer magnetization ferromagnetically aligned with H) and the AFM peak at low k (resulting from the noncollinear alignment of the Fe layers and corresponding to a doubling of the magnetic unit cell). By fitting the data, we were able to obtain the exact orientation of the spins of each layer. The Fe layers were aligned at close to 0° and 90° with respect to the field, but slightly canted.The canting was the result of the Zeeman energy term and became less as the field was reduced.

The presence of an AFM peak in the spin-flip reflectivity indicates that there was a perpendicular component of magnetization with a repeat distance of twice the superlattice spacing; this is a signature of the presence of interlayer coupling. The width of the AFM peak indicates that the magnetic structure was coherent throughout the thickness of the superlattice. The R^+ and R^- AFM peaks were shifted with respect to each other, the R^- peak being shifted to lower k (see Figure 1). The separation of the AFM peak was successfully modeled, assuming a single-domain sample; this results in the reflectivity being slightly weighted in favor of the front face of the sample because of attenuation of the neutron beam as it traverses the sample. (This weighting effect would be obscured in a multidomain sample.) In our case, the shift of the AFM peak indicates that the top Fe layer was magnetized perpendicular to H. Hence, by using PNR we were able to answer many questions about this system that were

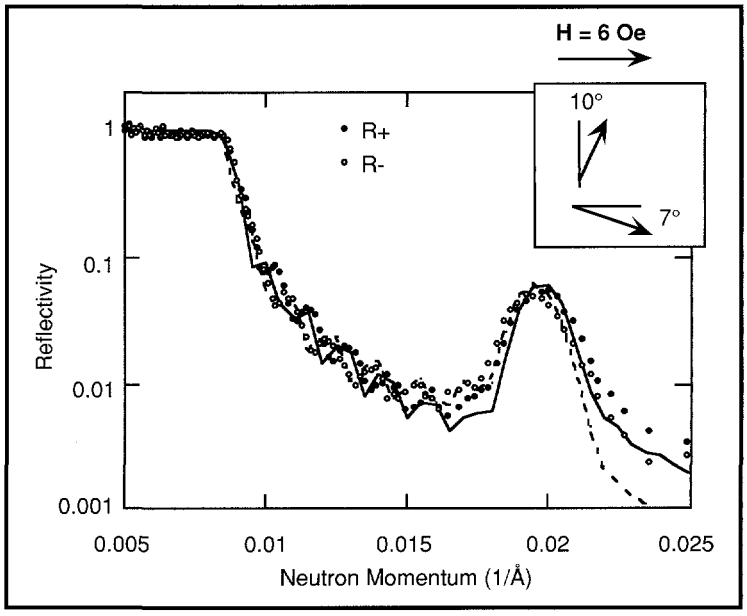

FIGURE 1.
Neutron reflectivity measured without polarization analysis along the easy [100] axis at H = 6 Oe and T = 205 K. The lines indicate the fit to the data for the spin structure shown in the inset.

not easily answered by bulk magnetization measurements; the question of whether or not the sample had a single domain, the fact that the structure was coherent, the exact direction of the magnetization of each layer, and the effect of field on the direction of the magnetization. The power of PNR lies in its depth-dependence profiling, which allows us to measure the magnetization as a function of depth in the sample.

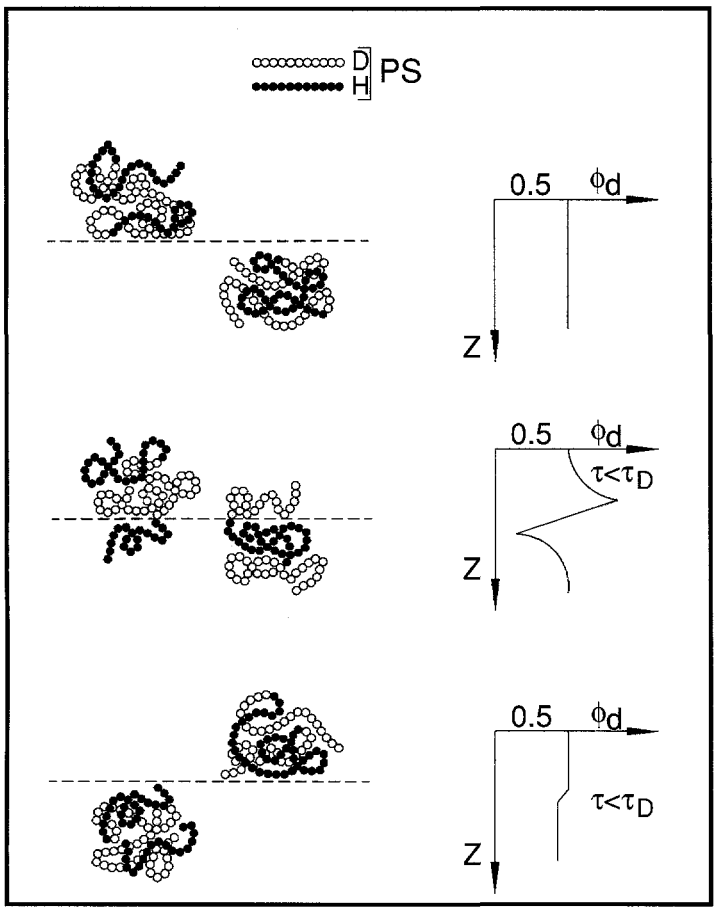

FIGURE 2.
Illustrative diagram for the interdiffusion between two oppositely deuterated polystyrene blends. The scattering density profiles at different stages are shown in the insets.

In 1994, we showed unequivocally on POSY II the first direct experimental evidence of the "reptation" motion of polymer chain diffusion (Agrawal et al., 1994). A polymer melt system is like a plate of spaghetti. For a particular polymer chain to move through the system, it has to perform a snake-like reptation movement to diffuse lengthwise along the chain direction through the network of polymer chains. By studying the interdiffusion between two species of polystyrene, we confirmed the reptation motion of polymer chains. The two species of polystyrene were deuterated at different portions of the polymer chains. The first species was deuterated at the middle one-third of the chain so that it was composed of linear hydrogenated-deuterated-hydrogenated polymer chains. The second species was deuterated at the opposite two-thirds so that it consisted of deuterated-hydrogenated-deuterated chains. Thin films of the two species of polystyrene were put in contact and neutron reflectivity was used to monitor the interface between the two films. At the beginning of the experiment, the neutron scattering contrast between the two species was not high. Subsequently, as the sample was annealed at elevated temperature for fixed intervals of time, interdiffusion between the two species of chain took place, and a clear bilayer of hydrogen-deuterium was observed as a result of the geometric arrangement of the deuteration. Upon further annealing, the bilayer was smeared again. Such a trend can be clearly observed in Figure 2, which shows the scattering length density profile

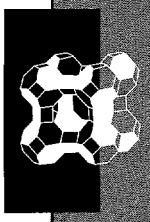

at various stages of annealing. This is the first direct observation of the polymer chains performing end-to-end reptation movements.

In addition to these exciting new developments, we are also committed to finding innovative ways to measure a variety of systems, including biological and colloidal systems, superconductors, and various magnetic systems. We are expanding the capabilities of the two POSY instruments; this includes devising methods to obtain in-plane structural information from the off-specular signal and measure all four components of the spin-dependent reflectivity (on POSY I).

In conclusion, the POSY instruments are versatile neutron reflectometers that can provide valuable information about such thin film problems as adhesion, diffusion, segregation, and growth modes. The user program is open to anyone who might have problems that can be resolved by reflectivity studies. Interested parties are encouraged to confer with either Gian Felcher (gian_felcher@qmgate.anl.gov) or Apollo Wong (apollo@anl.gov) about the possibility of running their experiments on the IPNS POSY facilities.

III

Quasielastic Scattering Spectrometer and Chemical Excitations Spectrometer

F. R. Trouw, IPNS Division, Argonne National Laboratory

Introduction

It is exciting and, at the same time, quite sobering to realize that the Quasielastic Scattering Spectrometer (QENS) is celebrating its tenth anniversary this year! We are fast approaching a total of 1800 useful data sets – quite a respectable number for this inelastic scattering instrument.

The instrument has undergone no significant modifications since the last progress report, but the "H" moderator viewed by QENS is now operated at 20 K using solid methane, in place of the previous 100 K liquid methane operation. This change has proven to be a great success: the flux at 3.65 meV, which represents the elastic scattering energy, has increased in intensity by approximately a factor of five. Moreover, the design of the new moderator maintained the pulse shape with such precision that this modification had essentially no effect on the resolution function of the instrument. Whereas most experiments previously required approximately 12 hours of measuring time to obtain acceptable statistical precision, this can now be achieved in about 3 hours.

The moderator enhancement is a great leap forward, and the future holds yet more possibilities. The current design of QENS is based on three simultaneous measurements at different momentum transfers, and the effective angular coverage is only 35 degrees out of a useable 300 degrees, which is clearly inefficient. A modification to QENS is being planned that would increase the number of simultaneous measurements by about a factor of five, resulting in a complete set of Q measurements at a single, fixed detector setting. This potential upgrade, in conjunction with the moderator modification, would result in a count-rate 25 times greater than was possible just two years ago. We hope QENS will be upgraded to this level of performance over the next two years.

Another exciting development has been the construction of the Chemical Excitations Spectrometer (CHEX). This inverse-geometry spectrometer is based on the neutron time-focusing principle used in early designs of such instruments at IPNS and KENS; the successful TFXA spectrometer located at ISIS is also based on this principle. Such an instrument has a number of attractive features for inelastic scattering experiments – for instance, in chemical spectroscopy, where the value of the momentum transfer does not play a significant role. Such instruments are capable of very respectable energy resolutions (1-3%) over a very large dynamic range (0-500 meV), and at the same time they are conceptually simple and relatively inexpensive to construct.

CHEX was built during the summer of 1995; the final quarter of the year was used to optimize the "prototype," which mainly involved making shielding modifications to address the neutron background (which represents the main limitation on such an instrument). This work was completed in December 1995, and the interim spectrometer (Figure 1) is now in routine use for chemical spectroscopy. An example of a spectrum measured on the instrument is given in Figure 2, which shows the vibrational spectrum of glycine anhydride. The final task is the fine-tuning of the calibration parameters, which is under way and should be completed by March 1996. The instrument uses only a part of the potential analyzer and detector area; a complete configuration of the spectrometer would increase the count rate by about a factor of six. Moreover, the detectors have not yet been matched to the rest of the instrument, and there is a potential for further improvements in energy resolution.

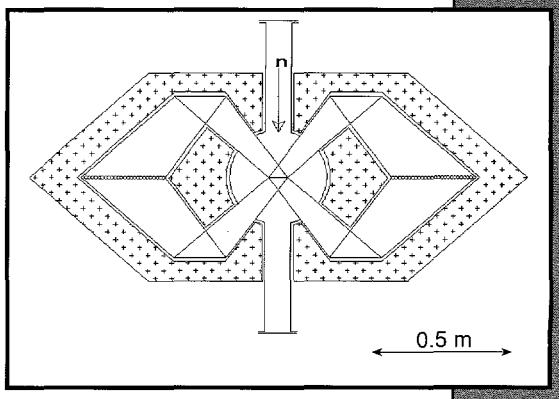

FIGURE 1.
Layout of the CHEX prototype. The current configuration has one-quarter of the possible graphite analyzer area, one-half of the detectors and room temperature beryllium.

Experimental Investigations

The type of science explored by means of QENS has continued to be broad-based, with a mixture of quasielastic and inelastic scattering measurements. Some examples of studies done on QENS in the last few years follow.

Early interest in using QENS for experiments on magnetic systems has continued; for instance, Rob Robinson (Los Alamos National Laboratory) and collaborators have characterized the inelastic scattering from the heavy fermion compound YbBiPt. This compound has a huge linear-temperature coefficient of specific heat $\gamma = 8$ mol^{-1} K^{-2} at low temperature. The low-energy dynamics of the compound have been characterized on LAM-40 at the KEK, on QENS at IPNS, and on the Cold-Neutron Fermi-Chopper Spectrometer at the NIST reactor. This comprehensive series of measurements has provided the necessary data for proposing a crystal field level scheme that is consistent with the measured heat capacity of the compound. The QENS data are shown in Figure 3, where the 6-meV excitation and two quasielastic components are clearly visible. One of the attractions of an inverse-geometry crystal analyzer spectrometer such as QENS for magnetic quasielastic scattering is the asymmetrical shape of the resolution function, where there is a sharp drop on the neutron energy-loss side of the peak. This is the critical side, because such experiments are carried

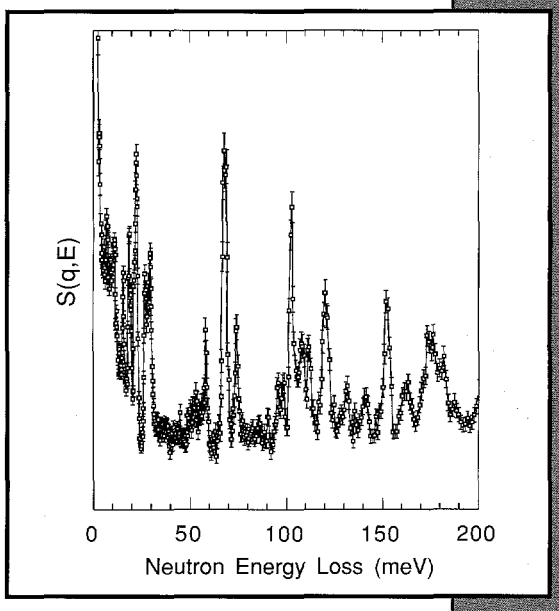

FIGURE 2.
Vibrational spectrum of glycine anhydride (15 K), measured on the new CHEX prototype.

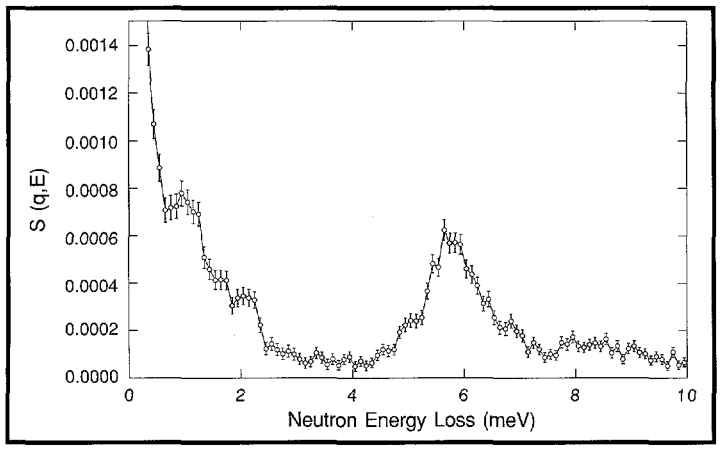

FIGURE 3.
Spectrum of YbBiPt measured on QENS at 1.5 K. The shoulders on the sharp side of the resolution function are clearly visible.

out at very low temperatures, and the sample does not have sufficient energy for there to be a significant number of neutron energy-gain events.

In the field of molecular sieves, mesoporous silicates with pore sizes in the tens of angstroms have recently been synthesized. The most familiar of these is MCM-41, a molecular sieve that contains one-dimensional pores of effectively infinite length, with a diameter of approximately 39 Å. John White (Australian National University) and collaborators have used this material as a substrate to study the dynamics of adsorbed methane; the adsorbate must consist of cylindrical tubes of methane with a cross-sectional area corresponding to only about 40 molecules. The low-temperature spectrum of bulk methane has peaks corresponding to the quantum rotor modes, and the measurements demonstrated that the adsorbed phase did not show similar excitations (Figure 4). Possible explanations for this result include the following:

- The temperature at which these modes are observable is depressed (the excitations in bulk methane are strongly temperature-dependent in the range 10-25 K);
- The methane has formed a disordered phase, which has broadened the excitations to such an extent that they are no longer visible; or
- The rotational splittings have moved to lower energies, out of the observable energy window of the instrument.

In addition to low-temperature inelastic scattering measurements, extensive quasielastic scattering measurements were also made; these gave results consistent with either a nonisotropic rotation of the adsorbate or a mixture of free and mobile species (Figure 4). Although the latter explanation is intuitively more satisfactory, a more definitive interpretation awaits the results of ongoing modeling efforts.

The dynamics of materials where the limitations of size play a role has been the focus of quasielastic scattering studies by Ken Herwig (University of Missouri-Columbia) and collaborators. They have investigated the mobility of water present as droplets in water-oil mixtures stabilized by a surfactant. The model system is a hexane/water/AOT mixture (AOT is the surfactant – sodium-di-2-ethylhexyl-sulfosuccinate), where the water forms clusters surrounded by the surfactant and dispersed in the organic phase. Because deuterium has a significantly lower cross section than hydrogen, the use of deuterated hexane means that

most of the signal comes from the water in the droplets. QENS is well-suited for studies of water dynamics, and a separation of rotational and translational diffusion can be done on the basis of the Q-dependence of the quasielastic scattering signal. The experiments were carried out on two different compositions, where the droplet sizes were 38 and 20 Å. The results consisted of a resolution-limited component (probably bound surface water) and the rotational and translational quasielastic scattering. The half-width at half-maximum of the translational scattering as a function of momentum transfer is shown in Figure 5. The droplet size-effect is quite pronounced, with the 38-Å translational diffusion constant already lower than that of bulk water, while the mobility of the water is dramatically affected in the 20-Å droplets. Because this well-defined system approaches the limits encountered in biological systems, such detailed information on water dynamics will be of use in understanding the behavior of small water clusters in, for instance, biological gels.

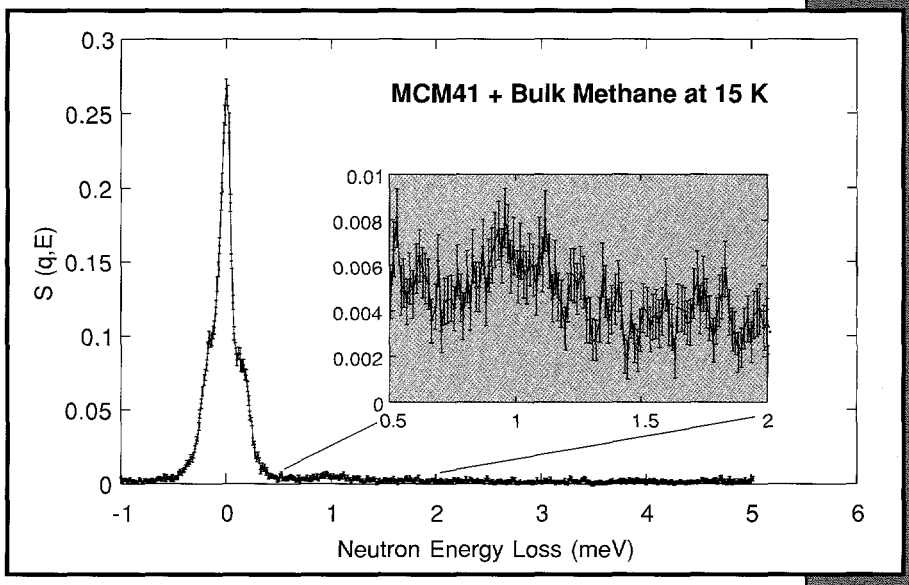

FIGURE 4.
Near-elastic scattering from bulk methane and adsorbed methane, each measured on QENS at approximately 15 K.

A final example is the very recent measurements on the inelastic spectrum of the bridging hydrogen in sodium hydrogen bis(4 nitrophenoxide) dihydrate ($Na.H.[OC_6H_4NO_2]_2.2H_2O$) by Maurice Kreevoy (University of Minnesota) and collaborators. This material gives rise to what is referred to as a Hadzi type ii infrared spectrum, which does not have a band in the usual O-H stretching region, 2500-3500 cm^{-1}, but instead has a very intense, very broad band with a width at half height that often exceeds 500 cm^{-1}, an ill-defined maximum that is frequently

less than 1000 cm^{-1}, and an integrated intensity that often appears to exceed the rest of the spectrum combined. The appeal of characterizing such compounds with neutron spectroscopy lies in the lack of such a broadening effect for neutron scattering. One of the other attractions of using neutron spectroscopy arises from the much-reduced cross section of deuterium and so selective deuteration of different parts of the molecule, giving rise to large intensity changes and frequency shifts. This provides a powerful method for the assignment of modes to particular spectral features, and this strategy has been used with success for many years. The spectra of a variety of partially deuterated compounds prepared for these experiments has provided a comprehensive set of spectra for the assignment of the modes, as well as the unequivocal identification of excitations involving the hydrogen-bond proton (Figure 6). It is clear (by inspection) that the bridging hydrogen gives rise to a peak at about 600 cm^{-1}, and the modes associated with the other hydrogen atoms on the aromatic ring can also be deduced from these spectra. These measurements represent an excellent example of the complementary nature of inelastic neutron scattering and optical spectroscopy, as well as the role of neutron spectroscopy in chemistry.

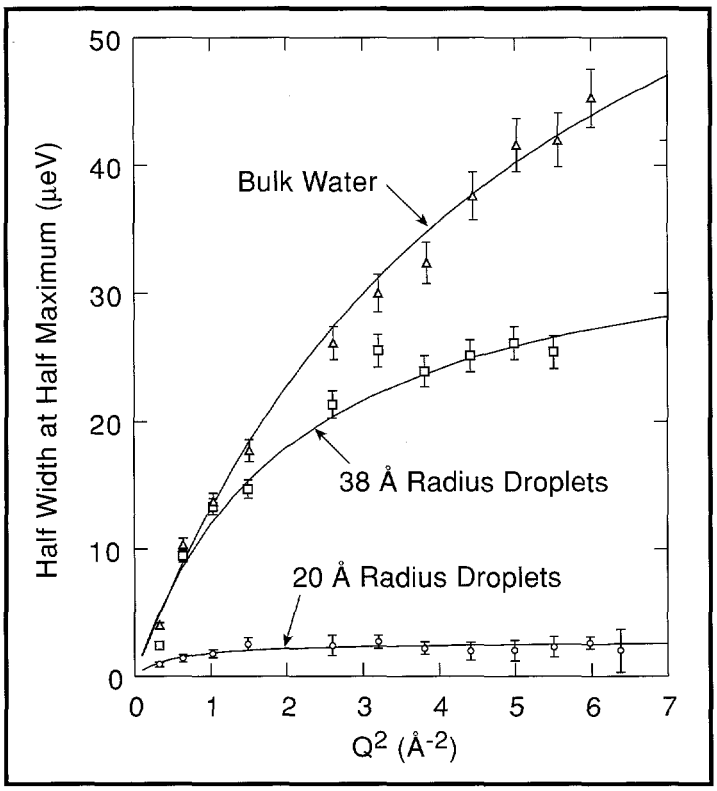

FIGURE 5.
Half-width at half-maximum of the translational component of quasielastic scattering from water in different-size droplets.

Conclusion

These studies represent projects that are typical of some of the science being done on QENS. There is a mix of quasielastic scattering and inelastic scattering measurements, since the spectrometer has the versatility to do both. This dual capability, made possible by the large dynamic range of the instrument, is often useful when both types of measurements are desired for a material. However, this is not always necessary, and CHEX represents a potentially better instrument for those experiments that are focused on inelastic scattering above about 100 cm^{-1}. It is anticipated that some of the inelastic scattering work will move to CHEX, allowing QENS to focus on quasielastic scattering measurements and those requiring better

elastic energy resolution. The next ten years will be an exciting time for inverse-geometry crystal analyzer spectrometers at IPNS; the anticipated QENS upgrade and the completion of CHEX will provide excellent opportunities for the scientific community.

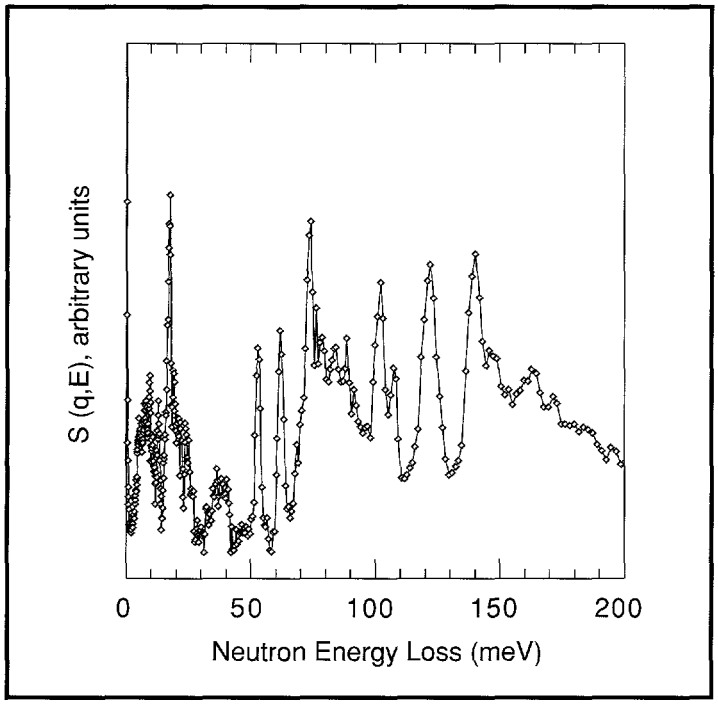

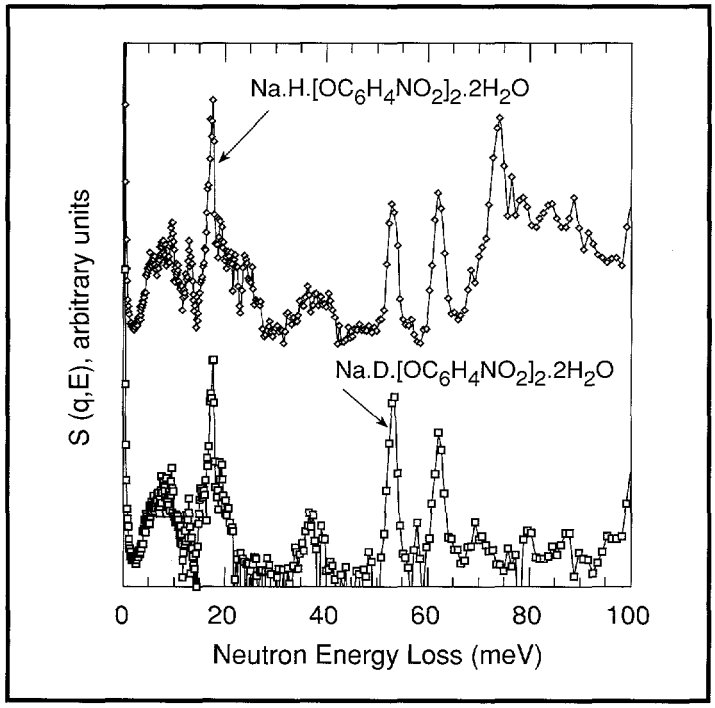

FIGURE 6.
(Top) low energy and (bottom) high energy vibrational spectra of $Na.H.[OC_6H_4NO_2]_2.2H_2O$ *and* $Na.D.[OC_6H_4NO_2]_2.2H_2O$*, measured on QENS at 15 K.*

HRMECS *(C.-K. Loong/D. Yocum)*
Incident energy (E_0)

5 — 1000 meV

Quasielastic	Inelastic	Deep-inelastic
Atomic diffusion	Magnetic/phonon	Momentum distribution
Magnetic fluctuations	excitations	Molecular spectroscopy

$0 \le E \le 800$ meV, $\Delta E/E_0 \cong 0.02$
$0.2 \le Q \le 30$ Å^{-1}, $\Delta Q/Q_0 \cong 0.01$

QENS *(F.R. Trouw)*
Energy Transfer

0 — 1000 meV

Quasielastic	Inelastic

$\Gamma_{elastic} = 35$ μeV, $\Delta E/E = 2$ - 4%
$0.5 < Q < 2.5$ Å^{-1}

GLAD *(D.L. Price/J.A. Johnson/K.J. Volin)*
Short and intermediate range order in glasses, liquids, amorphous and crystalline materials.
Downstream sample position: $0.2 \le Q \le 45$ Å^{-1}, $\Delta Q/Q_o \approx 0.01$ cotθ
Upstream sample position: $0.1 \le Q \le 25$ Å^{-1}, $\Delta Q/Q_o \approx 0.005$ cotθ

SCD *(A.J. Schultz)*
Single crystal time-of-flight Laue diffraction; nuclear and magnetic structures; phase transitions.
Position-sensitive area (30x30 cm^2) detector
d = 0.3 to 7.0 Å; $\Delta d/d$ = 0.02
Temperature = 4 to 1000 K; pressure = 0 to 5 kbar
Also, texture analyses of polycrystalline samples.

SEPD *(J.D. Jorgensen/S. Short)*

2θ (°)	145	90	60	30
d(Å)	0.4 - 3.9	0.6 - 5.4	0.8 - 7.7	1.5 - 14
Δd/d (%)	0.3	0.5	0.9	2.4

Special environments: Displex, furnaces, He-gas pressure cell.
Sample size: 0.02 - 20g
Nominal 2h data collection (for 5g sample)

LRMECS *(R. Osborn/L.I. Donley)*
Incident energy (E_0)

5 — 1000 meV

Quasielastic	Inelastic	Deep-inelastic
Atomic diffusion	Magnetic/phonon	Intermultiplet transitions
Magnetic fluctuations	excitations	Molecular spectroscopy

$0 \le E \le 800$ meV, $\Delta E/E_0 \cong 0.05$
$0.1 \le Q \le 35$ Å^{-1}, $\Delta Q/Q_0 \cong 0.02$

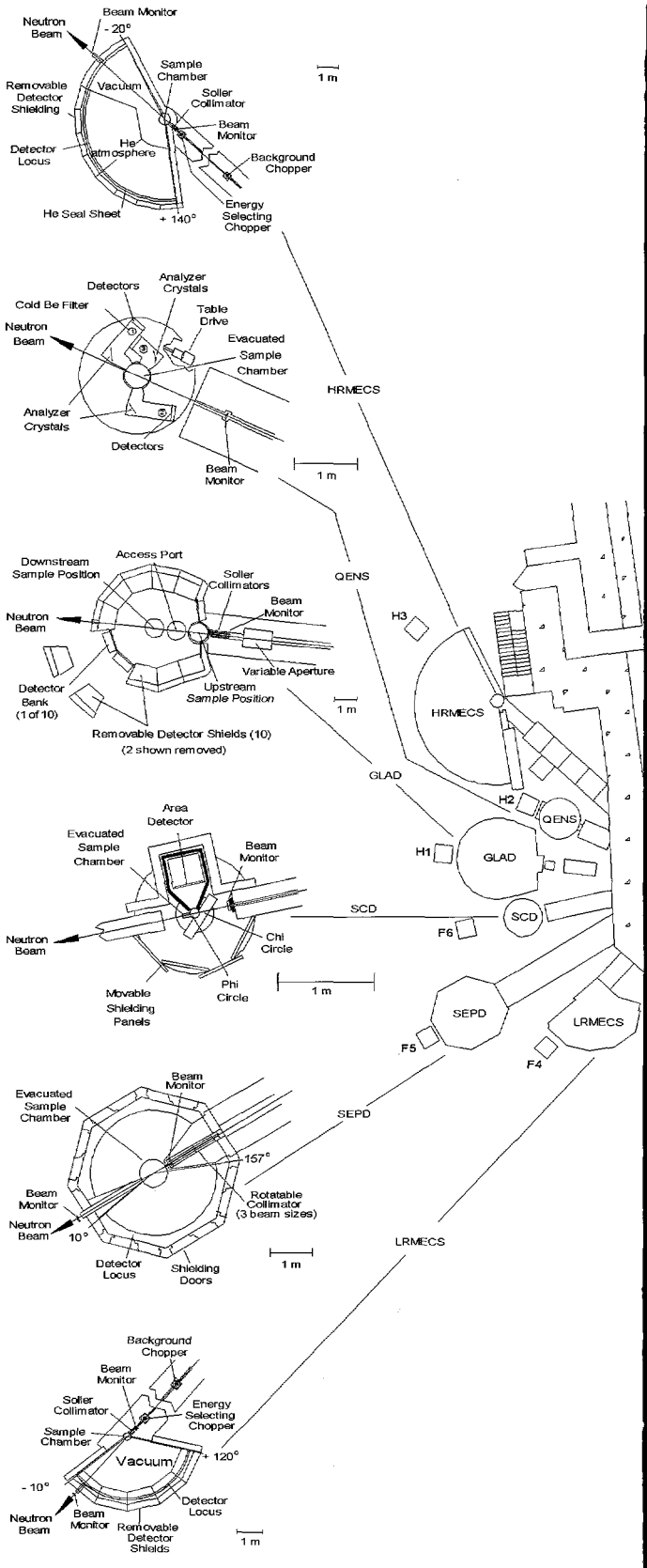

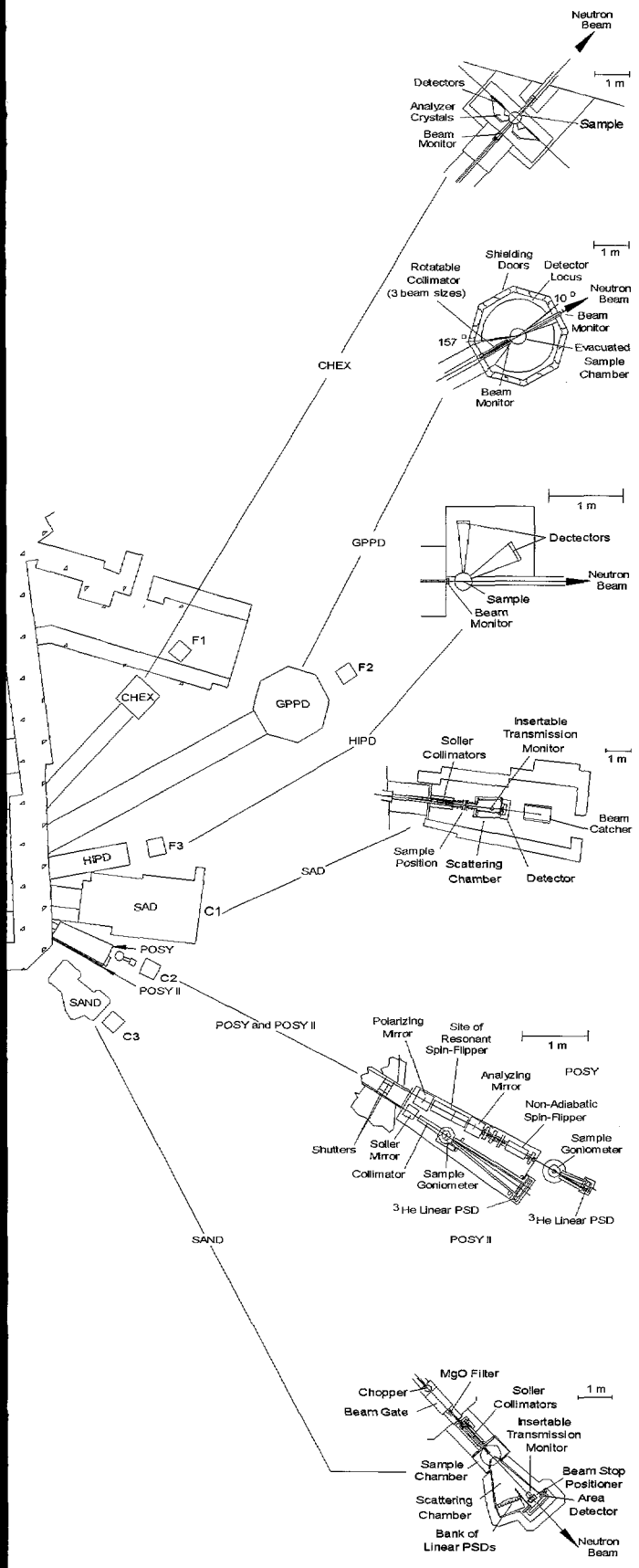

CHEX *(F.R. Trouw)*
Energy Transfer

5 — 1000 meV

Chemical Spectroscopy
ΔE/E = 1.5 - 3%

GPPD *(J.W. Richardson/R.R. Thomas)*

2θ (°)	148	90	60	30, 20
d(Å)	0.3 - 3.0	0.4 - 4.0	0.6 - 5.7	1.1 - 18.2
Δd/d (%)	0.25	0.4	0.8	2.3, 4.6

Special environments: Displex, furnaces, residual stress.
Sample size: 0.1 - 20g
Nominal 4h data collection (for 5g sample).

HIPD *(A.J. Schultz)*
Nuclear and magnetic powder diffraction.
30° detector bank: d_{max} = 29 Å; $\Delta d/d$ = 0.03
90° detector bank: d_{max} = 10 Å; $\Delta d/d$ = 0.01

SAD *(P. Thiyagarajan/D.G. Wozniak)*
Large-scale structures in biological, chemical, metallurgical, and magnetic systems.
$0.005 \leq Q \leq 0.35$ Å^{-1} (single measurement)

POSY *(G.P. Felcher/R.J. Goyette)*
Reflectivity/elastic scattering at grazing incidence of polarized neutrons.
Wavelength range: 2 - 16 Å (0.3 meV < E < 20 meV)
$4 \times 10^{-3} < Q < 0.5$ Å^{-1}, $\Delta Q/Q = 0.02$

POSY II *(A. Wong/R.J. Goyette)*
Reflectivity/elastic scattering at grazing incidence.
Wavelength range: 2 - 14 Å (0.4 meV < E < 20 meV)
$4 \times 10^{-3} < Q < 0.3$ Å^{-1}, $\Delta Q/Q = 0.025$

SAND *(P. Thiyagarajan/D.G. Wozniak)*
Large-scale structures (10-2000 Å) in biological, chemical, metallurgical, and magnetic systems.
$0.0035 \leq Q \leq 0.8$ Å^{-1} (single measurement)

III

Diffraction Studies of Hydrogenous Materials at GLAD

P. C. Trulove, D. Haworth, and R. T. Carlin, Division of Electrochemical Sciences, The Frank J. Seiler Research Laboratory
S. R. Nagel, R. L. Leheny, and N. Menon, James Franck Institute, The University of Chicago
P. Zhou and J. E. Fischer, Department of Materials Science and Engineering and Laboratory for Research on the Structure of Matter, University of Pennsylvania
N. Koura, Tokyo University of Science
A. K. Soper, Neutron Science Division, Rutherford Appleton Laboratory
A. J. G. Ellison, M.-L. Saboungi, K. Suzuya, S. Takahashi, and D. L. Price, Materials Science Division, and K. J. Volin, IPNS Division, Argonne National Laboratory

Introduction

The Glass, Liquid, and Amorphous Materials Diffractometer (GLAD) is proving itself to be a first-class instrument for structural analysis of a wide variety of disordered materials, including glasses, liquids, fibers and other amorphous solids, and disordered crystalline materials, including oxides exhibiting superconductivity and giant magnetoresistance. The quality of the data appears excellent, and the consistency over a wide range of angles and wavelengths is highly satisfactory.

Many interesting disordered materials contain hydrogen, either as a primary component or as a residual constituent left over from preparation from organic precursors. In these cases, the conventional "Placzek" approach for subtracting the self scattering, based on a mass expansion in powers of neutron mass: atomic mass, is inapplicable. The problem has been addressed by Soper and collaborators (Soper and Luzar, 1993) at ISIS, who have developed a procedure for estimating the self scattering by a Chebyshev polynomial fit to the structure factor, made consistent with Krogh-Moe normalization (essentially, the requirement that the radial distribution function $n(r)$ be zero below some minimum value of r) through a maximum-entropy method. This procedure has been implemented on the SMUG node at IPNS as a new analysis program, SUBSLFGLD. This report provides a brief description of some of the experiments performed on GLAD over the past two years on hydrogenous materials and a preliminary account of some of the results.

Neutron Diffraction Studies of an Ambient-Temperature Molten Salt

Ambient-temperature molten salts composed of mixtures of 1-ethyl-3-methylimidazolium chloride (ImCl) and hydrogen chloride (HCl) are part of an important class of nonaqueous solvents. These solvents have been used for studying the chemistry of a wide variety of both organic and inorganic solutes (Osteryoung, 1987; Hussey, 1983). Mixtures of ImCl and HCl are liquid at or below ambient temperature over a wide range of compositions. Recent spectroscopic

studies (Campbell and Johnson, 1993) have shown that the anionic speciation in ImCl:HCl molten salts varies significantly with relative amounts of ImCl and HCl. When ImCl is in molar excess, the anions present are primarily Cl^- and HCl_2^-, while a molar excess of HCl gives HCl_2^- and $H_2Cl_3^-$ as the primary anions. In the case of a large molar excess of HCl, additional polyanions of the form $Cl(HCl)_n^-$ may be present. When HCl and ImCl are mixed in nearly equal amounts, HCl_2^- is the primary anion (however, small amounts of Cl^- and $H_2Cl_3^-$ may be present). Since Im^+ is the sole cationic species, the equal molar mixtures of ImCl and HCl are often referred to as $ImHCl_2$.

The ring hydrogens on the 1-ethyl-3-methylimidazolium cation (Im^+) are known to hydrogen-bond to chloride ion in basic $AlCl_3$:ImCl molten salts (Dieter et al., 1988; Dymeck and Stewart, 1989). The existence of anions of the form $Cl(HCl)_n^-$ in the ImCl:HCl molten salts demonstrates the ability of HCl_2^- to act as a hydrogen-bond acceptor. Therefore, it is reasonable to conclude that HCl_2^- may hydrogen-bond to the ring hydrogens on Im^+ in ImCl:HCl molten salts. In addition, recent solid-state crystallographic studies of similar low-melting salts indicate that Im^+ cations tend to form p-stacks with d-d distances <4 Å (Wilkes and Zaworotko, 1993). These and other observations suggest significant ordering of the ions in ImCl:HCl molten salts. Consequently, a better understanding of the structure of ImCl:HCl would be of considerable aid in understanding its chemical and physical properties, as well as how these properties relate to those of other, like low-melting salts.

Neutron diffraction on GLAD was employed to investigate the structure of the ImCl:HCl ambient-temperature molten salt. For the investigation of the liquid structure of ImCl:HCl, judicious deuterium substitution was employed to isolate the interactions involving hydrogen. Experiments were performed on ImCl:HCl samples with differing combinations of H-D substitution on both the imidazolium cation ring and hydrogen chloride. The diffraction differences from the hydrogen-deuterium substitution were analyzed by using programs developed at ISIS (Soper and Luzar, 1993).

The analysis of first-order differences due to deuteration of HCl_2^- gave two intrastructural peaks. These results indicate that HCl_2^- exists as an asymmetric ion in the $ImHCl_2$ molten salt. This is quite remarkable, considering that the HCl_2^- ion in $AlCl_3$ImCl molten salts appears to be linear, with the hydrogen symmetrically placed between the two chlorides (Trulove and Osteryoung, 1992). Furthermore, to our knowledge, asymmetric HCl_2^- ions have only been observed in the solid state (Evans and Lo, 1966). An asymmetric HCl_2^- implies some type of interaction with an additional species. The samples of $ImHCl_2$ used for these experiments contained some free Cl^-. As shown in Figure 1(A), this free Cl^- could weakly hydrogen-bond to the hydrogen in HCl_2^-. However, because of the low actual Cl^- concentration, very few of the species shown in Figure 1(A) could actually form. A more plausible reason for an asymmetric ion is the

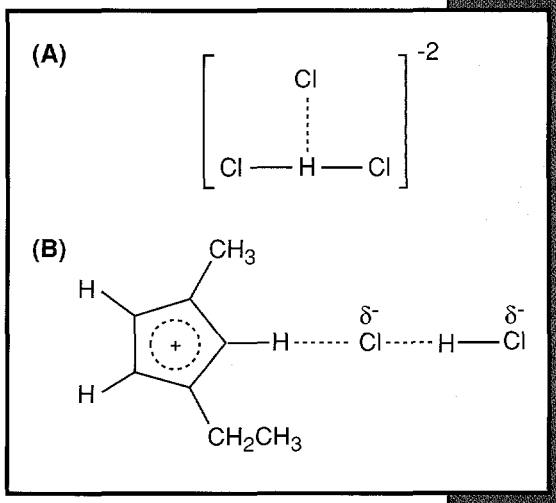

FIGURE 1.
Possible structures for the asymmetric HCl_2^- ion.

formation of a hydrogen-bond between one chloride from the HCl_2^- and a hydrogen on the imidazolium cation ring as shown in Figure 1(B). The chlorides in the HCl_2^- ion are capable of acting as hydrogen-bond acceptors, as demonstrated by the presence of anions of the type $Cl(HCl)_n^-$ in the $ImHCl_2$ melts containing excess HCl (Campbell and Johnson, 1993). In addition, the imidazolium ring hydrogens have been shown to strongly hydrogen-bond to Cl^- in $AlCl_3$:ImCl molten salts (Dieter et al., 1988). Analysis of second-order differences due to correlations between hydrogens on the imidazolium cation ring and HCl_2^- gave a pronounced peak near r = 4 Å. The area for this peak corresponded to 2-3 hydrogens about a hydrogen at the origin. These results are consistent with the p-stacking of the imidazolium cations.

Structural Studies of Organic Liquids through the Glass Transition

At temperatures below a liquid's melting point, the time scales that characterize its response to an external perturbation increase dramatically (Nagel, 1993). Extrapolations from measurements in this supercooled region suggest that for many liquids these time scales diverge at a finite temperature. Despite numerous studies to probe these slowing dynamics, the origin of this finite temperature divergence remains an outstanding problem. In contrast to the multitude of dynamical measurements, relatively few structural studies have attempted to identify changes in structure with the growing time scales. The main impediment to such work has been that the systems that show this finite temperature divergence most strongly are typically organic molecular liquids, in which significant intramolecular scattering and high hydrogen content complicate the analysis of structure data.

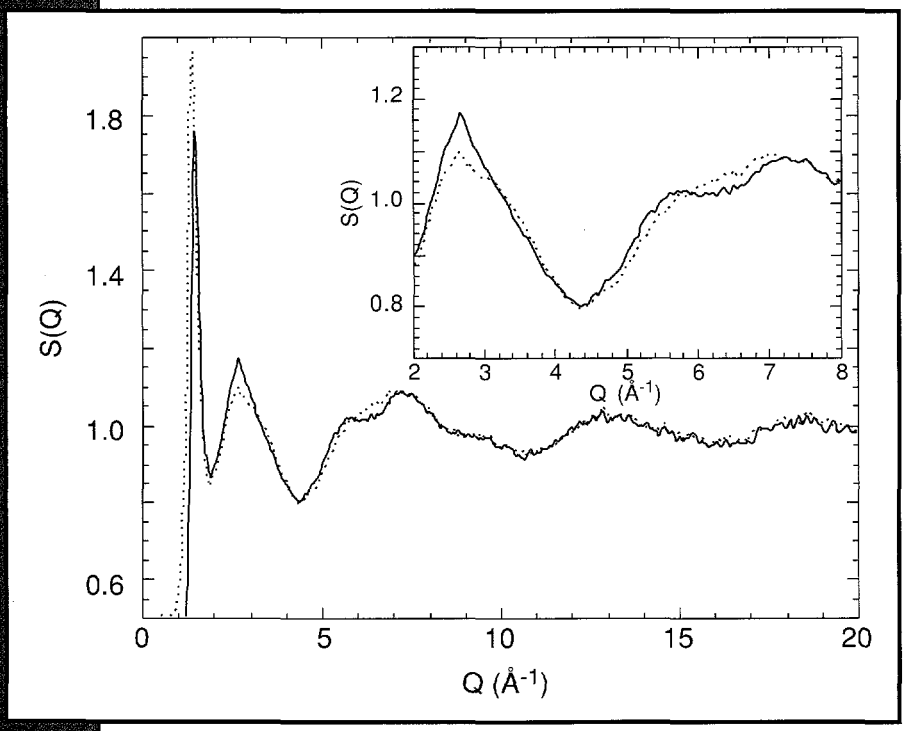

FIGURE 2.
The structure factor measured for D-propylene glycol ($C_3D_8O_2$) at 90 K (——) and 300 K (- · · · -). The inset shows an enlargement of the second and third peaks, whose shapes change systematically with temperature.

In experiments on supercooled D-propylene glycol ($C_3D_8O_2$) at GLAD, we have attempted to overcome some of these complications. We have collected diffraction data on the liquid at several temperatures from high in the liquid state to below the divergence temperature in an effort to

identify structural trends we can associate with the slowing dynamics. The combination of the liquid's light elements and large molecular weight makes the standard Placzek corrections for self scattering inappropriate for our data. In particular, application of this correction leads to much greater temperature dependence in S(Q) than the differential cross sections indicate. In the low-Q region, the good quantitative agreement of the differential cross sections from GLAD with data taken at SAD suggests that inelastic scattering plays a small role in our results, and in our analysis we have assumed a structureless, flat self scattering contribution. We have also applied a maximum entropy analysis to the data and find that the resulting structure factors closely approximate those calculated with the flat self scattering. In particular, much of the same temperature-dependent structure in S(Q) appears after application of each correction. Figure 2 shows the resulting S(Q) at our highest and lowest temperatures. The inset shows the second and third peaks, which reveal systematic changes with temperature.

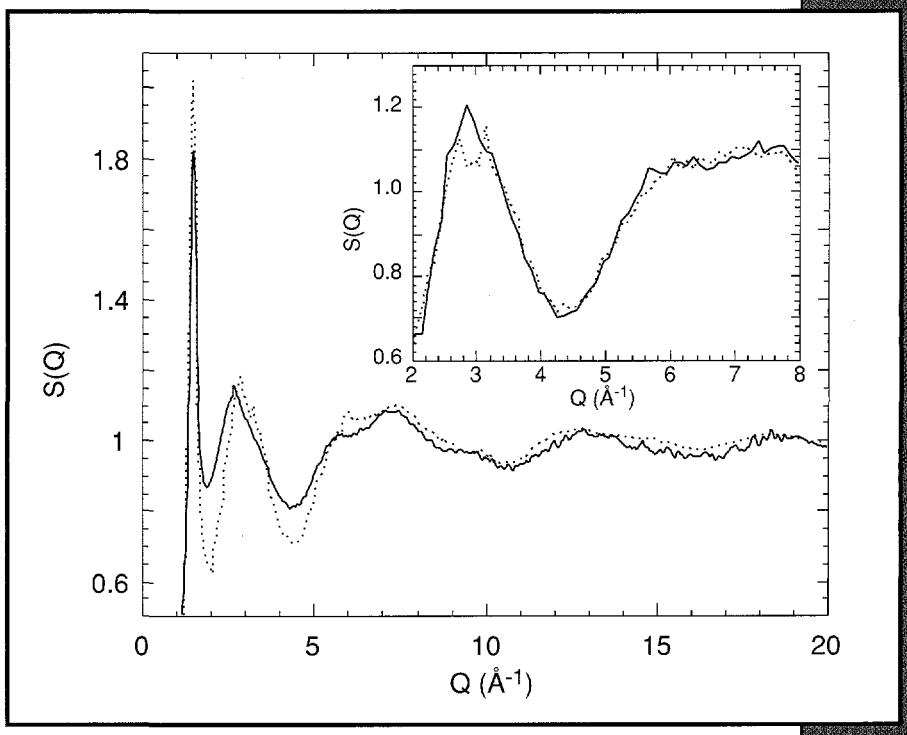

FIGURE 3.
The structure factor for D-propylene glycol measured (——) at 160 K and calculated from molecular dynamics simulations of the liquid (- · · -) at the same temperature. The inset shows the second and third peaks of the structure factor calculated from simulations at 90 K (——) and 300 K (- · · -). S(Q) for the simulations reveals the same trends with temperature seen in the experiment.

We have also performed molecular dynamics simulations of the liquid in an effort to isolate contributions from intermolecular scattering to the changes in S(Q). Figure 3 shows a comparison of the simulation results with the experimental data. As shown in the inset to Figure 3, the simulations possess the same trends in temperature as the experimental S(Q). Our analysis of the simulation results demonstrates that the intramolecular structure factor shows little temperature dependence and that much of the change in temperature can be identified with intermolecular scattering. Fourier analysis of the intermolecular scattering in the simulations reveals a sharpening of pair correlations at distances between 1.5 and 4 Å at low temperatures. Therefore, we tentatively identify the changes in S(Q) in Figure 2 with an enhanced orientational correlation between nearest neighbors as the temperature decreases.

III

Local Atomic Structures of Amorphous Carbons from Radial Distribution Function Analysis

Lithium-intercalated amorphous carbons have attracted enormous interest recently due to their applications as anode electrodes in lithium-ion rechargeable (rocking-chair) batteries (Dahn et al., 1995a; Zheng et al., 1995). The concept is that Li cations move back and forth between the anode and cathode during charge/discharge cycles without ever being reduced to hazardous metallic form. The prototype cells exhibit energy density four times that of conventional NiCAD batteries and much longer recycling lifetimes (as much as 3,000 cycles). The host carbons can be divided into three categories according to their structures and chemical compositions. First, graphitic carbons prepared at temperatures >2500°C with a maximum lithium capacity of, in electrochemistry terminology, 372 milliampere-hours per gram (mAAh/g) correspond to a stoichiometry LiC_6, the physics and chemistry of which are very well studied and understood (Fischer, 1987). Its exfoliation in electrolytes results in a very short lifetime, limiting its wide usage. The second category covers vitreous carbons from pyrolyzing polyaromatic hydrocarbons or polymers at moderate temperatures (800 to 1500°C). The lithium capacity of these materials ranges from 300 to 600 mAAh/g, as good as or better than LiC_6. One interpretation involves covering up with lithium on both sides of "single" graphitic sheets (Dahn et al., 1995b). The third category includes vitreous carbons from organic precursors pyrolyzed at lower temperatures (500 to 800°C). These carbons exhibit exceptionally high lithium capacity (600-1000 mAAh/g), most of which is irreversible (i.e., covalently bonded lithium atoms), an effect due to high hydrogen residual.

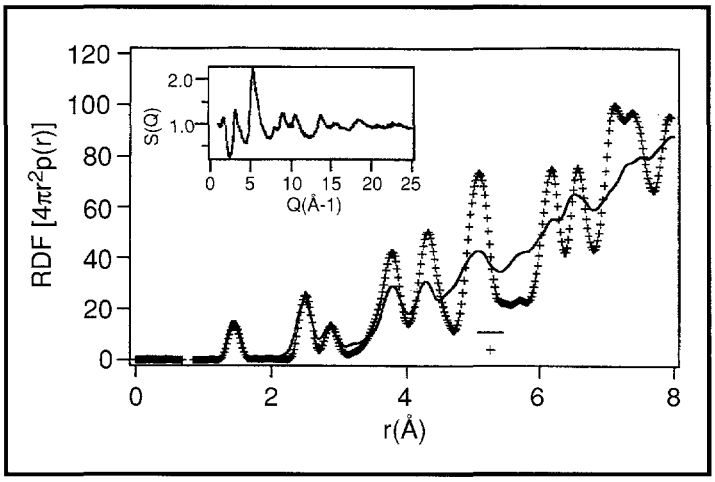

FIGURE 4.
Radial distribution function (rdf, $4\pi r^2\rho(r)$, solid curve) of the amorphous carbon containing 17 at.% hydrogen. The graphite rdf is also plotted as a reference (crosses). A Lorch-weighting factor was applied in both cases to remove spurious features due to truncation at 30 Å^{-1}. Inset: neutron-weighted structure S(Q). The incoherent and inelastic scattering backgrounds from hydrogen were fitted to a third-order Chebychev polynomial and removed.

Here, we address the local structures of amorphous carbons with large hydrogen concentration and the chemical bonding states of lithium, using time-of-flight (TOF) pulsed neutron diffraction. A carbon sample was prepared at Simon Fraser University, Canada (Dahn et al., 1995a) by pyrolyzing epoxy novolac resin (poly[(phenyl glycidyl ether)-co-formaldehyde], Dow Chemical Corp.) cured with phthallic anhydride (Aldrich). The cured monolith was ball-milled to fine powder prior to pyrolysis, which was performed in a tube furnace at 700°C in argon for one hour. Elemental chemical analysis determined

the hydrogen/carbon atomic ratio, H/C = 0.17. Electrochemical testing on a small aliquot of the sample revealed a lithium capacity of 650 mAAh/g. Neutron diffraction data were taken on GLAD. A vanadium can (7/16-in. OD) with an indium gasket seal was used to prevent moisture. Scattering from the instrument and the vanadium can was also measured and removed from the data. A graphite powder sample (Fisher, 1987) was also measured under the same conditions, as a control. Each data set was taken for eight hours. A large background was observed from the amorphous sample due to both incoherent and inelastic scattering from the hydrogen. We used the SUBSLFGLD program to remove the background and obtain the coherent scattering. No resonance was considered in the fitting procedures.

The neutron-weighted structure factor S(Q) (after removal of the background) is plotted in the inset to Figure 4. Only a few broad features can be seen due to the very amorphous nature of the sample. The radial distribution function ($4\pi r^2 \rho(r)$) was obtained from S(Q) via Fourier transformation; the result is plotted in Figure 4 along with that of graphite. A Lorch-weighting factor was used to remove the spurious features due to truncation at 30 $Å^{-1}$. The first peak, found at 1.44 Å, agrees very well with the C-C distance in graphite (1.42 Å). The coordination number (area under the first peak) and bond angle (from the second peak position at 2.47 Å) are 3.1 and 118°, respectively, consistent with an sp^2 type of bonding. The so-called intra-hexagonal peak is found at 2.85 Å, twice the bond length, a signature of planar hexagons. These results indicate that this particular material is remarkably similar to graphite on the length scale <1 nm. The decrease in peak intensities relative to those of graphite is due to small particle sizes. Real space modeling using plain graphite sheets reveals that the average size is around 10-20 Å, which would have 18% at. hydrogen atoms if they were all attached to the edges, consistent with the H/C ratio from the chemical analysis.

Neutron Diffraction Measurements of Imidazolium Chloroaluminates

Mixtures of aluminum chloride, $AlCl_3$, and 1-ethyl-3-methylimidazolium chloride (EMIC) have low melting points (well below room temperature), high electrical conductivity, and high current density of aluminum plating. These properties are strongly affected by the ionic species and the structures of the melts. Previous investigations of these melts have indicated that the major aluminum complex is $AlCl_4^-$ in basic melts ($AlCl_3$<50 mol%) and $Al_2Cl_7^-$ in acidic melts ($AlCl_3$>50 mol%).

Neutron diffraction studies were carried out on GLAD to obtain the structure and configuration of the ionic species. The samples were prepared by mixing highly anhydrous $AlCl_3$ with fully deuterated EMIC in a glove box, where the H_2O and O_2 levels were maintained at less than 2 ppm. The melts were sealed under vacuum in quartz tubes of 1-mm thickness and inner diameter of 3 mm. Four compositions, with 46, 50, 60, and 67 mol%

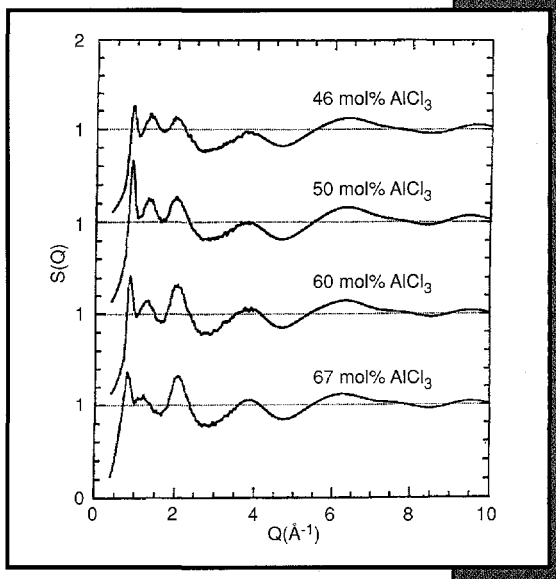

FIGURE 5.
Structure factors of fully deuterated $AlCl_3$-EMIC.

$AlCl_3$, were selected. Measurements were made on each sample at 298 K, followed by a similar measurement on an empty fused silica container of the same dimensions for purposes of instrument calibration and data normalization; measurements were also carried out on a 0.64-cm-diameter vanadium standard and with the spectrometer empty, both at 298 K. The data were analyzed with standard procedures developed at Argonne for glass and liquid diffraction data, incorporating simple corrections for multiple scattering and inelasticity effects.

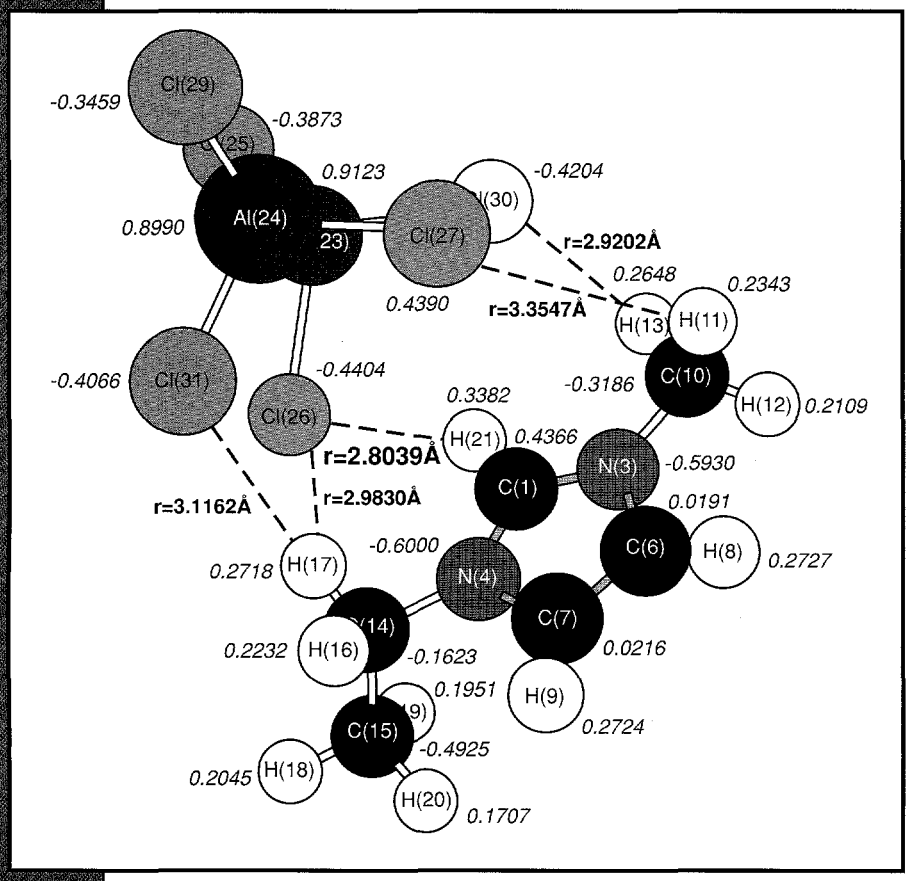

FIGURE 6.
Structure and Mulliken charges of the $Al_2Cl_7^-$ – EMI^+ complex.

Figure 5 shows the structure factors S(Q) measured for the four solutions. These are rather similar over the range $Q > 5A^{-1}$. However, they show differences at relatively low Q, in the range of 1-5 A^{-1}, which must be due to the interactions between the $AlCl_4^-$ and $Al_2Cl_7^-$ anions and the EMI^+ cation.

A better understanding of the structure of these melts can be achieved by combining *ab initio* quantum chemistry calculations with the neutron diffraction data. For the 67 mol% $AlCl_3$ melt, the calculations were carried out on the assumption that $Al_2Cl_7^-$ and EMI^+ were present. The neutron diffraction pattern derived is in good agreement with the experimental one. The structure of the $Al_2Cl_7^-$ and EMI^+ complex is shown in Figure 6.

References

J.L.E. Campbell and K.E. Johnson, Inorg. Chem. **32** (1993), 3809.

J.R. Dahn, A.K. Sleigh, H. Shi, B.M. Way, W.J. Weydanz, J.N. Reimers, Q. Zhong, and U. von Sacken, in: *Lithium Batteries – New Materials, Developments and Perspective*, G. Pistoia, Editor (Elsevier, 1995a).

J.R. Dahn et al., Science **270** (1995b), 590. The single-sheet model was derived from the widths of the (002) and (100) peaks in the X-ray diffraction patterns, using the Scherrer equation.

K.M. Dieter, C.J. Dymeck, N.E. Heimer, J.W. Rovang, and J.S. Wilkes, J. Am. Chem. Soc. **110** (1988), 2722.

C.J. Dymeck and J.J.P. Stewart, Inorg. Chem. **28** (1989), 1472.

J.C. Evans and G.Y-S. Lo, J. Phys. Chem. **70** (1966), 11.

J.E. Fischer, in: *Chemical Physics of Intercalation*, A.P. Legrand and S. Flandois, Editors (Plenum, N.Y., 1987), 59.

C.L. Hussey, Adv. Molten Salt Chem. **5** (1983), 185.

S.R. Nagel, in: *Phase Transitions and Relaxation in Systems with Competing Energy Scales*, T. Riste and D. Sherrington, Editors (Kluwer Academic Press, Boston, Mass., 1993), 259.

R.A. Osteryoung, in: *Molten Salt Chemistry*, G. Mamantov and R. Marassi, Editors (Reidel Publishing, Netherlands, 1987), 329.

A.K. Soper and A. Luzar, J. Chem. Phys. **97** (1993), 1320.

P.C. Trulove and R.A. Osteryoung, Inorg. Chem. **31** (1992), 3980.

J.S. Wilkes and M.J. Zaworotko, Supramolecular Chem. **1** (1993), 191.

T. Zheng, Y. Liu, E.W. Fuller, S. Tseng, U. von Sacken, and J.R. Dahn, J. Electrochem. Soc., (1995), in press.

III Advanced Technical Ceramics

C.-K. Loong, IPNS Division, Argonne National Laboratory

Potential benefits from applications of ceramic materials that utilize their unique properties are enormous. However, as a result of complex processing, alloying, transformation toughening, or composite reinforcement, practical ceramics inherently contain microstructures, defects, interfacial impurity phases, anisotropies, and inhomogeneities. Neutron scattering investigations yield information regarding the atomic organization and dynamics that is crucial to the eventual tailoring of the applied properties. Table 1 lists the major properties of interest to researchers and some recent user programs carried out at IPNS.

I. Lanthanide-Doped Zirconia and Alumina as Catalytic Materials

Zirconia, an active isosynthesis catalyst, is capable of selective conversion of synthesis gas into branched hydrocarbons. High-surface-area zirconia and alumina powders can be used as

PROPERTIES OF INTEREST	
MECHANICAL	*Toughness, Hardness, Strength, Creep Resistance, Residual Stress, Texture*
THERMAL	*Thermal Expansion, Shock Resistance, Refractoriness*
CHEMICAL	*Adsorpency, Catalytic Functions, Corrosion Resistance, Surface Chemistry*
OPTICAL	*Transparency/Dispersion, Luminescence, Photo-Sensitivity, Laser/Waveguide Applications*
ELECTRICAL/MAGNETIC	*Permittivity, Ferro-/Piezo-Electricity, Semi-, Ionic, Photo-, and Superconductivity, Magnetism, Memory Capacity*
BIOMEDICAL	*Bone Compatibility, Enzymatic Reactivity, Sensory Functions, Bioactivity*
MINERALOGICAL	*Crystal Phase and Transformation, Energetics, Thermodynamics, Ecology*

TABLE 1. Properties of Technical Ceramics at IPNS.

promoters and/or support components in automobile-exhaust emission-control catalysts to remove poisonous gases, such as CO, NO_x, and hydrocarbons. Doping lanthanides (Ln) into zirconia to form solid solutions of Ln-Zr is an effective approach to improve the stability of the catalysts at high temperatures. These mixed oxides are partially stabilized to the cubic and tetragonal phases and are free from any disruptive structural transformation over a wide temperature range. In addition, the difference in valency of the cations (Ln^{3+} versus Zr^{4+}) results in oxygen vacancies, which may lead to effective adsorption sites and/or strong metal-support interactions. Masakuni Ozawa (Nagoya Institute of Technology) holds a patent on the use of Ln-ZrO_2 for supporting precious metals in automobile three-way catalytic converters to improve durability and enhance de-NO_x performance. Recently, a series of neutron-scattering experiments were carried out to characterize the microscopic properties of fine Ln-doped zirconia and alumina powders:

1. From powder diffraction studies using GPPD, the crystal structure of high-surface-area (~80 m^2/g) $Ln_{0.1}Zr_{0.9}O_{1.95}$ (Ln = La and Nd) powders prepared by a coprecipitation method was found to be composed of mixed phases of tetragonal and cubic symmetry, which can be stabilized over a temperature range (up to ~1000°C) pertinent to catalytic applications (Ozawa et al., 1995). A real-space correlation function, obtained from a Fourier transform of the filtered residual diffuse scattering,

RECENT USER PROJECTS	
1	*Lanthanide-Modified Zirconia and Alumina (Ozawa and Suzuki, Nagoya Institute of Technology)*
2	*Silicon Nitride (Vashishta and Kalia, Louisiana State Univ.; Ebbsjö, Univ. of Uppsala)*
3	*Sialon and Aluminum Nitride Ceramics (Suzuki and Ozawa, Nagoya Institute of Technology; Kanda, NGK Spark Plug, Inc.)*
4	*$KTa_{1-x}Nb_xO_3$ Electroceramics (Boatner and Christen, Oak Ridge National Lab.)*
5	*Manganese Dioxide Cathode Materials (Thackeray, Argonne National Lab.)*
6	*Carbonate Fuel Cells (Koura and Idemoto, Science Univ. of Tokyo)*
7	*Forsterite and Enstatite (Ghose, Univ. of Washington; Choudhury, Bhabha Atomic Research Center)*
8	*Alunite (Lager, Univ. of Louisville)*
9	*Brucite (Chakoumakos, Oak Ridge National Lab.)*
10	*$Ba_{1-x}K_xBiO_3$ Superconductors (Vashishta and Kalia, Louisiana State Univ.)*
11	*Rare Earth Orthophosphates and Phosphate Glasses (Boatner and Sales, Oak Ridge National Lab.; Nipko, Colorado State Univ.)*

TABLE 1. Recent User Projects at IPNS.

showed evidence of static, oxygen-vacancy-induced atomic displacements along the pseudocubic <111> and other directions (Loong et al., 1994g, 1995c); see Figures 1 and 2.

2. The $\gamma \rightarrow \delta \rightarrow \theta \rightarrow \alpha$ transformations over a temperature range of 450-1300°C in pure and La-doped alumina were examined by in situ powder diffraction on GPPD. The effect of La doping on the up-shifting of the α-Al_2O_3 formation temperature was observed.

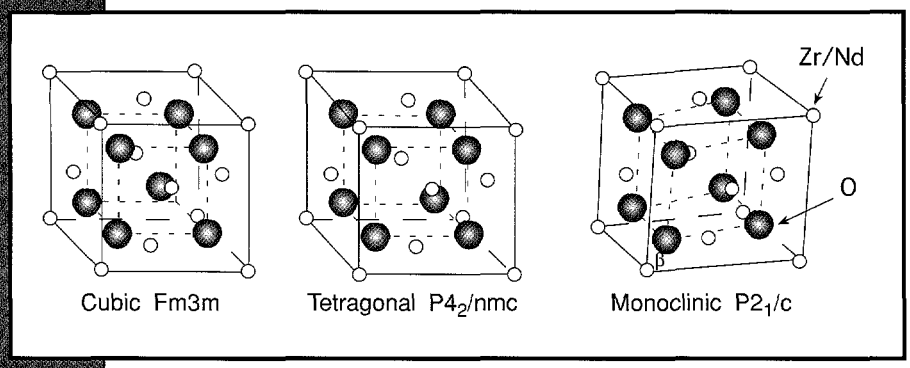

FIGURE 1.
Pure ZrO_2 has three polymorphs: a cubic fluorite structure (space group Fm3m) above 2640 K, a tetragonal structure ($P4_2/nmc$) between 1400 and 2640 K, and a monoclinic structure ($P2_1/c$) below 1400 K. In general, lanthanide-modified ZrO_2 exhibits mixed crystal phases and defects that are sensitive to processes of the synthesis, such as agglomeration in the precursor and heat treatments of the samples.

3. The dynamics of hydrogen atoms associated with the surface hydroxyl groups and adsorbed water molecules on $Ln_{0.1}Zr_{0.9}O_{1.95}$ and pure ZrO_2 over a frequency range of 0-4400 cm^{-1} was investigated by inelastic scattering using HRMECS. The stretch vibrations of surface hydroxyl groups on monoclinic ZrO_2 were found to have slightly higher frequencies than those for $Ln_{0.1}Zr_{0.9}O_{1.95}$. At a submonolayer coverage of water the O-H stretch bands broaden and shift to lower energies. At higher coverage three bands, corresponding to the O-H stretch, H-O-H bend, and librational motion

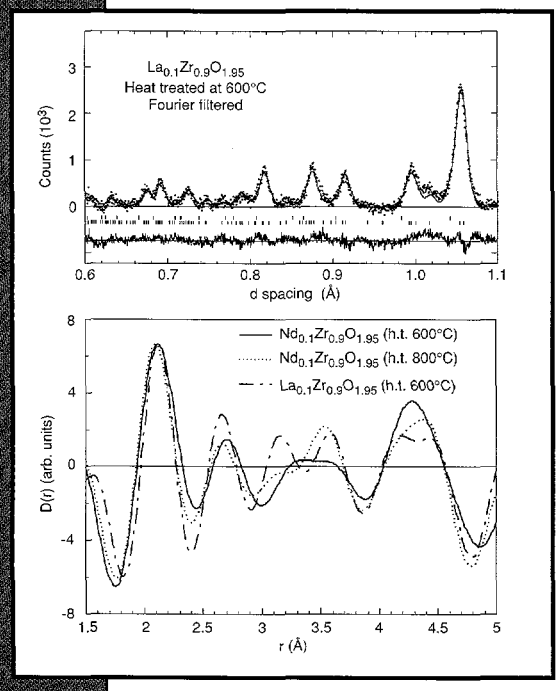

FIGURE 2.
(Top) The crystal structure of high-surface-area $Ln_{0.1}Zr_{0.9}O_{1.95}$ (Ln = La and Nd) powders prepared by a coprecipitation method were found to be composed of mixed phases of tetragonal and cubic symmetry, which can be stabilized over a temperature range (up to ~1000°C) pertinent to catalytic applications.(Bottom) A Fourier filtering technique was employed to examine the short-range defect structure in $La_{0.1}Zr_{0.9}O_{1.95}$ and $Nd_{0.1}Zr_{0.9}O_{1.95}$. The real-space correlation functions obtained show evidence of static atomic displacement along the pseudocubic <111> and other directions, probably due to relaxation of atoms near the oxygen vacancies. Oxygen vacancy sites in the present Ln-ZrO_2 samples play an important role in the removal of NO_x, CO, and hydrocarbons as a support component in a three-way catalytic converter for automobiles.

of water molecules, were observed, indicating the influence of hydrogen bonding (Loong et al., 1995c, 1996c).

4. Microstructural change and crystal growth in Ce- and Nd-doped ZrO_2, as well as in pure ZrO_2 powders, were studied by small-angle scattering using SAD. Different porosities and particle-size distributions were observed for these powders at various heat-treatment temperatures; this may be due to the different oxidation states of Ce and Nd ions.

II. Slip-Cast Sialon Ceramics as High-Temperature, High-Strength Materials

The outstanding high-temperature properties of silicon nitride (e.g., high strength and hardness, low thermal expansion, and superb chemical durability) make these ceramics of interest for applications as high-temperature structural materials. Substituting Al for Si and O for N to form a solid solution of Si-Al-O-N (sialon) adds new opportunities in tailoring material properties to suit different demands for technological applications (see Figure 3). The resulting ceramic alloys often exhibit varying microstructures and behaviors, depending on the processing route. Sialon ceramics as structural materials are usually densified by hot press or hot isostatic press methods. Recently, reaction-sintered sialons, $Si_{6-z}Al_zO_zN_{8-z}$ ($0 \le z \le 6$) ceramics, were fabricated by using aqueous slurries with a novel slip-casting method by Sugura Suzuki and co-workers (Nagoya Institute of Technology). Such a method has an obvious advantage, namely the capability of forming relatively complex shapes by using inexpensive plaster molds. It is desirable to characterize the crystal phases and atomic dynamics in conjunction with the macroscopic properties of these slip-cast sialon ceramic alloys. Such an effort was undertaken in a collaboration between the Nagoya and Argonne teams.

First, the crystal phases of the slip-cast $Si_{6-z}Al_zO_zN_{8-z}$ ($0 \le z \le 6$) ceramics were studied by diffraction measurements using GPPD. A Rietveld analysis of the diffraction patterns shows that samples of $z < 4$ form a single-phase solid solution of Si-Al-O-N isostructural to β-Si_3N_4 (space group $P6_3/m$), known as β-sialons (see Figure 4). Within this structure, there is a consistent preferred occupation of O on the 2c sites and N on the 6h sites. For $z > 4$, the materials exhibit multiple-phase structure, including β-sialon, θ-$Si_3Al_{12}O_9N_{10}$, α-Al_2O_3, β'-$SiAl_4O_2N_4$, and Al_3O_3N phases (Loong et al., 1996a). Second, the generalized

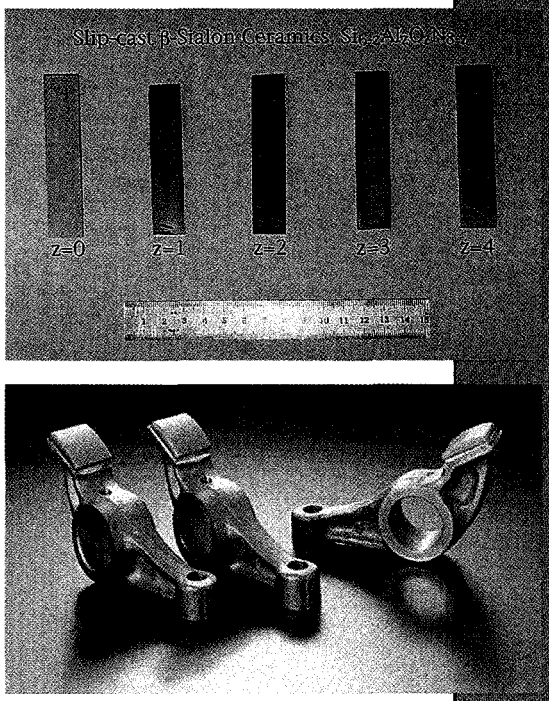

FIGURE 3.
(Top) Sialon ceramic alloys prepared by a slip-cast method at Nagoya Institute of Technology and characterized by neutron scattering at IPNS. Substituting Al for Si and O for N in Si_3N_4 to form a solid solution of Si-Al-O-N (sialon) adds new opportunities for tailoring the properties to suit different demands for technological applications. (Bottom) Rocker arms which are brazed with silicon nitride tips (NTK products) improve wear resistance and help maintain free operation for long periods.

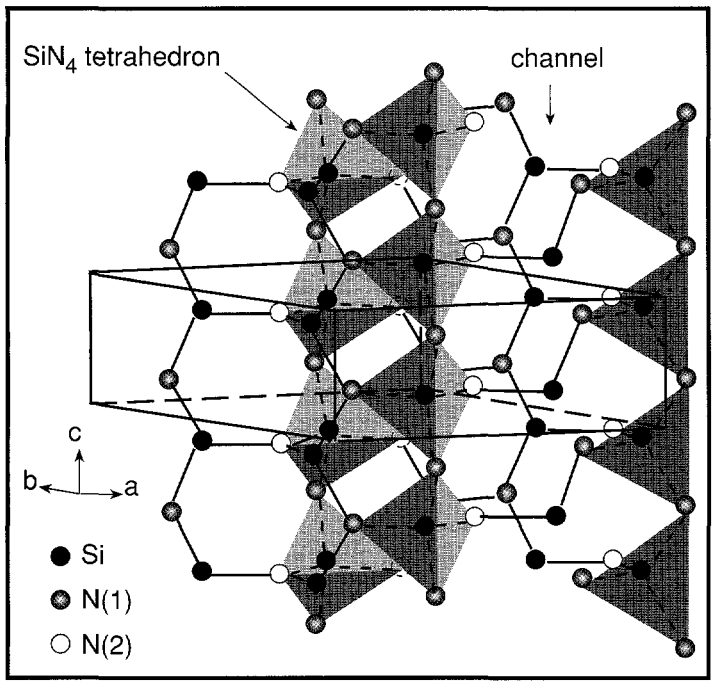

FIGURE 4.
The crystal structure of β-Si_3N_4. Under space group $P6_3/m$, all atoms situate in the mirror planes of heights at 1/4 and 3/4 parallel to the basal plane. Exemplifying SiN_4 tetrahedra chains and a channel running along the c-direction are indicated. The N(2) atoms join three neighboring Si atoms to form a coplanar Si3N unit parallel to the basal plane. β-sialons, $Si_{6-z}Al_zO_zN_{8-z}$ ($0 \le z \le 4$), were found to be isostructural to β-Si_3N_4, but there was a consistent preferred occupation of O on the N(1) or 2c sites and N on the N(2) or 6h sites.

phonon densities of states (PDOS) of the β-sialons were determined by inelastic-scattering experiments using HRMECS. The observed PDOS of the $0 \le z \le 4$ ceramics displays phonon bands at about 50 and 115 meV. These features are considerably broader than the corresponding ones in β-Si_3N_4 powder. As z increases, effects due to atomic disorder lead to an overlap of the two phonon bands and a complete filling up of the phonon gap at ~100 meV (Loong et al., 1996a). The combined characterization by neutron-scattering and mechanical-property measurements indicates that the slip-cast β-sialon ceramics are of comparable quality, in terms of structural integrity and mechanical strength, with other β-sialons prepared by hot press methods.

III. Calcium-Doped Potassium Tantalate Niobate as New Electroceramics for Varistors and Varicaps

The ferroelectric transition temperature of insulating $K(Ta_{1-x}Nb_x)O_3$ (KTN) varies with the Nb concentration, and the character of the transition changes from first order to second order to quantum ferroelectric with increasing x. Recently, high-quality ferroelectric $K(Ta_{1-x}Nb_x)O_3$ compounds with the addition of small amounts (~0.05 mol-%) of Ba, Ca, or Sr were prepared by Lynn Boatner and co-workers at Oak Ridge National Laboratory. The resulting material is a semiconductor with a high room-temperature electrical conductivity (a resistivity of about 0.06 W·cm as compared to 10^{16} W·cm for the corresponding undoped compound); see Figure 5. In sintered Ca-doped KTN ceramics, the semiconducting crystal grains are surrounded by thin insulating grain boundaries. Consequently, both the resistance and the capacitance of the material exhibit a sudden change as the potential barrier at grain boundaries is overcome

by an applied voltage. Devices using these resistance/capacitance vs. voltage characteristics are called varistors and varicaps, respectively.

Normally, neutron, x-ray, or dielectric measurements are suitable to study the properties of ferroelectric materials. However, due to the formation of insulating surface depletion layers in the Ca-doped KTN samples, dielectric measurements will only probe the behavior of the Ca-depleted layer, and x-rays do not have the penetrating power to reach the semiconducting part of the sample. Neutrons are the method of choice for the study of effects of Ca doping on the ferroelectric and structural transitions in KTN. Both single crystals and powders of Ca:KTN were investigated, using the SCD and GPPD diffractometers, respectively. In single-crystal samples of KTN, with and without Ca doping, the orthorhombic-to-tetragonal transitions were compared by monitoring the Bragg-reflection intensities as relief of extinction effects across the phase transition at low temperatures. In pure and Ca-doped $KNbO_3$ powders of controlled grain size (>150 μm) obtained from ground-up crystals, the orthorhombic-to-tetragonal (~230° C) and tetragonal-to-cubic (~430°C) transitions were analyzed by Rietveld refinements. Preliminary results show that both transition temperatures were shifted to slightly lower temperatures in Ca-doped materials (Christen et al., SCD: #2056).

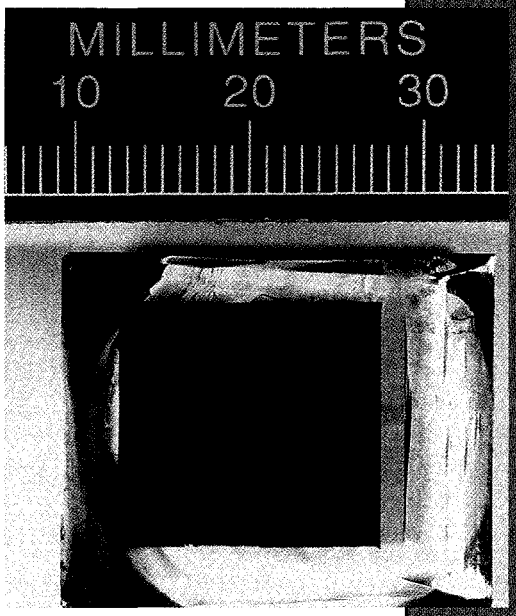

FIGURE 5.
Calcium-doped single crystal of potassium tantalate niobate, showing the dark semiconducting central portion of the crystal that contains the calcium dopant, which is characterized by a resistivity of ~0.06 Ω·cm, and the clear outer region, which is highly insulating (ρ = 10^{16} Ω·cm). Samples of this type are currently being used to investigate the effects of charge carriers on displactive ferroelectric phase transitions.

IV. Molten Alkali Carbonate as Next-Generation Fuel Cell Materials

Molten alkali carbonate is an important electrolyte for the next generation of fuel cells, which show promising efficiency and attractive environmental features. An intensive research effort has been undertaken by Nobuyuki Koura and co-workers at Science University of Tokyo. The design of this type of fuel cells calls for a molten Li_2CO_3·K_2CO_3 mixture as the electrolyte and porous metallic (Ni or Cu) anode and cathode. Electricity is produced from combining hydrogen and oxygen molecules (introduced through the anode and cathode) via the electrolyte, resulting in a release of only water vapor. Important technical issues, such as the relatively high operating temperature (~650°C) and corrosive behavior of the carbonates, have to be addressed immediately. It is known that the melting point, chemical reactivity, and corrosiveness of mixed Li_2CO_3·K_2CO_3 depend on the chemical balance of ionic species such as CO_3^- and

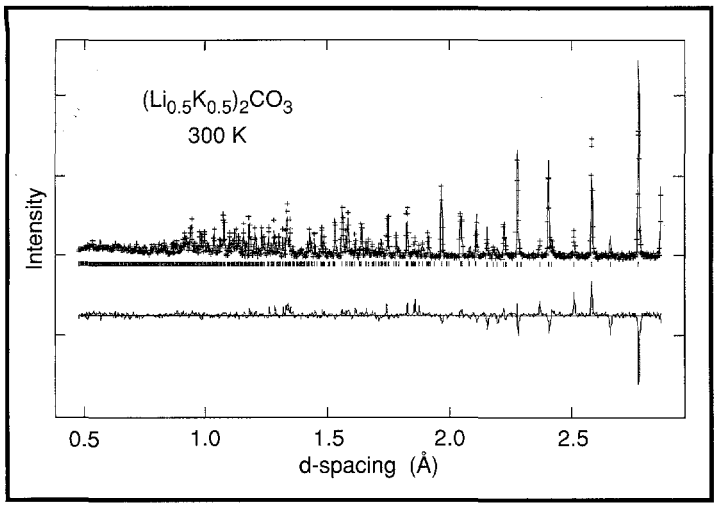

FIGURE 6.
Rietveld profile fit in the 0.5-2.8 Å region of d-spacing for $(Li_{0.5}K_{0.5})_2CO_3$ at room temperature. The symbols (+) are the observed, background-subtracted intensities. The solid line represents the calculated crystalline intensities. The tick marks indicate the positions of the Bragg reflections. The differences between the observed and calculated intensities are shown at the bottom of the figure. The large discrepancy of the large d-spacing reflections is due to absorption by the sample. More measurements using isotopic ^7Li samples have been planned.

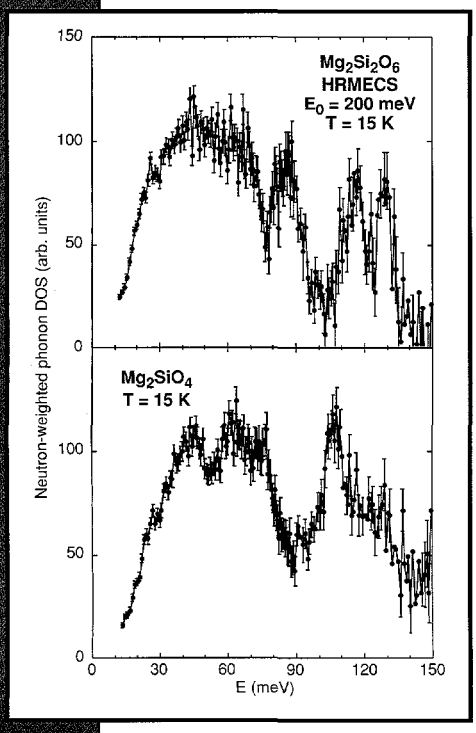

FIGURE 7.
The measured neutron-weighted phonon densities of states of polycrystalline orthoenstatite, $Mg_2Si_2O_6$ (top), and forsterite, Mg_2SiO_4 (bottom). The peak in the 80-100 meV range in the measured spectra of orthoenstatite has contributions mainly from the bridging oxygens and is absent in forsterite.

other metal cations. Neutron-scattering studies of the crystal structure and atomic dynamics in Li_2CO_3·K_2CO_3 solid solution have been conducted, using the GPPD and LRMECS instruments. The goal is to determine the short-range order structure of ionic species in the molten-salt state, eventually using the GLAD diffractometer. Figure 6 shows the powder pattern of a $(Li_2CO_3)_{50}$·$(K_2CO_3)_{50}$ solid solution (Koura et al., GPPD: #2250). A tentative crystal structure was obtained from a Rietveld analysis. This structural information is being used for ab initio molecular-orbital and molecular-dynamics calculations currently being carried out in Japan.

V. Enstatite as an Important Rock-Forming Silicate

Enstatite, the magnesium end-member of orthopyroxenes, which are important rock-forming minerals occurring in terrestrial and lunar rocks and meteorites, is considered to be an important constituent of the earth's upper mantle. It has three polymorphs: proto-, ortho-, and clinoenstatite. The structural building blocks of these minerals are single chains of SiO_4 tetrahedra and double bands of MgO_6 octahedra running parallel to the

crystallographic c-axis. Structurally, the polymorphs are distinguished by their various stacking sequences, which depend on the orientation of the MgO_6 octahedra with respect to the SiO_4 tetrahedra. Because of their closely related structures, the thermodynamic properties of the enstatite polymorphs are expected to be similar. Following a previous experiment on forsterite, Mg_2SiO_4, at IPNS, Subrata Ghose (University of Washington) and Narayani Choudhury (Bhabha Atomic Research Center) have performed similar PDOS measurements for orthenstatite, $Mg_2Si_2O_6$. The principal motivation for the lattice dynamic study is the eventual understanding of the thermodynamic properties as a function of pressure and temperature and the mechanism of phase transitions in this mineral. Figure 7 shows the measured PDOS of orthenstatite. The calculated lattice specific heat, obtained from a phonon model using the neutron data, is in good agreement with experimental values (Narayani et al., HRMECS: #1851).

VI. Rare-Earth Orthophosphates as Scintillators, Laser Crystals, and Magnetic Refrigerants

Rare-earth orthophosphates, RPO_4 (R = rare-earth elements), are known for their outstanding properties. Their high melting temperatures (about 2000°C), structural and chemical stability, and long-term corrosion resistance make these substances attractive for such applications as high-temperature components and nuclear waste storage media. The optical properties of the rare-earth ions in RPO_4 hosts, particularly rare-earth-activated luminescence, have found application in scintillators and phosphors. For example, in 1995, General Electric's lighting division introduced a new, long-life (10,000 h) household light bulb, known as the E-lamp. It employs $LaPO_4:Ce^{3+}$, Tb^{3+} as green phosphors. The lamp produces 75-watt-equivalent light while consuming 23 watts of electrical power. Moreover, cerium-doped $LuPO_4$ is found to be one of the most promising new scintillator materials. The magnetic phase transitions and Jahn-Teller effects associated with some RPO_4 compounds also have prompted many fundamental investigations, as well as suggesting magnetic refrigerant applications.

Mixed natural rare-earth orthophosphates form the minerals monazite (R = La-Gd) and xenotime (R = Tb-Lu). Pure crystalline forms of these compounds can be synthesized by controlled precipitation techniques, and single crystals can be grown by means of flux methods (see Figures 8 and 9). For over a decade, high-purity

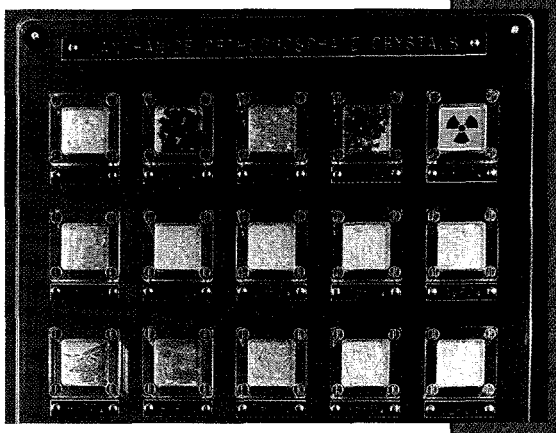

FIGURE 8.
Lanthanide orthophosphate crystals grown by L.A. Boatner and J.O. Remey (Oak Ridge National Laboratory). These crystals are known for their outstanding properties. However, puzzlingly different magnetic and optical behavior is often found in orthophosphates containing different rare-earth elements. The neutron study provides a basic understanding of many important thermodynamic properties, including magnetic susceptibility, specific heat, saturated magnetization, anomalous thermal expansion, and atomic migration and vibrations. It is hoped that the knowledge gained from systematic investigations will lead to the eventual development of new phosphate materials with properties tailored to advanced technological applications.

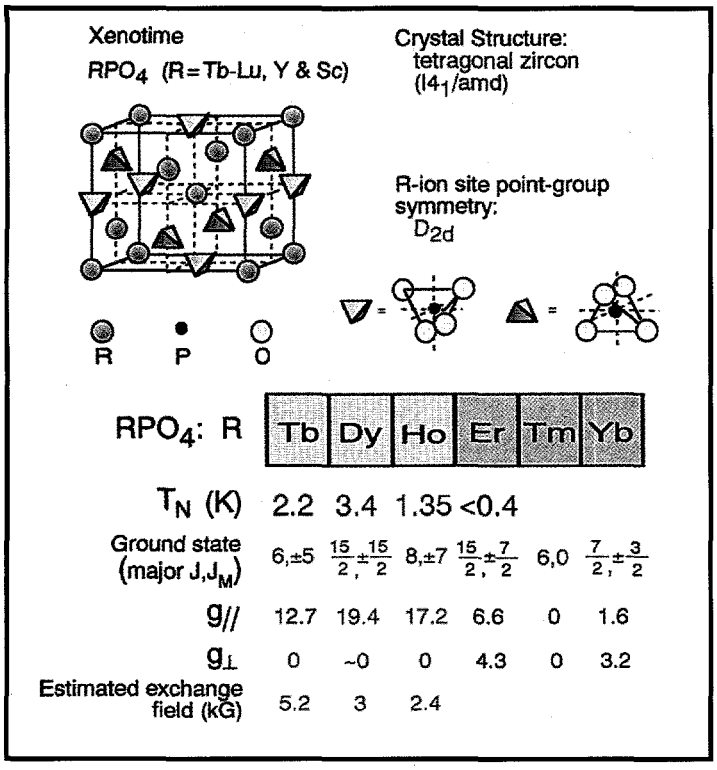

RPO_4: R	Tb	Dy	Ho	Er	Tm	Yb
T_N (K)	2.2	3.4	1.35	<0.4		
Ground state (major J,J_M)	$6,\pm5$	$\frac{15}{2},\pm\frac{15}{2}$	$8,\pm7$	$\frac{15}{2},\pm\frac{7}{2}$	$6,0$	$\frac{7}{2},\pm\frac{3}{2}$
$g_{//}$	12.7	19.4	17.2	6.6	0	1.6
$g_{\perp}$	0	~0	0	4.3	0	3.2
Estimated exchange field (kG)	5.2	3	2.4			

FIGURE 9.
(Upper portion) The unit cell of xenotime, which contains four formula units of RPO_4. (Lower portion) The Néel temperatures, JM of the major components $|J,M>$ in the ground-state wavefunctions, spectroscopic splitting g-factors of the ground state (// and ⊥ denote the magnetic field directions parallel and perpendicular to the c-axis, respectively), and the exchange field strength estimated from a molecular-field approximation.

RPO_4 compounds have been prepared and their chemical and physical properties characterized by Lynn Boatner and Marvin Abraham and co-workers at Oak Ridge National Laboratory. Recently, a systematic neutron-scattering study of the rare-earth energy levels and wavefunctions and possible interactions between f-electrons and the crystalline lattice in RPO_4 compounds was initiated at IPNS. It is hoped that the knowledge gained from these investigations will lead to the eventual development of new phosphate materials with properties tailored for advanced technological applications.

The rare-earth crystal-field split-level structure and the symmetry of the wavefunctions of six xenotime compounds are shown in Figure 10. They were derived from analyses of the observed energies and intensities of magnetic transitions, using a crystal-field (CF) model. The neutron results provide a means to calculate important magnetic properties, such as the paramagnetic susceptibility, specific heat, saturated magnetization, and effective exchange fields, permitting a direct comparison with experimental data (Loong et al., 1993c, 1993d, 1993e, 1993f, 1994d, 1994e).

In some RPO_4 compounds, strong rare-earth spin-lattice interaction produces two major effects: (1) a coupling of the elastic energy of the rare-earth subsystem with the lattice results in anomalous thermal expansion and elastic properties, and (2) a coupling of the rare-earth electronic states with optical phonons results in mode-mixing of CF-phonon excitations and relaxation. For example, diffraction measurements using GPPD reveal an anomalous temperature dependence of the lattice parameters of $HoPO_4$ and $HoVO_4$. Starting from room temperature, the lattice parameters decrease with decreasing temperature. But in $HoPO_4$, the basal-plane lattice parameter a reaches a minimum at about 100 K and then actually increases with

decreasing temperature. In $HoVO_4$, this anomaly occurs in the lattice parameter c instead of a. The magnetic origin of these anomalies is confirmed by similar measurements of the lattice parameters of nonmagnetic $LuPO_4$ and $LuVO_4$ compounds, where no anomaly is found. The situation is illustrated in Figure 11, where the magnetic contribution to the relative change in the lattice parameters for $HoPO_4$ and $HoVO_4$ is shown as a function of temperature. The anomalous behavior in thermal expansion coincides with the temperature dependence of the Ho^{3+} ion quadrupole moments in both compounds. The opposite behavior of the thermal expansion along the a- and c-axes between $HoPO_4$ and $HoVO_4$ is due to the opposite sign of the corresponding B_0^2 CF parameters. Neutron magnetic-scattering results indicate that $HoPO_4$ has a 98% pure $|8,7\rangle$ doublet Γ_5 ground state, whereas $HoVO_4$ has a 90% pure $|8,0\rangle$ singlet Γ_1 ground state. The difference in the ground and low-lying states' wavefunctions yields contrasting low-temperature magnetic anisotropy with respect to the c-axis and basal plane in these two compounds (Skanthakumar et al., 1995a, 1995b, 1995c). Strong CF-lattice strain coupling has also been observed recently in the elastic constant anomaly in $YbPO_4$ at low temperatures (Nipko, GPPD: #1967).

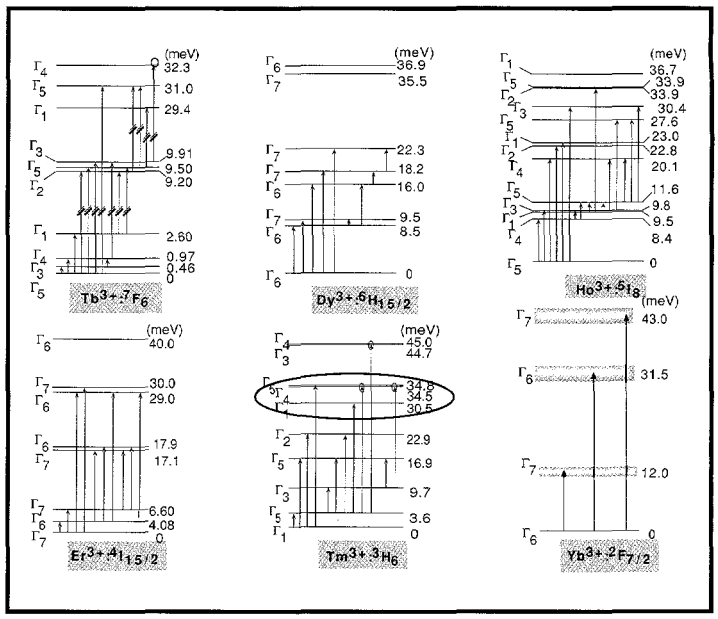

FIGURE 10.
A summary of the crystal-field (CF) structure of the six RPO_4 compounds. The arrows represent the observed CF transitions. In particular, the Γ_1 and Γ_4 states in $TmPO_4$ were clearly observed by neutrons, whereas they were missing in the Raman data. We found no anomalies in either the positions or intensities. Therefore, other workers' proposed decay mechanism through coupling to optical phonons can be ruled out entirely. The difficulty in observing these states in electronic Raman scattering must be related to the complexity of the theoretical calculation of two-photon processes.

VII. Lead-Indium-Phosphate Glasses as Optical Fibers

An important question in glass science is how the chemical durability and thermomechanical behavior of a glassy system change as a function of composition. The structure of vitreous P_2O_5 is thought to consist of a three-dimensional network of corner-sharing PO_4 tetrahedra, each of which is decorated with a nonbridging P=O bond. As M_2O (M = network-modifying elements, such as alkali and transition metals) is added to form a binary glass of composition $xM_2O+(1-x)P_2O_5$, a structural transformation from a 3-D network of P_2O_5 (x = 0) to a complex chain structure takes place through the generation of additional nonbridging oxygens. The

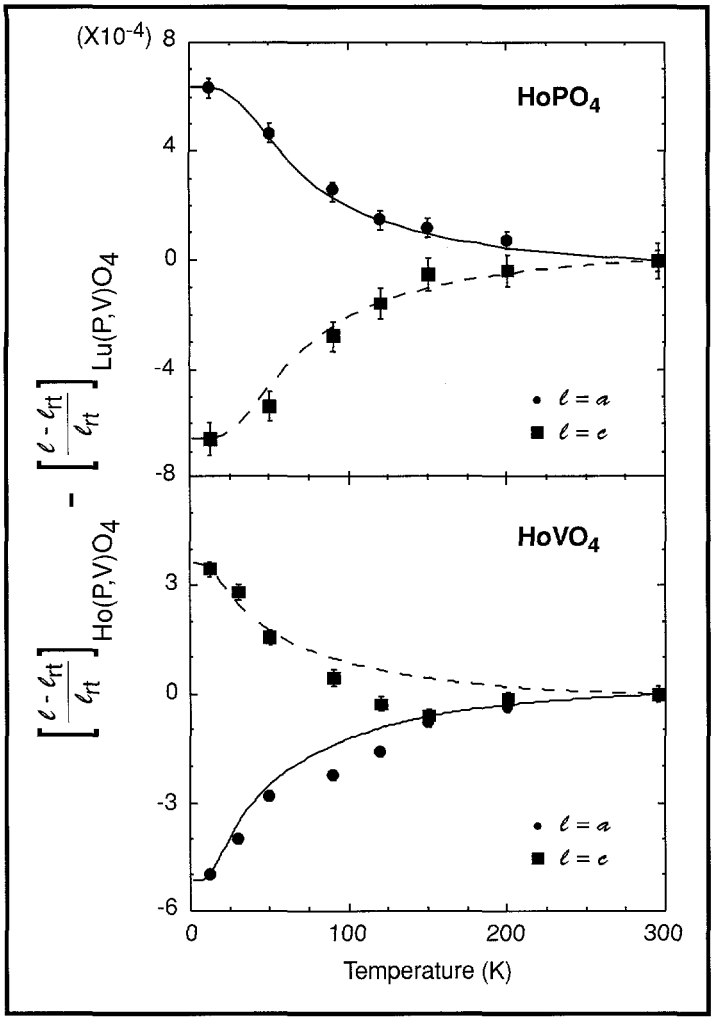

FIGURE 11.
The magnetic contribution to the relative change in the lattice parameters as a function of temperature for $HoPO_4$ and $HoVO_4$. The magnetic contribution is obtained by subtracting the relative change in the lattice parameters of the corresponding lutetium compounds. The lines represent the calculated quadrupole moment of the Ho^{3+} ion normalized to the data at 12 K (see text).

addition of metal ions into a phosphate glass may significantly modify the bonding between networking atoms, so that a rich variety of glasses of varying properties results. Table 2 lists some examples of varying properties of phosphate glasses and their potential applications. Understanding the correlation between the structural modifications induced by various metal-oxide additives and the physical and chemical properties represents one of the most important aspects of materials research on phosphate glasses.

Among the two-component phosphate glasses, lead-phosphate glasses have been studied extensively. Although the low softening temperature and melt viscosity of lead-phosphate glasses are attractive from the point of view of materials preparation, the relatively poor chemical durability when exposed to aqueous conditions was a major drawback to commercial utilization. Over the years, Brian Sales and Lynn Boatner of Oak Ridge National Laboratory have found that by adding a small amount (<10 wt %) of iron oxide, the resulting dark-brown ternary Pb-Fe-P glasses show a dramatic improvement in chemical durability without significantly raising the preparation temperature or the melt viscosity. In searching for an equally durable but optically clear glass, they have identified two useful candidates, Pb-In-P-O and Pb-Sc-P-O glasses. These glasses have an index of refraction of 1.75-1.83 in the visible region, an ultraviolet absorption edge at a wavelength near 300 nm, and strong infrared absorption beyond 2800 nm. The preparation temperatures are relatively low (900 to 1000°C), and the

PHOSPHATE GLASS EXAMPLES	
COMPOSITION	*Offer extremely wide range of compositions; possible to tailor chain-like polymeric structure, e.g., metaphosphate glasses; fibers*
PREPARATION TEMPERATURE	*Low, e.g., for Pb-In-P-O glass, T_{melt}=900°C, T_{pour}= 800-900°C, T_g=436°C, and T_{soft}=459°C; castable Pb-Sn-F-P glass lenses*
CHEMICAL DURABILITY	*Poor, but can be strengthened dramatically by incorporation of modifier oxides; e.g., Fe_2O_3, PbO, N, etc.*
THERMAL EXPANSION	*High, e.g., alkali-alkaline earth P-glass: 10-20 x 10^{-6}/C° for glass-to-metal seals*
ELECTRICAL CONDUCTIVITY	*e.g., AgI-Ag_2O-P_2O_5 glasses have $\rho \sim 10^{-3}$ to 10^{-2} $\Omega^{-1}cm^{-1}$*
INDEX OF REFRACTION	*High, 1.49-1.84*
DISPERSION	*Moderately low n_2 (nonlinearity), e.g., Pb-In-P-O glass: Abbe no. = 30*
UV TRANSPARENCY	*Higher energy excitations of the bridging O (9.5 eV) and nonbridging O (7.8 eV) lead to superior UV transparency*
STIMULATED EMISSION	*Large cross section (e.g., Nd^{3+}) due to narrow linewidths, large transition probabilities, and high refractive index; high spectral homogeneity permits high-average-power laser application*
SURFACE CHEMISTRY	*Hydrophilic, nonmisting surface; e.g., lenses for marine application*
NUCLEATION AND CRYSTAL GROWTH	*Controlled formation of randomly oriented or unidirectionally crystallized glass-ceramics, e.g., glass-ceramics for nuclear waste disposal; hydrogen-filled BPO_4 "gas-ceramic"*
BIOCOMPATIBILITY AND BIOACTIVITY	*Capable of bonding to living bone by glass formation of a Ca-P-rich surface film, e.g., Bioglass®, hydroxyl apatite (Ca_2PO_4OH)*

TABLE 2. Some examples of varying properties and applications of phosphate glasses.

chemical durability and resistance to both weathering and γ-radiation are good (see Figure 12). The length distribution of the PO_4 tetrahedral chains in Pb-In-P-O and Pb-Sc-P-O glasses was determined by a novel liquid chromatographic technique. These PO_4 chains are held together by bonds connecting the nonbridging O of the tetrahedra and the metal cations. In a recent collaborative study between Oak Ridge and Argonne, a neutron-diffraction study of the short-range atomic order in a Pb-In-O glass was carried out to make an identification of the In-O and Pb-O spatial coordination (Suzuya et al., 1996).

The neutron experiment was carried out using the GLAD diffractometer at IPNS. The use of cold-to-epithermal neutrons in conjunction with the large solid-angle coverage of the position-sensitive detectors on GLAD permits simultaneous measurements of coherent scattering from the sample over a wide range of wavevectors. Overlapping data sets from different detectors are combined, normalized to the incident flux, corrected for absorption, multiple scattering, and self-scattering, and then merged to obtain the structure factor S(Q). Figure 13 shows the neutron intensity spectra, I(Q), observed at two typical scattering angles of 27.5° and 92.5°, where strong absorption due to resonances of the ^{115}In nuclei at 1.46 and 3.86 eV was seen separately at 12.5 and 20 Å^{-1}, respectively. This makes it straightforward to identify the portions affected by the resonances and to avoid including them in the merged data set. As a result, the structure factor S(Q) can be obtained over a Q range of 0.5 to 25 Å^{-1}. This large Q range is essential to an accurate assessment of the near-neighbor atomic correlation in a glass.

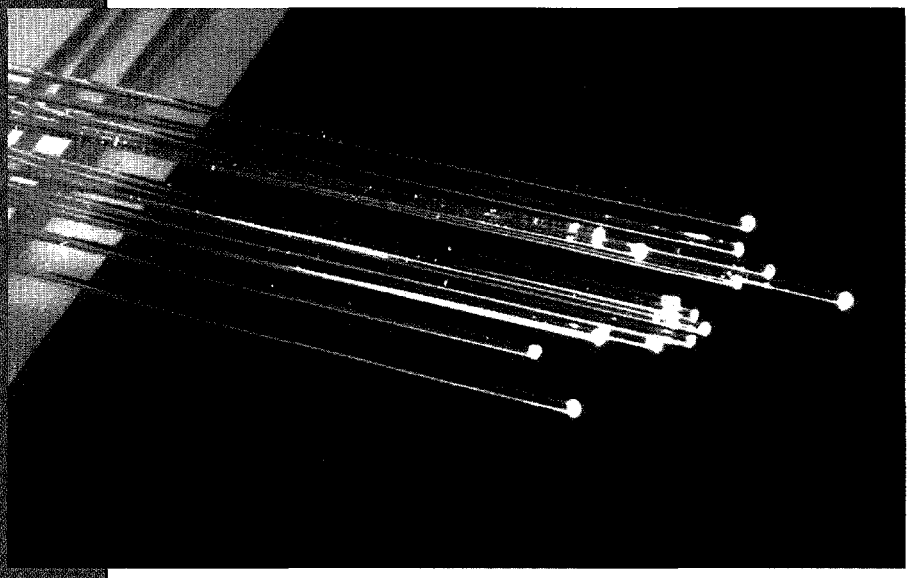

FIGURE 12.
High-numerical-aperture optical fibers drawn using a lead-indium-phosphate glass core and a calcium phosphate glass cladding developed at Oak Ridge National Laboratory.

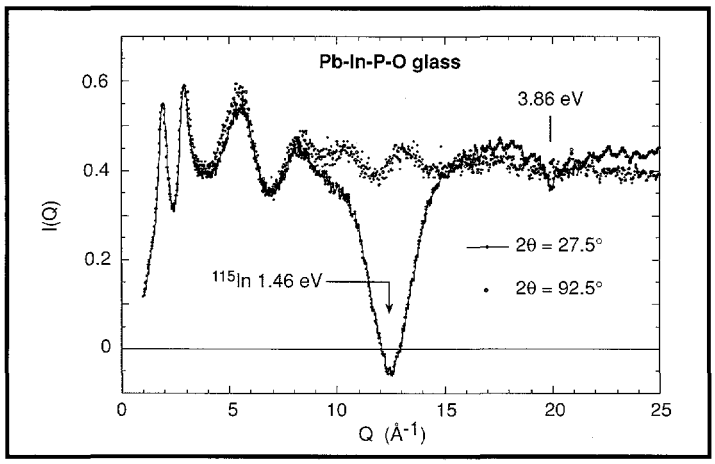

FIGURE 13.
The neutron-intensity spectra of Pb-In-P-O glass observed at scattering angles of 27.5 and 92.5°. In the 27.5° spectrum, resonances of the ^{115}In nuclei in the glass result in a depletion of intensity at 12.5 and 20 Å^{-1}. These resonances occur at much higher Q (>35 Å^{-1}) in the 92.5° spectrum.

Figure 14a displays the total distribution functions T(r) of Pb-In-P-O and pure P_2O_5 glasses. The peak centered at ~1.55 Å corresponds to the mean nearest P-O distance, as observed in the diffraction data of many phosphate glasses. The peak at ~2.5 Å in the T(r)of the Pb-In-P-O glass includes

a major contribution from the nearest O-O correlation as well as the Pb-O correlation. For $Q > 7$ Å^{-1}, the peak maxima in the S(Q) of pure v-P_2O_5 and the present Pb-In-P-O glass coincide. The main difference in the high-Q data between the two glasses is that the widths of the oscillations in S(Q) are somewhat sharper in pure v-P_2O_5. This indicates that, besides a narrower distribution of bond lengths and bond angles in pure v-P_2O_5, the short-range (r < 3 Å) P-O and O-O spatial correlations in these two glasses are similar. Therefore, the effects of structural modification by the metal cations occur mainly in the medium-range ordering. The residual T(r), obtained by subtracting the fitted gaussian functions for the T(r) of the P-O glass from the of the Pb-In-P-O glass, is shown in Figure 14b. This reveals two broad peaks that may be attributed to In-O and Pb-O correlations at about 2.1 and 2.5 Å, respectively, for the lead-indium-phosphate glass.

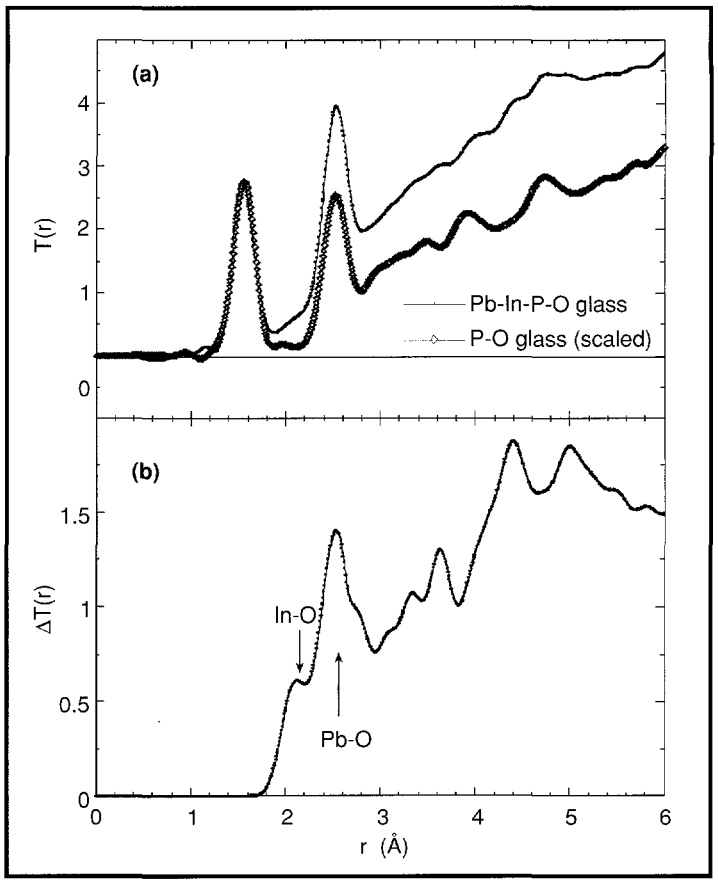

FIGURE 14.
(Top) The total distribution functions of Pb-In-P-O and P-O glasses. The T(r) of the P-O glass was scaled by a normalization factor of 0.6 so that both curves cover the same area under the first P-O peak. (Bottom) The residual T(r) obtained by subtracting the fitted gaussian functions for the P-O glass from the T(r) of the Pb-In-P-O glass. Small oscillations at r < 2 Å due to truncation errors in the Fourier transformation were ignored.

The combined neutron-diffraction data on pure v-P_2O_5, $(PbO)_{59}(P_2O_5)_{41}$, and Pb-In-P-O glasses, in conjunction with the liquid chromatographic results on lead-phosphate glasses, confirm that the major structural modification on the introduction of metal cations in phosphate glasses occurs in the medium range involving the PO_4 chains. The work has now been extended to lanthanide-bearing Pb-In-P-O glasses in which rare-earth-activated luminescence is of crucial importance to the development of high-performance fiber-optic devices.

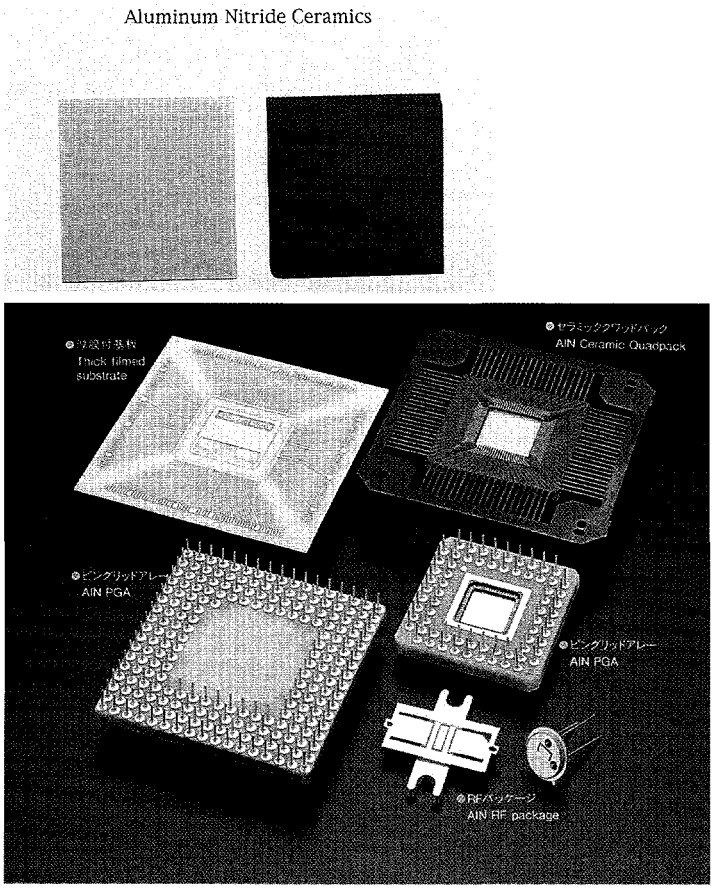

FIGURE 15.
(Top) Sintered AlN ceramics with (black) and without (white) TiN doping, prepared by NGK Spark Plug Co., Japan, and characterized at IPNS. (Bottom) High-density IC packages and multilayer substrates made with aluminum nitride ceramic components (NGK products).

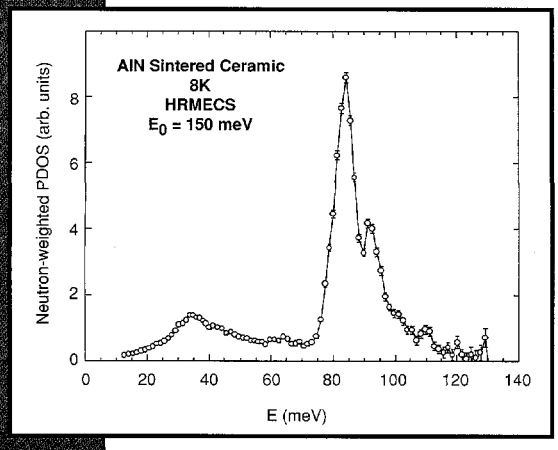

FIGURE 16.
The observed neutron-weighted phonon density of states of sintered AlN ceramic (no TiN doping).

VIII. Aluminum Nitride as a Substrate for High-Density Electronics Packages

The unique properties of aluminum nitride have attracted keen attention from materials scientists in recent years. It has a thermal conductivity comparable with those of most conductive metals (e.g., Al) and much greater than those of typical ceramics (~5 times that of alumina). The high electrical resistivity, good dielectric strength, a thermal expansion coefficient closely matching that of silicon, and lack of toxicity (like that associated with BeO) of AlN are ideal in heat-dissipating substrates for microelectronics applications (see Figure 15). Furthermore, AlN has high strength (a flexural strength equivalent to alumina), high temperature stability, and corrosion resistance. Therefore, "high-tech" AlN components can potentially be used under extreme conditions. In metals, heat is carried primarily by electrons, whereas in nonmetals such as AlN, heat is carried primarily by phonons. Therefore, determination of the phonon excitation spectra of AlN is a fundamental step toward the understanding of the thermophysical behavior of these materials.

In general, thermal conductivity of a solid depends on the microstructure and impurities within the system. Therefore, it is desirable to perform neutron-scattering measurements on well-characterized, sintered AlN ceramics. In a collaboration with Atsushi Kanda of NGK Spark Plug Co. and with Ozawa and Suzuki at Nagoya, neutron diffraction and inelastic experiments were conducted on sintered AlN ceramics, with and without TiN doping, for which mechanical, electrical, and thermodynamic properties had been determined. The generalized PDOS of these materials was measured using the HRMECS chopper spectrometer. The one-phonon DOS exhibits relatively sharp bands at about 33, 63, 83, and 91 meV (see Figure 16). In addition, distinct multiple-phonon excitations were observed up to ~300 meV. The neutron spectra are being compared with results of molecular-dynamics simulations and lattice-dynamics model calculations (Loong, 1996b).

III

The Structure and Dynamics of Zeolite Frameworks and Adsorbates

F. R. Trouw and J. W. Richardson, Jr., IPNS Division, Argonne National Laboratory

Zeolites represent an intriguing class of materials composed of infinite networks of silicon and aluminum atoms, interconnected by oxygen atoms. The crystals of such materials often contain significant void space consisting of open cages and/or cylindrical pores. The aluminum and silicon are four-coordinate, which means in practice that charge-compensating cations are present in the void space to take into account the fact that aluminum is usually three-coordinate.

The void space in such compounds provides a large effective surface area, and the aluminum in the framework acts as a reaction center, resulting in catalytically active materials. Furthermore, the products of reactions inside the void space must conform to the space and shape limitations imposed by the crystal structure. For these reasons, zeolites have been in use as shape-selective catalysts in the chemical industry for the last 40 years.

Active research in the area of molecular sieve materials continues, ranging from the search for novel materials to the modeling of zeolite frameworks and adsorbates. There has been an

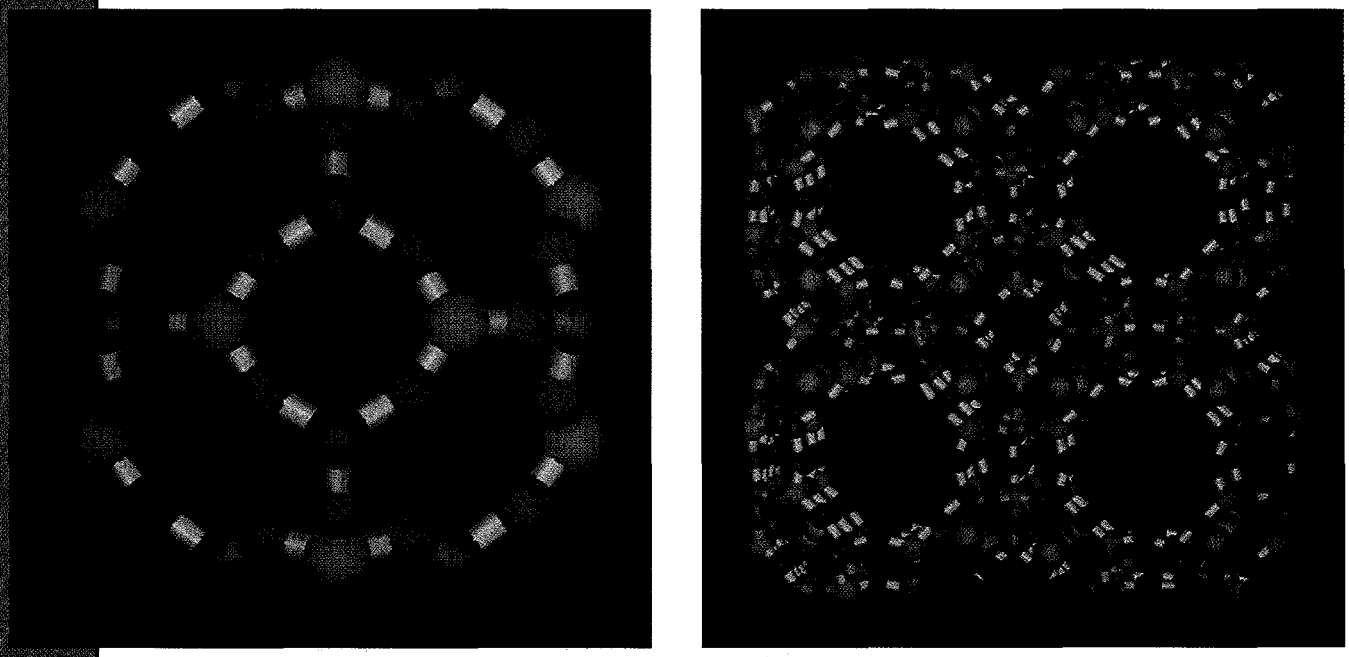

FIGURE 1.
(Left) Basic sodalite building block and (right) a view of a simulated cell of Ca-A zeolite at 300 K. Note the positions of the calcium ions (blue) on either side of the six-ring units.

active program of research in molecular sieves at IPNS for the last decade. Here, we present some recent results of a combined diffraction, inelastic scattering, and molecular dynamics (MD) simulation study of some of the Type-A zeolites.

The typical framework structure of the Type-A zeolite is shown in Figure 1, together with the basic sodalite cage building block. The sodalite cage (β-cage) is composed of six 4-ring and eight 6-ring units (the oxygen is ignored in this type of description), and the unit cell of the Type-A zeolite consists of eight of these building blocks interconnected via the 4-rings. This arrangement of building blocks gives rise to a larger cage at the center of the unit cell, which is referred to as the α-cage. This larger cage is accessible through the 8-ring openings created at the junction of the sodalite building blocks, while the β-cage is only accessible via a 6-ring or 4-ring opening.

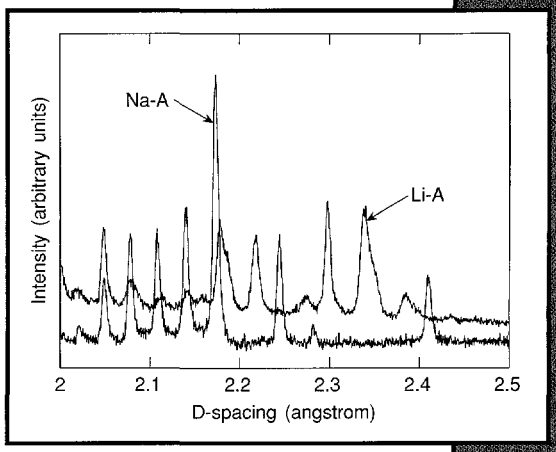

FIGURE 2.
Selected region of the diffraction patterns of Li-A and Na-A as measured on the GPPD diffractometer at IPNS.

The charge-compensating ions have been found at characteristic sites in the cages. There are basically three sites favored by such ions, and they are associated with the three different types of ring units found in the framework. For sodium and potassium, all ions are located in the α-cage, distributed over the 4-, 6-, and 8-ring sites. For the 4-ring sites, the ions are located off the surface, close to the 4-ring. For the 6-ring site, the sodium ion is located close to the plane of the ring, while the potassium projects more into the α-cage, as is to be expected for a larger cation. Both cations are located in the plane of the 8-ring, but off-center in order to maximize the favorable interaction between the cation and the framework oxygens.

Although the Type-A zeolites represent a well-characterized series of compounds, they are still interesting from several points of view. Some unanswered questions remain related to the structure of Li-A zeolite and the structure of Type-A zeolites containing ionic salts in addition to the charge-compensating cations (e.g., a mixture of Li, K, and Cl ions held within the zeolite-A framework). In addition, the vibrational spectroscopy of adsorbed water is still an area that has not been adequately explored by means of inelastic neutron scattering, and the vibrational spectroscopy of water in conjunction with ionic clusters represents completely new science. In particular, the competitive interactions in the ionic clusters themselves, the effect of the framework, and the selective hydration of particular species represent excellent opportunities for studying such clusters in a well-defined environment. Here, we attempt to provide a snapshot of such work, which is currently in progress at IPNS.

The first question that arose in this study involved the structure of Li-A zeolite, which is different from, for example, K-A, Na-A, and Ca-A. This difference can be readily appreciated from the dramatic differences in the neutron diffraction patterns for Li-A and Na-A as measured on GPPD (see Figure 2). The Li-A pattern demonstrates that the structure has a lower symmetry than is found for most of the other charge-compensating cations. Because lithium

is considerably smaller, it is possible that the ion is located off the center of the six-ring, as is found for the larger cations in the 8-rings. However, this would not change the symmetry of the structure; these locations of the lithium cations would still have a three-fold symmetry in the plane of the 6-ring.

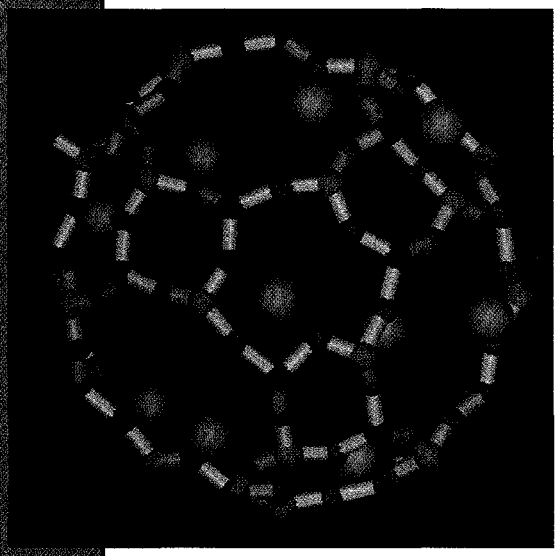

FIGURE 3.
Location of a lithium ion in the plane of a six-ring, as predicted by a molecular dynamics simulation. Note the off-center location of the cation and the resulting distortion of the ring, which removes the three-fold symmetry usually associated with this site.

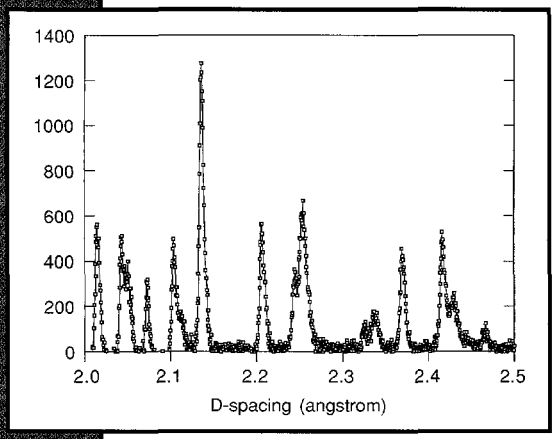

FIGURE 4.
Diffraction pattern of a Li,K,Cl-A zeolite, as measured on the GPPD diffractometer at IPNS.

At this point, a molecular dynamics simulation model developed at IPNS provides further insight into the structure of the Li-A zeolite. The likely explanation for the lower symmetry is illustrated in Figure 3. The high charge-to-radius ratio for the lithium cation is well known, and the simulation model predicts that this causes a characteristic distortion of the framework 6-ring, as the cation pulls in two of the framework oxygens to create a "pocket" with a very favorable lithium-oxygen coordination. This insight is the reason for the lowering of the symmetry in Li-A, as the three-fold symmetry at the 6-rings is lost, reducing the space group symmetry from cubic Fm3c to tetragonal I4/mcm. This suggestion was verified by Rietveld refinement of the Li-A diffraction data. From refinements in I4/mcm, Li ions are found off the centers of the 6- and 4-rings as well as the 8-rings, being in the latter two cases (4- and 8-rings) preferentially associated with pairs of oxygens linked to a common aluminum atom.

In addition to the work on Li-A, diffraction measurements have been extended to more complex systems. An example of a moderately more complex system is Li,K,Cl-A, where in addition to the charge-compensating cation, there is also an ionic cluster present in the cages. In such mixtures, the differentiation between charge-compensating cations and additional cations becomes artificial, but it is still possible to identify which cations bond to the classical 4-, 6-, and 8-ring sites. An example of a diffraction pattern from $Li_{120}K_{40}Cl_{64}$ $Si_{96}Al_{96}O_{384}$ as measured on GPPD is shown in Figure 4. Again, the pattern is complex, which is not surprising in light of the experience with Li-A. However, the material consists of two phases, possibly indicating a preference for a particular stoichiometry in the presence of the extra ions. The analysis of these complex mixtures is still underway, in conjunction with MD simulations; a preliminary MD result for this Li,K,Cl-A mixture is shown in Figure 5. Detailed inspection of the results shows that the chloride ions are closely associated with the lithium cations, which are located on the framework surface and in the cluster, and the chloride ions bridge two or more cations

to form chains of coordination. The potassium cations are predominantly located on the framework surface, but they are still coordinated with the chloride anions. These results reveal a small part of the wealth of information on the behavior of ionic clusters subjected to a periodic external field, in addition to providing basic information relevant to understanding the siting of ions in complex mixtures, which is in turn relevant to the macroscopic behavior of such materials.

A fundamental question that always arises regarding the predictions of theoretical simulation methods is the correctness of the model. As an integral part of the structural study of these Type-A zeolites, the predictions of this model have been compared with the structures of Na-, K-, and Ca-A zeolites known from X-ray single-crystal diffraction studies. What this comparison entails, for the MD simulation model, is an adjustment of the potential describing the interaction of the charge-compensating cation with the framework. This potential consists of two parameters (Lennard-Jones 12-6 form): the size of the cation and a parameter describing the strength of the potential. The siting of the charge-compensating cations is quite different for these three Type-A zeolites, and the location and occupancy (as determined by the simulations) represent a demanding test of the computational model. As is found experimentally, the simulations predict that all the calcium cations lie on either side of the 6-ring units, while the sodium cations are distributed over all three types of rings. Moreover, the predicted occupancies are also in excellent agreement with experimental data (for example, the occupancies for Na-A in the 4-, 6- and 8-rings are 64, 24, 5 from the simulation and 62.2, 23.2, and 6.3 from the experiment, with the simulation having three cations in the (1/4, 0, 0) position).

Having established excellent agreement between theory and experiment on the basis of position and occupancy, it would appear that the model is satisfactory. However, the neutron data provide a further stringent test of the computational model. The neutron powder diffraction profile can be readily extracted from the theoretical model. The resulting comparison for a small part of the profile, as shown in Figure 6, reveals a significant discrepancy between theory and experiment. On the basis of the magnitude of the contribution from the different atoms in the zeolite model, the main differences arise from peaks with a large oxygen contribution. Although

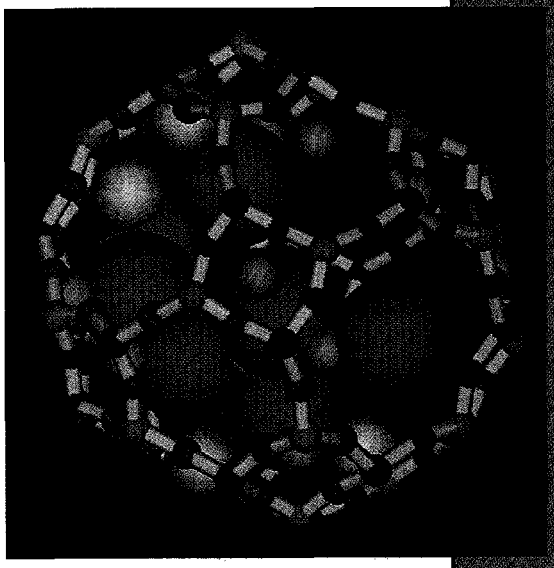

FIGURE 5.
Snapshot of the contents of a α-cage for the Li,K,Cl-A zeolite, from a molecular dynamics simulation. Lithium is shown as blue; potassium, yellow; and chlorine, purple.

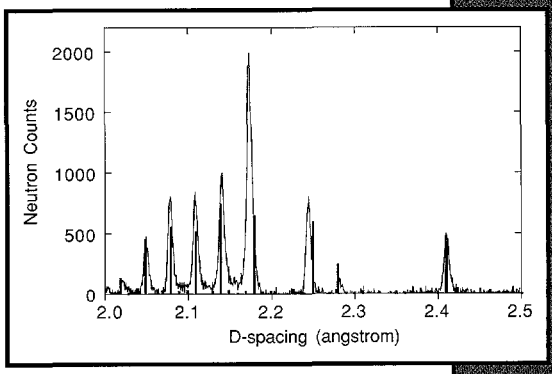

FIGURE 6.
Diffraction patterns of Na-A, as measured on GPPD, are directly compared with the pattern predicted by simulation. The relative normalization is arbitrary, but the predicted intensity at about 2.175 Å is clearly too low.

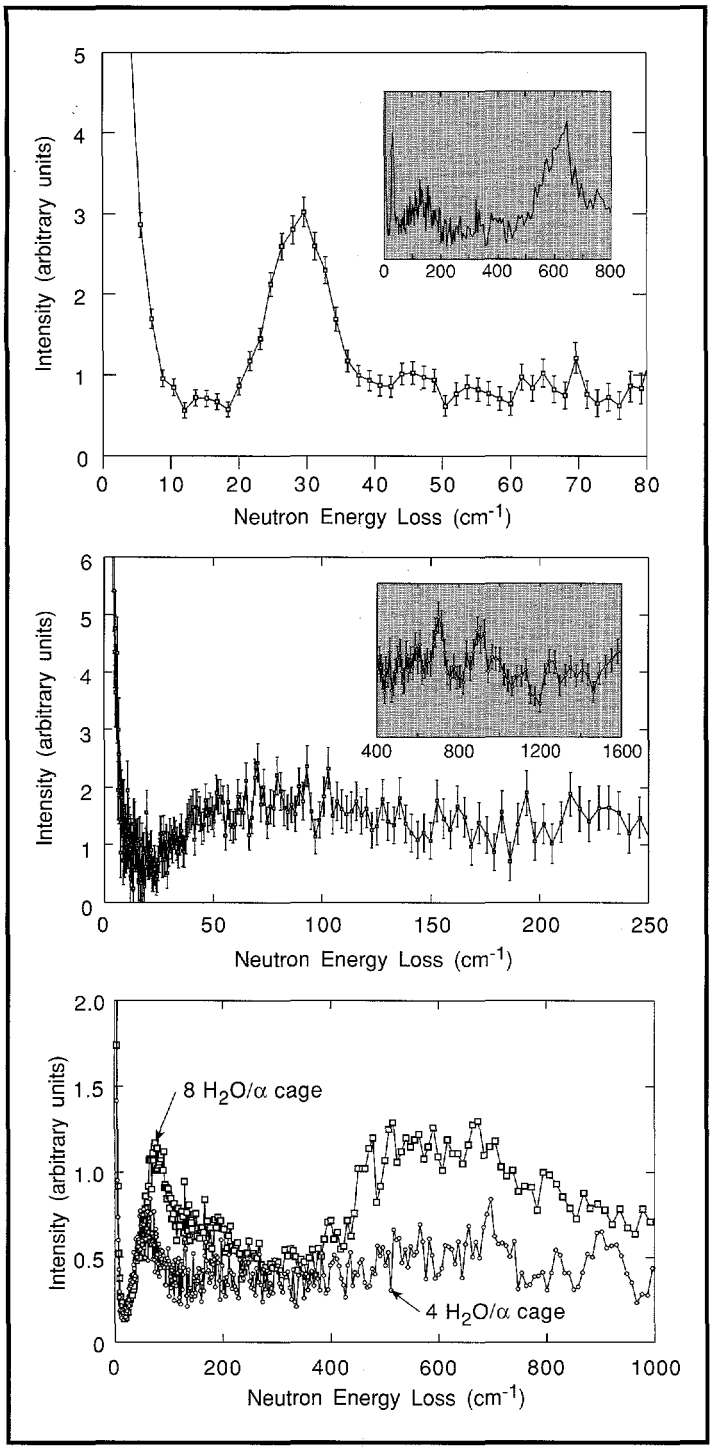

FIGURE 7.
Inelastic scattering spectra for hydrated sodium and calcium Type-A zeolites, as measured on the QENS spectrometer at 15 K: (top) Na-A with 3 H_2O/α-cage, (middle) Ca-A with 3 H_2O/α-cage, and (bottom) Ca-A with 4 and 8 H_2O/α-cage.

the framework structure appears to be satisfactory on the basis of average positions, there is clearly a distortion or disorder in the model that is incorrect, indicating that the framework potentials involving framework distortions need to be improved. This is a significant finding as the motion of the framework, and in particular the fluctuations in the 8-ring openings, are important for understanding transport processes in Type-A zeolites.

In addition to these structural studies, inelastic and quasielastic scattering on the QENS spectrometer at IPNS have provided insight into the dynamics of adsorbates in zeolites. In conjunction with the neutron diffraction work on GPPD, work has been started to characterize the dynamics of water adsorbed in Type-A zeolites. Although inelastic scattering has been used to characterize such compounds in the past, the work has frequently focused on the spectra from zeolites saturated with water and measured with neutron energy gain spectroscopy. The latter requires measurements at (for example) room temperature, with the attendant complications of large-amplitude motions, and possibly even translational and rotational diffusion.

To provide a baseline measurement of the spectra of water adsorbed in the Type-A zeolites, the vibrational spectra for Na-A and Ca-A have been measured on the QENS spectrometer at 15 K (neutron energy loss), using low doses of water. These spectra, shown in Figure 7, are quite different for the two compounds. The Na-A has essentialy three peaks: one at about 30 cm^{-1}, a broader and weaker feature at approximately 120 cm^{-1}, and a third band at about 610 cm^{-1}. The Ca-A has a low-frequency feature (but considerably broader than the low-frequency peak in the Na-A) and some ill-defined peaks at about 520, 680, and 900 cm^{-1}. In addition, there is an elevated "background" under the peaks over the whole frequency range shown.

Previous work on these hydrated zeolites assigned the low-frequency peak to the motion of the water/cation cluster and the higher-frequency features to the librational motion of the water molecules, based on the similarity to the inelastic spectrum of ice. These assignments are reasonable without further information, although the similarity of the librational spectrum in ice and water in zeolites is less appealing, particularly for the low loadings of water used in these experiments.

Fortunately, MD simulations provide the means to test these assignments. For the simulations of Na-A with adsorbed water, the model predicts that the first few water molecules will reside in the 8-ring units, coordinated to the framework and the sodium cations. There is sufficient space in the 8-ring for the oxygen on the water to attach to the sodium cation while also hydrogen-bonding to two of the 8-ring oxygens (see Figure 8). This result is consistent with thermodynamic expectations, because the water locates itself in an optimal environment for favorable interactions. Extending this model to the case of calcium, all the cations are located in the 6-ring sites, which are too small to accomodate an additional water molecule in the plane of the ring. The addition of water to the Ca-A simulations does not change the location of the cations at low water loadings (Figure 9).

The power spectra predicted for water in Na-A are shown in Figure 10 for the motion of the water hydrogen atoms, the water oxygen atoms, and the sodium cation. The low-frequency motion of the oxygen matches that of the water hydrogen atoms, while there is no such feature in the sodium spectrum. This means that the

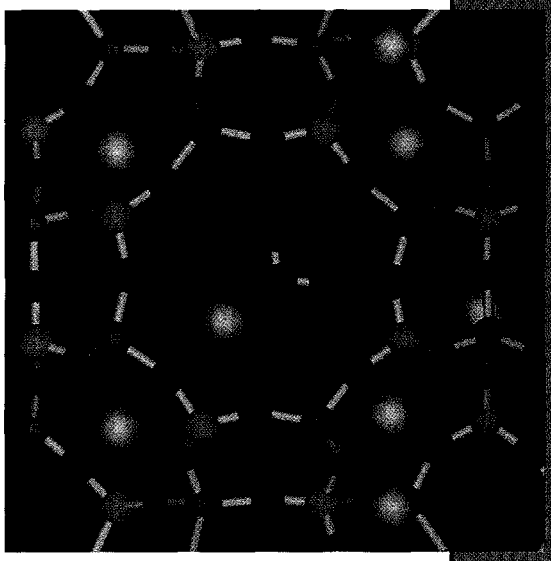

FIGURE 8.
Picture from the simulation of water in Na-A zeolite, showing the water located in an eight-ring, adjacent to the sodium ion (yellow).

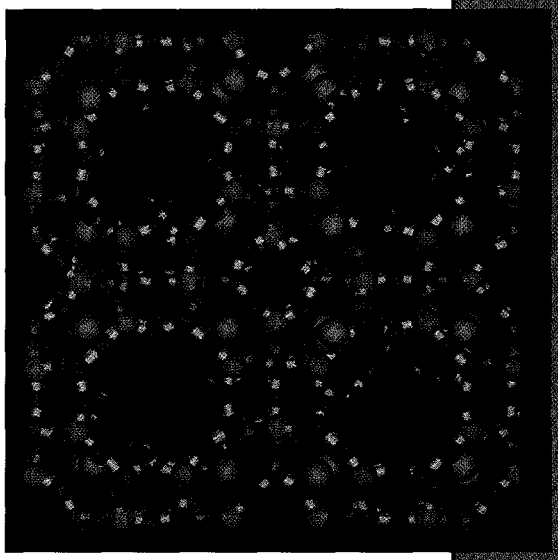

FIGURE 9.
Section of the simulation system for partially hydrated Ca-A. Note that the calcium ions (light blue) are still located on the six-rings.

lowest-frequency feature in the simulation model power spectrum for hydrogen at 30 cm^{-1} arises from the center-of-mass motion of the water molecule relative to the cation and the lattice. The higher-frequency feature in the calculated power spectra is present only in the hydrogen spectrum, which is consistent with a librational motion.

This theoretical result confirms the assignment of the librational peak, while it also suggests that the low-frequency assignment is not quite correct, because the water molecules vibrate in their adsorption sites at a lower frequency than do the neighboring cations.

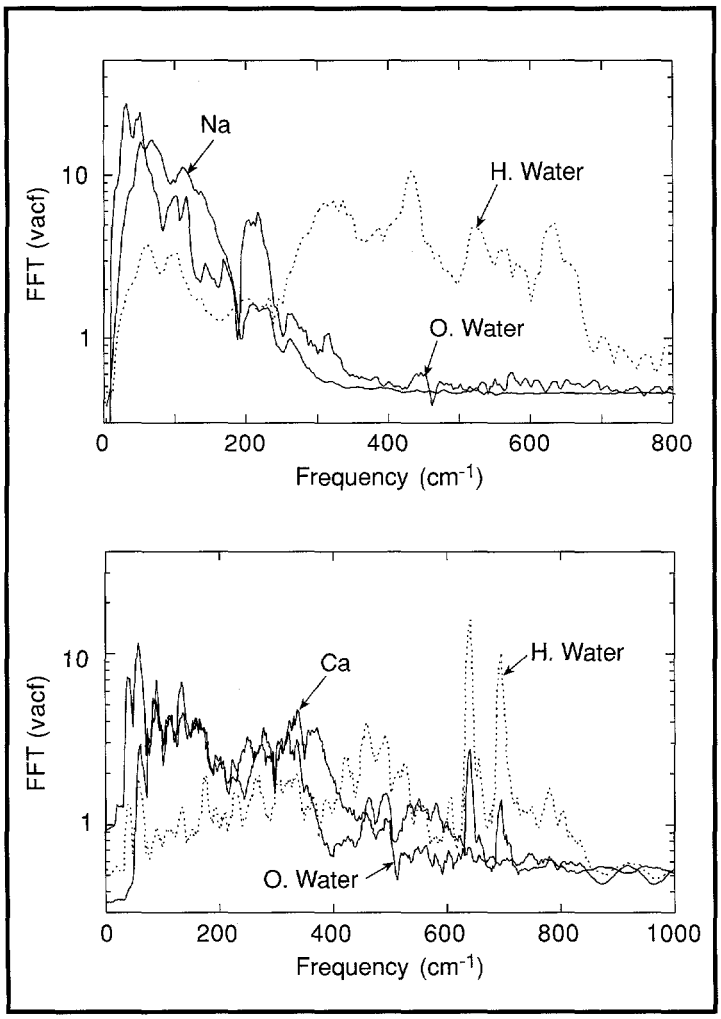

FIGURE 10.
Predicted power spectra of the water hydrogen atoms, oxygen atoms, and charge-compensating cations in (top) Na-A and (bottom) Ca-A hydrated to the level of three water molecules per α-cage. The power spectra intensities have not been scaled to allow for direct comparison with the neutron spectra. The inelastic neutron scattering spectra are dominated by the water proton motion.

For Ca-A, the MD power spectra have a low-frequency mode at about 47 cm^{-1}, which is again not present in the spectrum for calcium, a broad band from about 80 to 400 cm^{-1} that is featureless in the hydrogen spectrum, although it has structure in the other two spectra, and a distinct peak at about 480 cm^{-1} in the hydrogen spectrum. The low-frequency feature and the adjacent broad band of intensity is similar to the measured spectrum, but there is no higher-frequency feature in the experimental spectrum. The elevated "background" found in the experimental spectrum appears to be a major component of the scattering, and this could well be due to disordered water, as would be expected for molecules not bound to specific sites adjacent to the calcium cations.

For these two partially hydrated materials, the MD results are both promising and challenging. The Na-A simulations appear to be in good agreement with experimental data, while the Ca-A

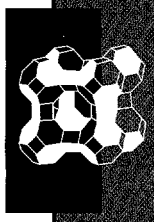

results are less so. Bearing in mind the excellent agreement between the predicted and measured structures of the anhydrous zeolites, it is somewhat surprising to find such discrepancies for the hydrated forms. Further work will be needed to achieve a better experimental and theoretical understanding of this modestly complicated system. It is only on the basis of a sound understanding of the hydrated forms of simple Type-A zeolites that we can attempt to understand more complicated hydrated clusters encapsulated in zeolitic materials.

These examples demonstrate the close relationship between the MD simulation method and neutron scattering. For the Li-A structure, where the distortions of the framework are readily apparent from simulations, the essential difference between this Type-A zeolite and others in the series can be readily appreciated. The interpretation of inelastic scattering data is difficult and, as demonstrated for hydrated Na-A, subject to peak assignment errors.

At the same time, the differences between the measured and predicted diffraction patterns highlight a shortcoming of the theoretical model, as is also the case with the less than satisfactory agreement between the calculated and measured vibrational spectra. A combined theoretical and experimental approach will be essential in coming to a full understanding of these simpler systems, as well as the much more complicated materials that are the goal of this program of zeolite science at IPNS, made possible by the capabilities of the GPPD diffractometer and the QENS spectrometer.

III Much Ado About Something

G. P. Felcher, Materials Science Division, and S. Adenwalla, IPNS Division, Argonne National Laboratory

It was the hyper-tall dutch Professor van Well who uttered the words "There must be a way to *uniquely* convert reflectivity data into a depth profile," while Victor de Haan, his eternally smiling student, and the two of us stared at a bundle of computer printouts. "Look here at this measured reflectivity and how good the fitting is in terms of two totally different models, that is to say, two different sequences of chemical layers in the samples we measured. Which one is the real one? Which one is fiction? Maybe the true profile is something else again. It all boils down to the fact that we measure the intensity of the reflectivity but not its phase, and with only that information our transformation from reflectivity to depth profile is not unique. But how do we get the phase?"

"Maybe we can put our sample close to a layer of a substance that we know well," someone interjected. "That would give us a handle. Actually, if that layer is magnetic we can have three different refractive indices: two obtained by magnetizing the layer in the plane of the film and looking at it with neutrons polarized parallel and antiparallel, and the third by magnetizing that layer perpendicular to the film." The speaker was on solid, but generic, ground: any prospector knows that having a reference point helps in measuring an object. Extracting the amplitude and phase of the reflectivity from such measurements is another matter – a matter that was solved in a set of lucid and elegant equations by the student with the eternal smile. By the time a paper, entitled "Retrieval of Phase Information in Neutron Reflectometry," was sent to *Physical Review*, all of us were smiling.

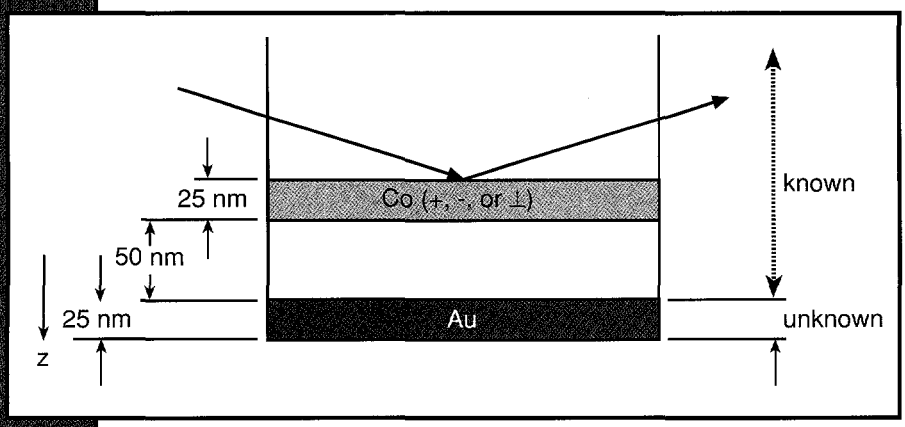

FIGURE 1.
Reflectivity "gedanken experiment" with the sample to be measured set in proximity to a known magnetic sample.

Ten days passed, and then on the desk of one of us a manuscript appeared, sent by *Physical Review* for refereeing. The title of this paper was "Exact Determination of the Phase in Neutron Reflectometry," by Majkrzak and Berk of NIST. Exactly the same equations, exactly the same results.... It looked as if Nature had decided to reveal one of her little secrets to many parties at once; at first, those parties were upset

and suspicious, but in the end they published their results back to back in the same journal, like good friends (Majkrzak and Berk, 1995; de Haan et al., 1995).

Is it true that once you have phase and amplitude the problem is solved? Together with a gallant mathematician from Iowa State University, Paul Sacks, we set about looking into the question by means of a "computer experiment." The experiment consisted in taking a sample composed of a magnetic standard, cobalt, with known properties and placing it in close proximity to another sample, which we called "gold" (Figure 1). This gold had, as determined by neutron optics, the scattering length density indicated by the solid line in Figure 2. The layer is sharply defined on one boundary, as if the surface were infinitely smooth; on the other side, the scattering length density gradually decreases, as if the sampling were taking place on a rough surface. With that initial profile, the reflectivities of the system cobalt + gold were calculated, and the phase and amplitude of the reflectivity due to gold only were extracted and back-transformed to recover a gold profile (solid points in Figure 2) that matches the original one well enough.

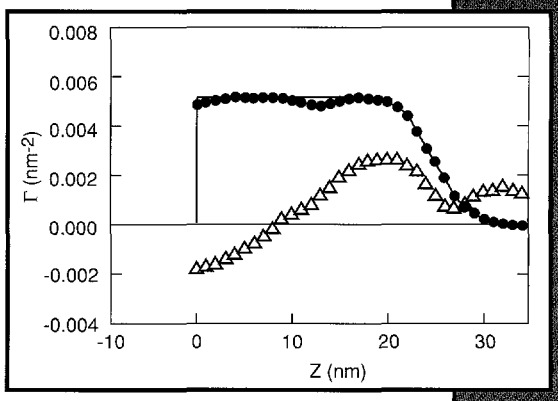

FIGURE 2.
Solid line: the neutron optical profile of a film (called "gold"). Solid points: profile recovered from perfect reflectivity data. Open triangles: profile recovered from reflectivity data with 5% jitter.

Great success? Well, a small success. In our calculation, we used exact data points for at least some of the reflectivity range; however, if a 5% jitter was introduced without applying other tricks, the "recovered" profile was very much ruined (triangles, Figure 2).

As experimentalists, we were not happy with computer simulation; we wanted to get our hands dirty with real samples and real neutrons. So we took a thin film of cobalt; on it we smeared, instead of gold, a thousand angstroms of deuterated polystyrene, and we stuck this sample in the neutron beam in the same configuration shown in Figure 1. The measurements with the magnetic field applied parallel to the surface went routinely. But on applying the magnetic field perpendicularly to the surface, we goofed big. A back-of-the-envelope calculation would have shown that the magnetic field necessary to magnetize cobalt perpendicularly to the surface was about 18 kOe, as indicated by the saturation value of the magnetization; instead, we used a value of 13 kOe. It was then that our detector showed a strange image.

Figure 3 gives a cartoon view of our sample/detector arrangement. All the neutrons elastically reflected are supposed to exit the surface at an angle equal to the angle of incidence, hitting one spot on the detector, where their wavelength is sorted out by time-of-flight. No neutrons are supposed to enter the detector at other angles, unless of course the sample is not exactly flat. Figure 4 gives a contour plot of the intensities collected in a magnetic field of 13 kOe. These intensities are given for the two neutron spin states (parallel [+] and opposite [-] to the field) as a function of the wavelength and of the reflection angle. Conventional reflectivity gives one stripe only, centered at one angle θ and extended at all wavelengths. In addition to

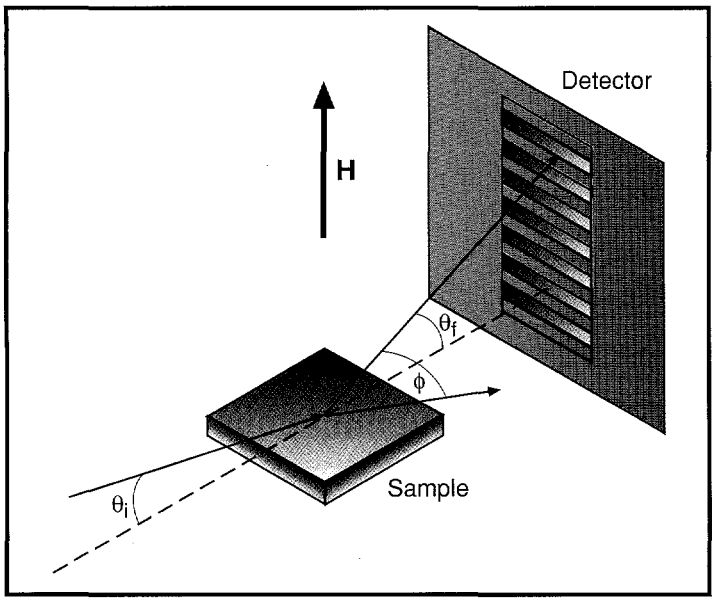

FIGURE 3.
Geometry of the sample-detector system.

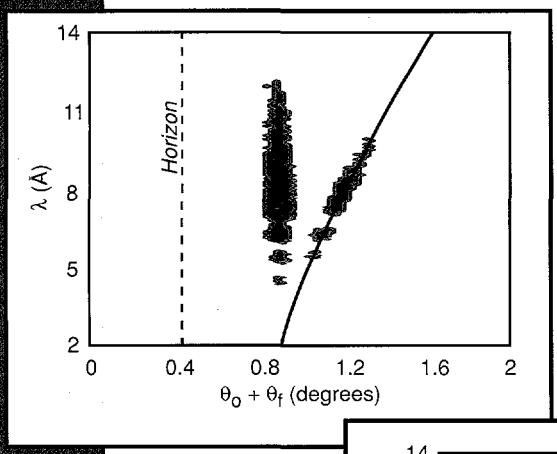

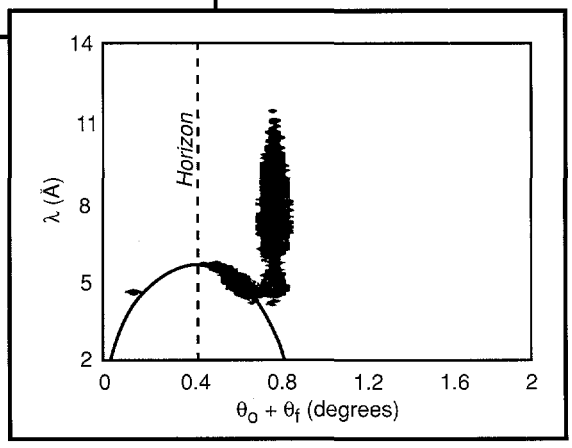

FIGURE 4.
Contour plots of the raw neutron intensities reflected from a cobalt/ polystyrene film. The angle of incidence is θ_i = 0.44°, and the magnetic field is 13 kOe. 4a (left), spin up; 4b (below), spin down.

that, you can see a mustache at the right for [+] neutrons (Figure 4a) and a mustache at the left for [-] neutrons (Figure 4b). To explain the effect, this time we went back and used that back of the envelope (Felcher et al., 1995).

The explanation is simple. The cobalt is not fully aligned in the magnetic field, and the neutron spins, upon reflection, can precess around the local moments. Even if no energy is exchanged between neutrons and sample, the flipped neutrons swap their Zeeman energy with kinetic energy. In mathematical terms, the total energy is conserved if

$$k_{zi}^2 + k_{xi}^2 \pm 8\pi^2 m\, \mu_n\, H/h^2 = k_{zf}^2 + k_{xf}^2 \mp 8\pi^2 m\, \mu_n\, H/h^2,$$

where μ_n is the neutron moment and H is the applied field (the term in which they enter is the Zeeman energy), h is Planck's constant, and $k_x = 2\pi \cos\theta/\lambda$, $k_z = 2\pi \sin\theta/\lambda$ are the momentum components parallel and perpendicular to the surface for neutrons incident at an angle θ_i or reflected at an angle θ_f from the surface. An added constraint is the conservation of the neutron momentum in the plane of the surface $k_{xi} = k_{xf}$. As a result, the exit angle is different from the entrance angle:

$$\theta_f^2 \sim \theta_i^2 \pm 1.47 \times 10^{-7} H \cdot \lambda^2,$$

with θ_i, θ_f expressed in radians, H in kOe, and λ in Å. The calculated loci of the spin-flipped, reflected neutrons, drawn in Figure 4, match well with the maxima of the observed ridges. What surprised us was that the effect was so visible, even though the splitting of the Zeeman levels was only 0.17 μeV at 13 kOe.

Does this represent the dawn of a new era of neutron surface spectroscopy? Honestly, we did not find any other case where we could apply these notions. If you find one, please drop us a note – or at least a preprint of your manuscript, on your way to sending it to *Physical Review Letters*.

Reference

C.F. Majkrzak and N.F. Berk, Phys. Rev. B **52** (1995), 10827.

III Neutron Irradiation Effect Studies at IPNS

R. C. Birtcher, Materials Science Division, Argonne National Laboratory

Radiation effect studies at IPNS have continued over the past five years at a relatively low but persistent level. Reduced from an initial facility consisting of a dedicated spallation target system optimized for radiation effects, the current program utilizes two thimbles in the Neutron Scattering Facility. One of the thimbles, located in the H2 beamline, is restricted to ambient-temperature irradiations; the second, located in Vertical Thimble 3, has been outfitted with a vacuum-isolated inner volume that permits irradiation at controlled temperatures up to 600°C. This second thimble, called the Radiation Effects Module (REM), began operations in 1992. The energy required to achieve the desired temperature is supplied by electrical heaters on experimental inserts. Since the energy deposited in the thimble from the neutron and gamma fluxes is very low, temperature control in the thimble (independent of IPNS operation) is better than 1°C, far superior to any other neutron irradiation facility. The REM is operated by the Materials Science Division at ANL, with experiments being approved through the IPNS experimental review process.

Irradiation experiments at IPNS have concentrated on studying the behavior of uranium silicide reactor fuels during early stages of their burnup. Changes in their crystallographic structure have been followed with neutron scattering in the General Purpose Powder Diffractometer (GPPD) at IPNS. The fuels under study are U_3Si and U_3Si_2. These are high-uranium-density materials for use in high-power or low-enrichment applications.

Neutron irradiations were performed at room temperature in the H2 facility. The neutron spectrum for this facility is characteristic of a reactor's neutron spectrum, with the addition of neutrons having energies up to 450 MeV. Damage in the specimens was primarily produced by uranium fission in a manner identical to damage production in operating nuclear reactor fuel. The nuclear-reaction cross sections for fast and thermal fission were determined by standard activation techniques to give a fission rate of 5.39×10^{-27}/proton for the uranium isotope ratio found in the specimens. The irradiations were performed in small steps, U burnup $<3 \times 10^{-8}$, in order to closely follow changes in the crystal structure; total uranium burnups amounted to about 2×10^{-6}. Average damage rates were 5×10^{-8} displacements per atom (dpa)/sec for U_3Si and 4×10^{-8} dpa/sec for U_3Si_2.

After each irradiation step, allowing an appropriate time period for radioactive decay (as long as 100 days), a time-of-flight powder pattern was measured on the GPPD, and the data were analyzed using the Rietveld profile refinement technique. For these experiments, only data from the highest resolution banks at $2Q = +148°$ [d ~ 0.4 to 2.9 Å, $\Delta d/d(FWHM) \sim 0.0025$] were processed. Data collection times varied from 12 hours for unirradiated specimens to 48 hours for highly irradiated specimens.

The diffraction peak shapes from the unirradiated material were the result of instrument resolution limitations. Repeated irradiation produced structural changes in both alloys that resulted in shifting and broadening of the Bragg peaks. In addition, the intensities of the Bragg peaks decreased as the background intensity from diffuse scattering (arising from lattice damage and amorphous material in the specimens) increased. The diffraction peak shifts arose from lattice distortions due to strains from defects and the increasing amorphous volume fraction. The irradiation dose at which all diffraction peaks disappeared was between 0.88 and 1.13 x 10^{17} fissions/cm^3, or 0.29 to 0.38 dpa, for both U_3Si and U_3Si_2. This is consistent with the results of Bethune (1969), who found amorphization between dose steps of 0.6 and 2 x 10^{17} fissions/cm^3.

The fractional changes in the lattice parameters from U_3Si and U_3Si_2 are shown in Figures 1 and 2 as functions of the amount of damage produced by the fission fragments. The response of the two compounds was quite different. In U_3Si, the a-axis expanded while the c-axis contracted, and the net volume change was positive. In U_3Si_2, the a-axis contracted strongly while the c-axis was little changed, and the net volume change was negative. These results explain the surface appearance of ion-irradiated U_3Si containing second-phase precipitates of U_3Si_2. After ion irradiation, the U_3Si_2 precipitates were rendered in negative relief after the U_3Si had expanded and the U_3Si_2 had contracted during irradiation.

The lattice dilation arose from the long-range strains due to cascade size volumes of amorphous material. At 30°C, both alloys were directly amorphized by irradiation. At low doses, when the volume fraction of amorphous material was small and localized in separated fission tracks, the lattice strain was equal to the product of the volume fraction of amorphous material times the volume dilation produced upon amorphization. At high doses, when the volume fraction of crystalline material was small, volumes of crystalline material were embedded in amorphous material, and the situation was much more complex.

Direct amorphization by the fission fragments resulted in the volume fraction of amorphous material, f_A, increasing as

$$f_A = (1 - e^{-\sigma A \Phi}) \qquad (1)$$

FIGURE 1.
Lattice parameter changes, $\Delta a/a$ (diamonds) and $\Delta c/c$ (squares), in U_3Si during neutron irradiation at room temperature. The lines are fits using Equation 1 (dashed lines) or Equation 2 (solid lines). The fitting parameters are given in the text and in Table 1.

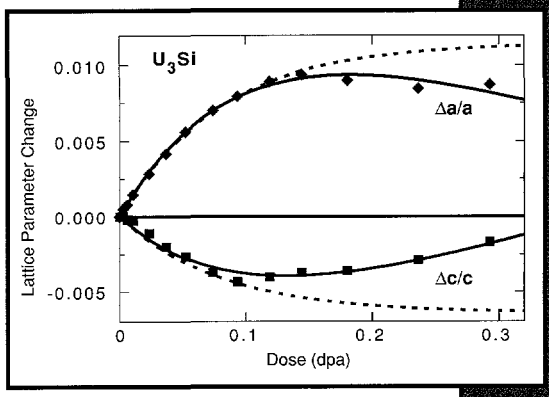

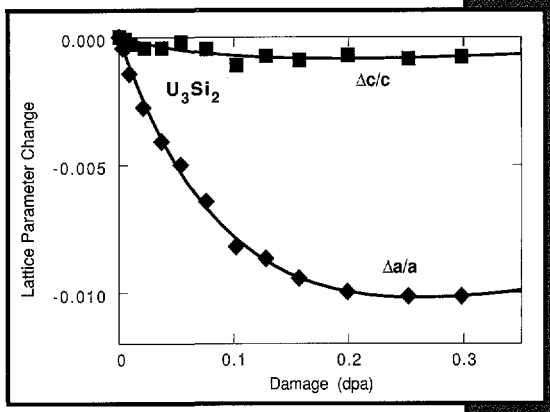

FIGURE 2.
Lattice parameter changes, $\Delta a/a$ (diamonds) and $\Delta c/c$ (squares), in U_3Si_2 during neutron irradiation at room temperature. The lines are fits using Equation 2. The fitting parameters are given in Table 1.

where Φ is the neutron dose and σ_A is the cross section for amorphization. As the specimen was amorphized, the scattering intensity in diffraction peaks decreased and the background scattering increased. Background scattering from U_3Si for d-spacings between 2.12 Å and 2.20 Å was determined by fitting a Lorentzian to the raw data. The ratio of background intensity to peak intensity is shown in Figure 3 as a function of the irradiation dose. The curve in Figure 3 is a fit based on Equation 1 with a cross section of 1/0.096 dpa. The increase of the background intensity indicates that amorphization was occurring directly within individual fission tracks and that the specimen was transforming from the crystalline state according to Equation 1. Two of the curves in Figure 1 are fits based on the assumption that the lattice parameter change is equal to the product of the volume dilation produced upon amorphization times the volume fraction of amorphous material given by Equation 1. Within the experimental uncertainty, U_3Si and U_3Si_2 amorphized at the same rate.

The exponential fits to the lattice parameter changes in Figure 1 indicate that for U_3Si the fractional increase in the a-axis saturated at 0.0115 while the c-axis contracted by 0.0065. The saturation value for the lattice volume expansion was 0.0165, although the maximum achieved was 0.0157. Walker and Morel (1971) found, with X-ray diffraction after ion irradiation, a saturation value for the lattice volume expansion of 0.012, based on a 0.4% shift of the <202> reflection. We found a total shift in the <202> d-spacing of 0.3725%, and we directly determined the change in the unit cell volume to achieve a maximum change of 0.0157; this value declined as the specimen became progressively more amorphous. Bethune (1969) found, using X-ray diffraction after a neutron dose equivalent to 0.17 dpa, that the a-axis had expanded by 0.0065 and the c-axis contracted by 0.0074, resulting in a volume expansion of 0.0056. After the same dose, we found the a-axis expansion to be 0.0087 and the c-axis contraction to be 0.0033, resulting in a volume expansion of 0.014. These X-ray diffraction results were based on a limited number of reflections, and peak broadening played a role in their interpretation. In addition, the X-ray diffraction results were sensitive to the surface treatment of the specimens, and cold work or surface deformation would result in the tetragonal-to-cubic transformation without amorphization.

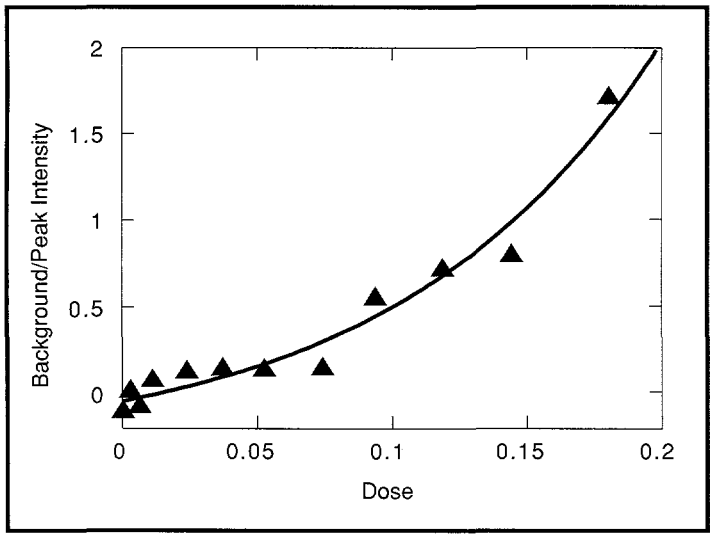

FIGURE 3.
Ratio of background intensity to peak intensity from U_3Si for scattering between d-spacings of 2.12 Å and 2.20 Å.

The exponential fits to the lattice parameter changes in Figure 2 indicate that for U_3Si_2, the fractional decrease in the a-axis saturated at -0.011 and the c-axis saturated at -0.00097. The saturation value for the lattice volume expansion of U_3Si_2 was -0.023. No comparable experimental results are available for U_3Si_2.

At damage levels greater that 0.1 dpa, the values of the lattice parameters of U_3Si deviated strongly from the exponential fits. The effect occurred, but less noticeably, for U_3Si_2. Deviations indicate that lattice strains were being relaxed as amorphous material filled the specimen and the remaining crystalline regions in the amorphous matrix became isolated from each other. Plastic flow of amorphous materials during irradiation is a universal behavior and occurs in response to any strain, such as that associated with the volume change upon amorphization. The specimens in this experiment consisted of 50- to 150-μm-diameter particles. For plastic flow to occur in these particles, an amorphous volume had to be connected to the surface so that it was free to expand. During ion irradiation, amorphous U_3Si undergoes rapid plastic flow, while the flow rate in U_3Si_2 is much lower. Thus, strain in the crystalline fraction of the specimens showed an initial increase due to the embedded amorphous regions, followed by a decrease in strain as the volume fraction of amorphous material increased. On the basis of the exponential fits to the data in Figures 1 and 2, strain relief becomes apparent in U_3Si and U_3Si_2 when the volume fraction of amorphous material is 70%. At this concentration, it is easy to visualize the remaining crystalline volumes becoming disconnected and the amorphous material yielding.

In general, our results were in agreement with the X-ray diffraction results; differences in the measured volume expansions were the result of stress relaxation due to plastic flow of the amorphous volume fraction. The rate of plastic flow depends on the mechanical constraints imposed on the system. In an unconstrained system, plastic flow is proportional to the irradiation dose. In order to gain insight into the strain relief, a linear relaxation term was added to Equation 1 so that the change in the a-axis lattice parameter was described as

$$\frac{\Delta a}{a} = -\alpha\Phi + \left.\frac{\Delta a}{a}\right|_{MAX} *(1 - e^{-\sigma A\Phi}) \qquad (2)$$

where α is a constant related to plastic flow and $\left.\frac{\Delta a}{a}\right|_{MAX}$ is the maximum lattice strain that would be measured without plastic flow. Values of the parameters are given in Table 1. A value of $\alpha = 0.026$ was found for both the a-axis and the c-axis of U_3Si, and a value of $\alpha = 0.0092$ for U_3Si_2. Due to the unknown mechanical constraints of the specimen particles, it is not clear how to interpret these values; however, a was larger, and unconstrained plastic flow was much more rapid, in U_3Si than in U_3Si_2. The volume change on amorphization is given by twice the change in the a-axis plus the change in the c-axis. The volume changes on amorphization were 0.0233 for U_3Si and -0.0301 for U_3Si_2. Density measurements on bulk U_3Si indicated a volume increase of 2.3%. The values agree, and there is no indication of excess vacancies or voids after amorphization. Discrepancies between previous X-ray measurements and bulk density measurements were due to strain relief in the crystalline material through plastic flow of the amorphous volume fraction. No comparable experimental results are available for U_3Si_2.

PARAMETER CHANGES DETERMINED BY NEUTRON DIFFRACTION						
	$\left.\frac{\Delta a}{a}\right\|_{MAX}$	$\left.\frac{\Delta c}{c}\right\|_{MAX}$	$\left.\frac{\Delta v}{v}\right\|_{MAX}$	$1/\sigma_a$ (fissions/cm^3)	$1/\sigma_a$ (dpa)	Plastic Flow Rate α
U_3Si	0.0166	-0.0099	0.0233	2.78×10^{16}	0.096	0.026
U_3Si_2	-0.0135	-0.0031	-0.0301	2.83×10^{16}	0.096	0.0092

Table 1. Parameters derived by fitting Equation 2 to lattice parameter changes determined by neutron diffraction.

In addition to changes in lattice parameters, U_3Si undergoes a phase transformation to its high-temperature cubic phase as atoms at the U_{II} position approach the idealized Cu_3Au position (1/4,3/4,0). This transformation has been detected by X-ray diffraction for neutron and ion irradiations. The cubic transformation is illustrated in Figure 4 by the convergence of the $(220)_T$ and $(004)_T$ reflections to the cubic $(200)_C$ diffraction peak with increasing damage. For purposes of display, the $(220)_T$ peaks have been normalized to unity and the curves shifted vertically with increasing dose. Not shown in this representation is the significant increase in diffuse background scattering with increasing dose. The apparent increase in noise as the irradiation dose increases is due to the decreasing volume fraction of crystalline material contributing to the diffraction peaks relative to the increasing scattering from defects and the amorphous volume fraction contributing to background scattering. The d-spacing of the $(220)_T$ and $(004)_T$ reflections is shown in Figure 5 as a function of the irradiation dose. Extrapolation of these peaks' positions to total convergence yields the high-temperature, cubic-phase lattice parameter. After peak convergence at a dose of 0.1 dpa, when the crystalline volume fraction is 0.1, the $(200)_C$ diffraction peak continues to shift, indicating additional lattice expansion, at a rate of 6.1%/dpa. These peak shifts indicate that the driving force of the transformation is the accumulation

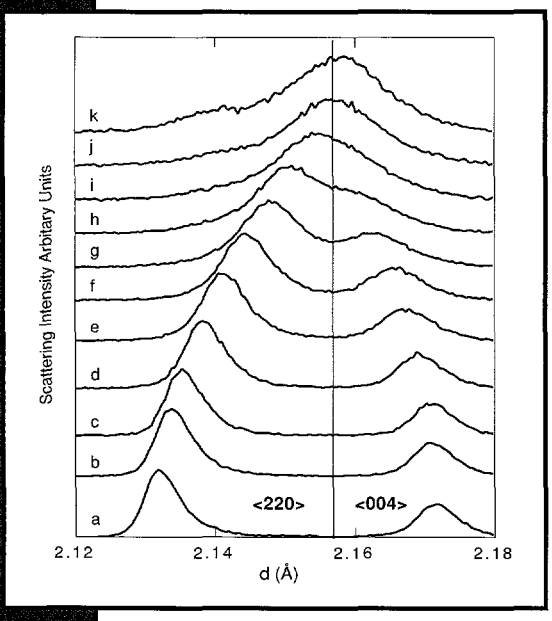

FIGURE 4.
Changes in the $(220)_T$ and $(004)_T$ reflections of U_3Si produced by neutron irradiation. Background intensities have been subtracted, and peak intensities have been normalized to unity. The different curves correspond to damage levels of a, 0; b, 0.003; c, 0.006; d, 0.011; e, 0.0235; f, 0.037; g, 0.052; h, 0.074; i, 0.093; j, 0.119; and k, 0.144 dpa. The vertical line at 2.157 Å represents the $(200)_C$ reflection of the high-temperature cubic phase.

of homogeneous lattice strains, without the direct formation of the cubic phase within the small volumes damaged by the fission fragments. Such direct formation of cubic material would be indicated by the growth of a $(200)_C$ diffraction peak at 2.156 Å, rather than the merging of the two tetragonal peaks. The homogeneous nature of the transformation may be enhanced by the powder specimen, which consists of unconstrained, single-crystal particles between 50 and 150 μm in diameter. Previous results based on X-ray diffraction claimed that the cubic phase was an intermediate phase before amorphization. We have shown that this is not the case, and that included amorphous volumes drive the tetragonal-to-cubic phase transformation much as internal stress from cold work or surface deformation can transform U_3Si to the cubic phase.

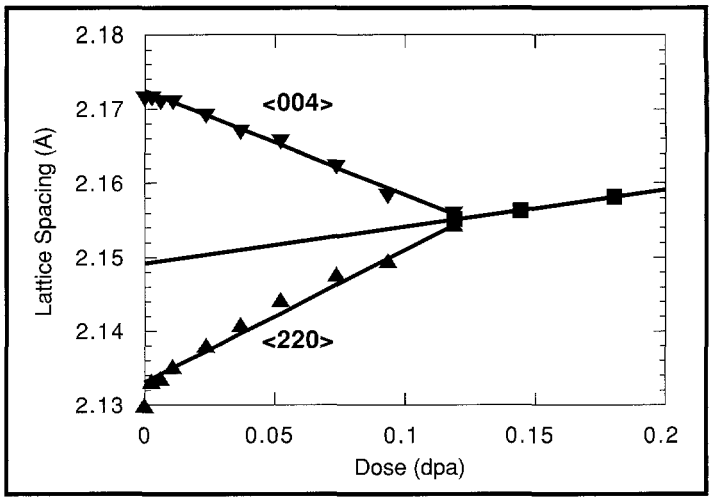

FIGURE 5.
Changes in the peak positions of the $(220)_T$ and $(004)_T$ reflections of U_3Si produced by neutron irradiation.

References

B. Bethune, J. Nucl. Mater. **31** (1969), 197.

D. G. Walker and P.A. Morel, J. Nucl. Mater. **39** (1971), 49.

Denis Wozniak aligns the beam stop on the new small-angle neutron diffractometer SAND at the Intense Pulsed Neutron Source. This instrument is used to study large-scale structures (10-1000 Å) in biology, chemistry, and metallurgy.

Chapter IV

INSTRUMENTATION AND COMPUTING DEVELOPMENTS AT IPNS

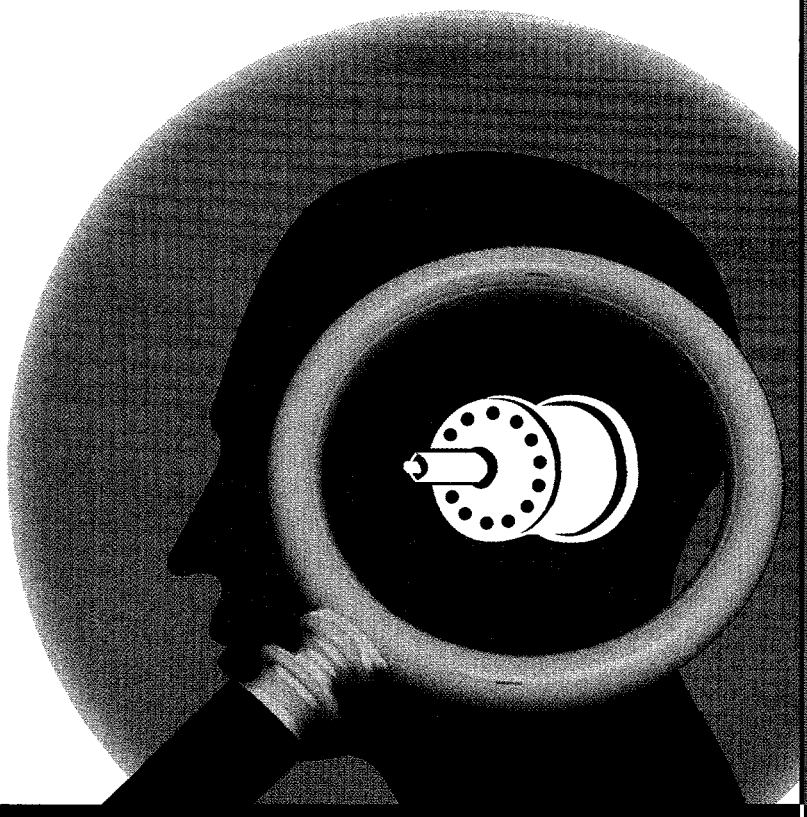

15TH ANNIVERSARY 1981–1996

IV

Instrumentation and Computing Developments at IPNS

R. K. Crawford, T. G. Worlton, and J. M. Carpenter, IPNS Division, Argonne National Laboratory

A number of developments have taken place in IPNS neutron scattering instrumentation and data handling since the 1991 IPNS Progress Report was published. In terms of instrumentation, the new glass diffractometer GLAD has been commissioned and is now included in the user program; the new small-angle diffractometer SAND is being commissioned and will soon be added to the user program as well; the mid-angle portion of the HRMECS chopper spectrometer flight path has been installed and is being commissioned; a new, prototype crystal-analyzer spectrometer CHEX has been installed, and its performance is being characterized; and design studies have begun for a major upgrade of the QENS crystal-analyzer spectrometer. In terms of data handling, we have replaced all the original PDP instrument computers with microVax computers; we have begun the design of a next-generation data acquisition system; the computer cluster used for data analysis has been significantly upgraded, and increasingly we are using workstations for data analysis; several interesting developments in data visualization have occurred; and we have made considerable progress in rationalizing and modernizing all the databases for equipment maintenance, the proposal system, etc. These various new developments are discussed briefly below.

GLAD is Commissioned

Until recently, neutron diffraction measurements of the structure of disordered materials were carried out at pulsed sources on diffractometers such as SEPD and GPPD, which are optimized for powder diffraction. Although much work of high quality has been performed in this manner, these instruments fall far short of meeting the requirements for state-of-the-art structure measurements on disordered systems. A few years ago, because of this shortfall, a group of Argonne and university scientists, organized as a Participating Research Team (PRT) led by the University of Houston, decided to build a new instrument optimized for structural measurements in glasses and liquids at IPNS. This new instrument, the Glass, Liquids, and Amorphous Materials Diffractometer (GLAD), was described in the IPNS Progress Report (1991). GLAD, now commissioned, was opened in 1992 to proposals from the PRT and outside users. Details of the performance of this instrument, including background, calibration, resolution, data rate, data quality, and data reduction and analysis, have been discussed elsewhere (Ellison et al., 1994a).

The analysis of neutron scattering from materials containing light atoms is plagued by the need for inelasticity corrections. Therefore, GLAD was designed to collect data over as broad a Q-range as possible, using the highest-energy neutrons collected over the smallest range of scattering angles, and to perform these experiments in the extremely limited amount of time typically allotted to experimenters. GLAD routinely collects data at neutron wavelengths between 0.05 and 5 Å, and it can obtain reliable data for scattering

angles between 4 and 95° (higher for the downstream sample position). For difficult samples, the data analysis can be restricted to a subset of angles and wavelengths to improve the quality of the data and minimize corrections. For example, an excellent-quality structure factor of D_2O out to 30 $Å^{-1}$ was obtained by using detector segments from 8 to 30° (over a wavelength range of 0.1 to 1.0 Å. When a broader range of scattering angles and/or a larger wavelength range can be employed, the statistics at all points are improved significantly, and the structure factor data can be extended to far higher Q (analyses are routinely performed using data through Q = 40 $Å^{-1}$, and occasionally to Q = 50 $Å^{-1}$).

GLAD is by far the most technically sophisticated instrument at IPNS, with two sample positions and 235 linear position-sensitive detectors (LPSDs) distributed around these sample positions. The use of LPSDs permits GLAD to handle high data rates and to cover low scattering angles. Crossed, converging Soller collimators focused on the forward detector bank collimate the thermal and epithermal neutrons used by GLAD. With this collimation scheme, the sample size does not contribute significantly to the resolution, so large samples can be used. We have devoted considerable attention to background sources in GLAD; over the wavelength range for which GLAD is optimized, its background is currently the lowest among diffractometers at IPNS. The data files are large and a typical experiment generates several such files in a short period of time, so efficient programs have been developed for analyzing and compressing the data to more manageable sizes.

The High-Intensity Powder Diffractometer

The High-Intensity Powder Diffractometer (HIPD) was built from spare detectors and shielding materials as an instrument with which to study surface diffraction from molecules adsorbed on large-surface-area substrates. The total amount of sample present in the adsorbed layers in these systems is small, and these types of studies do not require high resolution, so the instrument's design sacrifices resolution to provide intensities as high as practical. A low-angle detector bank covers scattering angles from 20 to 40° with resolution $\Delta d/d$ ranging from 1.8 to 3.5%. A second detector bank covers the range 84-96° with $\Delta d/d$ = 0.95%. This instrument has been very productive for the measurement of adsorbed species; since the ~90° bank has been added, it has also been useful for Rietveld refinements on certain classes of crystalline materials. The low-angle bank has also been particularly well suited to the study of magnetic structures. This instrument has proved to be so useful that it was added to the user program in 1992.

The HRMECS Intermediate-Angle Flight Path

The high-resolution chopper spectrometer HRMECS was initially designed to provide angular coverage of scattering angles from -20° to +140°. The scattering flight path was to be made in three parts, covering low, intermediate, and high scattering angles. However, because of funding limitations, the intermediate-angle portion of the flight path was not included as part of the initial instrument construction. For a number of years, HRMECS has operated with only the low- and high-angle portions of the flight path installed. Fortunately, we have now been able to rectify this situation.

The intermediate-angle section of the scattering flight path for HRMECS was fabricated and installed in 1994-1995. This section allows coverage of the intermediate scattering angles (20 to 80°) that previously were inaccessible on HRMECS. Additional detectors were procured to provide partial coverage of these angles, but the number of detectors currently available is still far from sufficient to provide complete angular coverage. This portion of the flight path became operational in late 1995.

FIGURE 1.
John Hammonds installs the detectors on the HRMECS intermediate-angle flight path, viewed from the HRMECS sample position.

The New Small-Angle Diffractometer SAND

In 1980, a prototype time-of-flight (TOF) small-angle diffractometer was operated at the prototype pulsed neutron source ZING-P' at Argonne National Laboratory; this instrument was later upgraded and operated at the IPNS pulsed source from 1982 through 1984. In late 1984, this instrument was further upgraded to become the current Small-Angle Diffractometer (SAD) at IPNS. Both Argonne researchers and outside users have performed many experiments on the SAD, and these have resulted in a large number of publications. The quality of this work, as well as that at other pulsed-source small-angle neutron scattering (SANS) instruments, clearly demonstrates that SANS using the TOF method at a pulsed source is now an established technique, capable of producing data of quality comparable with those taken on the more mature reactor instruments.

The SAD instrument at IPNS has been severely oversubscribed since its commissioning, with proposals exceeding operating time by a factor of two to three. Because of this, and because experience led us to believe we could now build a significantly improved instrument, consideration of a second SANS instrument at IPNS was begun in 1986. Design of this second small-angle diffractometer and development of the necessary components has proceeded slowly due to limited resources, but the new instrument (named SAND) is now being commissioned.

SAND is designed to provide all the capabilities now provided by SAD and to enhance those capabilities by extending the dynamic range and improving the ease of operation and the instrument reliability. One goal was to make a range of Q down to 0.002 $Å^{-1}$ readily accessible for those experiments that require it. SAND includes a chopper to allow operation with much longer wavelengths, and eventually it will have a second set of collimators with smaller angular divergence; both features will serve to reduce the minimum Q from that on SAD (0.005 $Å^{-1}$).

A second goal was to increase the maximum Q value accessible and to provide better counting statistics for the higher Q data, where the scattering cross section is usually quite small. This goal has already been partially addressed by procuring a position-sensitive detector with a 40 cm x 40 cm area for the new instrument. This is twice the linear dimensions of the SAD detector (four times the area). An array of LPSDs at higher scattering angles (up to 36°) is also included to provide large additional increases in the maximum Q.

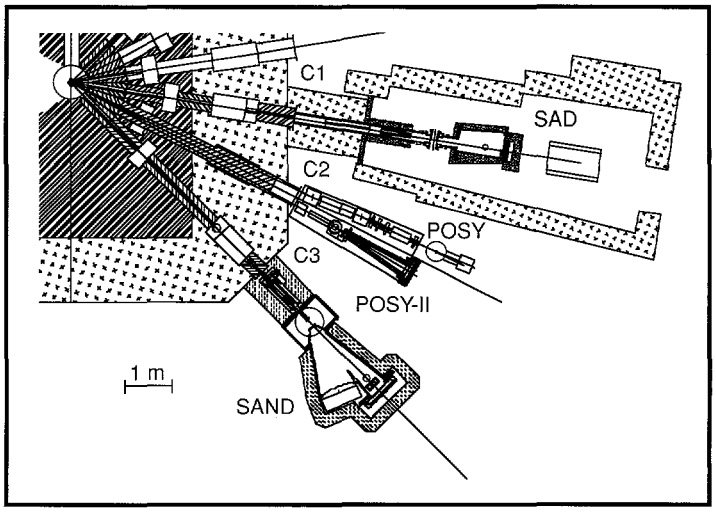

FIGURE 2.
Top view of a portion of the IPNS experiment hall, showing SAND and adjacent instruments.

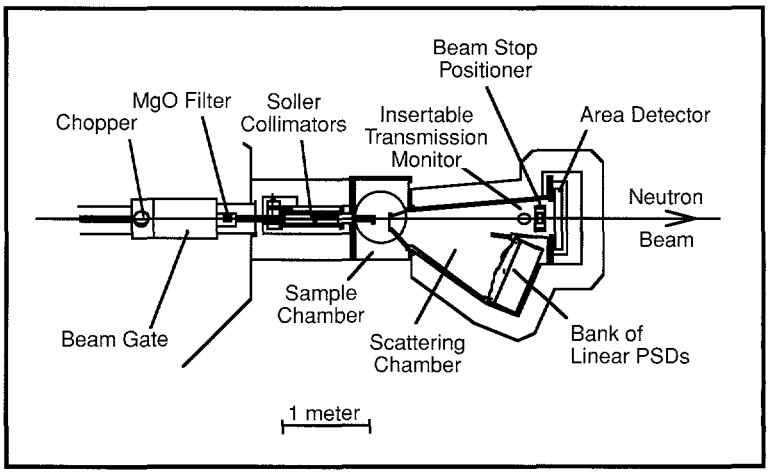

FIGURE 3.
Top view of SAND, showing major instrument components.

Details of SAND are available elsewhere (Crawford et al., 1995a), so only a few of the important features are summarized here. Figure 2 shows SAND in its location on the C3 beamline and indicates its relationship to its neighbors. Figure 3 shows the instrument in greater detail, indicating the geometry and relative placement of major components of the instrument. Major components include the moderator, incident beam filter, background chopper, collimation system, sample chamber, area detector, high-angle LPSD bank, and beam monitors and beamstops. Table 1 summarizes the instrument parameters for SAND. Figure 4 shows the SAND team in the process of installing the instrument.

A key component of SAND is the solid CH_4 moderator. The C3 beamline where SAND is located is one of three beamlines that view this cold moderator. SAD on beamline C1 also views the same moderator, as do POSY and POSY-II. From early 1985 until late 1988, and again since 1994, these beamlines have viewed a grooved solid CH_4 moderator (physical temperature ~20 K), which is an excellent source of long-wavelength neutrons. During the other operating periods,

PARAMETERS FOR SAND

PARAMETER	VALUE
Source frequency	*30 Hz*
Moderator	*decoupled solid CH_4*
Source-to-sample distance	*7.0 m*
Sample-to-area-detector distance	*2.0 m*
Collimator-to-sample distance	*0.5 m*
Sample-to-LPSD distance	*1.524 m*
Focusing collimators	
coarse	*0.0034 radians fwhm[a]*
fine	*0.0014 radians fwhm*
Beam size at moderator	*9.0 cm diameter*
Maximum beam size at sample	*2.0 cm diameter*
Beam size at area detector	
with coarse collimators	*17 mm full diameter*
with fine collimators	*6 mm full diameter*
Area detector	
active volume	*40 cm x 40 cm², 2.5 cm thick*
resolution	*4-6 mm*
max. scattering angle	*~9°*
LPSD	
active volume per detector	*1.1 cm diameter, 60 cm long*
number of detectors	*65*
resolution	*1-2 cm along detector*
max. scattering angle	*36°*
Wavelength range	*1-14 Å (5-14 Å for crystalline samples)*
Q_{max}	
λ_{min} = 1.0 Å (noncrystalline)	*>2.0 Å^{-1}*
λ_{min} = 5.0 Å (crystalline)	*~0.6 Å^{-1}*
Q_{min} (λ_{max} = 14 Å)	
coarse collimation	*~0.005 Å^{-1}*
fine collimation	*~0.002 Å^{-1}*
Q_{min} (λ_{max} = 28 Å, using chopper)	
coarse collimation	*~0.003 Å^{-1}*
fine collimation	*~0.001 Å^{-1}*

[a]fwhm = full width at half maximum.

TABLE 1. Parameters for SAND

the moderator can was filled with liquid H_2 instead. Measurements indicate that over most of the wavelength range of interest for small-angle diffraction, the solid CH_4 moderator provides a factor of ~3.5 times greater intensity than did the liquid H_2 moderator.

SAND uses crossed, converging Soller collimators (similar to those on SAD) to achieve good angular collimation with a short flight path. This permits the use of neutron wavelengths up to 14 Å without frame overlap. An MgO filter in the incident beam eliminates most of the fast neutrons, and a slow chopper minimizes the effects of delayed neutrons and frame-overlap neutrons. Both of these features improve the instrument background. The chopper can also be rephased to allow the use of neutron wavelengths up to 28 Å when desired.

An optical alignment system has been built into SAND to facilitate alignment of the Soller collimators, beamstop, and transmission monitor. This system includes a halogen lamp as a broad white-light source and a low-power laser for finer alignment. Both are directed along the surveyed axis of the instrument by a thin (3-mm-thick) single-crystal

silicon wafer permanently mounted in the neutron beam upstream from the Soller collimators and inclined at 45° to the beam. This wafer has minimal effect on the neutron beam. Transparent sapphire vacuum windows transmit the light from the halogen lamp or from the laser all the way to the area detector. This optical system has reduced the time required for the alignment process to a few minutes. It also provides a means for quick centering of the sample in the beam when nonstandard sample equipment is used.

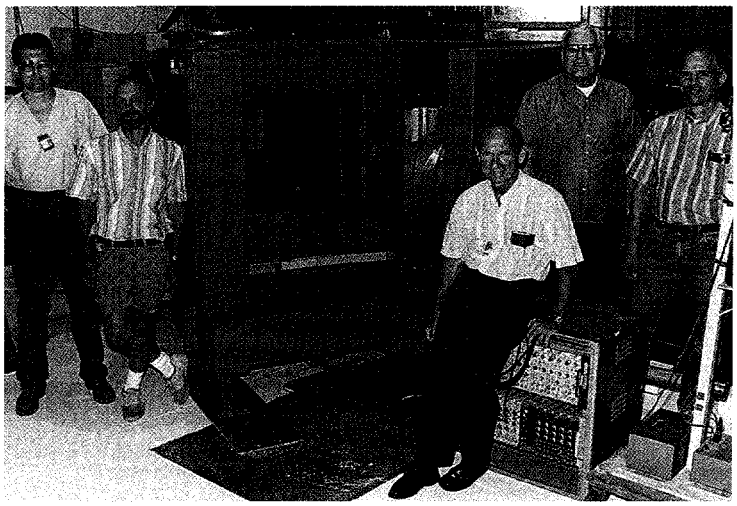

FIGURE 4.
The SAND team at work installing the instrument: (from left to right) Chris Piatak, Dave Leach, Don Bohringer, Bob Kleb and Kent Crawford.

A large sample region is provided in the instrument, with proper alignment fixtures so that a wide variety of sample environments can be easily interchanged. Included among environmental equipment and capabilities are cryogenic capabilities, temperature-controlled sample changers, furnace capabilities (with the sample in vacuum or in a controlled atmosphere), high-pressure cells, and magnetic fields.

On SAND, the Q-range extends up to 0.6 $Å^{-1}$ even when wavelengths are restricted to $\lambda > 5$ Å (above the Bragg cutoff for most crystalline samples), and much higher when the full wavelength range down to $\lambda = 1$ Å can be used. Much of the interesting data lies at these higher Q values, above 0.1 $Å^{-1}$. An increasing share of the experiments being proposed require such data, and these will greatly benefit from this extension of the Q-range.

With 14-Å neutrons and the coarse set of Soller collimators, the minimum Q on SAND is 0.005 $Å^{-1}$. When SAND is fully operational, the capability to use wavelengths out to 28 Å and the availability of a set of fine Soller collimators will extend the range down to 0.002 $Å^{-1}$ or possibly even to 0.001 $Å^{-1}$.

Improvements to the Quasielastic Spectrometer QENS

In crystal-analyzer spectrometers, the solid angle subtended by the analyzer arm can be increased by increasing the size of the analyzer crystal array. In order to do this without spoiling the energy resolution, focusing techniques are employed. The IPNS quasielastic spectrometer, QENS, and the planned improved instrument, QENS-Upgrade, utilize "fixed final energy focusing," in which all neutron paths between the sample and the detector make the

same Bragg angle θ with the analyzer array. These instruments are optimized for quasielastic scattering and for low-energy inelastic scattering.

The fixed final energy condition is satisfied for a point sample and a point detector if the analyzer crystals are located on a circle that passes through the sample and detector. The reflecting planes of the analyzer crystals are not in general tangent to this circle, however, and each individual crystal must be oriented so the normal to its reflecting planes bisects the sample-analyzer-detector angle. Both QENS and QENS-Upgrade have their analyzer-crystal arrays assembled in this geometry. With this focusing geometry, a number of closely spaced detectors can be used for each analyzer bank. Each of these detectors is also approximately "final-energy focused" for a different set of mosaic planes of this analyzer array. The final energy for each detector is thus slightly different, but since events from each detector are analyzed separately, this does not worsen the resolution. This ability to obtain high resolution from analyzer crystals with a broad mosaic spread, while utilizing the full reflectivity of the entire mosaic spread, greatly enhances the data rate of these instruments.

QENS is a crystal-analyzer spectrometer at IPNS optimized to provide ~70-μeV resolution for quasielastic scattering, but it also has very good resolution for chemical spectroscopy at excitation energies up to ~150 μeV. The "white" beam from the source is incident on the sample, so a separate detector can be mounted to monitor diffraction from the sample. This allows a careful following of phase changes, *in-situ* sample growth or modification, etc., concurrently with the quasielastic- and inelastic-scattering measurements. QENS has three focused-crystal-analyzer arms mounted on a rotating table so that a wide range of scattering angles can be covered. Figure 5 shows the layout of the present QENS. For the past year, QENS has been viewing a solid CH_4 moderator, and this has resulted in a factor of ~5 increase in data rate for most experiments, when compared to the previous liquid CH_4 moderator. This higher intensity has made the instrument even more attractive, and demand is rapidly increasing.

The upgrade of QENS, now in the planning stage, will replace the rotating instrument table having three detector banks (Fig. 5) with a fixed instrument having 16 analyzer-detector banks plus two diffraction detector banks. Figure 6 indicates this planned arrangement. Quasielastic resolution will be kept at ~70 μeV for each of the analyzer banks. The incorporation of 16 analyzer banks will allow sampling of the full angular range (~15-165°) for inelastic scattering without rotating the instrument. Eliminating the need for rotation will allow the use of improved shielding and will simplify the types of sample environment required. The

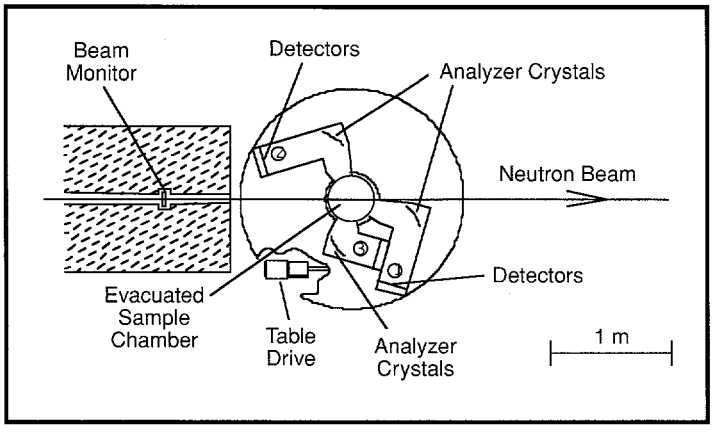

FIGURE 5.
Schematic layout of the present QENS. The three analyzer arms rotate about the sample in order to cover the full angular range.

upgrade will also result in a factor of ~5 increase in the analyzer solid angle, leading to an additional factor of ~5 increase in useful data rate. It is expected that with adequate funding this upgraded version of QENS will be operational in 2-3 years.

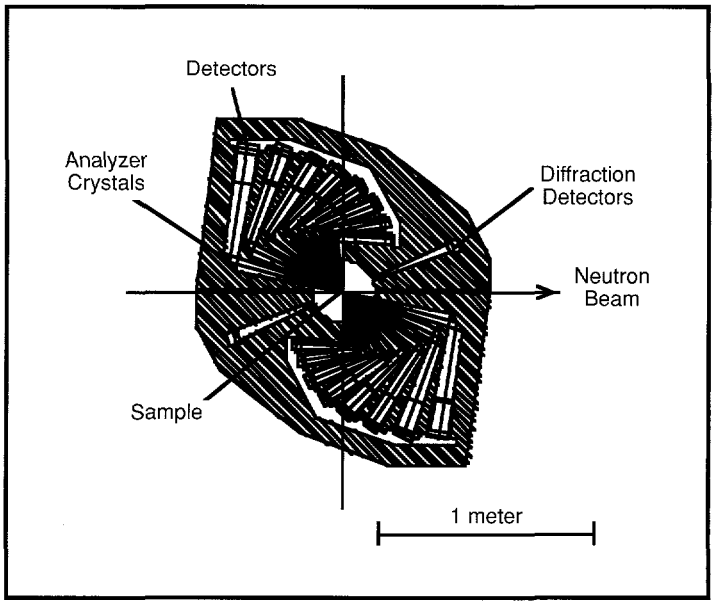

FIGURE 6.
Schematic layout of the proposed QENS-Upgrade instrument. The full angular range is covered without rotating the analyzer arms.

The Prototype Spectrometer CHEX

For higher-energy inelastic scattering, it becomes more important to keep the sample-detector flight time constant for all scattered neutron paths in the analyzer arm, in order to minimize the incident energy uncertainty δE_i. This "final-time-focusing" condition is achieved by placing the sample, analyzer crystals, and detectors on parallel planes. With this type of focusing, each neutron path from a point on the sample to a different point on the detector has a different Bragg angle θ, and hence a different final energy; if large samples and detectors are used to increase the data rate, this can lead to a relatively large spread in the final energy E_f. This spread is not particularly important if $E_f << E_i$, but it can be the dominant contribution to the resolution for $E_f \approx E_i$. Large samples can be used with this type of focusing, so this method can be very good for high-energy-transfer spectroscopy, but it is not as good as the fixed-final-energy focusing of QENS for low-energy transfers or for quasielastic scattering.

Fortunately, QENS (and soon, QENS-Upgrade) is already optimized to cover this low-energy-transfer range. However, because QENS is restricted to the use of small samples because of the type of focusing employed, it was decided to build a complementary crystal-analyzer spectrometer using the fixed-final-time focusing. This prototype Chemical Excitation spectrometer (CHEX) was installed on the F1 beamline in the summer of 1995, replacing the PHOENIX instrument that previously operated there. Figure 7 shows this instrument schematically. At present, this instrument is in the commissioning stage, but it is expected that it will soon be added to the user program.

Computing at IPNS

Introduction

The IPNS computer systems were first developed in 1980, about the same time as the first DEC VAX computers became available. We initially used a DEC VAX computer running the

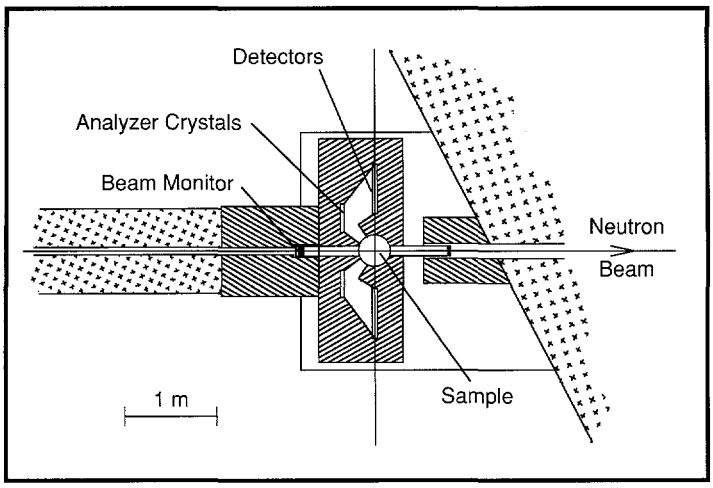

FIGURE 7.
Schematic representation of the prototype crystal-analyzer spectrometer CHEX. The location of sample, analyzers, and detectors on parallel planes provides the fixed-final-time focusing.

VMS operating system for shared data analysis and used PDP-11 computers for data collection. Because of developments in the computer industry, we have been converting from a primarily centralized computing system to a client-server system, with each scientist or other staff member having a workstation that is used for word processing, graphics, electronic mail, Internet access, etc. The original PDP-11 instrument computers have been replaced by VAXstation/VMS computers, and the data analysis computers have been replaced by RISC workstations running either DEC OpenVMS or UNIX software. Data analysis software has been converted to run on the new RISC workstations and to take advantage of newer software technologies. Graphical display of data is usually done by using X Windows/Motif with X Terminal emulation software on a personal computer. Text terminals and Tektronix graphics terminals are now seldom used.

While we have made good use of Motif and X Windows, we are also evaluating Microsoft Windows NT as a possible system to use for data analysis. Windows NT is the first portable, robust operating system that will run personal computer applications as well as support large scientific calculations. Most of the tools provided by UNIX are now available in VMS or on Windows NT. Our plan is to shift applications to the most suitable computing platform as improved systems become available. We have already shifted document sharing among personal computers from VMS to a Windows NT server. We are providing ftp servers on both Windows NT and VMS, and our Web servers are running on Windows NT.

New Data Acquisition System

Design of the present data acquisition system for the IPNS instruments was begun in 1977. This system has served us well, but many of the components are becoming obsolete, and it is difficult or impossible to find replacements. In the intervening years, electronics technology has made enormous advances. For these reasons, we believe that it is now time to embark on the design of a second-generation data acquisition system for the IPNS instruments. We are just beginning to define the parameters for this new system. We expect that development of the new system will take about 18 months, after which we will then start replacing the present systems at a rate determined primarily by the available funds. The entire changeover is expected to be completed before the end of this decade.

Collaboration on Data Analysis

In October 1994, IPNS organized the first workshop on Software for Neutron and Synchrotron Scattering (SOFTNESS-94), under the direction of Ray Osborn. This workshop succeeded in stimulating cooperation among neutron scientists in the United States and Europe. One of the recommendations from the first workshop was that a neutron mailing list, a neutron ftp site, and a neutron World Wide Web home page be established. These have all been set up at IPNS. To subscribe to the neutron mailing list, send a mail message to "neutron-request@anl.gov" with a first message line "SUBSCRIBE". No subject is necessary. You will be sent further instructions. The neutron WWW page is at "http://www.neutron.anl.gov", and the neutron ftp site is at "ftp.neutron.anl.gov". Subcommittees on a data format standard and on data collection and analysis were formed at the workshop; their reports can be found on the neutron ftp server.

Another recommendation from SOFTNESS-94 was that a second workshop be held to agree on a format for exchange of neutron and X-ray scattering data. The SOFTNESS-95 workshop was held at NIST in September 1995. At this workshop, it was agreed that we should base our standard on the Hierarchical Data Format (HDF) developed at the University of Illinois, NCSA. The data exchange format will be called NEXUS (Neutron and X-ray Unified Standard); the workshop attendees are working on standardized nomenclature and developing sample programs. Further developments will be reported on the mailing list and posted on the neutron home page. Contributions to the neutron ftp site and World Wide Web page are solicited.

Data Visualization

Visualization of experimental data and fitted or calculated functions are of prime importance in quickly analyzing the results of neutron scattering experiments. Historically, we have generated plots of our data and fitted curves through calls to a library of graphics routines, such as Computer Associates DISSPLA, or a similar library, GPLOT, written at IPNS for DEC GKS. Those types of programs are being converted to use PGPLOT, which was written by Tim Pierson at Cal Tech and is freely available on several computing platforms.

For more sophisticated visualization, we have purchased several licenses for IDL from Research Systems Incorporated. We have also collaborated with Dennis Mikkelson of the University of Wisconsin on a visualization package, TOF_VIS, which is useful for quickly viewing experimental data from large arrays of detectors. This has proven very valuable in assessing the functioning of instruments with large numbers of detectors. Originally written for the GLAD instrument and since generalized to be usable on other instruments, TOF_VIS runs on either UNIX or VMS.

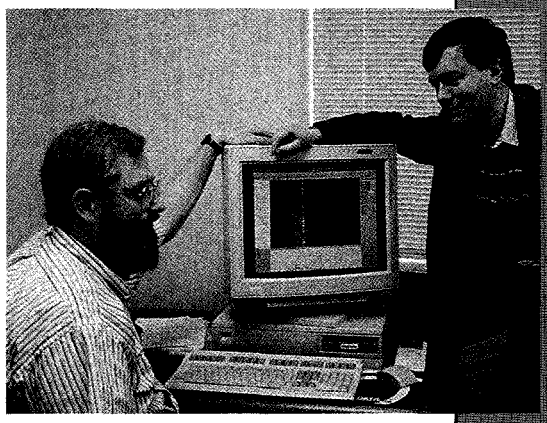

FIGURE 8.
Dennis Mikkelson demonstrates the TOF_VIS program to Ray Osborn.

Database Applications

As database requirements continue to increase, we have begun a program to create and manage databases with experiment, user, safety, maintenance, and other information. We have created database procedures for tracking proposals from submission to experiment completion and have automated the printing of experiment data sheets, equipment usage reports, and as-run reports. We have also created database procedures for tracking the qualification for beam gate keys for the various beamlines, as well as for various maintenance and safety issues. IPNS and Argonne have not had a unified approach to database applications. Argonne's business database applications have generally been on an IBM mainframe. This is being replaced by a client-server database system with UNIX servers and MS Windows PC clients. The UNIX servers use the Oracle database, and two or three client tools are used. IPNS has several databases using MASS11 Manager on a VAX and several using Filemaker Pro on a Macintosh. We are in the process of evaluating database products and converting applications to run on PC or Mac database systems.

Network Applications

IPNS is beginning to convert from a paper-based system for proposals etc. to a system that uses electronic media as much as possible in distributing and gathering information. IPNS has a home page at the URL "http://www.pns.anl.gov/ipns.htm", which is separate from the server we provide for the neutron community. Proposal forms are now available via ftp and can be submitted by Fax (708-252-4163) or regular mail. Since we have switched to an electronic mail system that supports attached documents, proposals may also be submitted via e-mail (to bamarzec@anl.gov). To obtain an IPNS proposal form, ftp to "ftp.pnstgw.pns.anl.gov" or use Netscape or Mosaic to follow the links on the IPNS home page. The forms are available both in MS Word Rich Text Format (RTF) and in Adobe Portable Document Format (PDF). You can view or print the PDF format document by means of a free Adobe Acrobat Reader from "http://www.adobe.com/", but if you intend to submit a proposal electronically, you need to use the RTF document and convert it to either MS Word or WordPerfect.

We have also begun a program of converting printed documents to electronic form for easier storage and access. The documents will be scanned into a computer and converted to Adobe Acrobat format using Adobe Acrobat Capture software. This approach will provide compact, searchable documents and free up considerable storage space. Eventually, it may also allow remote users to access documents, such as experiment reports and publications, electronically.

Other Developments

The increasing complexity of the experiments being proposed at IPNS places ever greater demands on the quality and types of sample-environment equipment required. One of the existing general-purpose, "workhorse" furnaces was extensively modified to meet these demands, an additional furnace was procured, and new furnace temperature controllers with improved capabilities were procured and interfaced to the data acquisition computers. A general upgrade of the sample and flight-path vacuum systems on all of the instruments was

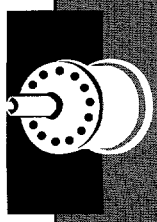

begun; the new systems will allow the vacuum information to be read out by the data acquisition computers. New higher-power, lower-temperature closed-cycle refrigerators have been procured to provide faster sample cooldown on the chopper instruments.

Working with an exchange student from Kyushu University, we have completed an accurate, absolute calibration of a set of beam monitor detectors. We have also been involved in an extensive effort to understand the performance of the rise-time-encoded, position-sensitive gas proportional counters used on several of the IPNS instruments. This program is now beginning to lead to improvements in the encoding speed and linearity and to increased lifetimes for these detectors.

A program of measurements has begun, aimed at understanding and optimizing mica and other analyzers for use in high-resolution spectrometers. Mica has the demonstrated potential to provide inexpensive, large, efficient monochromators. This effort is in conjunction with preliminary design studies aimed at the design of a high-resolution, backscattering crystal analyzer spectrometer. This instrument would allow the study of inelastic and quasielastic scattering with a resolution of 1-10 μeV. This would open up several important fields, including rotational tunneling and relatively slow diffusion effects, for study at IPNS.

Robert Kleb demonstrating a 1/4-scale model of the Intense Pulsed Neutron Source target handling arrangement, which he designed.

Chapter V

TARGET AND MODERATOR DEVELOPMENT

- IPNS TARGET EXPERIENCE
- COLD MODERATOR DEVELOPMENT
- A TRIBUTE TO BOB KLEB

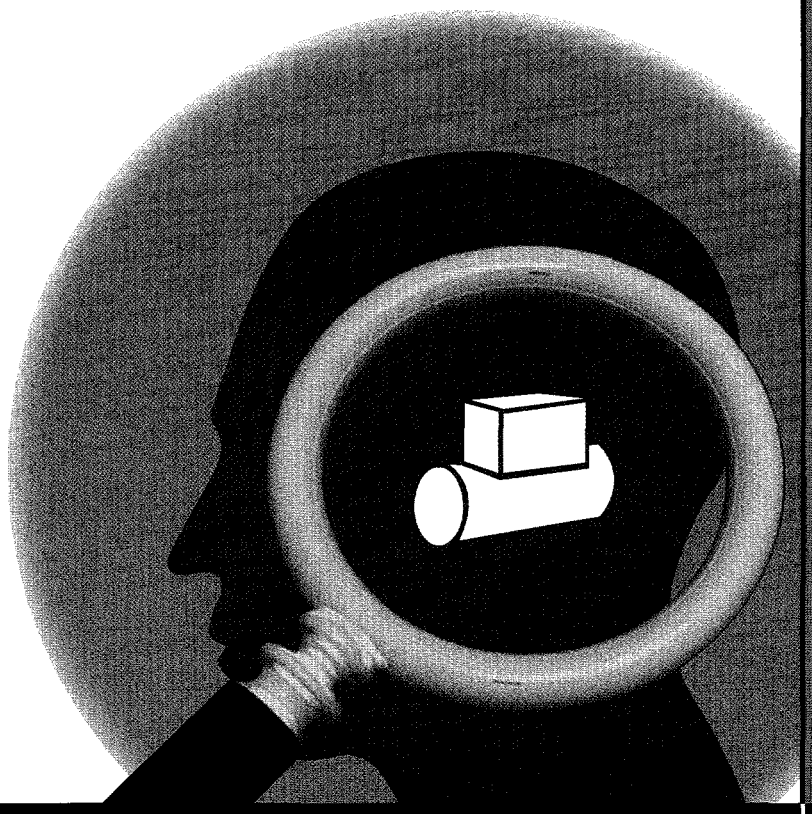

V IPNS Target Experience

J. M. Carpenter and W. G. Ruzicka, IPNS Division, Argonne National Laboratory

This section summarizes our experience with targets in IPNS and the origins of target developments in the prototypes ZING-P and ZING-P′. The targets used are as follows:

ZING-P	1/2 lead brick, soldered copper water cooling tube; 1974, 1975
ZING-P′	Tungsten cylinder with surrounding water cooling jacket; 1977, 1978 Zircaloy-clad depleted α-uranium cylinder with surrounding water cooling jacket; 1979, 1980
IPNS	Zircaloy-clad depleted α-uranium disks with cross-flow water cooling; same for neutron scattering and (until 1985) radiation effects targets; 1981-1988, 1991-1996(?) Zircaloy-clad enriched α-uranium disks; 1988-1991 Zircaloy-clad enriched γ-phase uranium-10 weight % molybdenum disks; 1996(?)-

The following describes design philosophies, operational experiences, observations of failures, and performance.

Experience, 1991-1996

The history of IPNS target developments until 1991 was traced in the 1991 IPNS Progress Report. These developments centered around the use of water-cooled Zircaloy-2-clad α-uranium (actually "Springfield" uranium, an α-phase alloy with a few hundred parts per million (ppm) of Fe, Al, Si, and C). Interesting events took place almost immediately after our last report. The enriched-uranium booster target developed a cladding leak in June 1991, when the xenon-135 monitoring system, working as planned, promptly indicated the presence of the fission product in the cooling system cover gas. To determine whether the xenon monitor was really indicating a leak, we pursued an intensive series of measurements to verify that fission products were getting out of the target and to quantify the effect. When we were satisfied that the target had developed a cladding break, we removed the booster and, in the fall of 1991, replaced it with the earlier-operated depleted-uranium target that we had reserved as a spare. No deleterious consequences, for the facility or the outside world, followed from the target failure. We had anticipated that the target would fail after about the accumulated operating time, on the basis of isotropic radiation-induced swelling of uranium. But because periodic monitoring (with an ultrasonic probe) of the growth indicated that growth was proceeding more slowly than anticipated, we were surprised by the leak.

The depleted-uranium target worked without trouble for about a year, at which time the xenon-135 monitor again indicated a leak. By then, that target had served for about eight years; we removed it and replaced it with a fresh spare. Subsequently, we modified the earlier-used depleted-uranium radiation effects target for service in the Neutron Scattering Facility (cooling connections had to be rearranged) and, to confirm that it would fit, installed it in September 1994. As this is written, that target is still in place, and the slightly-used second target is our spare.

We dispatched the spent booster target for safe disposal and sent the failed depleted target to Argonne's alpha-gamma hot cells for destructive examination by Al Hins, Bob Strain, and Larry Neimark and his crew. The first disk (facing the proton beam) had small cracks in the cladding of both the front and back faces. This was not entirely surprising; the xenon monitor had indicated two onsets in close succession. The cladding exhibited wavy distortion on several of the frontmost disks, more or less coinciding with the power density variation; the second disk, wavy as it was, was intact. Figure 1 shows the front surface of the first disk.

FIGURE 1.
Front face of Disk #1.

Cutting apart the first disk, we revealed a crack through the entire thickness, passing through the thermocouple well and extending from the cladding crack on the one side to that on the other. Figure 2 shows the sectioned first disk. We dug out some of the "grunge" that filled the crack, and other secondary cracks in the uranium metal, and put it into the General Purpose Powder Diffractometer for analysis. Although it was a rather small sample by common standards, Jim Richardson and Mel Mueller identified uranium hydride and several oxides, the products of uranium corrosion in water (even a small amount of gamma iron, residue of the pick used to remove the grunge and a testimony to the sensitivity of the analysis). The grunge analysis held no surprises, because the cracked disk had soaked in water for several months after failure.

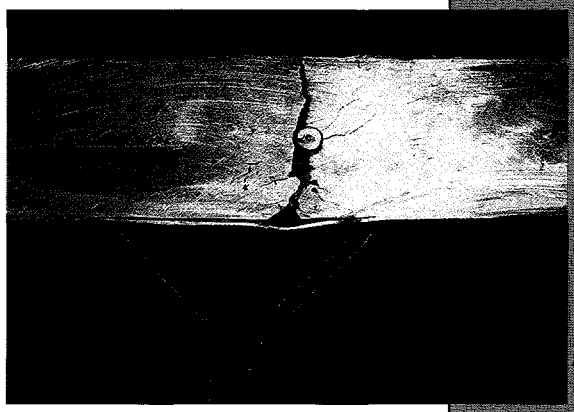

FIGURE 2.
Cross section revealed by cut through Disk #1.

We concentrated on the second disk, which was uncontaminated by the results of uranium corrosion due to water entering through any crack, to obtain evidence of the cause of failure. Figure 3 shows a micrograph of a section of the second disk. A system of cracks extends to the clad interface where, at a step in the metal surface, the uranium metal has separated from the cladding over a small region. The cladding remains intact at that point, and no evidence of corrosion is visible. The crack morphology indicates anisotropic growth. (α-Uranium is

V

rhombohedral in crystal structure; upon irradiation, it expands in the c-direction and contracts in the a- and b-directions, causing intergranular strain that eventually leads to cracking.)

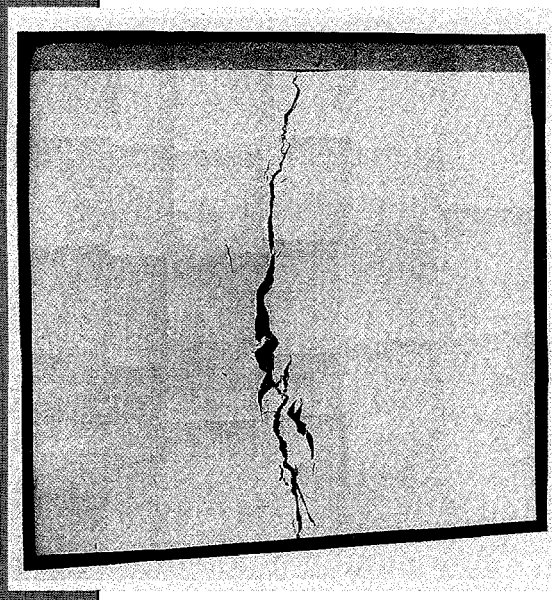

FIGURE 3.
Composite micrograph of the second sample from Disk #2 in the as-polished condition.

This experience is not unique. ISIS has used eight α-uranium targets, most of which have failed by externally similar mechanisms. The α-uranium target of KENS also failed recently, after about ten years of service. After the IPNS booster target failure, we looked at the records with Tim Broome (ISIS), seeking to identify the failure mechanism. We found that fission burnup correlated more closely with failure than did operating temperature or thermal cycling; this correlation would be expected if the root cause were anisotropic growth. However, these observations, based on a rather small number of rather approximately characterized examples, do not conclusively exclude another possible mechanism, failure due to hydride formation.

Future Plans

By informal agreement, IPNS and ISIS decided to take two different routes to solve the problem of shorter-than-desired uranium target lifetime: ISIS would try a target of finer-grained α-uranium (anisotropic on a smaller physical scale), and IPNS would work on a target of γ-uranium. ISIS has gone its route, fabricating a new target and operating it to end-of-life, with no resulting improvement in lifetime.

At IPNS, we have completed the analysis and design of a new booster target of enriched uranium-10 weight % molybdenum, a γ-phase (cubic, therefore isotropic) alloy. Information on this alloy exists from 30 or 40 years ago, when research was done to find a reactor fuel that could be operated in a water-cooled environment without cladding. Indeed, U-10Mo has corrosion behavior much superior to that of α-uranium (a significant advantage in hazards evaluation), but it still needs cladding. Tests done in support of the German SNQ (Spallations Neutronen Quelle) project confirm the expectation that (cubic, isotropic) U-10Mo is dimensionally stable under thermal cycling, while α-uranium is not. Other SNQ-sponsored tests have shown that zirconium or Zircaloy cladding can be applied by diffusion (hot isostatic pressure, HIP) bonding, the process used in all uranium targets so far. These data support our design.

The new IPNS booster target will have the same multiplication factor (k_{eff} = 0.80) as the previous partially enriched α-uranium booster target, and disks clad with HIP-bonded Zircaloy. The subcritical multiplication gain in the new booster target will be about the same as in the original, since we are essentially replacing U-238 atoms with Mo atoms in the new booster. (This has been verified in calculations by P.K. Job and R.N. Blomquist.) There will be

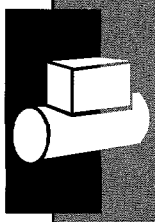

no internal thermocouples, since they were used only for measurements to confirm design calculations and were never intended for monitoring purposes. Furthermore, the thermocouple wells in the failed target disk that we examined had at least a partial role in weakening the disk with respect to cracking. U-10Mo is a metastable phase, which decomposes to a mixed $\alpha + \gamma$ phase after long times at temperature. Time/temperature transformation data do not extend to times comparable with the desired target lifetime, nor to the relatively low temperatures expected, and the consequences of transformation to the $\alpha + \gamma$ phase are not known. Nevertheless, we can reasonably expect the U-10Mo booster to last longer than the α-uranium booster, which had a lifetime that was, after all, satisfactory under IPNS conditions; we simply seek to do better.

The design and the safety analysis for the U-10Mo booster target are completed. We await administrative action on the level of hazards categorization and on security concerns. Due to changes in policy regarding enriched uranium, we also await decisions about the facility where the new target would be fabricated – the Oak Ridge Y-12 facilities. Y-12 built the original booster target, and we have negotiated tentative arrangements for manufacturing the new one there. However, those facilities have only recently started up after a shutdown.

We are ready to proceed with the new booster target, anticipating the same 2.5-times overall gain in IPNS beam intensities, and we are eager to carry out our part of the grand uranium target experiment. Meanwhile, we are down to one spare depleted-uranium target and are discussing producing another (just in case). We are also preparing plans to replace the graphite reflector with beryllium, to gain another 15 to 20% intensity in an arrangement that also will provide faster turnaround of moderator replacements.

V

Cold Moderator Development

T. L. Scott and J. M. Carpenter, IPNS Division, Argonne National Laboratory

Development of IPNS Moderators

The history of moderator development at IPNS from 1981 to 1991 was described in the IPNS 10th Anniversary Progress Report (1991). Here, we update that history to 1996.

Before 1988, the solid methane moderators had experienced numerous failures, which resulted in lost experimental time, costly replacements, and exposure of personnel to radiation. The cause was a pressure surge, caused by a combination of (1) the release of stored energy, which occurred when methane radiolysis products recombined, and (2) the expansion of hydrogen, which built up in the solid methane during irradiation. We formulated a theory about the effect to help us manage it.

From October 1988 to August 1991, we ran the moderators with an enriched uranium target, which increased the intensity of the neutron beams by about 2.5 times. However, the nuclear heating and radiation damage rates in the moderators also increased correspondingly. Because we had already experienced problems with solid methane in the C moderator with a depleted uranium target, we decided to use liquid hydrogen in the C moderator while continuing to use liquid methane in the H and F moderators. In August 1991, the enriched uranium target failed, so we returned to use of a depleted uranium target, with a resultant loss of intensity. Despite the history of solid methane moderator failures, we again ran a solid methane moderator in the C position to regain greater intensity at long wavelengths (about 3.5 times greater than was achieved with a liquid hydrogen moderator). We also formed a committee dedicated to moderator improvement. Committee members consulted with scientists at other facilities about how to avoid failures while operating solid methane moderators.

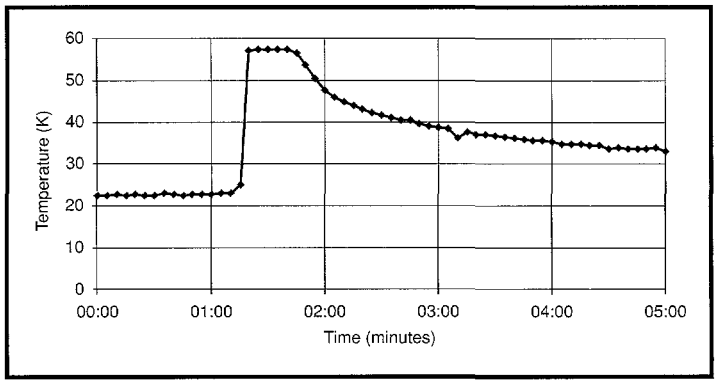

FIGURE 1.
Solid methane C moderator during annealing (after three days irradiation at 29 K).

Moderator Experiments

From December 1992 to March 1993, we tested the C moderator with cold solid methane to determine the

rate at which the stored energy built up during irradiation and the temperature at which hydrogen was released during annealing. We found that we could operate at about 28 K if we annealed the moderator to the melting point of methane (about 90 K) every two to three days. We determined this schedule on the basis of the stored energy that was released during recombination, as indicated by the rapid rise in temperature when the moderator warmed up during annealing. Figure 1 shows this energy release, which increased with (1) the irradiation time between annealings and (2) the lowering of the moderator operating temperature. We found that very little hydrogen gas evolved during warm-up, until a temperature of about 65 K was reached. Above this temperature, the hydrogen gas was released rapidly up to about 90 K, at which the methane melted. (We do not yet understand the physics involved in this threshold temperature for hydrogen release.) Figure 2 shows the hydrogen release as a function of annealing temperature, as measured with a residual gas analyzer (RGA). We continue using solid methane as the medium in the C moderator.

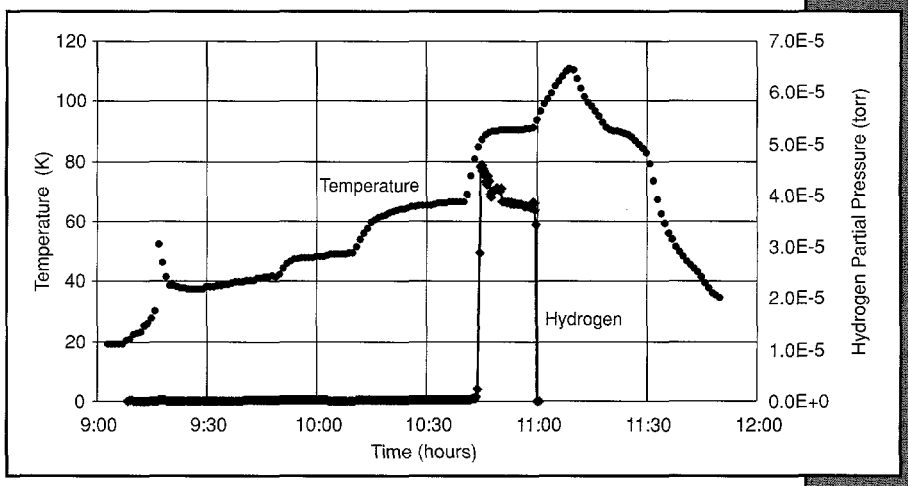

FIGURE 2.
Solid methane C moderator (hydrogen release during an anneal).

Moderator Changes

During the long, hot summer of 1994, the moderator crew, Terry Scott, Mark Schlueter, Richard Tafoya, and Denny Wozniak, installed a new moderator/reflector assembly, a liquid-helium refrigeration system, and a gas control system to convert operation of the H moderator from liquid to solid methane. The installation, completed in September 1994, included the following changes: the liquid methane moderator in the H position was replaced with a new solid methane moderator; a new solid methane moderator was placed in the C position; and the liquid methane moderator in the F position was replaced with a new one of identical design. The new H moderator, which serves three instruments (QENS, GLAD, and HRMECS), contains an aluminum-foam heat-transfer medium (like that always used in the C moderator) and an aluminum-17% gadolinium poisoning plate, 0.5-mm thick by 10-cm square, located 2.5 cm beneath the viewed surface.

Moderator Operation

Both solid methane moderator systems are operated at about 28 K and melted to approximately 95 K at intervals of two to three days to anneal the stored energy and remove accumulated hydrogen. The annealing schedule and operating temperature are dictated by the observation of spontaneous "burps" that take place somewhat irregularly in the C moderator,

at intervals of a little less than three days. Figure 3 shows such a burp of the C moderator that took place after about three days of irradiation of the depleted uranium target at a proton current of ~15 μA. Such burps do not remove all the stored energy; a subsequent scheduled annealing produced another release of stored energy following a relatively short (1-hour) irradiation.

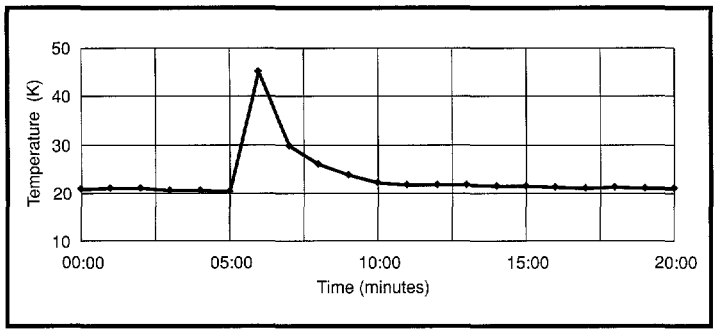

FIGURE 3.
Solid methane C moderator spontaneous burp (after three days of irradiation at 28 K).

Instrument Beam Improvements Accomplished by the H Moderator Change

The colder, solid methane H moderator (about 28 K, compared with the liquid methane H moderator at about 100 K) not only produces a greater flux of long-wavelength neutrons, it also extends the sharp "slowing-down" shape of the pulse to lower energies. However, there is some sacrifice of flux in the 10-meV region. This situation has enabled HRMECS to extend its useful range to E_0 below 4 meV, where ~150-μeV elastic resolution is achieved. The counting rate in QENS in the near-elastic range (E_f = 3.7 meV) has increased, with little change in resolution. The resolution of GLAD is also cleaner in the longer-wavelength range.

Calculations at the University of Illinois, Urbana-Champaign

We hope to modify the grooved C moderator to improve its performance for the reflectometers. We believe we can achieve this because the flux emerging from the bottoms of the (horizontal) grooves is about five times greater than the flux from the tips of the fins, while the (vertical) POSY beams average across tips and grooves. The idea is to change the moderator design so that the grooves are vertical and the bottoms of the grooves illuminate the POSY collimation. However, we are not certain what such a new geometry would do to the SAD and SAND instruments, which view the moderator ± 18° (horizontally) from the normal, whereas the POSY reflectometers view the moderator perpendicularly. If the moderator had vertical grooves, SAD and SAND would not see the bottoms of the grooves at all, and intensity might be lost. To answer the questions raised and guide the design of a modified moderator, we have begun a program of Monte Carlo neutron transport calculations, overseen by Brent Heuser and performed by student Steve Kramer at the University of Illinois's Department of Nuclear Engineering. Preliminary results, derived from an accurate representation of the IPNS arrangement with the grooves vertical, indicate that intensity in the directions of SAD and SAND is preserved, with the sides of the fins providing the principal illumination.

Cold Neutron Testing Facility at Pennsylvania State University

Thus far, our understanding of the burping phenomenon is based on relatively poorly controlled measurements taken on production versions of solid methane moderators. Varying the

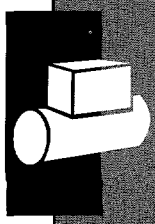

operating conditions systematically is too difficult, the number of installed monitoring instruments is too small, and the risk to continuing operations is too great for us to undertake a program of measurements on IPNS that could provide clearer insight into the basic phenomena. We have developed a design for a facility in which to make well-instrumented tests under controlled conditions in the Breazeale Nuclear Reactor at Penn State, and we have obtained safety approval to proceed. Paul Sokol leads the effort; Rob Dimeo carried out the design and safety analysis work. The project has been encouraged, assisted, and endorsed by Reactor Manager Marc Voth, Nuclear Engineering Department Chairman Ed Klevans, and visiting scientist and colleague Genja Shabalin from the Frank Laboratory for Neutron Physics (Dubna, Russia).

We look forward to carrying out a program of measurements that will offer us a better understanding of the burping phenomenon, provide the basis for improving the design of production moderators, determining operating temperatures and annealing schedules, and generate information on the stresses encountered during operation and annealing.

V

A Tribute to Bob Kleb

J. M. Carpenter, IPNS Division, Argonne National Laboratory

The two best sculptures on the Argonne site both fascinate and mystify most people. This response is fitting for the work of any artist, but both of these works were created by an engineer. They were components of an important particle-physics detector of the 1970s: the 12-foot Hydrogen Bubble Chamber. One part, the piston, stands majestically outside the central administration building; the other, the "Omega bellows," rests near the High Energy Physics offices. Their creator, neither a common artist nor a common engineer, is Bob Kleb. Bob designed those parts and, with his colleague, Lyle Genens, made the bellows himself. Although these are two rather big items, they represent only a tiny fraction of Bob Kleb's contributions to the research tools, large and small, of Argonne National Laboratory. And they worked! Everything Bob has designed or built works!

In the 1960s, Bob Kleb went to work in the neutron scattering program at the CP-5 reactor, where he took part in many important developments. We met when I first began visiting Argonne in the late 1960s, and I learned then of his already-legendary skills. In the early 1970s, I began working at Argonne for David Price, then Solid State Science Division Director. Our goal was to build a pulsed source at Argonne. I was to manage the project but needed engineering assistance. I waited to learn who would be assigned. David announced that Bob Kleb would work with me. I had thought that that was impossible even to hope for and rejoiced in my excellent luck. It was luck widely spread, for our collaboration, which succeeded only because of Bob Kleb's numerous contributions, led to a new generation of neutron scattering facilities. Bob's mark is on the target, moderator, reflector, shielding, and general designs for the earliest prototypes – ZING-P and ZING-P'; on all the proposed larger versions, both built and unbuilt – ZING, IPNS-I, IPNS-II, IPNS Upgrade; and on all the neutron scattering instruments – in sample cells, cryostats, pressure cells, sample changers, ovens, countless choppers, detector rigs, shields, moderators, windows.... Bob's work is everywhere. And everything works! (Well, he has done some "experiments.")

To say that Bob is a brilliant engineer is to say only part of what he is, for, as a highly skilled craftsman, he builds with his own hands much of what he designs. The artist is there in him because he cares deeply about what he does. If "form follows function" is a maxim for beauty in design, then the origin of beauty in Bob's creations is obvious. "Easy to work with," "an idea man," "a patient teacher," "an honest critic" – all these phrases describe Bob Kleb. As Bob moves toward retirement, I acknowledge my own huge debt to him for his contributions to the work of pulsed spallation neutron source development.

The following comments are from a few of Bob's colleagues. One thing is clear from them: we are all talking about the same person.

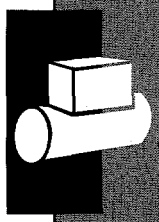

G. P. Felcher, Senior Scientist, Materials Science Division,
Argonne National Laboratory

"Bob, here is what I want: I want a superconducting magnet composed of two circular coils, coaxially placed. I want a magnetic field up to 100 kilooersted in the center, where I am going to place my sample. I want to change the sample with utmost ease, to control its temperature between 1 K and room temperature, and to be able to orient it in any direction. Oh, I forgot ... I want the two coils to be spaced 2 inches apart, and I would like to shine (neutron) light in any direction in the gap. And I do not want any material around that could become magnetic. No steel."

"Okay, Gian, let me think about it."

This exchange of words took place in 1970. At the time, production had just started of niobium-tin ribbon, the only material capable of attaining that magnetic field. At the time, also, I was a young man with no qualms for asking the Moon. In 1972, the magnet was ready and running. True, I had to descend to grievous compromises. For instance, the gap between the two coils was not clear over 360° but *only* over 330°. The coils were not kept apart *just* by vacuum (when energized, they were pulling together with the force of 100 tons, the weight of a small bridge) but by a box made of thin, concentric aluminum rings, carved out of a solid block and prestressed in the ensemble. On the other hand, the mechanism to orient the sample, made of heavily anodized aluminum – synthetic sapphire – would have been the envy of any Swiss watchmaker.

Many years have passed since then, and I came to know better Bob and his "creatures". As always, one goes to Bob wanting something – something that has a special job to do – and Bob creates it. Large or small, his creatures have come to life to fulfill their appointed goals simply but marvelously. In the musing of an esteemed Cornell professor: "This looks a Rube Goldberg thing, but it works."

Bob loves his creatures. The only times I saw him upset were when somebody (and sometimes it was I) mistreated them, or abused them with no concern about their working. For Bob, the working of things constitutes their inherent beauty, and I suspect that if sometimes he was tempted to go beyond and add something purely for aesthetic value, he refrained because that would have been (where did I hear that?) "gilding the lilies."

J. M. Rowe, Chief, Reactor Radiation Division,
National Institute of Standards and Technology, Gaithersburg, Maryland

Of the many surprises awaiting me when I arrived at Argonne to take up a postdoctoral position in August 1966, the one that has given me the most long-term problems was the existence of an engineer named Bob Kleb. Bob did not behave like an engineer; his only answer to any request was "Yes, we can do it, and now let's see how long it will take and at what cost." After he had worked on it for a while, the time and cost were always less than I had feared or guessed. This may not seem to be a problem of any kind, let alone a long-lasting one, but I can assure you that it was!

V

I spent many years after leaving Argonne looking for "another Bob Kleb," and to those who know Bob, it will be no surprise that my search was unsuccessful. He is without question the most talented and creative design engineer that I have ever had the good luck to meet, and those of you at Argonne must have found, as I have, that there is only one of him.

The fruits of Bob's labor surround you at IPNS, many dating from the days of CP-5 at ANL, including the LRMECS flight path. I had the great good fortune to work with Bob at a time of excitement and accomplishment at ANL, when there were many young and talented scientists just starting their careers. Some of those scientists were less skilled than others at some of the more practical aspects of our work, and Bob was unfailingly pleasant, supportive, and a good teacher. At this time of his retirement, I want to thank him for all that he has done, not only for Argonne and IPNS, but also for the entire field of neutron scattering.

J. J. Rush, Group Leader, Neutron Condensed Matter Science,
National Institute of Standards and Technology, Gaithersburg, Maryland

In 1963, I arrived at Argonne as the first of a cadre of young Turks who joined Don Connor's leap into time-of-flight neutron scattering at the CP-5 reactor. Being a chemist among physicists and engineers, with a strong sense of mission and confidence and an urge to get on with it, I needed tempering and guidance, which Don Connor understood better than I did at the time. He introduced me in short order to a young engineer named Bob Kleb he had rescued from the Argonne Central Shops. My job was to "design" and carry out the tests of a D_2O-ice moderator for the CP-5 and NBS reactors and to start a research effort in chemical spectroscopy with neutrons. It was during those early days that I experienced and came to understand the special qualities and genius of Bob Kleb as an engineer and designer.

With a smile on his face and his special blend of kindness and directness, Bob managed to blunt and redirect my sometimes bizarre (but creative) plans and suggestions. Quite simply, he (and Don) taught me in those days a lot of what I know about doing things right, in neutron instrumentation, in cryogenics, in sample containment, and a host of other issues. I never got very good at it, but with their guidance I did develop a better sense of things and a nose for detecting potential problems. So Bob Kleb was both a tutor and a friend to me in those early days. Also, he was always available to Bob Carter, Mike Rowe, and me for valuable consultations in later years, in spite of his increasing responsibilities. Bob is perhaps the most multitalented engineer I have ever had the privilege to work with. I know he will be sorely missed at Argonne, but he has certainly earned an active and joyful retirement. I wish him the best.

D. L. Price, Senior Scientist, Materials Science Division,
Argonne National Laboratory

During the quarter century of our association, Bob has been responsible for many facilities and pieces of apparatus for our neutron scattering research. These cover an enormous variety of sizes, shapes, and functions, but all have two features in common: an outstanding simplicity and an infallible capability for doing the job. This unique performance testifies to the unique genius of their creator: an uncanny ability to distill the often wild and misarticulated demands of the scientist into essential technical requirements and produce a finished piece of equipment that never ceases to amaze in its simplicity and its match of

function to purpose. This rare engineering talent is combined in Bob with a delightful personality; an unflagging interest in, and a mine of information about, all diverse things; a quizzical sense of humor; and a humane interest in his fellow beings. We shall not look upon his like again.

J. D. Jorgensen, Senior Scientist, Materials Science Division,
Argonne National Laboratory

When I arrived at Argonne in 1974, I quickly realized that Bob Kleb was a critical part of a highly developed infrastructure that allowed unique experiments to be done at the CP-5 research reactor in spite of its modest flux. His contributions included high-speed neutron choppers of various designs, a superconducting high-field magnet with a large aperture to accommodate samples in the neutron beam, and specialized sample cells that would enable the measurement of the antiferromagnetic order in high pressure, ultracold solid ^{3}He.

My arrival coincided with the beginnings of the pulsed neutron effort at Argonne, which would prove to depend heavily on Bob's skills. It's not hard to understand Bob's contributions to the pulsed neutron source effort. Originally, there was the series of ZING prototypes, where Bob did everything from target/moderator design to instrument design to the buildings and hutches that housed them. It all needed to be done on a tight budget. I can still picture my beam path, made from hardware-store downspout and borax, passing though a torch-cut hole in a large cooling-fan plenum that happened to be in the desired path. His later contributions to IPNS are simple to define. Consider an empty Building 375 – a bare floor. Everything other than that was engineered partly or solely by Bob.

An amazing quality of Bob's engineering is that he often executed the fabrication himself in order to make sure it was done correctly. The computer-controlled sample changers on the SEPD and GPPD are examples. Responding to my request for a sample changer (I was tired of changing samples in the middle of the night), Bob went into the neutron group's shop in Building 223 to fabricate a prototype based on his idea of using a Geneva drive to achieve accurate (within 0.025 cm) sample positioning. He made the critical components himself. Other components were made in Central Shops. The changer was so successful in its first test on the SEPD that GPPD immediately wanted one. Bob took the prototype apart to measure the components and make drawings for the shop. The installation of these changers on the SEPD and GPPD yielded an increase of about 50% in the overall throughput of samples on these instruments. Bob's ingenuity proved again that productivity in neutron scattering depends on more than the neutron flux.

The amount of creative engineering done at the lunch table also amazes me. Concepts that led to air-tight vanadium sample cans that could be sealed in a few seconds and techniques for the study of small samples (smaller than 100 mg) by hanging them on amorphous boron fibers were developed in just this way, with the first prototypes often fabricated the same afternoon.

Few people have contributed as much to the overall success of Argonne's neutron scattering effort. At a lunch honoring Bob's 70th birthday, some of us joked about how productive he still was, but it's actually a sobering thought to consider his retirement. Thanks for all the contributions that only you could have made, Bob! I'm going to start trying to learn how to take care of that helium pressure cell myself.

Shireen Adenwalla and Apollo P. Y. Wong adjust the alignment of the polarized neutron beam with the super mirror analyzer on the POSY diffractometer at the Intense Pulsed Neutron Source. POSY is used to study near-surface behavior – for example, polymer bonding and diffusion.

Chapter VI

ORGANIZATION AND USER PROGRAM

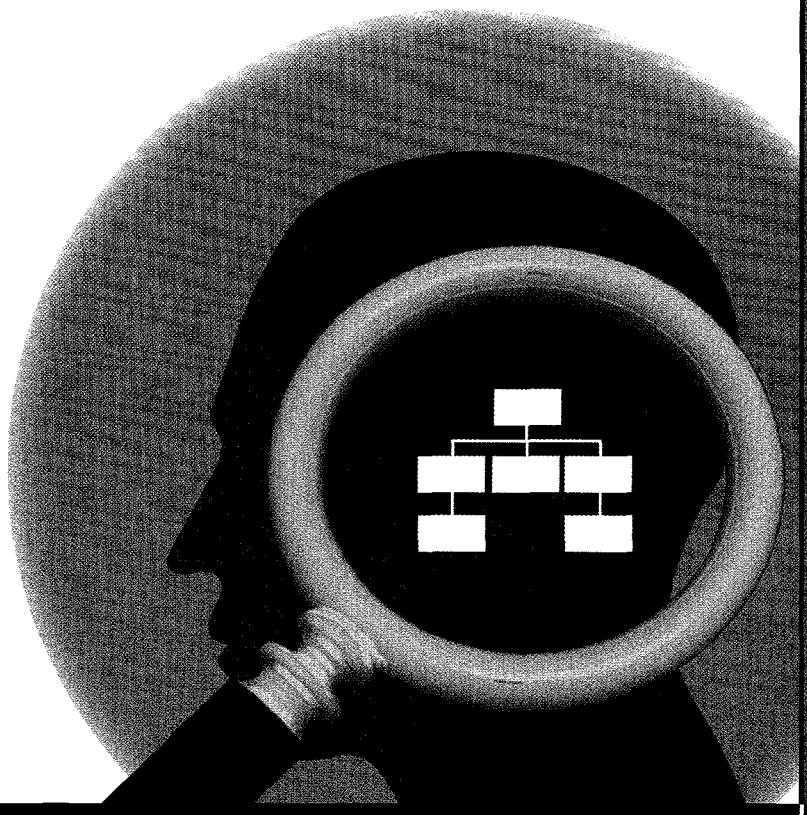

15TH ANNIVERSARY 1981 - 1996

IPNS

VI Organization and User Program

B. A. Marzec, IPNS Division, Argonne National Laboratory

IPNS is operated by the IPNS Division (Figure 1). The IPNS management team – which includes the Division Director, Technical Director, Operations Manager, Accelerator Facilities Manager and Deputy Manager, Assistant Division Director, Instrumentation Scientist, Group Leader for Neutron Scattering, and Data Analysis System Manager – provides strategic direction for the organization's mission, vision, values, and goals and defines the personnel roles and responsibilities to attain these objectives. The management team takes a positive, pro-active approach in developing new or revised IPNS strategies and in integrating such strategies into the operational program. These strategies include modes of operation, staffing plans, new instruments, new advanced sources, and external interactions.

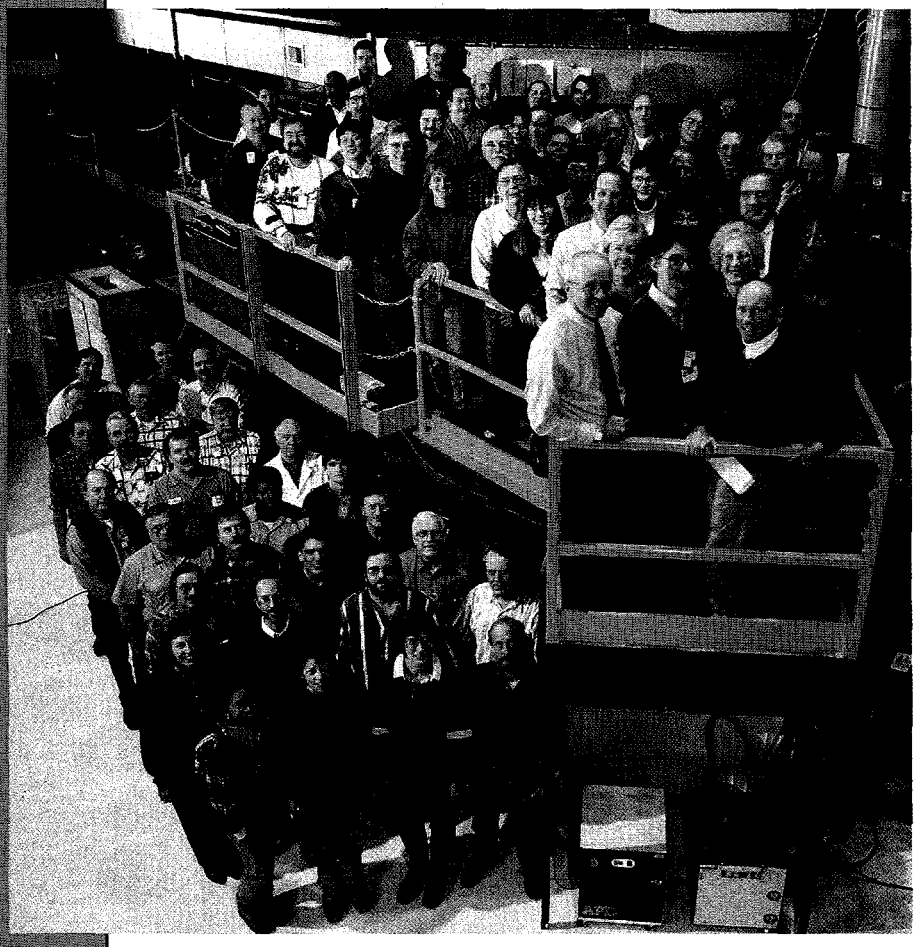

FIGURE 1.
IPNS Division personnel.

IPNS itself has a permanent scientific and technical staff to maintain and run the accelerator, target and moderator systems, and instruments (and to pursue development where necessary), as well as to serve the user program. Many of the Ph.D. scientists who spend full time in neutron scattering and serve as Instrument Scientists for IPNS instruments are members of the Materials Science Division at Argonne. Service personnel, administratively part of other Laboratory organizations, are dedicated to work closely with the IPNS organization to provide support. In addition, at any

given time, a number of visiting faculty members, post-doctoral appointees, and students spending extended periods at Argonne add a welcome diversity to the in-house neutron scattering community.

Neutron Scattering Instruments

IPNS currently has eleven operating neutron scattering instruments, plus two more under development:

General Purpose Powder Diffractometer *(GPPD)*
Glass, Liquid, and Amorphous Materials Diffractometer *(GLAD)*
High-Intensity Powder Diffractometer *(HIPD)*
High-Resolution Medium-Energy Chopper Spectrometer *(HRMECS)*
Low-Resolution Medium-Energy Chopper Spectrometer *(LRMECS)*
Neutron Reflectometer *(POSY II)*
Polarized Neutron Reflectometer *(POSY)*
Quasielastic Neutron Spectrometer *(QENS)*
Single Crystal Diffractometer *(SCD)*
Small-Angle Diffractometer *(SAD)*
Special Environment Powder Diffractometer *(SEPD)*
Chemical Excitation Spectrometer *(CHEX, under development)*
Small-Angle Neutron Diffractometer *(SAND, under development)*

These instruments are the result of a continuous series of developments that began with the early prototypes. Ancillary equipment, available for all of these instruments, includes various capabilities for measurements at high temperature, low temperature, high pressure, and high magnetic field, as well as under various gaseous conditions. A majority of users come from outside Argonne, representing universities, industrial corporations, and government-sponsored research laboratories throughout the nation and overseas, as shown in Figure 2.

User Program

IPNS is by far the most user-oriented of the U.S. Department of Energy's (DOE's) neutron source facilities. IPNS personnel believe that to properly run a user program, it is necessary to provide creative, Ph.D.-level scientists whose primary responsibility is to aid users of the IPNS neutron scattering instruments in the planning and performance of experiments. This involves providing individual help through the whole experiment process, beginning with sample preparation; followed by sample environment, experiment setup, and data collection; and concluding with data evaluation. Other services provided for users include helping with travel and lodging arrangements, site entrance assistance, and site-specific IPNS orientation and training. In addition, training and safety-related information are provided to users to facilitate independent future experiments, permitting the Instrument Scientist to work with other new users and thereby expanding our user base.

In meeting one of the primary user requirements, IPNS has attained an enviably high reliability record (of which we have always been extremely proud) for its accelerator system. Operating reliability is defined as the percentage of scheduled operating time during which the

IPNS USER PROGRAM

	FY82	FY83	FY84	FY85	FY86	FY87	FY88	FY89	FY90	FY91	FY92	FY93	FY94	FY95
NO. OF EXPERIMENTS PERFORMED	94	110	210	180	212	223	257	323	330	273	210	248	281	279
VISITORS TO IPNS FOR AT LEAST ONE EXPERIMENT:														
ARGONNE	37	41	49	44	52	55	57	60	61	60	53	48	49	55
OTHER GOVT. LABS	8	9	8	7	11	15	18	16	19	15	14	18	13	16
UNIVERSITIES	27	33	45	51	79	78	89	94	120	92	62	64	63	83
INDUSTRY	5	5	9	7	13	24	20	24	36	18	20	16	15	12
FOREIGN	12	18	39	35	27	24	17	26	18	27	14	25	32	33
TOTAL	89	106	150	143	182	196	201	220	254	212	163	171	172	199

FIGURE 2.
A majority of users come from outside Argonne, representing universities, industrial corporations, and government-sponsored research laboratories throughout the nation and overseas.

accelerator, target, and moderators are all functioning to deliver useful beams to the instruments. From the beginning, the operating reliability of IPNS has been consistently above 90%, and in recent years this has increased to 95%. Reliability is especially important because the typical experiment lasts only a few days. IPNS's high reliability has made it possible for users to schedule their visits comfortably and to count on collecting their data during their scheduled time. In those few cases where problems have been encountered in neutron source operation, in operation of the specific instrument, or in the user's own equipment, the dedicated operation of the accelerator system for IPNS has usually permitted the flexibility to arrange the scheduling changes necessary to complete the experiment (for example, by extending the run). Two weeks of operation per year have been supported by the NSF Science and Technology Center for Superconductivity.

IPNS/LANSCE Program Advisory Committee

The Program Advisory Committee (PAC) for IPNS and the Los Alamos Neutron Scattering Center (LANSCE) meets twice a year to review proposals for beam time at the two neutron facilities. The PAC has a majority of non-Argonne members, with its membership chosen to span the diverse types of science typically proposed (Figure 3). Current members of the committee and their institutions are:

Elastic Subcommittee
Anthony K. Cheetham *(University of California)*
David E. Cox *(Brookhaven National Laboratory)*

Andrew C. Lawson *(Los Alamos National Laboratory)*
Kenneth R. Poeppelmeier *(Northwestern University)*
James D. Jorgensen *(Argonne National Laboratory)*

Inelastic Subcommittee
Jurgen Eckert *(Los Alamos National Laboratory)*
Priya D. Vashishta *(Louisiana State University)*
Gabriel Aeppli *(AT&T Bell Laboratories)*
Raymond Osborn *(Argonne National Laboratory)*
Brian M. Powell *(Chalk River Laboratory)*

Small-Angle Diffractometer and Reflectometer Subcommittee
Robert Briber *(University of Maryland)*, PAC Chairman
Brent Heuser *(University of Illinois)*
Pappannan Thiyagarajan *(Argonne National Laboratory)*
Gregory S. Smith *(Los Alamos National Laboratory)*

For most instruments, 75% of the beam time is allocated by the PAC to the users, on the basis of proposals submitted by the users, and 25% is reserved for the Instrument Scientists, who operate, maintain, and improve the instruments and carry out their own scientific programs. In December 1995, the PAC met to schedule experiments for the 26th operating cycle. Most instruments have been oversubscribed by factors of 2-3 since their commissioning, and no instruments are undersubscribed. For experiments on publishable research accepted by the PAC or done in collaboration with an Argonne Instrument Scientist, the neutron beam time, complete scientific and technical assistance, and the use of the relevant IPNS instrument, analysis codes, and computing facilities are provided free of charge. Some support is also available to cover travel and lodging for those university users who are unable to arrange this support otherwise. The IPNS computers can be easily accessed remotely, permitting scientists to complete data analysis from their home institutions. Beam time for proprietary work or for publishable work that is not accepted by the PAC can be purchased under a rate structure established by the DOE.

FIGURE 3.
IPNS/LANSCE Program Advisory Committee members present at the December 1995 review meeting. From left to right, they are Andrew (Angus) Lawson, James Jorgensen, Brent Heuser, Gregory Smith, and Kenneth Poeppelmeier (standing); Raymond Osborn, Robert Briber, Gabriel Aeppli, and Brian Powell (seated).

VI

Application for Beam Time

To apply for neutron beam time at IPNS, a proposal must be submitted on a proposal form. The IPNS/LANSCE Program Advisory Committee meets twice a year to consider these proposals. Proposal forms are sent to a large subset of our mailing list approximately one month in advance of each deadline.

Proposal forms are now available via ftp and can be submitted by fax (708-252-4163) or regular mail. Because we have switched to an electronic mail system that supports attached documents, proposals may also be submitted via e-mail (to bamarzec@anl.gov). To obtain an IPNS proposal form, ftp to "ftp.pnstgw.pns.anl.gov" or use Netscape or Mosaic to follow the links on the IPNS home page. The forms are available both in MS Word Rich Text Format (RTF) and in Adobe Portable Document Format (PDF). You can view or print the PDF format document by means of a free Adobe Acrobat Reader from "http://www.adobe.com/", but if you intend to submit a proposal electronically, you need to use the RTF document and convert it to either MS Word or WordPerfect.

The proposal form is an important input to the PAC for allocation of beam time. The form should be as comprehensive as possible; use of figures is extremely useful to the committee. However, the available space on the proposal form must be strictly respected. It is essential to complete and sign the safety box on the proposal form. Desired and impossible dates should also be indicated. The PAC will review only those proposals submitted on the most current proposal form. All other submitted forms or incomplete forms will be returned.

Those who have already run experiments must submit a report on the standard IPNS report form. Further beam time will not be granted unless reports on all previous experiments have been submitted. Referencing and discussing all previous work at IPNS is extremely useful to the PAC and can enhance your proposal's prospects for acceptance.

Assistance for University Users of IPNS

A policy has been established, with support from the University of Chicago Board of Governors for Argonne National Laboratory, for limited financial assistance for IPNS users from North American universities. The University of Chicago Board of Governors for Argonne National Laboratory has also supplied a car, which is available to IPNS users during their stay.

Purchase of Proprietary Beam Time

Beam time for experiments can be purchased under a rate structure approved by the Department of Energy. For proprietary work or publishable work that is not of direct interest to the DOE, the full-cost-recovery rate of ~$5000 per instrument per day (effective October 1995) will be applicable. For information, contact the IPNS Division Director, Bruce Brown, at 708-252-4999.

Other IPNS Activities

IPNS activities are related to many other DOE programs, such as fossil energy, energy efficiency, nuclear waste management, transportation, defense, and biological research. Many

industrial users have performed experiments at IPNS, and some of them have paid for beam time for proprietary research. Many of these experiments are collaborations with Argonne and IPNS scientists and result in joint publications.

IPNS and the Neutron Scattering Group in the Argonne Materials Science Division have continued to develop on-site Ph.D. thesis participation programs in collaboration with the Division of Educational Programs (DEP) at Argonne. In addition to trips to Argonne during the year, faculty advisors have frequently come to Argonne for the summer as part of a faculty research program. Some IPNS personnel have served as regional university adjunct faculty.

Argonne sponsors a Laboratory Open House every few years. IPNS has always participated in this Open House, and several thousand people routinely tour IPNS during the event. IPNS tour guides inform the public about IPNS activities and share information on the type of research performed at the facility (Figure 4). Visitors are provided with information about Argonne and IPNS, enhancing public understanding about the Laboratory and how it conducts its important national mission. The Open House demonstrates both the high quality of our research and concern for our neighbors. The next Open House is planned for the fall of 1996 to celebrate the 50th Anniversary of Argonne National Laboratory.

FIGURE 4.
IPNS Division tour guides for the May 1994 Open House.

Conferences and Workshops

With financial and technical assistance from both the University of Chicago and Argonne's Division of Educational Programs, IPNS has sponsored conferences and workshops to inform and educate the outside community about the usefulness of neutrons across a spectrum of scientific disciplines and to train newcomers in the applications. In the early years of IPNS, an average of five conferences and workshops were held per year. More recently, the average has decreased due to budget restrictions.

IPNS celebrated its **10th Anniversary** on July 10, 1991, with a day-long workshop followed by a reception. Similar plans are being made to celebrate the 15th Anniversary of IPNS on May 7, 1996.

The **Frontiers of Liquid and Amorphous States International Symposium** was held on August 13-15, 1991. The goals of this symposium were to (1) focus on recent advances in the

chemistry and physics of disordered materials; (2) emphasize the interplay between physico-chemical properties and atomic structure, as probed by neutron and x-ray scattering and computer simulation; and (3) discuss selected topics related to the liquid and amorphous states.

In planning for very large projects, such as the new IPNS Upgrade source that is being proposed, IPNS received considerable input from the users. A large workshop for users was held at Argonne on May 13-16, 1993, on **Scientific Opportunities at Future Spallation Neutron Sources.**

The **Workshop on Software Development at Neutron Scattering Sources, SOFTNESS-94,** was held on October 6-7, 1994. The purposes of the workshop were to (1) promote the exchange of information concerning software developments for the visualization and analysis of neutron scattering data; (2) establish a formatting standard for the interchange of neutron scattering data between neutron sources and the user community; and (3) assess the capability of proprietary and public domain software for general data analysis problems and discuss the potential for standardization by U.S. neutron scattering centers.

In April 1995, the **IPNS Upgrade Workshop** was held to examine the Feasibility Study for an IPNS Upgrade. The workshop was a substantial peer review of the proposed accelerator system, conventional facilities, cost, and schedule. The target stations had been previously reviewed. The above study was carried out as a collaboration between IPNS and Advanced Photon Source (APS) personnel at Argonne. The successful IPNS operational, experimental, and target experience were augmented with APS accelerator and project management expertise to produce concepts with high technical, cost, and schedule credibility.

The **Fourth International Conference on Surface X-Ray and Neutron Scattering** was held on June 26-30, 1995. The following topics were discussed during the conference: depth profile in polymers, semiconductors, and magnetic materials; roughness at surfaces and at the interfaces of multilayers; structure of overlayers and surface layers; and in-situ studies of vapor, liquid, and solid interfaces in special environments.

The **Ninth International Conference on Liquid and Amorphous Metals** was held on August 27-September 1, 1995. Highlighted topics included new structural materials and applications in energy conversion, electronics, optics/electro-optics, and waste storage.

The **International Collaboration on Advanced Neutron Sources (ICANS)** was founded at Argonne in 1977. Argonne hosted the sixth ICANS meeting in 1982 and will be hosting the 14th meeting in the spring of 1998. For further information, contact John M. Carpenter (JMCarpenter@anl.gov) or consult our Web description, "http://www.pns.anl.gov/icans/icansdescript.html".

IPNS Advisory Committee

The IPNS Advisory Committee was established in 1986 to represent the mix of disciplines of the users and to assist users with any problems or issues arising at IPNS where consultation could be useful. The committee reviews and advises on all aspects of the IPNS operation, including scientific programs, user programs, planned upgrades, and other programmatic

issues as requested by the IPNS Division Director. The purview of the committee has expanded to include advising on short- and long-term plans for the facility. The members are chosen to represent the various scientific research areas that utilize IPNS. The committee is being expanded and will report to the University of Chicago's Board of Governors for Argonne National Laboratory. The next meeting will be in the spring of 1997.

Awards and Recognition

Recognizing employee contributions is paramount to a continuing successful program. Performance awards may be given to individual employees in recognition of performance achievements, as set forth in the specific award program criteria. IPNS personnel have been nominated for and received numerous awards. In October 1995, IPNS facility personnel were honored to be recognized by the U.S. Department of Energy and the Energy Quality Council; the facility was presented the Energy Quality Commendation Award for exemplary achievements in demonstrating the quality ethic (Figure 5).

FIGURE 5.
Beverly Marzec accepted the 1995 DOE Energy Quality Award for IPNS from Secretary of Energy Hazel O'Leary. Also attending the awards ceremony were H. Sue Morss (left), representing the ANL Associate Laboratory Director for Physical Research, and Arthur J. Goldman (right), Director of ANL Quality Management.

Since 1991, the following IPNS personnel have received awards:

The 1992 Federal Laboratory Consortium Award for Excellence in Technology Transfer
James Richardson, Jr.

The University of Chicago Outstanding Service Award
Franklin Brumwell
David Leach

The Argonne Director's Award
Julie Hanebuth
Kenneth Volin

VI

The Argonne Pacesetter Award

Roger Blackman and Lawrence Johns

Roger Blackman, Donald Bohringer, Merlyn Faber, John Hammonds, Lawrence Johns, David Leach, Beverly Marzec, William Ruzicka, Terry Scott, Kenneth Volin, and Robert Zolecki

John Hammonds

Julie Hanebuth

Terry Scott and Al Paugys

Jeffrey Toeller and Frans Trouw

IPNS Facility Personnel – March 1996

Specific job responsibilities of IPNS personnel are listed. IPNS instrument responsibility is given in parentheses.

PNS DIVISION ADMINISTRATION

Bruce Brown	-	*Division Director*
Diane Hoffmann	-	*Secretary*
Ira Bresof	-	*Assistant Division Director*
Jack Carpenter	-	*Technical Director*
Julie Hanebuth	-	*ESH Coordinator, Quality Assurance*
Beverly Marzec	-	*Staff Assistant, Scientific Secretary*

USER SUPPORT

Kent Crawford	-	*Instrumentation Scientist*
Chun Loong	-	*Group Leader for Neutron Scattering, Inelastic Scattering (HRMECS)*
George Ostrowski	-	*Software Development*
Jim Richardson	-	*Powder Diffraction (GPPD)*
Art Schultz	-	*Single Crystal Diffraction (SCD), High-Intensity Powder Diffraction (HIPD)*
Thiyagu Thiyagarajan	-	*Small-Angle Diffraction (SAD/SAND)*
Frans Trouw	-	*Quasielastic and Inelastic Scattering (QENS/CHEX)*
Apollo Wong	-	*Neutron Reflection (POSY II)*
Tom Worlton	-	*Computer Systems Manager, Network Manager*
Shireen Adenwalla	-	*Neutron Reflection (POSY)*
Gary Burr	-	*Powder Diffraction (GPPD)*
Millie Firestone	-	*Molecular Diffusion, Synthesis (QENS)*
Jackie Johnson	-	*Glass, Liquid, and Amorphous Materials (GLAD)*
Jamie Ku	-	*Colloidal Systems (SAD/SAND)*
Cheok Tam	-	*Molecular Spectroscopy,Chemical Excitation (CHEX)*
Dianna Young	-	*Chemical Crystallography (SCD)*

NEUTRON OPERATIONS

Bill Ruzicka	-	*Operations Manager*
Cathy Riblon	-	*Secretary*
Henry Belch	-	*Design Engineer*
Don Bohringer	-	*Neutron Facilities Supervisor*
Lawrence Donley	-	*(LRMECS), Choppers, Accelerator Kicker System*
Rick Goyette	-	*Neutron Reflection (POSY/POSY II), Mac Computers*
John Hammonds	-	*Data Acquisition*
Lynette Jirik	-	*Operations*
Chris Johnson	-	*Operations, (QENS)*
John Kowalski	-	*Ancillary Equipment Engineer*
Dave Leach	-	*Group Leader - Operations*

Martha Miller	-	*Cryogenic Engineer, Moderators*
Dean Peters	-	*Cryogenics, Moderators*
Chris Piatak	-	*Operations*
Mark Schlueter	-	*Operations*
Terry Scott	-	*Lead Engineer for Moderators, Cryogenics*
Tony Tafoya	-	*Operations*
Ray Thomas	-	*Powder Diffraction Instrumentation (GPPD)*
Jeff Toeller	-	*Chief Technician - Operations*
Rich Vitt	-	*Operations, (SCD)*
Ken Volin	-	*Glass, Liquid, and Amorphous Materials (GLAD)*
Tom Walsh	-	*Operations*
Denny Wozniak	-	*Small-Angle Scattering Instrumentation (SAD/SAND)*
Dan Yocum	-	*Inelastic Scattering (HRMECS), Choppers*

ACCELERATOR OPERATIONS

Gerry McMichael	-	*Accelerator Facilities Manager*
Frank Brumwell	-	*Deputy Accelerator Facilities Manager*
Carolyn Tobin	-	*Secretary*
Jerome Ballentine	-	*Linac, Mechanical Systems*
Tom Beilfus	-	*Linac, Power Supplies*
Roger Blackman	-	*Synchrotron Power Supplies and Magnets, Procurement*
Wally Czyz	-	*Operations, Instrumentation and Controls*
Jim Davis	-	*Assistant Chief of Operations, Kicker System*
Tony DeWitt	-	*Preaccelerator and Linac Systems*
Joe Dittrich	-	*Operations, Electronics*
Merle Faber	-	*Chief Technician - Operations, PC Computers*
Mark Gibson	-	*Operations, Electronics*
Jeff Goetzen	-	*Operations, Electronics*
Larry Johns	-	*Group Leader - Synchrotron*
Ray Krell	-	*Operations, Mechanical Systems*
Frank Nelson	-	*Synchrotron, Mechanical Systems*
Don Piatak	-	*Linac, Vacuum and Mechanical*
Garrett Rinehart	-	*Computer Control and Diagnostics*
Jim Spindler	-	*Assistant Chief of Operations, Kicker System*
Vern Stipp	-	*Group Leader - Linac*
Bill Sullivan	-	*Assistant Chief of Operations, Controls*
George Vasilopulos	-	*Assistant Chief of Operations, Electronics*
Bob Zolecki	-	*Synchrotron RF System, Instrumentation and Controls*

USER SUPPORT AND TECHNICAL ASSISTANCE FROM OUTSIDE IPNS

MATERIALS SCIENCE DIVISION

Bob Birtcher	-	*Radiation Effects*
Gian Felcher	-	*Neutron Reflection (POSY)*
Jim Jorgensen	-	*Powder Diffraction (SEPD)*
Ray Osborn	-	*Inelastic Scattering (LRMECS)*
David Price	-	*Glass, Liquid, and Amorphous Materials (GLAD)*
Simine Short	-	*Powder Diffraction (SEPD)*
Ray Ziegler	-	*Instrument Support*

ENVIRONMENT, SAFETY AND HEALTH DIVISION

Marcia Torres	-	*Health Physicist*
Bill Krueger	-	*Health Physics Technician*
Sue Rhodes	-	*Health Physics Technician*

James Spindler at the controls of the Intense Pulsed Neutron Source accelerator, which produces a 500-MeV proton beam for use by the IPNS spallation neutron source.

Chapter VII

FUTURE PLANS

- ENHANCED OPERATION
- SPALLATION NEUTRON SOURCE PLANS AT ARGONNE

IPNS

VII Enhanced Operation

B. S. Brown, IPNS Division, Argonne National Laboratory

The DOE budget proposal for FY 1996 includes a Scientific Facilities Initiative (SFI) that will lead to the more effective use of a remarkable array of research facilities throughout the United States, many of which have no counterpart in any other country. These innovative, state-of-the-art resources represent a large federal investment in specialized energy, environmental, medical, physics, and industrial research. The facilities include high-energy and nuclear physics accelerators, neutron and synchrotron-light sources, and smaller facilities, such as electron microscopy centers.

The SFI provides $100 million per year to meet the increasing demand for operating time at these unique facilities involved in the basic energy sciences, high-energy physics, and nuclear physics. Although that sum represents a funding increase of about 10% for user facilities, it will actually increase operations at such facilities by about 30%, thereby leveraging both federally and privately sponsored research. The initiative recognizes the president's pledge and the Administration's commitment, as articulated in *Science in the National Interest*, to invest in fundamental science as a top priority.

One goal of the SFI is to double the IPNS's operation time and provide the scientific and technical support needed to permit all instruments in the user program to be operated fully. The additional operating funds represent a 50% increase over FY 1995's funding from DOE.

Upon receiving news of the possible increase, ANL solicited opinions from outside users, as well as its own scientists and technical support personnel, on the best use of the prospective funds. Discussions were held within the IPNS division and throughout the Laboratory, and a plan was formulated. A decision was made to add staff at the post-doctoral level, scientific staff to support the instrument scientists, and engineering and technical staff to support the accelerator and neutron operations groups. Ads were placed, and Argonne received many inquiries and applications from outstanding candidates. The interview process, which is still going on, involves many members of the IPNS team. The first "new faces" began to appear in December 1995, and by March 1996, over half of the new personnel were on board. So far, ANL has been very pleased with the new additions.

The goal is to build up the amount of time the IPNS operates to 32 weeks per year. During the first year, while people are being hired and trained, IPNS will operate for 25 weeks. The transition to greater availability is already under way; it started in October, the beginning of the new fiscal year. At its December meeting, the Program Advisory Committee (PAC) increased the amount of time it will allocate by 50% for most instruments and by 100% for the two powder diffractometers. The funding increases under the SFI are being immediately translated into additional beam time for IPNS users.

Spallation Neutron Source Plans at Argonne

B. S. Brown, IPNS Division, Argonne National Laboratory

In the fall of 1995, after the Advanced Neutron Source (ANS) was cancelled, DOE's Basic Energy Sciences Advisory Committee (BESAC) established three subcommittees to update its review of future U.S. neutron sources. One subcommittee was to review possible upgrades to existing reactors; the second was to review possible upgrades to existing spallation sources; and the third was to guide DOE's conceptual design of a new spallation neutron source.

For the past three years, Argonne has been examining the feasibility of upgrading the IPNS. Page iii of this report shows the layout of the IPNS Upgrade. Based on a proton accelerator producing 500 μA at 2 GeV, the upgrade could provide a total beam power of 1 MW. It would have two target stations; one would operate at 10 Hz, for high-resolution and long-wavelength instruments; the other would operate at 30 Hz, for high-intensity applications. The IPNS could be upgraded in 4-1/2 years through a modest extension of existing technology, for a total construction cost estimated at $559 million. Using existing Argonne buildings would save $175 million over using a new (greenfield) site. Argonne printed and distributed its *IPNS Upgrade: A Feasibility Study* in April 1995, and since that time, the report has been subject to many peer reviews. The target stations, accelerator system, conventional facilities, cost, and schedule have all been endorsed.

The choice of 30 Hz as the source repetition frequency was based on a survey of scientific requirements and an evaluation of preliminary designs for neutron scattering instruments for a 1-MW pulsed source. The study found that scattering instruments could be put into two categories: those for which 30 Hz would be preferable, and those that would require a lower frequency, for which 10 Hz would be satisfactory. Few of the instruments considered could efficiently use frequencies higher than 30 Hz. Therefore, Argonne determined that two targets operating at different frequencies would provide the flexibility to serve both categories of instruments while doubling the number of available beamlines and instruments.

The preferred option is to operate at the highest possible energy and lowest possible current. This preference would not affect the neutron production rate, which is proportional to the proton beam power at the energies under consideration. High-energy protons can be obtained by accelerating protons through a linear accelerator or a circular machine. Because single-pass machines such as linacs tend to have high construction and operating costs, proton linacs tend to be lower-energy machines. The highest-energy proton linac is the 800-MeV linac at Los Alamos National Laboratory. Because circular machines take advantage of multiple traversals of the particles, the energy level at which they operate can be very high. Construction and operating costs for circular machines are substantially lower than those for linacs of similar energy. Circular machines can accelerate a time-averaged current of 0.5-1.0 mA to several GeV. Argonne chose to use a linac to provide a 400-MeV H^-

beam for injection into a rapid cycling synchrotron (RCS). The RCS is designed to accelerate an average proton beam current of 0.5 mA to 2 GeV.

Shielded transport lines would carry two extracted proton beams to the two target stations. Each station would contain a neutron-producing target consisting of water-cooled tungsten plates in two sections. Moderators positioned close to each target would slow down neutrons from the primary source energies (about 1 MeV) to useful energies (less than about 10 eV). Water, liquid methane, and liquid hydrogen moderators would be used. Reflectors of beryllium metal or of beryllium and heavy metal would surround the moderators to enhance the intensities of the neutron beams. Decouplers and heterogeneous poisons within the moderator-reflector system would tailor the spectra and pulse characteristics of the neutron beams. Massive steel and concrete shields would surround the targets and moderators and provide multiple levels of confinement for the radioactive materials within. Because some components of the target would have finite lifetimes, and because alterations would need to be made over the years to accommodate changing demands, each target station would be equipped with a hot cell and remote handling equipment and designed to facilitate the movement and servicing of the internal components. Cross-sectional views of the biological shield and hot cell are shown in Figure 1. Irradiation facilities for neutron activation and fast-neutron materials irradiation applications would be arranged close to the targets. These irradiation facilities would not interfere with neutron scattering applications and would be accessible during operation.

The IPNS Upgrade would provide 36 beam ports for neutron scattering instruments, 18 at the 30-Hz target station and the other 18 at the 10-Hz station. Because neutron beams for more than one instrument would be extracted from a single beam port in some cases, more than 36 neutron scattering instruments could be supported at this facility. There would be a total of 12 moderators, one for every three beam ports, so the moderator characteristics could be optimized to meet the requirements of the individual instruments.

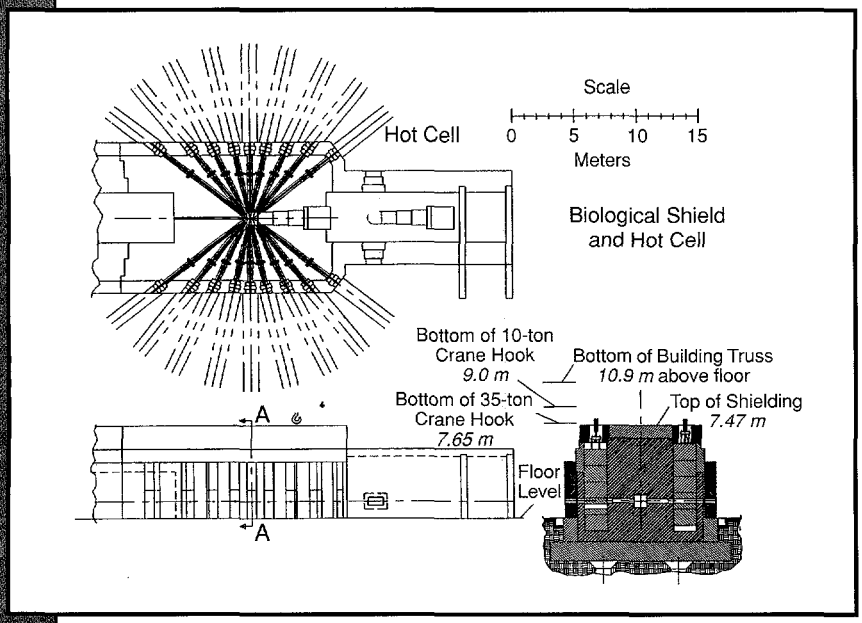

FIGURE 1.
Plan, elevation and cross-sectional views of the biological shield and hot cell.

The IPNS Upgrade would provide 27 instruments for 24 of the 36 beam ports. The remaining 12 uninstrumented beam ports would be available for later development and the installation of both state-of-the-art

instruments and specialized instruments developed by participating research teams. Chapter V of the *IPNS Upgrade: A Feasibility Study* outlines a reference set of 27 instruments that would be well-balanced and capable of carrying out a wide range of neutron scattering activities. This reference set was used in selecting the target station parameters, laying out the locations of the target stations within the experiment halls (page iii), and making cost estimates. Up to 10 of the instruments that are presently operating at IPNS would be refurbished and transferred to the IPNS Upgrade as part of this initial instrument complement. This approach would provide a core of proven instruments ready for operation at start-up. The neutron scattering instruments are located in existing experiment halls that provide internal space for beamlines up to 50 m long. Longer beamlines can be extended outside the buildings, if necessary.

Most of the neutron scattering instruments use the neutron time-of-flight (TOF) principle for determining neutron wavelengths. The majority of these instruments, in turn, require good wavelength resolution. For such instruments, the IPNS Upgrade target stations would provide 25 to 50 times the intensity available at IPNS. However, for those instruments that do not require good wavelength resolution (for example, small-angle-scattering instruments), the coupled liquid hydrogen moderators would be used to provide 100 to 200 times the intensity available at IPNS.

If the IPNS Upgrade were a 1-MW source, it could easily be upgraded to 5 MW by injecting the beam from the 2-GeV RCS into a 10-GeV RCS. Studies on this option have been under way since the 1-MW feasibility study was completed. A viable concept that takes ANL site considerations into account has been developed. This design has the advantage of permitting full operation of the 1-MW source while the 10-GeV ring and target areas are under construction. The 2-GeV and 10-GeV rings could be connected quite quickly. Furthermore, the 1-MW facility would require no additional capabilities to be enhanced to 5 MW; thus, there would be no extra costs associated with the initial 1-MW source.

A downsized version of the 1-MW IPNS Upgrade has also been under study; the design was presented to the second BESAC subcommittee in January 1996 and to the full BESAC in February 1996. The downsized source would use the same conceptual linac-synchrotron accelerator system, operating at 30 Hz. The beam would be delivered to only one target (not two), and the number of instrument beamlines would also be halved. The beam power would be 400 kW (2.5 times that of ISIS, the most powerful spallation source in the world), and the cost would be about half that of the 1-MW source. Using existing Argonne buildings would save $155 million over using a new site. Not only would this proposed downsized IPNS Upgrade be considerably less expensive, it would also take less time to build (less than 4 years, rather than 4-1/2 years), thereby helping the United States regain its leadership position in neutron research. A reference set of instruments was chosen; it includes five existing, upgraded instruments that would be moved from IPNS. The layout of the reference set is shown in Figure 2, and the corresponding requirements are listed in Table 1.

Since the BESAC review, an effort has begun on designing and costing an ISIS-level source of 150 kW. This would consist of a linac and 1.5-GeV synchrotron operating at 30 Hz and producing 100 μA. There would be one target station, and instruments would be moved from IPNS

BEAMLINE REQUIREMENTS					
INSTRUMENT	L_i (m)	L_f (m)	MODERATOR	COUPLING[b]	BEAM PORT[c]
*SEPD	12	1.5	H_2O		B-3
*GPPD	25	1.5-4	H_2O		B-2
hi res[d] powder	50	2	H_2O		E-1
residual stress	25	1.5-3	H_2O		E-2
*GLAD	16.5[e]	1.5	H_2		D-3
single crystal	10	0.6	H_2O		E-3
*HRMECS	18	4	H_2		F-1
quasielastic	9	≤1	H_2		F-2
*SAND	12	2	H_2	coupled	A-2
hi res small-angle	20	5	H_2	coupled	A-3
reflectometer	13[f]	≤2	H_2		F-3
cold neutron chopper	20	4	H_2		D-1
hi res backscattering	30	3	H_2		D-2

* Instruments transferred from IPNS.

[a] The reference set of instruments is selected to show that a balanced set of instruments can be suitably placed to utilize the experiment hall (Building 370). This reference set occupies 13 of the 18 beam ports. It includes the five instruments transferred from IPNS, with the remainder being selected from among the instruments described in Reference 1.

[b] All moderators are decoupled, unless otherwise noted.

[c] Beam ports are numbered clockwise from the proton beam, as viewed from above. Numbering scheme is moderator (A through F) and beam port on that moderator (1 through 3).

[d] "hi res" = high-resolution.

[e] To low-resolution sample position.

[f] Flight path shortened for 30-Hz operation.

TABLE 1. Beamline requirements for a reference set[a] of instruments.

and/or provided by Participating Research Teams. The construction schedule would be somewhat shorter than the 400-kW Upgrade, and the cost would be slightly more than half that of the latter source.

All of the above studies have been carried out as collaborations between the IPNS and APS (Advanced Photon Source) personnel at Argonne. Augmenting the successful operational, experimental, and target experience gained at IPNS with the accelerator and project management expertise developed at APS has resulted in concepts that are very credible in terms of their technical merit, cost, and schedule.

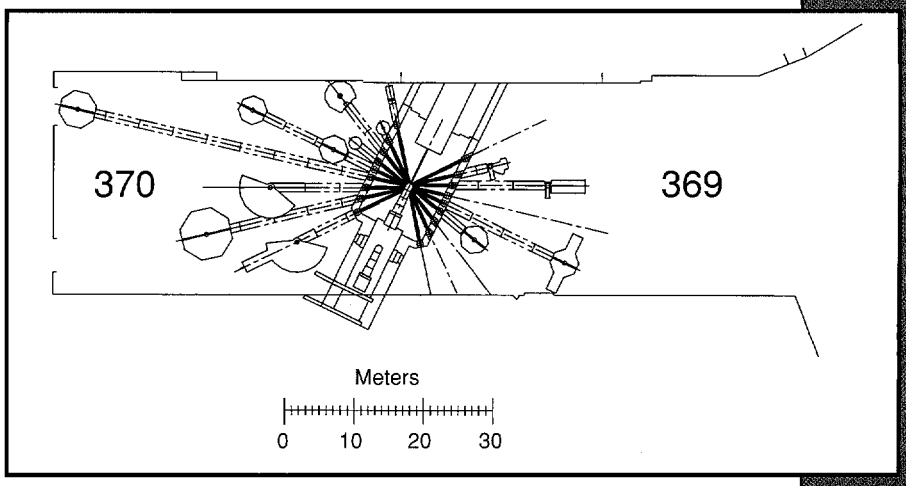

FIGURE 2.
Location of the reference set of instruments on the neutron beamlines in Building 370.

Reference

IPNS Upgrade: A Feasibility Study, Argonne National Laboratory Report ANL-95/13 (April 1995).

Lawrence Donely examines a bakeable cell designed for in-situ neutron studies of atomic diffusion and excitations in hydrogen-charged zeolites and proton conductors.

Chapter VIII

PUBLICATIONS

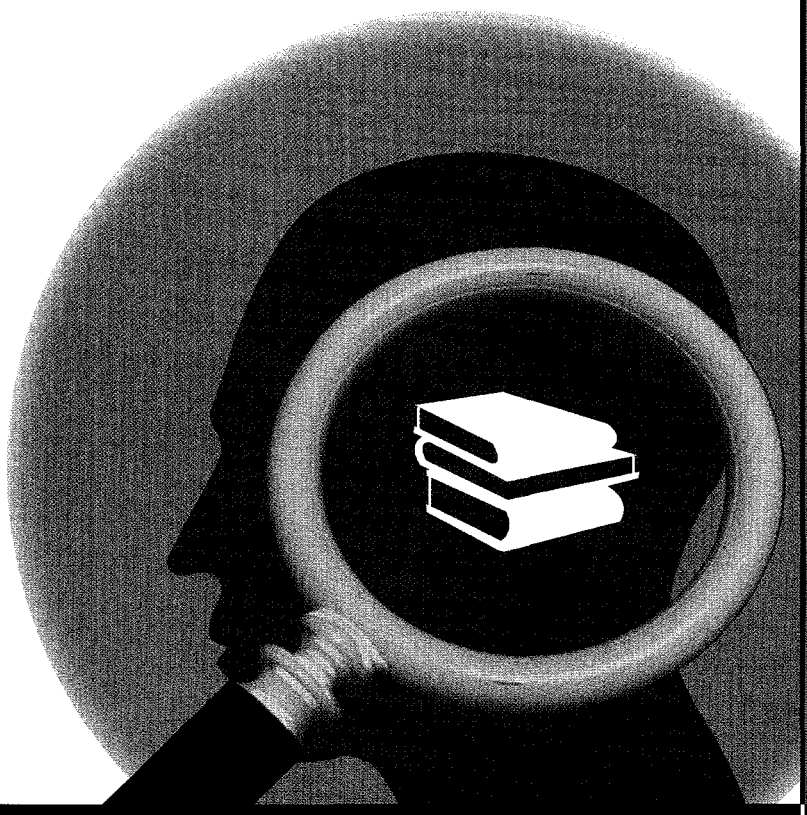

VIII Publications

Authors should be reminded that IPNS is funded by the Department of Energy (DOE) and appropriate acknowledgement is important. Authors are encouraged to acknowledge IPNS and DOE support in all relevant papers and abstracts. A recommended acknowledgement citation is the following:

> *This work has benefited from the use of the Intense Pulsed Neutron Source at Argonne National Laboratory. This facility is funded by the U.S. Department of Energy, BES-Materials Science, under Contract W-31-109-Eng-38.*

Please pay particular attention to items which are to be copied by direct method; cover page acknowledgements are not normally copied. Since publications are the "product" of IPNS experiments, all authors are requested to send a copy of all publications arising from IPNS work to the IPNS Division office. If you send a preprint, please remember to follow up either with a reprint or at least a note giving the precise publication details. This request applies irrespective of whether an Argonne scientist is co-author of the paper.

Please remember that the Argonne staff have spent considerable effort building up the facilities which are made available to users. We consider it natural that Argonne staff participating extensively in the performance of user experiments will have the opportunity to be co-authors of any resulting publication. If in doubt, co-authorship should be discussed at the beginning of an experiment.

These publications, resulting from work done at IPNS since 1991, have been compiled.

S. Adenwalla, Y. Park, G. P. Felcher, and M. Teitelman, "Magnetic Response of Ultrathin Fe on MgO: A Polarized Neutron Reflectometry Study," J. Appl. Phys. **76** (1994), 6443-6445.

S. Adenwalla, G. P. Felcher, E. Fullerton, and S. Bader, "Polarized Neutron Reflectivity Confirmation of 90 Degree Magnetic Structure in Fe/Cr(001) Superlattices," Phys. Rev. **53**(5) (1996), 2474-2480.

G. Agrawal, R. Wool, W. Dozier, G. P. Felcher, T. Russell, and J. Mays, "Short-Time Interdiffusion at Polymer Interfaces," Macro. **27** (1994), 4407-4409.

P. A. Alekseev, V. N. Lazukov, R. Osborn, I. P. Sadikov, E. S. Konolova, Y. B. Paderno, and B. Rainford, "Magnetic Excitations in Inelastic Neutron Scattering Spectra on Sm(M)B_6 where (M=Ca, Ba, La) Intermediate Valent Compounds," Zh. Eksp. Teor. Fiz. **208**(3) (1995), 1064-1080.

P. Alekseev, V. Lazukov, R. Osborn, B. Rainford, I. Sadikov, E. Konolova, and Y. Paderno, "Neutron Scattering Study of the Intermediate-Valent Ground State in SmB_6," Europhys. Lett. **23**(5) (1993), 347-353.

C. Allen, S. Ohnuki, and H. Takahaski, "Facilities for In Situ Ion Beam Studies in Transmission Electron Microscopes," Proc. 3rd IUMRS Int. Conf. on Adv. Mater. **17** (1994), 93-96.

P. Allenspach, J. Mesot, U. Staub, M. Guillaume, A. Furrer, S.-I. Yoo, M. J. Kramer, R. W. McCallum, H. Maletta, H. Blank, H. Mutka, R. Osborn, M. Arai, Z. Bowden, and A. D. Taylor, "Magnetic Properties of Nd^{3+} in Nd-Ba-Cu-O Compounds," Z. Phys. B **95**(3) (1994), 301-310.

A. Alvarenga, M.-L. Saboungi, L. Curtiss, M. Grimsditch, and L. McNeil, "Structure and Dynamics of Molten Aluminum and Gallium Trihalides II: Raman Spectroscopy and ab-initio Calculations," Mol. Phys. **81** (1994), 409-420.

M. Anderson and K. Poeppelmeier, "La_2CuSnO_6: A New Perovskite-Related Compound with an Unusual Arrangement of B Cations," Am. Chem. Soc. (1991), 476-482.

M. Arai, A. Hannon, A. Taylor, A. Wright, R. Sinclair, and D. L. Price, "Neutron Scattering Law Measurements for Vitreous Silica," Trans. Amer. Cryst. Assoc. **27** (1993), 113-131.

M. Arai, A. Hannon, A. Taylor, A. Wright, R. Sinclair, and D. L. Price, "High Resolution S(Q,E) Measurement on g-SiO_2," Physica B **180-181** (1992), 779-781.

M. Arai, A. Hannon, A. Taylor, A. Wright, R. Sinclair, and D. L. Price, "Neutron Scattering Law Measurements on Vitreous Silica," The Phys. of Non-Crystall. Solids, edited by L. Pye, W. LaCourse, and H. Stevens (Taylor and Francis, London, 1992), 479-483.

R. Arendt, M. Garbauskas, C. Meyer, F. Rotella, J. D. Jorgensen, and R. L. Hitterman, "Thermal Expansion Measurements Using Neutron Diffraction of $(Bi,Pb)_2Ca_2Sr_2Cu_3O_x$," Physica C **194** (1992), 397-402.

R. Arendt, M. Garbauskas, C. Meyer, F. Rotella, J. D. Jorgensen, and R. L. Hitterman, "Thermal Expansion Measurements Using Neutron Diffraction of $Bi_2CaSr_2Cu_2O_x$," Physica C **182**(1-3) (1992), 73-78.

D. Argyriou, J. D. Jorgensen, R. L. Hitterman, Z. Hiroi, N. Kobayashi, and M. Takano, "Structure and Superconductivity without Apical Oxygens in $(Ca,Na)_2CuO_2Cl_2$," Phys. Rev. B **51**(13) (1995), 8434-8437.

D. Argyriou, J. Garcia, J. Mitchell, J. D. Jorgensen, and D. G. Hinks, "Phase Development of Bi-2212 Superconductor: A Time-Resolved Neutron Powder Diffraction Investigation," J. Mater. Res. (1996), in press.

P. Armand, M. Beno, A. J. G. Ellison, G. Knapp, D. L. Price, and M.-L. Saboungi, "Local and Intermediate-Range Order in Cesium Germanate Glass," Europhy. Lett. **29** (1995), 549-553.

M. C. Aronson, R. Osborn, R. A. Robinson, J. W. Lynn, R. Chau, C. L. Seaman, and M. B. Maple, "Non-Fermi Liquid Scaling of the Magnetic Response in $UCu_{5-x}Pd_x$(x=1, 1.5)," Phys. Rev. Lett. **75**(4) (1994), 725-728.

M. C. Aronson, R. Osborn, R. A. Robinson, J. W. Lynn, R. Chau, C. L. Seaman, and M. B. Maple, "Non-Fermi Liquid Scaling in UPd_xCu_{5-x}(x=1,1.5)," Physica B **206-207** (1995), 108-111.

V. Arrogjo, J. Higgins, A. Burgess, and W. Howells, "Rotation of Methyl Side Groups in Polymer: A Fourier Transform Approach to Quasielastic Neutron Scattering. 1. Homopolymers," Macromolecules **28** (1995), 2745-2753.

R. T. Azuah, W. G. Stirling, J. Mayers, I. F. Bailey, and P. E. Sokol, "Concentration Dependence of the Kinetic Energy in ^3He-^4He Mixtures," Phys. Rev. B **51** (1995), 6780-6783.

D. Basov, T. Timuk, B. Dabrowski, and J. D. Jorgensen, "C-axis Response to $YBa_2Cu_4O_8$: A Pseudogap and Possibility of Josephson Coupling of CuO_2 Planes," Phys. Rev. B **50** (1994), 3511-3514.

M. Beno, G. Knapp, P. Armand, D. L. Price, and M.-L. Saboungi, "Application of New Synchrotron Powder Diffraction Techniques to Anomalous Scattering in Glasses," Rev. Sci. Instrum. **66**(2) (1995), 1308-1310.

A. C. Biondo, J. S. Kallend, A. J. Schultz, and K. C. Goretta, "Texture Evolution during Sintering of Y-Ba-Cu-O," High Temperature Superconducting Compounds III: Processing and Microstructure Property Relationships, edited by S. H. Whang, A. Dasgupta, and E. Collings, The Minerals, Metals and Mater. Soc. (1991), 119-127.

A. C. Biondo, J. S. Kallend, A. J. Schultz, and K. C. Goretta, "Texture Analysis of Bulk $YBa_2Cu_3O_x$ by Neutron Diffraction," In Second World Congress on Superconductivity, Progress in High Temperature Superconductivity, Vol **28,** edited by C. G. Burnham (World Scientific: Singapore, 1992), 361-369.

R. C. Birtcher, J. W. Richardson, Jr., and M. H. Mueller, "Amorphization of U_3Si by Ion or Neutron Irradiation," Met. Trans (1996a), in press.

R. C. Birtcher, J. W. Richardson, Jr., and M. H. Mueller, "Amorphization of U_3Si_2 by Ion or Neutron Irradiation," J. Nucl. Mater. (1995), in press.

M. Blander, E. Bierwagen, K. Calkins, L. Curtiss, D. L. Price, and M.-L. Saboungi, "Structure of Acidic Haloaluminate Melts: Neutron Diffraction and Quantum Chemical Calculations," J. Chem. Phys. **97**(4) (1992), 2733-2741.

A. Boothroyd, S. Doyle, and R. Osborn, "The Magnetic State of Pr in $PrBa_2Cu_3O_7$," Physica C **217** (1993), 425-438.

K. F. Bradley, S.-H. Chen, and T. O. Brun, "Quasielastic Neutron Scattering Measurements of N-butane in Its Crystalline, Plastic and Liquid Phases," J. Chem. Phys. **95**(7) (1991), 5273-5280.

K. F. Bradley, S.-H. Chen, and P. Thiyagarajan, "Observation of Micellar Formation in the Cavity of Porous Silica Glass," Mat. Res. Soc. Symp. Proc. **166** (1990), 403-408.

H. Brand, L. Curtiss, L. E. Iton, F. Trouw, and T. O. Brun, "Theoretical and Inelastic Neutron Scattering Studies of Tetraethylammonium Cation as a Molecular Sieve Template," J. Phys. Chem. **98** (1993), 1293-1301.

B. S. Brown, "Technology and Science at a High-Power Spallation Source," Proc. Sci. Opportunities at Future Spallation Neutron Sources Workshop (Argonne National Laboratory, 1994).

B. S. Brown, F. Brumwell, J. M. Carpenter, R. K. Crawford, A. Rauchas, W. G. Ruzicka, and T. G. Worlton, "Intense Pulsed Neutron Source Status Report," ICANS-XII Facility Status Reports (1993).

B. S. Brown, "A Feasibility Study for the IPNS Upgrade, a 1-MW Pulsed Spallation Neutron Source," Neutron News (1995), 18-20.

B. S. Brown and R. K. Crawford, "IPNS Neutron Scattering Instrumentation. A. Existing and Planned. B. Possibilities for IPNS Upgrade, a 1-MW Spallation Source," Mat. Res. Soc. Symp. Proc. **376** (1994), 47-58.

B. S. Brown, J. M. Carpenter, and R. Kustom, "Outline of a Proposal for a New Neutron Source: The Pulsed Neutron Research Facility," Proc. Int. School of Phys. Enrico Fermi, Ind. and Technol. Appl. of Neutrons, edited by M. Fontana and F. Rustichelli (1992), 511-523.

B. S. Brown, J. M. Carpenter, Y. Cho, R. K. Crawford, and A. E. Knox, "IPNS Upgrade—A 1-MW Spallation Neutron Source," Proc. ICANS-XII **RAL 94-025** (1993), P13-P20.

R. M. Bullock, L. Brammer, A. J. Schultz, A. Albinati, and T. Koetzle, "Low-Temperature Neutron Diffraction Study of $HMn_2Re(CO)_{14}$ and Studies of a Metal-Metal Exchange Equilibrium that Converts $HMn_2Re(CO)_{14}$ into $HMnRe_2(CO)_{14}$," J. Am. Chem. Soc. **114**(13) (1992), 5125-5130.

B. Butler and J. Cohen, "What the Latest Diffraction Techniques Can Tell Us About an Old Material: Steel," Ultramicroscopy **52** (1993), 238-242.

P. Canfield, R. Moshovich, R. Robinson, J. Thompson, Z. Fisk, W. Beyermann, A. Lacerda, M. Hundley, and F. Trouw, "The Low Temperature Groundstate of YbBiPt," Physica B **197** (1994), 101-108.

C. Carlile, R. Durand, W. Fullagar, P. Reynolds, F. Trouw, and J. W. White, "Inelastic Neutron Scattering and Superconductivity of $Rb_3C_{60}(NH_3)_x$," Molecular Phys. **86** (1995), 19-37.

J. M. Carpenter, D. F. R. Mildner, J. W. Richardson, Jr., and W. C. Dimm, "Correcting Beam Monitor and Diffraction Data for Chopped Delayed Neutron Backgrounds," Proc. ICANS-XI (1990), 1044-1053.

J. M. Carpenter, "IPNS Upgrade: Plan for a Neutron Scattering Facility Based on a 1-MW Proton Beam," Asian Neutron Network News (Hamon) **3**(2) (1994), 17-20.

J. M. Carpenter, "Beam Catcher for Unstripped 400 MeV Protons," Accelerator Note NSA-94-6 (1994).

J. M. Carpenter, R. K. Crawford, R. Kleb, and A. E. Knox, "Conceptual Design of the Target Stations of the IPNS Upgrade," Proc. ICANS-XII **RAL 94-025** (1993), T95-T104.

J. M. Carpenter, Y. Kiyanagi, N. Watanabe, H. Iwasa, and M. Nakajima, "Tailoring Intensities and Pulse Shapes in Coupled Moderator-Reflector Systems," Proc. ICANS-XII **RAL 94-025** (1993), T164-T171.

J. M. Carpenter, "Studies for a 1-MW Pulsed Spallation Source in the United States," Physica B **213-214** (1995),1042-1047.

J. M. Carpenter, "Deconvoluting Source Pulse Broadening in Pulsed Source Time-of-Flight Measurements," Proc. ICANS-XIII (1995), 175-183.

J. M. Carpenter, "Feasibility Study for the IPNS Upgrade, A 1-MW Pulsed Spallation Neutron Source, Target Stations," Proc. ICANS-XIII (1995), 7777-7788.

J. M. Carpenter, "ICANS on the World Wide Web," Proc. ICANS-XIII (1995), 22-27.

J. M. Carpenter and A. G. Hins, "Experience with IPNS Targets," Proc. ICANS-XII **RAL 94-025** (1993), T1-T11.

J. M. Carpenter and D. Mildner, "Improving the Resolution of Chopper Spectrometers at Pulsed Neutron Sources," Nucl. Instrum. and Methods in Phys. Res. **A325** (1993), 255-265.

K. A. Carrado, P. Thiyagarajan, R. E. Winans, and R. E. Botto, "The Hydrothermal Crystallization of Porphyrin-Containing Layer Silicates," Inorg. Chem. **30** (1990), 794-799.

K. A. Carrado, P. Thiyagarajan, and D. L. Elder, "Synthetic Polymer-Layer Silicate Clay Composites," Proc. Int. Symp. Synthesis of Zeolites, Expanded Layered Compounds (1996), in press.

K. A. Carrado, P. Thiyagarajan, and D. L. Elder, "Synthetic Polymer-Layer Silicate Clay Composites," Prepr. Pap. - Am. Chem. Soc., Div. Petroleum Chem. **40** (1995), 310-313.

K. A. Carrado, P. Thiyagarajan, and D. L. Elder, "Porous Networks Derived from Synthetic Polymer-Clay Complexes," Synthesis of Microporous Materials: Zeolites, Clays and Nanostructures, edited by M. L. Occelli and H. Kessler (Marcel Dekker, 1996), in press.

K. A. Carrado, P. Thiyagarajan, and K. Song, "A Study of Organo-hectorite Clays Crystallization," Clay Minerals (1996), in press.

K. A. Carrado, P. Thiyagarajan, and D. L. Elder, "Polyvinyl Alcohol-Clay Complexes Formed by Direct Synthesis," Clay and Clay Minerals **44** (1996), in press.

S.-H. Chen, S. L. Chang, R. Strey, and P. Thiyagarajan, "Small Angle Neutron Scattering Investigation of Structural Inversion in a Three-Component Ionic Micro-Emulsion," J. Phys. Condensed Matter **3** (1991), F91-F107.

H. Chen and J. E. Epperson, "Multidisciplinary Study of Phase Separation in a Supersaturated Ni-Si Alloy," TMS-AIME Mtg., M.E. Fine Symp., edited by J. Weertman, H. Marcus, and J. Santner (1991), 17-28.

O. Chmaissem, D. Argyriou, D. G. Hinks, J. D. Jorgensen, B. Storey, H. Zhang, L. Marks, Y. Wang, V. Dravid, and B. Dabrowski, "Chromium Clustering and Ordering in $Hg_{1-x}Cr_xSr_2CuO_{4+\delta}$," Phys. Rev. B **52**(21) (1995), 636-643.

Y. Cho, J. Bailey, B. Brown, F. Brumwell, J. M. Carpenter, R. K. Crawford, D. Horan, D. Jerng, R. Kleb, A. Knox, R. Kustom, E. Lessner, D. McGhee, F. Mills, H. Moe, R. Nielsen, C. Potts, A. Rauchas, and K. Thompson, "Conceptual Design for One Megawatt Spallation Neutron Source at Argonne," Proc. 1993 Particle Accel. Conf. **5** (IEEE 1993), 3757-3759.

Y. Cho, J. Bailey, B. Brown, F. Brumwell, J. M. Carpenter, R. K. Crawford, D. Horan, D. Jerng, R. Kleb, A. Knox, R. Kustom, E. Lessner, D. McGhee, F. Mills, H. Moe, R. Nielsen, C. Potts, A. Rauchas, and K. Thompson, "Conceptual Design for 1-MW Spallation Neutron Source at Argonne," Proc. ICANS-XII, **RAL 94-025** (1993), A57-A63.

G. Cody, P. Thiyagarajan, R. Botto, J. Hunt, and R. Winans, "The Solution Structure of Coal Macromolecules in Deuteropyridine: Small Angle Neutron Scattering Analysis of Untreated and O-Methylated Coal Extracts," Energy and Fuels **8** (1994), 1370-1378.

F. Cotton, L. Daniels, L. Falvello, C. Murillo, and A. J. Schultz, "Solid Solutions of a Jahn-Teller Compound in an Undistorted Host. 4. Neutron and X-ray Single-Crystal Structures of a Cr/Zn Tutton Salt Solid Solution, and Their Implications for the Determination of Homogeneity," Inorg. Chem. **33** (1993), 5396-5403.

F. Cotton, L. Falvello, C. Murillo, and A. J. Schultz, "The Neutron Crystal Structure of the Saccharinate Complex $[Cu(C_7H_4NO_3S)_2(H_2O)_4].2H_20$," Eur. J. Solid State Inorg. Chem. (1992), 311-320.

F. Cotton, L. Falvello, C. Murillo, I. Pascual, A. J. Schultz, and M. Tomas, "The Neutron and X-ray Structural Characterization of the Hexaaquavanadium (II) Compound $VSO_4.7H_2O$," Inorg. Chem. **33** (1994), 5391-5395.

R. K. Crawford, "Celebration of the Tenth Anniversary of IPNS at Argonne," Neutron News **3** (1992), 4-5.

R. K. Crawford, P. Thiyagarajan, and J. Chen, "Linearity and Calibration of Charge-Division and Rise-Time Encoded Gas PSDS," Proc. ICANS-XII (1994), I208-I215.

R. K. Crawford, "Reference Instrument Complement for IPNS Upgrade," Proc. ICANS-XII (1994), I24-I31.

R. K. Crawford, "Position-Sensitive Detection of Slow Neutrons - Survey of Fundamental Principles," Conf. on Slow Neutron Imaging Detectors, SPIE Proc. **1737** (1992), 210-223.

R. K. Crawford, "Gas Detectors for Neutrons, New Tools for Neutron Instrumentation Workshop," J. Neutron Res. (1996), in press.

R. K. Crawford, P. Thiyagarajan, J. Epperson, F. Trouw, R. Kleb, D. Wozniak, and D. Leach, "The New Small-Angle Diffractometer SAND at IPNS," Proc. ICANS-XIII **95-02** (1995a), 99-117.

R. K. Crawford and N. Niimura, "Instrument Workshop Summary on New Components - Detectors," Proc. ICANS-XI (1991), 975-978.

S. Crennell, A. Cheetham, R. Jarman, R. Thrash, and J. Kaduk, "Isomorphous Substitution in Non-Linear $KTiOPO_4$: Neutron Powder Diffraction Study of $KTiO(P_{0.5}As_{0.5})O_4$," J. Mater. Chem. **2** (1992), 383-386.

S. Crennell, A. Cheetham, J. Kaduk, and R. Jarman, "Isomorphous Substitution in Non-Linear Optical Potassium Titanate Phosphate ($KTiOPO_4$). Time-of-Flight Neutron Powder Diffraction Study of Potassium Rubidium Titanate Phosphate ($K_{0.5}Rb_{0.5}TiOPO_4$)," J. Mater. Chem. **1** (1991), 297-298.

S. Crennell, A. Cheetham, J. Kaduk, and R. Jarman, "Isomorphous Substitution in Non-Linear Optical $KTiOPO_4$: A Powder Diffraction Study of $K_{1/2}Na_{1/2}Ti_{1/2}Sn_{1/2}OPO_4$, $Na_{1/2}Rb_{1/2}Ti_{1/2}OPO_4$, $K_{1/2}Rb_{1/2}Ti_{1/2}Sn_{1/2}OPO_4$, and $K_{1/2}Rb_{1/2}Ti_{1/2}Sn_{1/2}OPO_4$," J. Mater. Chem, **2** (1992), 785-792.

A. Cuclol, R. Leo, P. Romano, B. Dabrowski, D. G. Hinks, and P. Radaelli, "Tunneling Spectroscopy into $YBa_2Cu_4O_8$: Intralayer and Interlayer Analysis," Phys. Rev. B **50** (1994), 10397-10400.

B. Dabrowski, Z. Wang, J. D. Jorgensen, R. L. Hitterman, J. Wagner, B. Hunter, P. Radaelli, and D. G. Hinks, "Suppression of Superconductivity by Structural Distortion of the CuO_2 Planes in Orthorhombic $La_{2-x}M_xCuO_4O_4$ (M=Nd,Ca,Sr)," Physica C **235-240** (1994), 339-340.

B. Dabrowski, D. Richards, J. D. Jorgensen, D. G. Hinks, S. Pei, Y. Zheng, and A. Mitchell, "Defects, Oxygen Ordering and Properties of La-Cu-O and Ba-Bi-O Superconductors," 26th Winter School Theoretical Phys. Ordering Phenomena in Condensed Phys. (1990), 88-110.

B. Dabrowski, J. D. Jorgensen, D. G. Hinks, C. Segre, S. Pei, D. Richards, and L. Soderholm, "La2CuO4+δ: A Superconductor Doped by Excess Oxygen Defects," Mat. Res. Soc. Proc. **156** (1989) 69-76.

B. Dabrowski, J. D. Jorgensen, R. L. Hitterman, J. Wagner, Z. Wang, B. Hunter, P. Radaelli, and D. G. Hinks, "Suppression of Superconductivity in Orthorhombic $La_{2-x}M_xCuO_4$ (M=Ca,Sr)," Physica C **235-240** (1995), 339-340.

B. Dabrowski, V. Zhang-MacCoy, R. Hannon, B. Hunter, J. D. Jorgensen, J. Wagner, and R. L. Hitterman, "New 1212 Structural Analog of $YBa_2Cu_3O_7$: The Sr-Based Superconducting," Physica C **208** (1993), 183-188.

B. Dabrowski, Z. Wang, J. D. Jorgensen, R. L. Hitterman, J. Wagner, B. Hunter, and D. G. Hinks, "Suppression of Superconducting Transition Temperature in Orthorhombic $La_{2-x}Ca_xCuO_4$," Physica C **217** (1993), 455-460.

V.-O. de Haan, A. A. Van Well, S. Adenwalla, and G. P. Felcher, "On the Retrieval of Phase Information in Neutron Reflectometry," Phys. Rev. B **52** (1995), 10831-10833.

V.-O. de Haan, A. Van Well, P. Sacks, S. Adenwalla, and G. P. Felcher, "Toward the Solution of the Inverse Problem in Neutron Reflectometry," Physica B (1995a), in press.

R. J. Dejus, S. Susman, K. J. Volin, D. G. Montague, and D. L. Price, "Structure of Vitreous Ag/Ge/Se," J. Non-Cryst. Solids **143** (1990), 162-180.

R. J. Dejus, D. J. LePoire, S. Susman, K. J. Volin, and D. L. Price, "Dynamics of Vitreous Ag/Ge/Se II," Phys. Rev. B15 **43** (1991), 1194-1197.

T. Den, T. Kobayashi, F. Izumi, T. Kamiyama, Y. Shimakawa, J. D. Jorgensen, F. Rotella, and R. L. Hitterman, "Electrical Properties and Crystal Structures of a Homologous Series of Oxides $Nd_2Ba_2Ca_mCe_n/Ti_{2-\delta}O_{11+m+2n}$ (m,n = O or 1)," Physica C **225** (1995), 37-52.

M. Dong, M. Marchetti, A. Middleton, and V. Vinokur, "Elastic String in a Random Potential," Phys. Rev. Lett. **70** (1993), 6562-6565.

W. D. Dozier, P. Thiyagarajan, D. G. Peiffer, M. Rabeony, M. Y. Lin, G. Agrawal, and R. P. Wool, "Small Angle Neutron Scattering and Neutron Reflectometry Studies of a Model Graft Copolymer," Polymer **35** (1994), 3116.

W. D. Dozier, D. G. Peiffer, M. Y. Lin, M. Rabeony, P. Thiyagarajan, S. K. Behal, and M. M. Disko, "Microphase Separation in a Model Graft Copolymer," Int. J. Polymer Analysis and Characterization **1** (1995), 259-275.

W. Dozier and C. Platt, "Graphoepitaxy of $YBa_2Cu_3O_7$ Thin Films," Appl. Phys. Lett. **62** (1992), 2048-2050.

R. Durand, W. Fullagar, G. Lindsell, P. Reynolds, and J. W. White, "X-ray and Neutron Powder Diffraction from $Rb_3C_{60}(NH_3)_x$ - The Approach to Quasicrystallinity?" Mol. Phys. **86** (1995), 1-18.

K. Edler, J. Dougherty, R. Durand, L. Iton, G. Kirton, G. Lockhart, Z. Wang, R. Withers, and J. W. White, "Small Angle X-ray Scattering from MCM41 and Its Synthesis Gels - Optimization of the Synthesis Parameters," Colloids and Surf. (1995), in press.

T. Egami, "Role of Local Polarizations in Superconductivity of High T_c Oxides," Ferroelectrics **130** (1992), 15-26.

T. Egami, B. Toby, S. Billinge, H. Rosenfeld, J. D. Jorgensen, D. G. Hinks, B. Dabrowski, M. Subramanian, R. K. Crawford, W. Farneth, and E. Mccarron, "Local Structural Anomaly Near T_c Observed by Pulsed Neutron Scattering," Physica C **185-189** (1991), 867-868.

T. Egami, H. Rosenfeld, B. Toby, and A. Bhalla, "Diffraction Studies of Local Atomic Structure in Ferroelectric and Superconducting Oxides," Ferroelectrics **120** (1991), 11-21.

T. Egami, B. H. Toby, W. Dmowski, J. D. Jorgensen, and D. G. Hinks, "Local Atomic Displacements in High T_c Oxides Studied by Pulsed Neutron Scattering," in Oxygen Disorder Effects in High-T_c Superconductors, edited by J. L. Moran-Lopez and I. K. Schuller (Plenum, N.Y., 1992), 47-54.

H. Ehrenberg, G. Wltschek, H. Weitzel, F. Trouw, J. Buettner, T. Kroener, and H. Fuess, "Ferrimagnetism in $Ni_4Nb_2O_9$," Phys. Rev. B **52** (1995), 9595-9600.

H. Ehrenberg, G. Wltschek, F. Trouw, T. Kroener, H. Weitzel, and H. Fuess, "Magnetic Structures of α-$FeMoO_4$ and α-$CoMoO_4$," J. Magn. and Magn. Mater. **135** (1994), 355-360.

H. Ehrenberg, I. Svoboda, G. Wltschek, M. Wiesmann, F. Trouw, H. Weitzel, and H. Fuess, "Crystal and Magnetic Structure of α-$NiMoO_4$," J. Magn. and Magn. Mater. **150** (1995), 371-376.

A. J. G. Ellison, K. Volin, D. L. Price, and R. K. Crawford, "Performance of the Amorphous Materials Diffractometer "GLAD" at IPNS," Proc. ICANS-XII **RAL-94-151** (1994a), I144-I151.

A. J. G. Ellison, C.-K. Loong, and J. Wagner, "Neutron-Scattering Studies of Yb-bearing Silicate Glasses," J. Alloys Cmpd. **207-208** (1994), 170-173.

A. J. G. Ellison, C.-K. Loong, and J. Wagner, "The Structure and Spin Dynamics of Lanthanide-Bearing Silicate Glasses," J. Appl. Phys. **75** (1994b), 6825-6827.

A. J. G. Ellison, R. K. Crawford, D. Montague, K. Volin, and D. L. Price, "The New Glass, Liquids, and Amorphous Materials Diffractometer (GLAD) at IPNS," J. of Neutron Res. **1** (1993), 61-70.

A. J. G. Ellison, D. L. Price, J. Dickinson, and A. Hannon, "The Effect of Phase Separation on Short- and Intermediate-Range Order in High-Silica Li_2O-SiO_2 Glasses," J. Chem. Phys. **102** (1995), 9647-9652.

A. Faldi, J. Genzer, R. Composto, and W. Dozier, "Segregation at the Interface Between a Homopolymer and a Binary Polymer Blend," Phys. Rev. Lett. **74** (1994), 3388-3391.

M. Fang, Y. Wang, and P. E. Sokol, "Structure of D_2 Adsorbed in Zeolites," Phys. Rev. B **50** (1994), 12291-12297.

M. P. Fang and P. E. Sokol, "The Structure of Helium and Neon in Zeolites," Phys. Rev. B (1995), 12614-12617.

G. P. Felcher and Y. Y. Huang, "Magnetism of Thin Film Multilayers: An Analogue of Interacting Platelets," Structure and Dynamics of Supramolecular Aggregates and Strongly Interacting Colloids, S.-H. Chen, J. S. Huang, and P. Tartaglia, edited by NATO ASI Series **C369** (Kluwer Academic Publishers, 1992), 691-711.

G. P. Felcher, Y. Y. Huang, M. Carey, and A. Berkowitz, "Polarized Neutron Reflection Study of the Unidirectional Magnetic Anisotropy of Permalloy on $Ni_{0.5}CO_{0.5}O$," J. Magn. and Magn. Mater. **121** (1993), 105-108.

G. P. Felcher, "Forward Scattering of Neutrons from Polymeric and Magnetic Multilayers," Physica B **198** (1993), 150-155.

G. P. Felcher, R. J. Goyette, S. Anastasiadis, T. P. Russell, M. Foster, and F. Bates, "Topology of Forward Scattering of Neutrons from Imperfect Multilayers," Phys. Rev. B **50** (1994), 9565-9568.

G. P. Felcher, "Magnetic Depth Profiling Studies by Polarized Neutron Reflection," Physica B **192** (1993), 137-149.

G. P. Felcher, S. Adenwalla, V.-O. de Haan, and A. A. Van Well, "Zeeman Splitting of the Surface-Scattered Neutrons," Nature **377** (1995), 409-410.

G. P. Felcher, A. Karim, and T. P. Russell, "Interdiffusion at the Bilayer Polymer Interface: Evidence for Interdiffusion?" J. Non-Cryst. Solids **131** (1991), 703-708.

G. P. Felcher, "Applications of Neutron Reflectivity: Polymers and Magnetism," International School of Physics E. Fermi, Course CXIV on the Industrial and Technological Applications of Neutrons, edited by M. Fontana, F. Rustichelli, and R. Coppola, (North Holland, Amsterdam 1992), 325-340.

G. P. Felcher, W. D. Dozier, Y. Y. Huang, and X. L. Zhou, "Total Neutron Reflection: Experiments and Analysis," Proc. II Conf. Surface X-Ray and Neutron Scattering, edited by H. Zabel and I. K. Robinson, (Springer, 1992), 99-103.

G. P. Felcher, "Of Butterflies and Terraces," Neutron News **5**, no. 4, (1994), 18-22.

G. P. Felcher, S. Adenwalla, V.-O. de Haan, and A. A. Van Well, "Observation of the Zeeman Splitting for Neutrons Reflected by Magnetic Layers," Physica B (1996), in press.

J. Fortner and M.-L. Saboungi, "Raman Scattering in Liquid K-Te," Europhysics Lett. **22** (1992), 359-364.

J. Fortner, M.-L. Saboungi, and J. Enderby, "Charge Transfer in Liquid Semiconductors: The K-Te System," Phys. Rev. Lett. **150** (1992), 287-291.

J. Fortner, M.-L. Saboungi, and J. Enderby, "Electrical Properties of an Unusual Liquid Semiconductor: K-Te," Phil. Mag. Lett. **68** (1993), 85-91.

J. Fox, G. Lopinski, J. Lannin, G. Adams, J. Page, and J. Fischer, "Neutron Diffraction and Modeling of Rb_1C_{60} Phases," Chem. Phys. Lett. (1995), in press.

W. Fullagar, D. Cookson, J. W. Richardson, Jr., P. Reynolds, and J. W. White, "Disproportionation of Rb_3C_{60} by Ammonia to Produce Two New Ammoniated Fullerides," Chem. Phys. Lett. **245** (1995), 102-106.

W. Fullagar, J. W. White, and F. Trouw, "Superconductivity, Vibrational and Lattice Dynamics of Rb_3C_{60}," Physica B **213-214** (1995), 16-21.

E. E. Fullerton, J. E. Mattson, S. R. Lee, C. H. Sowers, Y. Y. Huang, G. P. Felcher, and S. D. Bader, "Non-oscillatory Antiferromagnetic Coupling in Sputtered Fe/Si Superlattices," J. Magn. and Magn. Mater. **117** (1992), L301-L306.

E. E. Fullerton, J. E. Mattson, S. R. Lee, C. H. Sowers, Y. Y. Huang, G. P. Felcher, and S. D. Bader, "Magnetic Decoupling in Fe/Si Superlattices and Multilayers," J. Appl. Phys. **73** (1993), 6335-6337.

E. Fullerton, S. Adenwalla, G. P. Felcher, K. Riggs, C. Sowers, S. Bader, and J. Robertson, "Neutron Diffraction and Reflectivity Studies of the Cr Neel Transition in Fr/Cr(001)," Physica B (1996), in press.

A. A. Golestaneh and J. M. Carpenter, "Study of the Martensitic Transformation in Shape-Memory Nitinol Alloy by Time-of-Flight Neutron Diffraction Techniques," Acta Metall. Mater. **38** (1990), 1291-1305.

G. L. Goodman, C.-K. Loong, and L. Soderholm, "Crystal-Field Properties of f-Electron States in $RBa_2Cu_3O_7$ for R = Ho, Nd and Pr," J. Phys.: Cond. Matter **3** (1991), 49-67.

E. A. Goremychkin, R. Osborn, and A. Y. Muzychka, "Crystal Field Potential of $PrCu_2Si_2$: An Evaluation of Evidence for Heavy Fermion Behavior," Phys. Rev. B **50** (1994), 13863-13866.

E. A. Goremychkin and R. Osborn, "Neutron-Spectroscopy Study of the Heavy Fermion Compound $CeCu_6$," Phys. Rev. B **47** (1993), 14580-14583.

E. A. Goremychkin and R. Osborn, "Crystal Field Excitations in $CeCu_2Si_2$," Phys. Rev. B **47** (1993), 14280-14290.

E. A. Goremychkin, A. Y. Muzychka, and R. Osborn, "Crystal Field Potential of $NdCu_2Si_2$: A Comparison with $CeCu_2Si_2$," Physica B **179** (1992), 184-190.

P. Goyal, S. Menon, B. Dasannacharya, and P. Thiyagarajan, "SANS Study of Micellar Structure and Inter-Particle Interactions in Triton X-100 Solutions," Phys. Rev. E **51** (1995), 2308-2315.

M. Grimsditch, S. Popova, and D. L. Price, "Structural Investigation of the Proposed Specific Heat Anomaly in Liquid $ZnCl_2$," Proc. 185th Mtg. Electrochem. Soc., Inc., Ninth Int. Symp. on Molten Salts (1994), 58-68.

M. Guillaume, P. Allnespach, J. Mesot, U. Staub, A. Furrer, R. Osborn, A. D. Taylor, F. Stucki, and P. Unternährer, "Neutron Spectroscopy of the Crystalline Electric Field in High-T_c $YbBa_2Cu_3O_7$," Solid State Commun. **81** (1992), 999-1002.

W. Hahn, M. Loewenhaupt, G. P. Felcher, Y. Y. Huang, and S. S. P. Parkin, "Fe/Cr Multilayers: Effect of Annealing on Spin Structure and Magnetoresistance," J. Appl. Phys. **75** (1994), 3564-3570.

W. Hahn, M. Loewenhaupt, Y. Y. Huang, G. P. Felcher, and S. S. P. Parkin, "Experimental Determination of the Magnetic Phase Diagram of Gd/Fe Multilayers," Phys. Rev. B **52** (1995), 16041-16048.

P. J. Hall, M. Antxustegi, A. Mackinnon, P. Burchill, R. Winans, and P. Thiyagarajan, "Small Angle Scattering Evidence for the Formation of Microporosity in Pittsburgh #8 Coal Following Liquefaction Pre-Treatment by Solvent," Energy and Fuels **8** (1994), 1526-1527.

A. Hannon, R. Sinclair, and A. Wright, "The Vibrational Modes of Vitreous B_2O_3," Physica A **201** (1993), 375-380.

A. Hannon, R. Sinclair, and A. Wright, "Inelastic Neutron Scattering Studies of the Vibrational Modes of Vitreous B_2O_3," Proc. VII Intl. Conf. Phys. of Non-Crystalline Solids (1992), The Phys. of Non-Crystalline Solids edited by L. D. Pye, W. LaCourse, and H. Stevens (Taylor and Francis, London, 1992), 67-71.

W. Harrison, T. Gier, G. Stucky, and A. J. Schultz, "Structural Study of the Ferroelectric to Paraelectric Phase Transition in $TlTiOPO_4$," Mater. Res. Bulletin **30** (1995), 1341-1349.

D. Haskel, E. Stern, D. G. Hinks, A. Mitchell, J. D. Jorgensen, and J. Budnick, "Dopant and Temperatue Induced Structural Phases Transitions in $La_{2-x}Sr_xCuO_4$," Phys. Rev. Lett. **76** (1996), 439-442.

K. He, S. J. Ludtke, H. W. Huang, and D. L. Worcester, "Antimicrobial Peptide Pores in Membranes Detected by Neutron In-Plane Scattering," Biochemistry (1996), in press.

R. Hempelmann, D. Richter, and D. L. Price, "Kinetic Energy of Hydrogen in β-V_2H Studied by Neutron Compton Scattering," J. Less-Common Metals **172-174** (1990), 301-306.

K. W. Herwig, J. Gavilano, M. Schmidt, and R. O. Simmons, "Density Dependence of the Single-Particle Kinetic Energy of Solid Hydrogen," Phys. Rev. B **41** (1990), 96-102.

K. W. Herwig and F. Trouw, "Ethanol on Graphite: The Influence of Hydrogen-bonding on Surface Melting," Phys. Rev. Lett. **69** (1992), 89-92.

R. P. Hjelm, P. Thiyagarajan, and M. H. Alkan-Onyuksel, "A Small Angle Neutron Scattering Study of the Effects of Dilution on Particle Morphology in Mixture of Glycholate and Lecithin," J. Appl. Cryst. **21** (1988), 858-863.

R. P. Hjelm, P. Thiyagarajan, and M. H. Alkan-Onyuksel, "The Organization of Phoshatidylcholine and Bile Salt in Rod-Like Mixed Micelles," J. Phys. Chem. **96** (1992), 8653-8661.

R. P. Hjelm, P. Thiyagarajan, C. Schteingart, A. F. Hofmann, and M. H. Alkan-Onyuksel, "Structure of Mixed Micelles Present in Bile and Intestinal Content Based on Studies of Model Systems," Falk Symposium: Bile Acids in Gastroenterology: Basic and Clinical Advances, edited by A. F. Hofmann, G. Paumgartner, and A. Stiehl **80** (1995), 41-58.

R. P. Hjelm, P. A. Seeger, and P. Thiyagarajan, "Small-Angle Neutron Scattering at Pulsed Sources Compared to Reactor Sources," Proc. ICANS-XI (1990), 673-676.

R. P. Hjelm, J. Wilcoxon, P. Thiyagarajan, and M. H. Alkan-Onyuksel, "Nonequilibrium Behavior in Egg Phosphatidyl-Bilesalt Mixed Aqueous Colloids," Non-Equilibrium States in Mole. Aggregation and Fractals in Chem. edited by D. Tezak and M. Shera, Croatica Chirmica Acta **65** (1992), 367-377.

R. P. Hjelm, P. Thiyagarajan, and M. H. Alkan-Onyuksel, "Small Angle Neutron Scattering Studies of Morphology and Transformation in Mixed Bile Salt-Lecithin Colloids," Mol. Cryst. Liq. Cryst. **80A** (1990), 155-164.

G. L. Hofman, J. W. Richardson, Jr., and R. C. Birtcher, "Crystal and Microstructure of U_3Si_2 Fuel Plates after Reactor Irradiation," Met. Trans. (1996), in press.

V. Homer and R. Edge, "Polarization Relaxation in KDP-Isomorph Ferroelectrics," Mater. Res. Soc. Symp. Proc. **166** (1990), 175-180.

H. Horiuchi, T. Kobayashi, and A. J. Schultz, "Time-of-Flight Pulsed Neutron Diffraction Study on Uniaxial Stress-Induced Domain Switching in $LaNbO_4$," J. Appl. Phys. (1991), 2035-2039.

R. Hu, T. Egami, F. Li, and J. Lannin, "Local Intermolecular Correlation in C_{60}," Phys. Rev. B **45** (1992), 9517-9520.

Y. Huang, G. P. Felcher, and S. Parkin, "Antiferromagnetic and Ferromagnetic Order in Co/Ru Multilayers," J. Magn. and Magn. Mater. **99** (1991), 131-138.

Y. Huang, C. Liu, and G. P. Felcher, "Magnetization of Ultrathin bcc Fe Films on MgO," Phys. Rev. B **47** (1993), 183-189.

B. Hunter, J. D. Jorgensen, J. Wagner, P. Radaelli, D. G. Hinks, H. Shaked, and R. L. Hitterman, "Pressure-Induced Structural Changes in Superconducting $HgBa_2Ca_{n-1}Cu_nO_{2n+2\delta}$ (n=1,2,3) Compounds," Physica C **221** (1994), 1-10.

L. Iton, F. Trouw, T. Brun, and J. E. Epperson, "Small-Angle Neutron-Scattering Studies of the Template-Mediated Crystallization of ZSM-5-Type Zeolite," Am. Chem. Soc. (1993), 1045-1048.

F. Izumi, J. D. Jorgensen, Y. Shimakawa, Y. Kubo, T. Manako, S. Pei, T. Matsumoto, R. L. Hitterman, and Y. Kanke, "Pressure-Induced Structural Changes and Charge Transfer in $Tl_2Ba_2CuO_{6+z}$," Physica C **193** (1991), 426-436.

W. Jauch, A. Palmer, and A. J. Schultz, "Single-Crystal Pulsed Neutron Diffraction from NiF_2 and FeF_2: The Effect of Magnetic Order on the Fluorine Positions," Acta Cryst. B **49** (1993), 984-987.

P. Jemian, J. Enderby, A. Merriam, D. L. Price, and M.-L. Saboungi, "Modulated Anomalous X-Ray Scattering," Acta Crystallogr. **A49** (1992), 743-749.

D. W. Jerng and J. M. Carpenter, "Heat Generation and Neutron Beam Characteristics in a High Power Pulsed Neutron Source," Proc. ICANS-XII **RAL 94-025** (1993), T105-T114.

W. Jin, M. H. Degani, R. K. Kalia, P. Vashishta, and C.-K. Loong, "Superconductivity in $Ba_{1-x}K_xBiO_3$ Cubic Oxides," Cond. Matter Theories **7**, edited by A. N. Proto and J. Aliaga (Plenum, New York, 1992), 253-268.

D. Johnston, F. Borsa, P. Canfield, J. Cho, F. Chou, L. Miller, D. Torgeson, D. Vaknin, J. Zarestky, J. Ziolo, J. D. Jorgensen, P. Radaelli, A. J. Schultz, J. Wagner, S. Cheong, W. Bayless, J. Schirber, and Z. Fisk, "The Phase Diagrams and Doped-Hole Segregation in $La_2CuO_{4+\delta}$ and $La_{2-x}Sr_xCuO_{4+\delta}$ ($X \leq 0.15$, $\delta \leq 0.12$)," Proc. 2nd Workshop on Phase Separation in Cuprate Superconductors, edited by E. Sigmund and K. Muller (Springer-Verlag, Heidelberg, 1993), 82-100.

D. Johnston, F. Borsa, J. Cho, F. Chou, D. Torgeson, D. Vaknin, J. Zarestky, J. Ziolo, J. D. Jorgensen, P. Radaelli, A. J. Schultz, J. Wagner, and S. Cheong, "Phase Diagram and Phase Separation in $La_{2-x}Sr_xCuO_{3+\delta}$," J. Alloys Compd. **207-208** (1994), 206-212.

D. Johnston, W. Bayless, F. Borsa, P. Canfield, S. Cheong, J. Cho, F. Chou, Z. Fisk, J. D. Jorgensen, A. Lascialfari, L. Miller, P. Radaelli, J. Schirber, A. J. Schultz, D. Torgeson, D. Vaknin, J. Wagner, J. Zarestky, and J. Ziolo, "Phase Separation and Doped-Hole Segregation in $La_2CuO_{4+\delta}$ and $La_{2-x}SrCuO_{4+\delta}$," Proc. 4th Intl. Conf. on Mater. and Mech. of Superconductivity and High Temp. Superconductors, Physica C **235** (1994), 257-260.

R. A. L. Jones, E. J. Kramer, L. J. Norton, K. R. Shull, G. P. Felcher, A. Karim, and L. J. Fetters, "Interfacial Segment Density Profiles of End-Anchored Polymers in a Melt," Macromolecules **25** (1992), 2359-2368.

J. D. Jorgensen, D. G. Hinks, P. Radaelli, S. Pei, P. Lightfoot, B. Dabrowski, C. Segre, and B. Hunter, "Defects, Defect Ordering, Structural Coherence and Superconductivity in the 123 Copper Oxides," Physica C (1991), 184-189.

J. D. Jorgensen, D. G. Hinks, B. Hunter, J. Wagner, P. Radaelli, E. Larson, B. Dabrowski, R. L. Hitterman, A. Mitchell, and H. Takahashi, "Structural Coherence of the CuO_2 Planes of Oxide Superconductors: Is It a Requirement for Superconductivity?" Lattice Effects in High-T_c Superconductors, edited by Y. Bor-Yom, T. Egami, J. Mustre-de Leon, and A. Bishop (World Sci. Publ., 1992), 84-92.

J. D. Jorgensen, P. Radaelli, H. Shaked, J. Wagner, B. Hunter, J. Mitchell, R. L. Hitterman, and D. G. Hinks, "Roles of Oxygen Defects in Copper-Oxide Superconductors," 1993 Int. Workshop on Superconductivity (ISTEC) **7** (1993a), 145-149.

J. D. Jorgensen, "Time-of-Flight Diffraction at Pulsed Neutron Sources: An Introduction to the Symposium," Proc. Symp. on Time-of-Flight Diffraction at Pulsed Neutron Sources, edited by J. D. Jorgensen and A. J. Schultz, Trans. Am. Crystall. **28** (1994), 1-10.

J. D. Jorgensen, P. G. Radaelli, D. G. Hinks, J. L. Wagner, S. Kikkawa, G. Er, and F. Kanamaru, "Structure of Superconducting $Sr_{0.9}La_{0.1}CuO_2$(T_c=42K) from Neutron Powder Diffraction," Phys. Rev. B **47** (1993b), 14654-14656.

T. Kamiyama, F. Izumi, H. Takahashi, J. D. Jorgensen, B. Dabrowski, R. L. Hitterman, D. G. Hinks, H. Shaked, T. Mason, and M. Seabaugh, "Pressure-induced Structural Changes in $Nd_{2-x}Ce_xCuO_4$ (x=0 and 0.165)," Physica C **229** (1994), 377-388.

A. Karim, B. H. Arendt, R. Goyette, Y. Y. Huang, R. K. Kleb, and G. P. Felcher, "An Automated Neutron Reflectometer (POSY II) at the Intense Pulsed Neutron Source," Physica B **173** (1991), 17-24.

A. Karim, N. Singh, M. Sikkak, F. Bates, W. Dozier, and G. P. Felcher, "Ordering in Asymmetric Poly (Ethylene-Propylene)- Poly (Ethylethylene) Diblock Copolymer Thin Films," J. Chem. Phys. **100** (1994), 1620-1629.

A. Karim, G. P. Felcher, and T. Russell, "The Interdiffusion of Polymers at Short Times," Macromolecules **27** (1994), 6973-6979.

A. Karim, B. H. Arendt, G. P. Felcher, and T. P. Russell, "Preparation and Characterization of Thin Polymer Bilayer Films by Neutron Reflection," J. Thin Solid Films **202** (1991), 345-350.

G. Kearley and F. Trouw, "A High-Resolution Inverted Time-of-Flight Spectrometer for Reactor Cold-Sources," Neutron News **1** No.3 (1992),45-60.

G. J. Kellogg, P. E. Sokol, S. K. Sinha, and D. L. Price, "Momentum Distributions of H_2 Monolayers on Grafoil," Phys. Rev. B **42** (1990), 7725-7737.

S. Kern, G. H. Lander, L. Soderholm, C.-K. Loong, F. Trouw, M. West, D. Hoisington, B. Cort, and U. Welp, "Neutron Inelastic Scattering Studies of UF_4 and NpF_4," J. Chem. Phys. **101** (1994a), 9338-9343.

S. Kern, J. Hayward, S. Roberts, J. W. Richardson, Jr., F. Rotella, L. Soderholm, B. Cort, M. Tinkle, M. West, D. Hoisington, and G. H. Lander, "Temperature Variation of the Structural Parameters in Actinide Tetraflourides," J. Chem. Phys. **101** (1994b), 9333-9337.

Y. Kiyanagi, J. M. Carpenter, N. Watanabe, H. Iwasa, and M. Nakajima, "Studies of Decoupled Composite Moderators of Liquid Hydrogen and Zirconium Hydride," Proc. ICANS-XII **RAL 94-025** (1993), T206-T212.

W. Kohn, D. L. Price, and J. Rush, Editors, "Neutron Sources for America's Future," U.S. Department of Energy Report DOE/ER-0576P (1993).

N. Koura, K. Takeishi, S. Takahashi, L. A. Curtiss, K. Suzuya, M.-L. Saboungi, and D. L. Price, "Aluminum Chloride-1-Butylpyridinium Chloride Melts as an Electrolyte for Aluminum/Polyaniline Cells," Proc. IXth Intl. Symp. on Molten Salts, edited by C. L. Hussey, D. S. Newman, G. Mamantov, and Y. Ito (Electrochemical Society, Pennington, N.J., (1994), 728-735.

M. Kunz, T. Armbruster, G. Lager, A. J. Schultz, R. Goyette, W. Lottermoser, and G. Amthauer, "Fe, Ti Ordering and Octahedral Distortions in Acentric Neptunite: Temperature Dependent X-ray and Neutron Structure Refinements and Mossbauer Spectroscopy," Phys. Chem. Minerals **18** (1991), 199-213.

D. S. Kupperman, "Neutron-Diffraction Determination of Residual Stresses in Advanced Composites," Ann. Rev. Mater. Sci. **24** (1994), 265-291.

R. Kustom and D. Horan, "IPNS-Upgrade RF System Design," Proc. ICANS-XII **RAL 94-025** (1993), A64-A72.

R. Kustom, "A 2-Stage 5-MW FFAG," Proc. ICANS-XII **RAL 94-025** (1993), A159-A167.

A. C. Lawson, J. Goldstone, B. Cort, R. Sheldon, and E. Foltyn, "Atomic Thermal Vibrations of the Light Actinide Elements," J. Alloys and Cmpd. **213-214** (1994), 426-428.

A. C. Lawson, J. Goldstone, B. Cort, R. Sheldon, and E. Foltyn, "Debye-Waller Factors of the Light Actinide Metals," Actinide Processing: Methods and Materials, edited by B. Mishra, The Minerals, Metals, and Materials Society (1995), 31-43.

A. C. Lawson, J. A. Goldstone, B. Cort, R. J. Martinez, T. G. Zocco, J. W. Richardson, Jr., and M. H. Mueller, "Structure of ζ-Plutonium-Uranium," Acta Cryst. B (1996), in press.

J. Lee, J. Swinnia, H. Steinfink, W. Reiff, S. Pei, and J. D. Jorgensen, "The Crystal Chemistry and Physical Properties of the Trip Layer Perovskite Intergrowths $LASR_3Fe_3O_{10-\delta}$ and $LaSr_3(Fe_{3-x}Al_x)O_{10-\delta}$)," J. Solid State Chem. **104** (1993), 1-15.

Y. Li, C. Polaczyk, F. Klose, C. Rehm, H. Maletta, D. Reigel, G. P. Felcher, and S. Adenwalla, "Magnetic Depth Profile of Fe/Ni Bilayers," Physica B (1996), in press.

F. Li, D. Ramage, and J. Lannin, "Confirmation of the Structure of Fullerene," Phys. and Chem. of Finite Systems, (Kluwer, 1992), 1341.

F. Li, D. Ramage, J. Lannin, and J. Conceicao, "Radial Distribution Function of C_{60}: Structure of Fullerene," Phys. Rev. B **44** (1991), 13167-13170.

Z. Li, J. E. Epperson, Y. Fang, and S.-K. Chan, "The Tetragonal-Monoclinic Transformations of Zirconia Studied by Small Angle Neutron Scattering and Differential Thermal Analysis," Sci. and Tech. Zirconia V (1993), 49-58.

M. Y. Lin, S. K. Sinha, J. Drake, P. Thiyagarajan, X. Wu, and H. Stanley, "SANS Studies of Fluid Phase Transitions in Porous Media," Physique IV, Colloque **C8**(3) (1993), 109-115.

M. Y. Lin, S. K. Sinha, J. Drake, X. L. Wu, P. Thiyagarajan, and H. B. Stanley, "Study of Phase Separation of a Binary Fluid Mixture in Confined Geometry," Phys. Rev. Lett. **72** (1994), 2207-2210.

G. K. Liu, C.-K. Loong, J. J. Beitz, R. Cao, Y. H. Chen, and K. Suzuya, "Raman Heterodyne Detection of Magnetic Resonance in a Phosphate Glass," J. Appl. Phys. (1996), in press.

G. K. Liu, C.-K. Loong, and F. Trouw, "Spectroscopic Studies of Magnetic Transitions in $TbPO_4$," J. Appl. Phys. **75** (1994), 7030-7032.

M. Loewenhaupt, W. Hahn, Y. Y. Huang, G. P. Felcher, and S. S. P. Parkin, "Determination of Spin Structures of Magnetic Multilayers by Polarized Neutron Reflectometry," J. Modern Phys. B **7** (1993), 438-445.

M. Loewenhaupt, W. Hahn, Y. Y. Huang, G. P. Felcher, and S. S. P. Parkin, "Spin Structure of Fe/Gd and Fe/Cr Multilayers Determined by Polarized Neutron Reflectometry," J. Magn. and Magn. Mater. **121** (1993), 173-176.

M. Loewenhaupt, C.-K. Loong, P. Tils, and W. Hahn, "Crystal Field and Exchange Interactions in DyT_4Al_8 (T=Fe,Mn)," Mat. Res. Soc. Symp. Proc. **376** (1996), 725-730.

C.-K. Loong, D. G. Hinks, W. Jin, M. H. Degani, D. L. Price, J. D. Jorgensen, B. Dabrowski, A. W. Mitchell, D. Richards, R. K. Kaila, Y. Zheng, and P. Vashishta, "Electron-Phonon Coupling, Oxygen Isotope Effect, and Superconductivity in $Ba_{1-x}K_xBiO_3$," in "Electron-Phonon Interactions in Oxide Superconductors edited by R. Baquaro (World Scientific: Singapore, 1990b), 122-145.

C.-K. Loong and L. Soderholm, "Crystal-Field Excitations in RE_2CuO_4 (RE = Pr and Nd)," J. Less-Common Met. **181** (1992a), 241-247.

C.-K. Loong, P. Vashishta, R. K. Kalia, W. Jin, M. H. Degani, D. G. Hinks, D. L. Price, J. D. Jorgensen, B. Dabrowski, A. W. Mitchell, D. R. Richards, and Y. Zheng, "Phonon Density of States and Oxygen Isotope Effect in $Ba_{1-x}K_xBiO_3$," Phys. Rev. B **45** (1992b), 8052-8064.

C.-K. Loong, L. Soderholm, M. M. Abraham, L. A. Boatner, and N. M. Edelstein, "Crystal-Field Excitations and Magnetic Properties of $TmPO_4$," J. Chem. Phys. **98** (1993c), 4214-4222.

C.-K. Loong, L. Soderholm, J. P. Hammonds, M. M. Abraham, L. A. Boatner, and N. M. Edelstein, "Neutron Study of Crystal-field Transitions in $ErPO_4$," J. Appl. Phys. **73** (1993d), 6069-6071.

C.-K. Loong, L. Soderholm, J. P. Hammonds, M. M. Abraham, L. A. Boatner, and N. M. Edelstein, "Rare-Earth Energy Levels and Magnetic Properties of $HoPO_4$ and $ErPO_4$," J. Phys. Cond. Matter **5** (1993f), 5121-5140.

C.-K. Loong, L. I. Donley, G. E. Ostrowski, R. Kleb, J. P. Hammonds, L. Soderholm, and S. Takahashi, "The Use of Chopper Spectrometers for Cold-to-Epithermal Neutron Scattering at IPNS," Proc. ICANS-XII **RAL 94-025** (1994b), I36-I43.

C.-K. Loong, L. Soderholm, J. S. Xue, M. M. Abraham, and L. A. Boatner, "Rare Earth Energy Levels and Magnetic Properties of $DyPO_4$," J. Alloys and Cmpd. **207-208** (1994e), 165-169.

C.-K. Loong, J. W. Richardson, Jr., M. Ozawa, and M. Kimura, "Crystal Structure and Short-Range Oxygen in La- and Nd-Modified ZrO_2," J. Alloys and Cmpd. **207-208** (1994g), 174-177.

C.-K. Loong, L. Soderholm, G. L. Goodman, M. M. Abraham, and L. A. Boatner, "The Ground-State Wavefunctions of Tb^{3+} Ions in Paramagnetic $TbPO_4$: A Neutron Scattering Study," Phys. Rev. B **48** (1993e), 6124-6131.

C.-K. Loong, F. Trouw, and L. E. Iton, "Formic Acid, Ethanol in Vycor Glass, and Water in Aluminosilicate Zeolites," Hydrogen Bond Networks, edited by M.-C. Bellissent-Funel and J. Dore (Kluwer Academic Publishers, 1994f), 231-238.

C.-K. Loong, L. E. Iton, and M. Ozawa, "Hydrogen Vibrational Density of States of Adsorbed Water on Rare-earth Modified Zirconia," Phys. B **213-214** (1995a), 640-642.

C.-K. Loong, P. Vashishta, R. K. Kalia, and I. Ebbsjo, "Crystal Structure and Phonon Density-of-States of High Temperature Ceramic Silicon Nitride," Europhys. Lett. **31** (1995b), 201-206.

C.-K. Loong, J. W. Richardson, Jr., and M. Ozawa, "Crystal Phases, Defects, and Dynamics of Adsorbed Hydroxyl Groups and Water in Pure and Lanthanide Modified Zirconia: A Neutron Scattering Study," J. Catalysis **157** (1995c), 636-644.

C.-K. Loong, "The Phonon Densities of States of Wurtzite AlN and ZrN," Mat. Res. Soc. Symp. Proc., "Gallium Nitride and Related Materials" (1996b), in press.

C.-K. Loong, G. L. Goodman, L. Soderholm, B. Dabrowski, and D. G. Hinks, "Crystal-field Excitations and Superconductivity in $Nd_{1+x}Ba_{2-x}Cu_3O_7$," J. Appl. Phys. **67** (1990), 4536-4538.

C.-K. Loong, J. W. Richardson, Jr., S. Suzuki, and M. Ozawa, "Crystal Phases and Lattice Dynamics of Slip-cast β-sialons," Mat. Res. Soc. Symp. Proc. "Covalent Ceramics III: Science and Technology of Non-Oxides" (1996a), in press.

C.-K. Loong, J. W. Richardson, Jr., L. E. Iton, and M. Ozawa, "Crystal Structure, Short-Range Oxygen Defects, and Water Adsorption in La- and Nd-Modified ZrO_2," Mat. Res. Soc. Symp. Proc. **376** (1996c), 627-634.

C.-K. Loong and L. Soderholm, "Superconductivity and Rare-Earth Paramagnetism in $Pr_{185}Ce_{0.15}CuO_4$," J. Alloys and Cmpd. **193** (1993b), 142-144.

C.-K. Loong and L. Soderholm, "Rare Earth Crystal Field Spectroscopy by Neutron Magnetic Scattering: From Xenotime to High-T_c Superconductors," J. Alloy and Cmpd. **207-208** (1994d), 153-160.

C.-K. Loong and L. Soderholm, "Rare-Earth Energy Levels in Nd_3CuO_4, Pr_2CuO_4 and the Electron Superconductor $Pr_{1.85}Ce_{0.15}CuO_4$," Phys. Rev. B **48** (1993a), 14001-14004.

C.-K. Loong and L. Soderholm, "Rare Earth Magnetism and Superconductivity in $Pr_{2-x}Ce_xCuO_4$ and $Y_{1-x}Pr_xBa_2Cu_3O_7$: A Neutron Scattering Study," Physical and Mechanical Properties of High Temperature Superconductors, edited by S. K. Malik and S.S. Shah (Nova, N.Y., 1994c), 257-282.

C.-K. Loong, J. M. Carpenter, and S. Ikeda, "A Parametric Formulation of the Resolution Function of a Pulsed-Source Chopper Spectrometer," Proc. ICANS-XII **RAL 94-025** (1994a), I320-I327.

C. Lowe, A. J. Schultz, R. Shaviv, and R. Carlin, "Magnetochemistry of the Tetrahaloferrate (II) Ions. 7. Crystal Structure and Magnetic Ordering in $(pyridinium)_3Fe_2Br_9$," Inorg. Chem. **33** (1993), 3051-3054.

M. Maple, M. de Andrade, J. Herrmann, Y. Dalichaouch, D. Gajewski, C. Seaman, R. Chau, R. Movshovich, M. Aronson, and R. Osborn, "Non-Fermi Liquid Ground States in Strongly Correlated f-Electron Materials," J. Low Temp. Phys. **99** (1994), 223-249.

D. Mari, A. D. Krawitz, J. W. Richardson, Jr., and W. Benoit, "Residual Stress in WC-Co Measured by Neutron Diffraction," Mat. Sci. and Engineer. (1996), in press.

D. Marx, P. Radaelli, J. D. Jorgensen, R. L. Hitterman, D. G. Hinks, S. Pei, and B. Dabrowski, "Metastable Behavior of the Superconducting Phase in the $BaBi_{1-x}Pb_xO_3$System," Phys. Rev. B **46** (1992), 1144-1156.

J. E. Mattson, E. E. Fullerton, C. H. Sowers, Y. Y. Huang, G. P. Felcher, and S. D. Bader, "Oscillatory Interlayer Magnetic Coupling of Sputtered Fe/Nb Superlattices," J. Appl. Phys. **73** (1993), 5969-5971.

D. G. McGhee, "Study of 1-MW Neutron Source Synchrotron Dual Frequency Power Circuit for the Main Ring Magnets," Proc. ICANS-XII **RAL 94-025** (1993), A73-A79.

D. G. McGhee and M. Fathizadeh, "Basis for the Power Supply Reliability of the 1-MW Neutron Source," Proc. ICANS-XII **RAL 94-025** (1993), A80-A84.

Yu. Mel'nichenko, J. Schuller, R. Richert, B. Ewen, and C.-K. Loong, "Dynamics of Hydrogen-Bonded Liquids Confined to Mesopores: A Dielectric and Neutron Spectroscopy Study," J. Chem. Phys. **103** (1995), 2016-2024.

W. Meng, J. Faber, P. Okamoto, L. Rehn, B. Kestel, and R. L. Hitterman, "Neutron Diffraction and Transmission Electron Microscopy Study of Hydrogen-Induced Phase Transformations in Zr_3Al," J. Appl. Phys. **67** (1990), 1312-1319.

S. V. G. Menon, P. S. Goyal, B. A. Dasannacharya, and P. Thiyagarajan, "Power-law Variations of Small-Angle Neutron Scattering Intensities from Triton X-100 Solutions," Phys. Rev. E (1996), in press.

J. Mesot, P. Allenspach, U. Staub, A. Furrer, H. Mutka, R. Osborn, and A. Taylor, "Neutron-Spectroscopic Studies of the Crystal Field in $ErBa_2Cu_3O_x$ ($6<x<7$)," Phys. Rev.B **47** (1993), 6027-6036.

D. Mikkelson, A. J. G. Ellison, D. L. Price, and T. G. Worlton, "Visualization of Time-of-Flight Neutron Diffraction Data," Nucl. Instr. Methods **354** (1995), 112-120.

D. F. R. Mildner, M. Arif, C. Stone, and R. K. Crawford, "The Neutron Transmission of Single-Crystal Sapphire Filters," J. Appl. Cryst. **26** (1993), 438-447.

D. F. R. Mildner and J. M. Carpenter, "Improvements to the Chebyshev Expansion of Attenuation Correction Factors for Cylindrical Samples," J. Appl. Cryst. **23** (1990), 378-386.

C. Milne, P. Lightfoot, J. D. Jorgensen, and S. Short, "Synthesis and Structure of Bi_2LaO_4Ll, a Novel Variant of the Sillen Phases," J. Mater. Chem. **5** (1995), 1419-1421.

L. Morss, E. Appelman, R. Gerz, and D. Martin-Rovet, "Structural Studies of Li_5ReO_6, Li_4NpO_5 and Li_5NpO_6 by Neutron and X-ray Powder Diffraction," J. Alloys Cmpd. **203** (1994), 289-295.

M. H. Mueller, J. W. Richardson, Jr., R. V. Strain, and G. L. Hofman, "Phase Analysis of Metallic Plutonium-Containing Fuel Alloys Using Neutron Diffraction," Advances in X-Ray Analysis **34** (1990), 447-457.

A. E. Munter, S. Adenwalla, G. P. Felcher, and X.-L. Zhou, "Reflection of Neutrons from an Optical Grating," Mat. Res. Soc. Symp. Proc. **376** (1994), 199-202.

G. Muralidharan, H. Chen, and J. E. Epperson, "A Small Angle Neutron Scattering Study of Coarsening in Ni-Si-Al Alloys," Proc. Symp. TMS-AIME Mtg. edited by H. Chen and V. Vasudevan (1992), 367-379.

A. P. Murani, Z. A. Bowden, A. D. Taylor, R. Osborn, and W. G. Marshall, "Evidence for Localized 4f States in α-Ce," Phys. Rev. B **48** (1993), 13981-13984.

A. P. Murani, A. D. Taylor, R. Osborn, and Z. A. Bowden, "Evolution of the Spin-orbit Excitation with Increasing Kondo Energy in $CeIn_{3-x}Sn_x$," Phys. Rev. B **48** (1993), 10606-10609.

T. Nguyen, S. E. Nagler, R. A. Cowley, T. Perring, and R. Osborn, "Energy Levels of Co^{2+} in CoF_2 and $CsCoCl_3$," J. Phys.: Cond. Matt. **7** (1995), 2917-2929.

J. B. Nicholas, F. Trouw, J. Mertz, L. Iton, and A. Hopfinger, "Molecular Dynamics Simulation of Propane and Methane in Silicalite," J. Phys. Chem. **97** (1993), 4149-4163.

J. B. Nicholson, T. Finerman, and B. Crist, "Thermodynamics of Polyolefin Blends: Small-Angle Neutron Scattering Studies with Partially Deuterated Chains," Polym. **31** (1990), 2287-2293.

J. Nipko, M. Grimsditch, C.-K. Loong, S. Kern, M. M. Abraham, and L. A. Boatner, "Elastic Constant Anomalies in $YbPO_4$," Phys. Rev. B **53** (1996), 2286-2290.

L. J. Norton, E. J. Kramer, R. A. L. Jones, F. S. Bates, H. R. Brown, G. P. Felcher, and R. Kleb, "Resonantly Enhanced Neutron Intensity in a Surface Segregated Polymer Blend," J. Physique **4** (1994), 367-376.

L. J. Norton, E. J. Kramer, F. S. Bates, M. D. Gehlsen, R. A. L. Jones, A. Karim, G. P. Felcher, and R. Kleb, "Neutron Reflectometry Study of Surface Segregation in an Isotopic Poly (ethylene propylene) Blend: Deviation from Mean Field Theory," Macromolecules **28** (1995), 8621-8628.

D. Novikov, J. Freeman, and J. D. Jorgensen, "Electronic Structure of Superconductors Without Apical Oxygen: $Sr_2CuO_2F_2$, $Sr_2CuO_2Cl_2$," Phys. Rev. B **51** (1994), 6675-6679.

R. Osborn, "Quadrupolar Effects in $PrCu_2Si_2$," J. Appl. Phys. **76** (1994), 6124-6126.

M. Ozawa, T. Noritake, S. Suzuki, and C.-K. Loong, "Phase Examination of 5 mol% Nd_2O_3 Doped ZrO_2 from Coprecipitation Process," J. Mater. Sci. Lett. **14** (1995), 796-798.

J. Parise, A. Yeganeh-Haeri, D. Widner, J. D. Jorgensen, and M. Saltzberg, "Pressure Induced Phase Transition and Pressure Dependence of Crystal Structure in Low (α) and Ca/Al-doped Cristobalite," J. Appl. Phys. **75** (1993), 1361-1367.

Y. Park, S. Adenwalla, G. P. Felcher, and S. Bader, "Superparamagnetic Relaxation of Fe Deposited on MgO (001)," Phys. Rev. B **52** (1995), 12779-12783.

D. Peek, I. Fujita, M. Schmidt, and R. O. Simmons, "Single-Particle Kinetic Energies in Solid Neon," Phys. Rev. B **45** (1992), 9680-9687.

D. Peek, M. Schmidt, I. Fujita, and R. O. Simmons, "Single-Particle Kinetic Energies in Liquid Neon," Phys. Rev. B **45** (1992), 9671-9679.

S. Pei, A. Paulikas, B. Veal, and J. D. Jorgensen, "Structural Refinement of Y_2BaCuO_5 Using Neutron Powder Diffraction," Acta. Cryst. C**46** (1990), 1986-1988.

S. Pei, J. D. Jorgensen, D. G. Hinks, Y. Zheng, D. Richards, B. Dabrowski, and A. Mitchell, "Structure and Chemistry of $Ba_{0.6}K_{0.4}BiO_y$ at High Temperature," J. Solid State Chem. **95** (1991), 29-38.

S. Pei, N. J. Zalvzec, J. D. Jorgensen, D. G. Hinks, B. Dabrowski, D. Richards, and A. Mitchell, "Charge Density Waves in the Superconducting $Ba_{1-x}K_xBiO_3$ System," Phys. Rev. B **39** (1989), 811-814.

T. G. Perring, A. D. Taylor, R. Osborn, D. McK. Paul, A. T. Boothroyd, and G. Aeppli, "MAPS: A Chopper Spectrometer to Measure High Energy Magnetic Excitations in Single Crystals," Proc. ICANS-XII **RAL 94-025** (1993), I60-I72.

V. Plakhty, A. Stratilatov, Yu. Chernenkov, V. Fedorov, S. K. Sinha, C.-K. Loong, B. Gaulin, M. Vlasov, and S. Moshkin, "X-Ray Studies of the $YBa_2Cu_3O_{6+x}$ Superstructures in the Range of $0.40(3) \leq x \leq 0.73(3)$," Solid State Comm. **84** (1992), 639-644.

D. L. Price, M.-L. Saboungi, S. Moss, and S. Hashimoto, "Structure of Molten Iron Chloride," Proc. 8th Int. Symp. on Molten Salts, edited by R. J. Gale, A. Blomgren, and H. Kojima, (Electrochem. Soc., 1992), 14-21.

D. L. Price, "Analysis of Disordered Materials by Neutron and X-Ray Diffraction," Plenary Lecture at 2nd European Powder Diffraction Conf., Mater. Sci. Forum, **133-136** (1992), 411-422.

D. L. Price, M.-L. Saboungi, W. Van Der Lugt, and G. De Wijs, "Structure of Liquid Cesium-Lead Alloys," 8th Int. Conf. on Liquid and Amorphous Metals, J. Non-Cryst. Solids **156-158** (1992), 34-37.

D. L. Price and A. J. G. Ellison, "Atomic Structure and Dynamics of Fast-Ion Conducting Glasses," Proc. ACS PAC RIM, J. Non-Cryst. Solids (1994), 293-298.

D. L. Price and J. Rush, Editors, "Neutron Sources and Applications," U.S. Department of Engergy Report DOE/ER-0607P (1994).

D. L. Price and M.-L. Saboungi, "Melting in Alkali-Metal - Lead Alloys: KPb and CsPb," Phys. Rev. B **44** (1991), 7289-7296.

D. L. Price, A. J. G. Ellison, C.-K. Loong, and S. Susman, "Atomic Structure and Dynamics of Fast-Ion Conducting Glasses," Am. Ceram. Soc. 1993 PAC RIM Conf. **177** (1993), 293-298.

D. L. Price, M.-L. Saboungi, and W. S. Howells, "Rotor Phases in Compound Semiconductors," Proc. Int. Conf. on Neutron Scattering, Physica B **213-214**, (1995), 547-551.

D. L. Price, M.-L. Saboungi, S. Susman, K. Volin, J. Enderby, and A. Barnes, "Structure of Two Liquid Semiconductors: $Ag_{1-x}Se_x$ and $Ag_{0.67}Te_{0.33}$," J. Phys.: Cond. Matt. **5** (1993), 3087-3094.

D. L. Price, M.-L. Saboungi, J. Fortner, J. W. Richardson, and W. S. Howells, "Rotator Phases in Narrow-Gap Semiconductors," Proc. Second Int. Conf. Quasielastic Neutron Scattering, Quasielastic Neutron Scattering edited by J. Colmenero, A. Alegria, and F. J. Bermejo (World Scientific: Singapore, 1994), 3-14.

D. L. Price, M.-L. Saboungi, and W. S. Howells, "Orientational and Translational Disorder in Semiconducting Zintl Compounds," Phys. Rev. B **51** (1995), 14923-14929.

D. L. Price, M.-L. Saboungi, S. Susman, K. Volin, and A. Wright, "Neutron Scattering Function of Vitreous and Molten Zinc Chloride," J. Phys.: Cond. Matt. **3** (1991), 9835-9842.

D. L. Price, M.-L. Saboungi, W. S. Howells, and M. Tosi, "Structure of Liquid Trivalent Salts," Proc. Int. Symp. on Molten Salt Chem. and Tech., edited by M.-L. Saboungi and H. Kojima, Electrochem. Soc. **93** (9) (1992), 1-5.

D. L. Price, S. Ghose, N. Choudhury, S. L. Chaplot, and K. R. Rao, "Phonon Density of States in Fayalite, Fe_2SiO_4," Physica B **174** (1991), 87-90.

M. Rabeony, D. Peiffer, S. Behel, M. Disko, W. D. Dozier, P. Thiyagarajan, and M. Y. Lin, "Self-Organization of Graft Copolymers at Surfaces, Interfaces and in Bulk," J. Chem. Soc. Faraday Trans. (1995), 2855-2861.

M. Rabeony, D. Peiffer, W. Dozier, and M. Lin, "Evolution of Structure in a Graft Copolymer under Strain," Macromolecules **26** (1993), 3676-3680.

P. Radaelli and J. D. Jorgensen, "Pressing for Better Results," Nature **364** (1993a), 286-287.

P. Radaelli, B. Hunter, J. Wagner, D. G. Hinks, A. Mitchell, B. Dabrowski, K. Vandervoort, H. Viswanathan, and J. D. Jorgensen, "Structural and Superconducting Properties of $La_{2-x}Sr_xCuO_4$ as a Function of Sr Content," Phys. Rev. B **49** (1993), 4163-4175.

P. Radaelli, C. Segre, D. G. Hinks, and J. D. Jorgensen, "Structural Inhomogeneities in Oxygen-Deficient $ErBa_2Cu_3O_{6+x}$ Associated with the Tetragonal-to-Orthorhombic Transition: Evidence of First Order Behavior," Phys. Rev. B **45** (1991), 4923-4949.

P. Radaelli, J. D. Jorgensen, A. J. Schultz, J. Peng, and R. Greene, "Evidence of Apical Oxygen in Nd_2CuO_4 by Single Crystal Neutron Diffraction," Phys. Rev. B **49** (1994), 15322-15326.

P. Radaelli, J. D. Jorgensen, A. J. Schultz, B. Hunter, J. Wagner, F. Chou, and D. Johnston, "Structure of the Superconducting $La_2CuO_{4+\delta}$ Phases (δ ~0.08,0.12) Prepared by Electrochemical Oxidation," Phys. Rev. B **48** (1993b), 499-510.

P. Radaelli, J. D. Jorgensen, R. Kleb, B. Hunter, F. Chou, and D. Johnston, "Miscibility Gap in Electrochemically Oxygenated $La_2CuO_{4+\delta}$," Phys. Rev. B **49** (1993), 6239-6245.

P. Radaelli, J. Wagner, B. Hunter, M. Beno, G. Knapp, J. D. Jorgensen, and D. G. Hinks, "Structure, Doping and Superconductivity in $HgBa_2CaCu_2O_{6+x}$ ($T_c \leq 128K$)," Physica C **216** (1993), 29-35.

W. Rauw, H. Ahsbahs, M. Hitchman, S. Lukin, D. Reinen, A. J. Schultz, C. Simmons, and H. Statemeier, "Pressure Dependence of the Crystal Structures and EPR Spectra of Potassium Hexaaquacopper (II) Sulfate and Deuterated Ammonium Hexaaquacopper (II) Sulfate," Inorganic Chem. (1996), in press.

P. Reynolds, B. Figgis, and A. J. Schultz, "$Ru(ND_3)_6(SCN)_3$ at 20K by Time-of-Flight Neutron Diffraction," Acta Cryst. C**51** (1995), in press.

J. W. Richardson, Jr. and E. T. C. Vogt, "Structure Determination and Rietveld Refinement of Aluminophosphate Molecular Sieve $AlPO_4$-8," Zeolites **12** (1992a), 12-19.

J. W. Richardson, Jr., "Background Modeling in Rietveld Analysis," Rietveld Method, edited by R. A. Young, (Oxford University Press, 1992), 102-109.

J. W. Richardson, Jr., "Residual and Applied Stress Measurements at IPNS," NATO Adv. Res. Workshop: Measurement of Residual and Appl. Stress Using Neutron Diffraction edited by M. T. Hutchings and A. D. Krawitz, (Kluwer Academic, 1992), 363-367.

J. W. Richardson, Jr., M. Lewis, and B. McCart, "Cation Segregation in Simulated Radioactive-Waste Zeolite-A Mixtures," Zeolites and Related Microporous Materials: State of the Art, edited by J. Weitkamp et al.(1994a), 741-747.

J. W. Richardson, Jr., D. L. Price, and M.-L. Saboungi, "Crystal Symmetry Lowering at an Order-Disorder Transition," Phys. Rev. Lett. (1996), in press.

J. W. Richardson, Jr., R. C. Birtcher, and S.-K. Chan, "Deconvolution of Neutron Scattering Data from a Pulsed Spallation Source," Mat. Res. Soc. Symp. Proc. **376** (1994b), 137-142.

J. W. Richardson, Jr., "Time-of-Flight Neutron Powder Diffraction," Proc. Workshop on Neutron Appl. in Mater. Sci. and Eng. (1996), in press.

R. Robinson, M. Kohgi, T. Osadabe, F. Trouw, J. Lynn, P. Canfield, J. Thompson, Z. Fisk, and W. Beryermann, "Low-Energy Excitations and the Electronic Specific Heat of YbBiPt," Phys. Rev. Lett. **75** (1995), 1194-1197.

R. Robinson and J. M. Carpenter, "On the Use of Switch Functions in Describing Pulsed Neutron Moderators," Nucl. Instrum. Methods A**307** (1991), 359-365.

M. Rodriguez, R. Snyder, J. Simmins, Y. Guo, R. Condrate, F. Rotella, and J. D. Jorgensen, "Structure of the $Y_1Ba_4Cu_2(CO_3)O_{5.5+\delta}$ Oxycarbonate," J. Appl. Cryst. **28** (1994), 429-435.

H. D. Rosenfeld and T. Egami, "The Local Atomic Structure of Superconducting $Ba_{0.6}K_{0.4}BiO_3$: Temperature Dependence Near T_c," Proc. Conf. Lattice Effects in High-Tc Superconductors, edited by Y. Bar-Yam, T. Egami, J.Mustre-de Leon, and A. R. Bishop, (World Scientific Publishing Co., 1992), 105-110.

T. Russell, V. Deline, W. Dozier, G. P. Felcher, G. Agrawal, R. Wool, and J. Mays, "Direct Observation of Reptation at Polymer Interfaces," Nature **365** (1993), 235-236.

M.-L. Saboungi, J. Fortner, J. W. Richardson, and J. Enderby, "Liquid Tellurides: Structure and Properties," 8th Int. Conf. on Liquid and Amorphous Metals, J. Non-Cryst. Solids **156-158** (1992), 356-361.

M.-L. Saboungi and D. L. Price, "A Novel Phase Transition in Alloys," J. Non-Cryst. Solids **150** (1992), 260-265.

M.-L. Saboungi, D. L. Price, P. Jemian, A. Merriam, and J. Enderby, "Modulated Anomalous X-Ray Scattering," Acta Cryst. A**49** (1993), 743-749.

M.-L. Saboungi, G. Johnson, and D. L. Price, "Orientational Phase Transitions in Alloys," Proc. NATO Advanced Study Institute on Statics and Dynamics of Alloy Phase Transformations, edited by A. Gonis and P. Turchi (1992), 195-201.

M.-L. Saboungi, J. Fortner, D. L. Price, and W. S. Howells, "Reorientations in Plastic Crystal Phases of Zintl Alloys," Physica A **201** (1993), 421-424.

M.-L. Saboungi, J. Fortner, W. S. Howells and D. L. Price, "Dynamic Enhancement of Cation Migration in a Zintl Alloy by Polyanion Rotation," Nature **365** (1993), 237-239.

M.-L. Saboungi, M. Howe, and D. L. Price, "Structure and Dynamics of Molten Aluminum and Gallium Trihalides I: Neutron Diffraction," Mol. Phys. **79** (1992), 847-858.

A. Saigal, D. Kupperman, J. Singh, D. Singh, J. W. Richardson, and R. Bhatt, "Thermal Residual Strains and Stresses in Silicon Carbide-Fiber-Reinforced Silicon Nitride Composites," Composites Eng. **3** (1993), 1075-1086.

L. Satek, J. Kaduk, and P. McMahon (Ed., W. E. Pascoe), Catalysis of Organic Reactions, "Characterization, Structure, and Active Site Hypothesis for Novel Copper Aluminum Borate Dehydrogenation and Dehydrochylization Catalysts," Catalysis of Organic Reactions, (New York: Marcel Dekker, 1991).

B. S. Schirato, M. Fang, P. E. Sokol, and S. Komarnani, "The Structure of Oxygen in a Sol-Gel Glass," Science **267** (1995), 369-371.

J. Schirber, G. Kwei, J. D. Jorgensen, R. L. Hitterman, and B. Morosin, "Room-temperature Compressibility of C_{60}: Intercalation Effects with He, Ne, and Ar," Phys. Rev. B **51** (1995), 12014-12017.

S. Schneider, U. Geyer, P. Thiyagarajan, R. Busch, R. Schulz, K. Samwer, and W. L. Johnson, "Phase Separation and Crystallization in the Bulk Amorphous $Zr_{41.2}Ti_{13.8}Cu_{12.5}Ni_{10}Be_{22.5}$ Alloy," Proc. Int. Symp. on Metastable, Mechanically Alloyed and Nanocrystalline Materials, Quebec, July 24-28, 1995, (1996a), in press.

S. Schneider, P. Thiyagarajan, and W. L. Johnson, "Formation of Nanocrystals Based on Decomposition in the Amorphous $Zr_{41.2}Ti_{13.8}Cu_{12.5}Ni_{10}Be_{22.5}$ Alloy," Appl. Phys. Lett. (1996b), in press.

A. J. Schultz, "Single-Crystal Time-of-Flight Neutron Diffraction," Trans. Am. Crystallogr. Assoc. **29** (1994), 29-41.

A. J. Schultz and R. Carlin, "Single-Crystal Pulsed Neutron Diffraction Structure of the Antiferromagnet $K_2[FeCl_5(H_2O)]$ With and Without Applied Pressure," Acta Crystallog. B**51** (1995), 43-47.

A. J. Schultz, H. Wang, J. Williams, L. Finger, R. Hazen, C. Rovira, and M-H Whangbo, "X-Ray Diffraction and Electronic Band Structure Study of the Organic Superconductor κ-$(ET)_2Cu[N(CN)_2]Cl$ at Pressures up to 28 kbar," Physica C **234** (1994), 300-306.

A. J. Schultz, J. D. Jorgensen, J. Peng, and R. Greene, "Single-Crystal Neutron Diffraction Structures of Reduced and Oxygenated $Nd_{2-x}Ce_xCuO_y$," Phys. Rev. B (1996), in press.

A. J. Schultz, U. Geiser, H. Wang, J. Williams, L. Finger, and R. Hazen, "High Pressure Structural Phase Transitions in the Organic Superconductor κ-$(ET)_2Cu[N(CN)_2]Cl$," Physica C **208** (1993), 277-285.

K. Schwartz, D. Leong, and R. McConville, "Structural Chemistry of Synthetic Cordierite: Evidence for Solid Solutions and Disordered Compositional Domains in Bi-Flux-Grown Mg-Cordierites," Phys. Chem. Minerals **20** (1994), 563-574.

T. Sendyka, T. Egami, B. Hunter, J. D. Jorgensen, D. G. Hinks, A. Mitchell, B. Dabrowski, R. L. Hitterman, P. Radaelli, and J. Wagner, "Local Orthorhombic Structure Observed in $La_{2-x}Sr_xCuO_4$ for x = 0.075 to 0.25," Proc. Conf. Lattice Effects in High-T_c Superconductors, edited by Y. Bar-Yam, T. Egami, J. Mustre-de Leon, and A. R. Bishop, (World Scientific Publishing Co., 1992), 111-117.

H. Shaked, J. D. Jorgensen, D. G. Hinks, R. L. Hitterman, and B. Dabrowski, "Structural Properties of $YBa_2Cu_3O_{6+x}$ at Elevated Temperatures in Controlled Oxygen Atmospheres," Physica C **205** (1992), 225-239.

H. Shaked, J. D. Jorgensen, B. Hunter, and R. L. Hitterman, "Defect Structure and Superconducting Properties of $La_{1.8}Sr_xCa_{1.2-x}Cu_2O_{6-\delta}$," Phys. Rev. B **48** (1993), 12941-12950.

H. Shaked, Y. Shimakawa, B. Hunter, P. Radaelli, B. Dabrowski, R. L. Hitterman, J. D. Jorgensen, P. Han, D. Payne, S. Kikkawa, G. Er, and F. Kanamaru, "Structural Effects of Hydrostatic Pressure in $Sr_{1-x}M_xCuO_2$ (M=La,Ca) and $Sr_4Cu_6O_{10}$," Phys. Rev. B **50** (1994a), 12752-12756.

H. Shaked, J. D. Jorgensen, B. Hunter, R. L. Hitterman, A. Paulikas, and B. Veal, "Local Ordering and Charge Transfer During Room-Temperature Annealing of Quenched Tetragonal $YBa_2Cu_3O_{6.25}$," Phys Rev. B **51** (1994), 547-552.

H. Shaked, Y. Shimakawa, B. Hunter, R. L. Hitterman, J. D. Jorgensen, P. Han, and D. Payne, "Superconductivity in the Sr-Ca-Cu-O System and the Phase with Infinite-Layer Structure," Phys. Rev. B **51** (1995), 11784-11790.

H. Shaked, J. D. Jorgensen, D. G. Hinks, R. L. Hitterman, and B. Dabrowski, "Structural Properties of $YBa_2Cu_3O_{6+x}$ at Elevated Temperatures in Controlled Oxygen Atmospheres," Physica C **205** (1993), 225-239.

R. P. Sharma, F. J. Rotella, J. D. Jorgensen, and L. E. Rehn, "Neutron Diffraction and Ion-Channeling Investigations of Atomic Displacements in $YBa_2Cu_3O_{7-\delta}$ Between 10 and 300 K," Physica C **174** (1991), 409-422.

E. Sheu, "Colloidal Properties of Asphaltenes in Organic Solvents," Asphaltenes-Fundamentals and Applications, edited by E. Sheu and O. Mullins (1995), 1.

E. Sheu, "Characterization of Colloidal Aggregates," Advances in the Applications of Membrane-Mimetic Chemistry, edited by T. Yen, R. Gilber, and J. Fendler (Plenum Press, New York, 1995), 105-138.

E. Sheu, D. Storm, and M. DeTar, "Structure and Interaction of Asphaltene Colloids in Organic Solvents," Asphaltene Particles in Fossil Fuel Exploration, Recovery, Refining, and Production Processes (Plenum, N.Y., 1994), 155.

E. Sheu, D. Storm, and M. DeTar, "Asphaltenes in Polar Solvent," J. Non-Cryst. Solid **131** (1991), 341-347.

E. Sheu, M. DeTar, and D. Storm, "Solution Properties of Colloids Formed by Petroleum Vacuum Residues," Macromolecular Report A**28** (1991), 159-176.

Y. Shimakawa, J. D. Jorgensen, D. G. Hinks, H. Shaked, R. L. Hitterman, F. Izumi, T. Kawashima, E. Takayama-Muromachi, and T. Kamiyama, "Crystal Structure of (Cu,C) $Ba_2Ca_3Cu_4O_11_{+\delta}$ (T_c = 117K) by Neutron Powder Diffraction Analysis," Phys. Rev. B **50** (1994a), 16008-16014.

Y. Shimakawa, J. D. Jorgensen, H. Shaked, R. L. Hitterman, T. Kondo, T. Manako, and Y. Kubo, "Underdoped, Optimally Doped, and Overdoped Superconductors in $T1Sr_2(R_{1-x}Ca_x)Cu_2O_{7-\delta}$ (R=Lu or T1)," Phys. Rev. B **51** (1994b), 568-575.

Y. Shimakawa, J. D. Jorgensen, J. Mitchell, B. Hunter, S. Shaked, D. G. Hinks, R. L. Hitterman, Z. Hiroi, and M. Takano, "Structural Study of $Sr_2CuO_{3+\delta}$ by Neutron Powder Diffraction," Physica C **228** (1994c), 73-80.

Y. Shimakawa, J. D. Jorgensen, B. Hunter, H. Shaked, R. L. Hitterman, Y. Kubo, T. Kondo, T. Manako, H. Takahashi, and N. Mori, "Pressure Effects on T_c and Structure in Overdoped $TlSr_2CaCu_2O_{7-\delta}$," Physica C **253** (1995), 71-78.

Y. Shimakawa, J. D. Jorgensen, T. Manako, and Y. Kubo, "Overdoped Metals in the $Tl_2Ba_2CuO_{6+\delta}$ and $TlSr_2CaCu_2O_{7-\delta}$ Systems," Phys. Rev. B **50** (1994), 16033-16039.

P. Shukla, P. Cotts, R. Miller, T. Russell, B. Smith, G. Wallraff, M. Baier, and P. Thiyagarajan, "Conformational Transition Studies of Organosilane Polymers by Light and Neutron Scattering," Macromolecules **24** (1991), 5606-5613.

C. Simmons, M. Hitchman, H. Stratemeier, and A. J. Schultz, "High Pressure, Low Temperature, Single Crystal Neutron Diffraction Study of Deuterated and Hydrogenous Ammonium Switchable Jahn-Teller Distortion," J. Am. Chem. Soc. **115** (1993), 11304-11311.

S. Skanthakumar, C.-K. Loong, L. Soderholm, J. W. Richardson Jr., M. M. Abraham, and L. A. Boatner, "Quadrupolar Effects in the Temperature Dependence of the Lattice Parameters of $HoP_{1-x}V_xO_4$," Phys. Rev. B **51** (1995a), 5644-5648.

S. Skanthakumar, C.-K. Loong, L. Soderholm, M. M. Abraham, and L. A. Boatner, "Crystal Excitations and Magnetic Properties of Ho^{3+} in $HoV0_4$," Phys. Rev. B **51** (1995b), 12451-12457.

S. Skanthakumar and L. Soderholm, "The Oxidation State of Ce in $Pb_2Sr_2Ce_{1-x}Ca_xCu_3O_8$," Phys. Rev. B (1996), in press.

S. Skanthakumar, C.-K. Loong, L. Soderholm, J. Nipko, and J. W. Richardson, Jr., "Anomalous Temperature Dependence of the Lattice Parameters in $HoPO_4$ and $HoVO_4$: Rare Earth Quadrupolar Effects," J. Alloys Cmpd. **225** (1995c),595-598.

A. Smith, R. Benedek, F. Trouw, M. Minkoff, and L. Yang, "Quasi-Two Dimensional Quantum States of H_2 in Stage-2 Rb-Intercalated Graphite," Phys. Rev. B (1996), in press.

A. Smith, R. Benedek, F. Trouw, and L. Yang, "Atomic Potentials for Rb and K Graphite Intercalation Compounds," Phys. Rev. B **49** (1994), 5050-5053.

W. M. Snow, Y. Wang, and P. E. Sokol, "Temperature and Density Dependence of the Condensate Fraction in Liquid ^{4}He," Europhys. Lett. **19** (1992), 304-308.

W. M. Snow and P. E. Sokol, "Temperature and Density Dependence of the Momentum Distribution in Liquid ^{4}He," J. Low. Temp. Phys. (1996), in press.

L. Soderholm, C.-K. Loong, G. L. Goodman, and B. D. Dabrowski, "Crystal-Field Splittings and Magnetic Properties of Pr^{+3} and Nd^{+3} in $RBa_2Cu_3O_7$," Phys. Rev. B **43** (1991), 7923-7935.

L. Soderholm, C.-K. Loong, and S. Kern, "Inelastic Neutron Scattering Study of the Er^{3+} Energy Levels in $ErBa_2Cu_3O_7$," Phys. Rev. B **45** (1992), 10062-10070.

L. Soderholm, C.-K. Loong, J. P. Hammonds, J. E. Greedan, and M. Maric, "Electronic Transitions of Ho in $Pb_2Sr_2HoCu_3O_{9-x}$ Observed by Inelastic Neutron Scattering," J. Appl. Phys. **73** (1993), 6314-6316.

L. Soderholm, C.-K. Loong, J. S. Xue, J. P. Hammonds, J. E. Greedan, and M. Maric, "The Magnetic Properties of R in $Pb_2Sr_2RCu_3O_8$ (R = Ho, and Er)," Physica C **246** (1995), 11-21.

L. Soderholm, U. Staub, S. Skanthakumar, and M. R. Antonio, "The Oxidation State and Magnetic Behaviour of Tb in High-T_c Related Materials," Mat. Res. Soc. Symp. Proc. **376** (1994), 529-534.

L. Soderholm and C.-K. Loong, "Pr and Cm in Superconductor-Related Oxides," J. Alloys Cmpd. **193** (1993), 125-128.

L. Soderholm, C.-K. Loong, and S. Kern, "A Crystal Field Analysis of the Energy Level Splittings for Erbium in $ErBa_3Cu_3O_7$," J. Alloys Cmpd. **181** (1992), 225-231.

P. E. Sokol, W. J. Ma, W. M. Snow, Y. Wang, K. W. Herwig, J. Koplik, and J. R. Banavar, "Freezing in Confined Geometries," Appl. Phys. Lett. **61** (1992), 777-780.

P. E. Sokol, "Bose-Einstein Condensation in Liquid Helium," in Bose-Einstein Condensation, edited by A. Griffin (1995).

U. Staub, L. Soderholm, R. Osborn, E. Balcar, and V. Trounov, "Observations of CEF-Split Intermultiplet Transitions in Optically Opaque Eu, $Ba_2Cu_3O_7$ Using Inelastic Neutron Scattering," Mat. Res. Soc. Symp. Proc. **376** (1994), 535-540.

U. Staub, L. Soderholm, R. Osborn, M. Guillaume, A. Furrer, and V. Trounov, "Intermultiplet Transitions in Optically Opaque $EuBa_2Cu_3O_7$: An Inelastic Neutron Scattering Study," J. Alloys Compd. **225** (1995), 591-594.

U. Staub, L. Soderholm, S. Skanthakumar, and M. Antonio, "Oxidation State and Magnetic Properites of $Pb_2Sr_2Tb_{1-x}Y_xCu_3O_8$," Phys. Rev. B **52** (1995), 9736-9745.

U. Staub, R. Osborn, E. Balcar, L. Soderholm, and V. Trounov, "Crystal Field-Split Intermultiplet Transitions and Their Q-Dependence in $EuBa_2Cu_3O_7$," Europhy. Lett. **31** (1995), 175-180.

R. Stoddary, M. Conradi, A. McDowell, M.-L. Saboungi, and D. L. Price, "Atomic Motions in an Unusual Molecular Semiconductor: NaSn," Phys. Rev. B **52** (1995), 13998-14009.

H. Stokes, D. Decker, H. Nelson, and J. D. Jorgensen, "Structure of Potassium Cyanide at Low Temperature and High Pressure Determined by Neutron Diffraction," Phys. Rev. B **47** (1993), 11082-11092.

R. Strain and J. M. Carpenter, "Examination of Disks from the IPNS Depleted Uranium Target," Proc. ICANS-XIII (1995), 697-706.

H. L. Strauss, Z. Chen, and C.-K. Loong, "The Diffusion of H_2 in Hexagonal Ice at Low Temperatures," J. Chem. Phys. **101** (1994), 7177-7180.

I. W. Sumarlin, J. W. Lynn, D. A. Neumann, J. J. Rush, C.-K. Loong, J. L. Peng, and Z. Li, "Phonon Density-of-States in R_2CuO_4 and Superconducting $R_{1.85}Ce_{0.15}CuO_4$ (R = Nd, Pr)," Phys. Rev. B **48** (1993), 473-482.

T. Sun and K. Seff, "The Location of Deuterium Ions in Zeolite Y by Pulsed-Neutron Powder Diffraction," J. Catalysis **138** (1992), 405-408.

K. Suzuya, D. L. Price, C.-K. Loong, B. C. Sales, and L. A. Boatner, "Structure of Lead-Indium Phosphate Glasses," Res. Soc. Symp. Proc. **367** (1996), 661-666.

H. Takahashi, J. D. Jorgensen, B. Hunter, R. L. Hitterman, S. Pei, F. Izumi, Y. Simakawa, Y. Kubo, and T. Manako, "Anomalous Behavior of the Pressure Dependence of Lattice Constants in $Tl_2Ba_2CuO_{6+x}$," Physica C **191** (1992a), 248-254.

S. Takahashi, L. A. Curtiss, D. Gosztola, N. Koura, C.-K. Loong, and M.-L. Saboungi, "Dialkylimidazolium Chloroaluminates: ab initio Calculations, Raman and Neutron Scattering Measurements," Proc. Intl. Symp. on Molten Salts Chem. and Tech. **93-9** (Electrochemical Society, Pennington, N.J., 1993), 622-631.

H. Takahashi, H. Shaked, B. Hunter, P. Radaelli, R. L. Hitterman, D. G. Hinks, and J. D. Jorgensen, "Structural Effects of Hydrostatic Pressure in Orthorhombic $La_{2-x}Sr_xCuO_4$," Phys. Rev. B **50** (1994), 3221-3229.

S. Takahashi, M.-L. Saboungi, K. Suzuya, and N. Koura, "Aluminum Chloride-1-Butylpyridinium Chloride Melts as an Electrolyte for Aluminum/Polyaniline Cells," 185th Mtg. Electrochem. Soc., Inc., Ninth Int. Symp. on Molten Salts **94** (1993), 728-735.

S. Takahashi, M.-L. Saboungi, R. Klingler, M. Chen, and J. Rathke, "Dynamics of Room-Temperature Melts: Nuclear Magnetic Resonance Measurements of Dialkylimidazolium Haloaluminates," J. Chem. Soc. Faraday Trans. **89** (1993), 3591-3595.

S. Takahashi, M.-L. Saboungi, K. Suzuya, and N. Koura, "Neutron Diffraction Study of Aluminum Chloride Imidazolium Chloride Molten Salts," 185th Mtg. Electrochem. Soc., Inc. Ninth Int. Symp. on Molten Salts **94** (1993), 69-76.

S. Takahashi, M.-L. Saboungi, R. Klingler, M. Chen, and J. Rathke, "NMR Measurements in Solutions of Dialkylimidazolium Haloaluminates," Proc. Eighth Int. Symp. on Molten Salts, The Electrochem. Soc. **92** (1992), 345-350.

S. Takahashi, L. A. Curtiss, D. Gosztola, N. Koura, and M.-L. Saboungi, "Molecular Orbital Calculations and Raman Measurements for 1-Ethyl-3-methylimidazolium Chloroaluminates," Inorganic Chem. **34**(11) (1995), 2990-2993.

J. Tallon, C. Bernhard, H. Shaked, R. L. Hitterman, and J. D. Jorgensen, "Generic Superconducting Phase Behaviour in High-T_c Cuprates: T_c Variation with Hole Concentration in $YBa_2Cu_3O_{7-\delta}$," Phys. Rev. B **51** (1995), 12911-12914.

P. Thiyagarajan, J. E. Epperson, R. K. Crawford, J. M. Carpenter, and R. Hjelm, "Comparison of SANS Instruments at Reactors and Pulsed Sources," Proc. Int. Seminar Structural Investigation at Pulsed Neutron Sources, Report **E3-93-65** (1992), 194-211.

P. Thiyagarajan, D. J. Chaiko, and R. Hjelm, "A Neutron Scattering Study of Poly(ethylene glycol) in Electrolyte Solutions," Macromolecules **28** (1995), 7730-7736.

P. Thiyagarajan, J. E. Hunt, R. E. Winans, K. B. Anderson, and J. T. Miller, "Temperature-Dependent Structural Changes in 1-methylnaphthalene," Energy and Fuels **9** (1995), 829-833.

P. Thiyagarajan, S. J. Henderson, and A. Joachimiak, "Solution Structure of GroEL and Its Complex and Rhodanese by Small Angle Neutron Scattering," Structure **4** (1996), 79-88.

P. Thiyagarajan, G. D. Cody, J. E. Hunt, and R. E. Winans, "Small Angle Neutron Scattering Applications in Fuel Science," Proc. 210th ACS National Mtg. **40** (1995), 397-401.

P. Thiyagarajan, K. A. Carrado, S. R. Wasserman, K. Song, and R. E. Winans, "Anomalous Small Angle X-ray Scattering Study of Layered Silicate Clays Containing Ni (II and Er(III)," Rev. Sci. Instrum. (1996), in press.

P. Thiyagarajan and D. M. Tiede, "Detergent Micelle Structure and Micelle-Micelle Interactions Determined by Small Angle Neutron Scattering in Solution Conditions Used for Membrane Protein Crystallization," J. Phys. Chem. **98** (1994), 10343-10351.

P. Thiyagarajan, K. Bradley, R. K. Crawford, J. E. Epperson, D. Wozniak, and J. M. Carpenter, "Characterization of ^{3}He Area Sensitive Proportional Counters at IPNS for SANS Applications," SPIE 1992 Int. Symp. on Optical Appl. Sci. and Eng., SPIE Proc. **1737** (1992), 243-254.

D. M. Tiede, P. Marone, A. M. Wagner, and P. Thiyagarajan, "Characterization of Photosynthetic Supramolecular Assemblies Using Small Angle Neutron Scattering," Photosynthesis from Light to Biosphere, edited by P. Mathis, (Kluwer Academic Publishers: Netherlands, 1995), 431-436.

D. M. Tiede, P. Marone, A. M. Wagner, and P. Thiyagarajan, "Characterization of Photosynthetic Supramolecular Assemblies Using Small Angle Neutron Scattering," Proc. Xth Int. Photosynthetic Congress, (1996b), in press.

D. M. Tiede and P. Thiyagarajan, "Biophysical Techniques in Photosynthesis," Biophysical Techniques in Photosynthesis, edited by J. Amez and A. Huff, (Academic Press, 1996a), in press.

B. Toby and T. Egami, "Accuracy of Pair Distribution Function Analysis Applied to Crystalline and Non-Crystalline Materials," Acta. Cryst. A**48** (1992), 336-346.

B. Toby, T. Egami, J. D. Jorgensen, and M. Subramanian, "Observation of a Local Structural Change at T_c for $Tl_2Ba_2CaCu_2O_8$ by Pulsed Neutron Diffraction," Phys. Rev. Lett. **64** (1990), 2414-2417.

I. Tomaskzkiewicz, S. Susman, K. Volin, and P. O'Hare, "Fluorine-Combustion Calorimetric Determinations of the Standard Molar Enthalpy Changes for the Formation of $SiSe_2$(cr), $SiSe_{1.94}$(cr), and $SiSe_{1.94}$(vit), and for the Transition: $SiSe_{1.94}$(cr) at Temperature T=298.15K. Implications of the Results for the Enthalpies of Dissociation D°m (Si-SiSe) and D°m (SiSe). Thermodynamic Properties of SiSe(g)," J. Chem. Thermodynamics **26** (1994), 1081-1093.

M. Tosi, D. L. Price, and M.-L. Saboungi, "Ordering in Metal Halide Melts," Ann. Rev. of Phys. Chem. **44** (1993), 173-211.

M. Tosi, G. Pastore, M.-L. Saboungi, and D. L. Price, "Liquid Structure and Melting of Trivalent Metal Chlorides," Phys. Scripta **15** (1991), 283-288.

F. Trouw, "Molecular Dynamics Simulation and Inelastic Neutron Scattering," Spectrochimsica Acta **48A** (1990), 455-476.

F. Trouw, L. Iton, and M. Davis, "Inelastic Neutron Scattering and Molecular Dynamics Simulation of Water Adsorbed in the Molecular Sieves $AlPO_4$-11, $AlPO_4$-5, $AlPO_4$-8 and VPI-5," Zeolites and Related Microporous Materials: State of the Art 1994, edited by J. Weitkamp, H. G. Karge, H. Pfeifer, and W. Holderich (Elsevier, 1994), 851-858.

P. Trulove, D. Haworth, R. Carlin, A. Soper, A. J. G. Ellison, and D. L. Price, "Structural Investigations of 1-Ethyl-3-Methylimidazolium Hydrogen Dichloride: Neutron Diffraction Studies of an Ambient-Temperature Molten Salt," Proc. IXth Int. Symp. on Molten Salts, edited by C. Hussey, D. Newman, G. Mamantov, and Y. Ito (1994), 50-57.

J. Wagner, B. Hunter, D. G. Hinks, and J. D. Jorgensen, "Structure and Superconductivity of $HgBa_2Ca_2Cu_3O_{8-\delta}$," Phys. Rev. B **51** (1994), 15407-15414.

J. L. Wagner, P. Radaelli, D. G. Hinks, J. D. Jorgensen, J. Mitchell, B. Dabrowski, G. Knapp, and M. Beno, "Structure and Superconductivity of $HgBa_2CuO_{4+\delta}$," Physica C **210** (1993), 447-454.

X. L. Wang, C. Stassis, D. C. Johnson, P. C. Leung, J. Ye, B. N. Harmon, G. H. Lander, A. J. Schultz, C.-K. Loong, and J. M. Honig, "Neutron Diffraction Study of the Antiferromagnetic Form Factor of La_2NiO_4," Phys. Rev. B **45** (1992), 5645-5653.

S.-L. Wang and J. W. Richardson, Jr., "Neutron Powder Diffraction Study of the Mixed-Valence Vanadium Pyrophosphate $RbV_3P_4O_{16.97}$," Zeit Krist. **202** (1992), 227-236.

Y. Wang, H. Zhang, V. Dravid, D. Shi, D. G. Hinks, Y. Zheng, and J. D. Jorgensen, "Evolution of the Low-Energy Excitations and Dielectric Function of $Ba_{1-x}K_xBiO_3(0<\xi<0.50)$," Phys. Rev. B **47** (1993), 14503-14509.

Y. Wang and P. E. Sokol, "Kinetic Energy and Condensate Fraction in Liquid ^3He-^4He Mixtures," Phys. Rev. Lett. **72** (1994), 1040.

U. Welp, G. Crabtree, J. Wagner, D. G. Hinks, P. Radaelli, J. D. Jorgensen, J. Mitchell, and B. Dabrowski, "The Irreversibility Line of $HgBa_2CuO_{4+x}$," Appl. Phys. Lett. **63** (1993), 693-695.

H.-R. Wenk, "Standard Project for Pole-Figure Determination by Neutron Diffraction," J. Appl. Cryst. **24** (1991), 920-927.

H.-R. Wenk, A. Larson, P. Vergamini, and A. J. Schultz, "Time-of-Flight Measurements of Pulsed Neutrons and 2d Detectors for Texture Analysis of Deformed Polycrystals," J. Appl. Phys. **70** (1991), 2035-2040.

T. Wiencek, H. Thresh, and J. Summers, "Development of a Boron-Copper Neutron Absorber Composite," **ANL-91/44** (1991), 1-34.

R. E. Winans, R. L. Mcbeth, R. S. Scott, P. Thiyagarajan, R. E. Botto, and R. Hayatsu, "Chemical and Physical Structures of Coals," Proc. Second Coal Res. Conf., **1** (Coal Res. Assoc. New Zealand, 1989), R13.1 1-14.

P. Worchner, Q. J. Wang, S. C. Moss, S. K. Sinha, G. Grübel, H. Chou, J. E. Berman, J. D. Axe, C.-K. Loong, J. B. Liu, W. D. Mosley, P. Klavins, and R. N. Shelton, "X-Ray Search for CDW Satellites in Single Crystal $Ba_{1-x}K_xBiO_3$," Phys. Rev. B **47** (1993), 9120-9123.

H. Zhang, Y. Wang, V. Dravid, B. Dabrowski, K. Zhang, D. G. Hinks, and J. D. Jorgensen, "Anisotropy of Charge Carriers and Dielectric Function of $YBa_2Cu_4O_8$ (Y124)," Physica C **208** (1993), 231-237.

X. Zhou, G. P. Felcher, and S.-H. Chen, "The Closed-Form Expressions for the Neutron and X-Ray Reflection and Transmission Coefficients of a One-Dimensional Profile," Physica B **173** (1991), 167-179.

X. Zhou, S.-H. Chen and G. P. Felcher, "Inverse Problem in Neutron Reflection," Proc. NATO Advance Reseach Workshop on Inverse Problems in Scattering and Imaging, edited by M. Bertero and E. R. Pilde (Adam Hilger, Bristol, 1992), 109-130.

X. Zhou, S.-H. Chen, and G. P. Felcher, "Improved Analytical Formulas for X-Ray and Neutron Reflection from Surface Films," Phys. Rev. A **46** (1992), 1839-1843.

X. Zhou, S.-H. Chen, and G. P. Felcher, "A New Analytical Formula for Neutron Reflection From Surface Films," J. Phys. Chem. **95** (1991), 9025-9029.

This progress report was prepared by the staff of Argonne's Intense Pulsed Neutron Source.

Editor
Beverly Marzec

Scientific Advisor
Chun-Keung Loong

Secretarial Assistance
Diane Hoffmann
Cathy Riblon
Carolyn Tobin

CAD Design
Philip Calahan

Publishing support services provided by Argonne's Information and Publishing Division.

Design
Daniel Sarro
Tami Sharley

Photography
George Joch

Technical Editors
Floyd Bennett
Marita Moniger

Additional Assistance
Linda Graf
Linda Haley
Lisa Hundley

Argonne National Laboratory
Operated by the University of Chicago
for the U.S. Department of Energy

Printed on recycled paper